Improved Numerical Simulation of Non-Thermal Enhanced Heavy Oil Recovery

By

Usman Habu Taura

BEng., MSc.

Submitted for the degree of Doctor of Philosophy

Institute of Petroleum Engineering

School of Earth Geoscience Infrastructure and Society

Heriot-Watt University

Dec 2016

ABSTRACT

The dependence on unconventional resources such as heavy oil is on the rise due to geometric increase in demand for energy and the decline of production from mature conventional oil reservoirs. Heavy oil reservoirs contain oil that has some limited mobility under reservoir conditions and only a small fraction of the oil-in-place can be recovered by primary technique which involve harnessing the internal reservoir energy. The remaining oil after the primary depletion is still mostly continuous and present a valuable target for enhanced recovery. However, most of these reservoirs are relatively thin, making them poor candidates for thermal methods, in addition to associated high energy requirement and adverse environmental effects of the heating process. Therefore, any incremental oil recovery must be through non-thermal methods, such as waterflooding, chemical and gas injection. These methods however suffer from adverse mobility ratio which significantly affect the efficiency of the displacement process. The simulation of these processes for the purpose of reservoir prediction and performance is a herculean task due to the complex physics of instability and compositional effect taking place that is not fully understood.

In this thesis, the results of improved numerical simulation techniques of non-thermal heavy oil recovery were presented, demonstrating the viability of the techniques as simulation methods heavy oil non-thermal enhanced heavy oil recovery (EHOR). Several displacement mechanisms were identified through the simulation of the secondary and tertiary processes that contributed to significant incremental heavy oil recovery. A systematic lumping scheme of the heavy oil components into pseudo-components based on the behaviour of the produced oil was proposed. A new methodology for the estimation of relative permeability from displacement with instability and compositional effect using a two-dimensional (2D), high-resolution model to effectively capture the finger, and a versatile, three-parameter function (L.E.T correlation) was demonstrated. A semi-analytical approach through a combination of theoretical and an empirical prediction method based on the famous works of Koval, and Todd and Longstaff on viscous fingering was employed for the verification of the estimated relative permeability. Lastly, a multiscale approach to history matching, for the estimation of unstable relative permeability that is computationally more efficient, was proposed. It involves the history

matching of a set of coarse grid models to predict the fine-scale relative permeability. In this approach, fine-scale information was resolved without direct solution of the global fine-scale problem. The results showed that the time required to estimate relative permeability using the multiscale approach was only about 35% required to estimate the same relative permeability using a single high-resolution model. The memory requirement for the approach was also about 50% required for simulation of the single high-resolution model. Therefore, the lower memory size and computations required in the multiscale approach mean that a less powerful computer can be used to estimate the relative permeability curves for unstable displacements with accuracy similar to that obtained using a high-resolution model approach.

DEDICATION

I wholeheartedly dedicate this work to my mum, Hajia Barira Umaru

ACKNOWLEDGEMENT

I would like to foremost, express sincere appreciation, to my Supervisor, Prof Mehran Sohrabi, for not only giving me the opportunity to be part of a world renown research team but for his unwavering support, guidance and mentorship throughout the duration of my programme. I would also like to thank immensely, my second supervisor, Dr Pedram Mahzari, for his tremendous contribution, valuable suggestions and criticisms, without which the programme would not have been a success.

Special thanks also go to Dr Hamidreza Shahvardi for his guidance at the early stage of my research. Many thanks also go to Amir Farzaneh for his generosity with experimental data. I would also like to thank all the students and staff of Centre for Enhanced Oil Recovery and CO_2 solutions for their invaluable companionship and timely assistance whenever and wherever it was required. Thanks, are also due to all staff and students of the institute of Petroleum Engineering at heriot-Watt University for their support, warm hospitality and respect to diversity.

Finally, I would like to express special appreciation to my mum, Hajia Barira Umaru, my family and friends for their love and continued support. The deepest thanks are expressed to my wife, Aisha Saleh, for her endless love, care, support and encouragement. To my daughter Barira, I say thank you for adding more joy to our family.

ACADEMIC REGISTRY

RESEARCH THESIS SUBMISSION

Name*:*	USMAN HABU TAURA		
School/PGI:	EGIS/IPE		
Version: *(i.e. First, Resubmission, Final)*	First	Degree Sought (Award **and** Subject area)	Doctor of Philosophy in Petroleum Engineering

Declaration

In accordance with the appropriate regulations I hereby submit my thesis and I declare that:

1) the thesis embodies the results of my own work and has been composed by myself
2) where appropriate, I have made acknowledgement of the work of others and have made reference to work carried out in collaboration with other persons
3) the thesis is the correct version of the thesis for submission and is the same version as any electronic versions submitted*.
4) my thesis for the award referred to, deposited in the Heriot-Watt University Library, should be made available for loan or photocopying and be available via the Institutional Repository, subject to such conditions as the Librarian may require.
5) I understand that as a student of the University I am required to abide by the Regulations of the University and to conform to its discipline.

* *Please note that it is the responsibility of the candidate to ensure that the correct version of the thesis is submitted.*

Signature of Candidate*:*		Date:	10/02/2017

Submission

Submitted By *(name in capitals):*	USMAN HABU TAURA
Signature of Individual Submitting:	
Date Submitted:	

For Completion in the Student Service Centre (SSC)

Received in the SSC by *(Name in capitals):*			
Method of Submission *(Handed in to SSC; posted through internal/external mail):*			
E-thesis Submitted *(Mandatory for final theses)*			
Signature:		Date:	

TABLE OF CONTENTS

LIST OF FIGURES

LIST OF TABLES

GLOSSARY

ρ	Density
k	Permeability
μ	Viscosity
λ	Mobility
v	Front velocity
BT	Breakthrough
ccOil/ccInj	Volume of produced oil in cc per volume of injected fluid in cc at lab conditions (unit for oil production rate)
ccCO2/ccOil	Volume of produced CO2 in cc per volume of produced oil in cc at lab conditions (unit for gas/oil ratio)
GOR	Gas/Oil ratio
IFT	Interfacial Tension
volume OOIP	Original oil in place
PV	Pore volume
SWAG	Simultaneous water alternating CO2 injection
Swi	Connate water saturation
Sorw	Waterflood residual oil saturation
Sorg	Gas flood residual oil saturation
EOS	Equation of State
PR	Peng-Robinson
SCN	Single Carbon Number
1D	One-Dimensional
2D	Two-Dimensional
Kr	relative permeability
L	Lower curve exponent
E	Middle curve exponent
T	Top of the curve exponent
DECE	Designed Exploration and Controlled Evolution
DP	Differential pressure
GC	Gas chromatography
GM	Gas meter

LIST OF PUBLICATIONS

- Taura, U. H., Mahzari, P., Soharbi, M., (2016) "A new methodology for Improved Estimation of Two-Phase Relative Permeability Functions for Heavy Oil Displacement Involving Compositional Effects and Instability", *SPE International Heavy Oil Conference and Exhibition*, Mangaf, Kuwait, 6-8, December.

- Taura, U. H., Mahzari, P., Sohrabi, M., (2017) "A Multiscale Approach to Estimation of Two-Phase Relative Permeability from Unstable Displacement by History Matching Technique", *SPE Nigeria Annual International Conference and Exhibition*, Lagos, Nigeria, 31 July – 2 August.

- Taura, U. H., Mahzari, P., Sohrabi, M., (2017) "A New Approach for Improved Estimation of Three Phase Relative Permeability Functions for Heavy Oil Displacement", *SPE Nigeria Annual International Conference and Exhibition*, Lagos, Nigeria, 31 July – 2 August.

- Taura, U. H., Mahzari, P., Sohrabi, M., (2017) "A New methodology for Improved Estimation of Two-Phase and Three Phase Relative Permeability Functions for Heavy Oil Displacement Involving Instability and Compositional Effect", *Journal of Petroleum Science and Engineering*, Elsevier, Under Review

CHAPTER 1

INTRODUCTION

1.1 HEAVY OIL RESOURCE

Heavy Oil is a type of hydrocarbon resource that is characterised by high viscosity and density and can exist in liquid, semi-solid or even solid state. The world is blessed with abundant quantities of this resource as according to International Energy Agency, there is currently an estimated over two trillion barrels of recoverable reserve of heavy-oil including medium-heavy-oil, extra-heavy-oil and bitumen (OECD/IEA, 2013). This amount is more than two-third of remaining conventional oil reserve (Figure 1-1). Although current production of this resource is far below that of conventional oil, the world reliance on non-conventional oil including heavy oil is on the rise and has the potential to be a major source of energy in the near future. This is mainly driven by higher oil prices as a result of ever-escalating demand for energy as well as improvement in technology.

The high viscosity of the oil at reservoir condition limits its mobility under primary depletion mechanism and conventional techniques are highly inefficient, and in most cases, unfeasible (Mai et al., 2009). For these reasons, improved recovery processes that are geared towards reducing the viscosity of the hydrocarbon, thereby making it easier to flow, have gained wider acceptance (Garcia, 1983, Nehring, 1983, Sankur and Emmanuel, 1983, Miller, 1994) . These techniques are broadly classified into two main classes; the thermal processes and the non-thermal processes (Figure 1-2). In the thermally improved recovery process, heat is added to reduce the viscosity of the oil and increase its mobility (Shu and Hartman, 1986, Butler, 1991). These include steam injection and in-situ combustion recovery techniques that are highly capital intensive ventures with significant undesirable environmental impact and high carbon footprint (Farouq Ali, 1974). In addition to these concerns, many heavy oil reservoirs are not suitable for thermal methods due to the reservoir geometry and hence it cannot be efficiently and

economically applied to these types of reservoirs (Farouq Ali, 1974, Mai et al., 2009). For these reasons, several non-thermal methods are being investigated, these include waterflood, gas flooding and chemical injections.

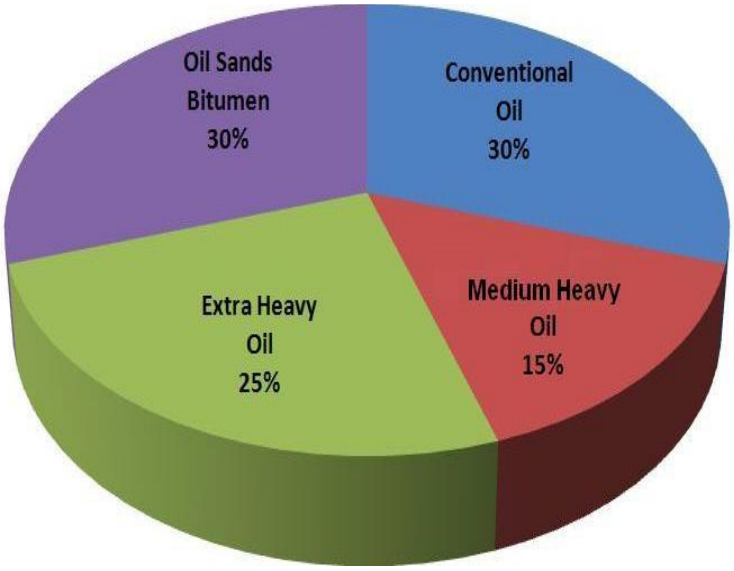

Figure 1-1: Total world oil resources. Medium-heavy, extra-heavy and bitumen make up to 70% of the world's total oil resources.

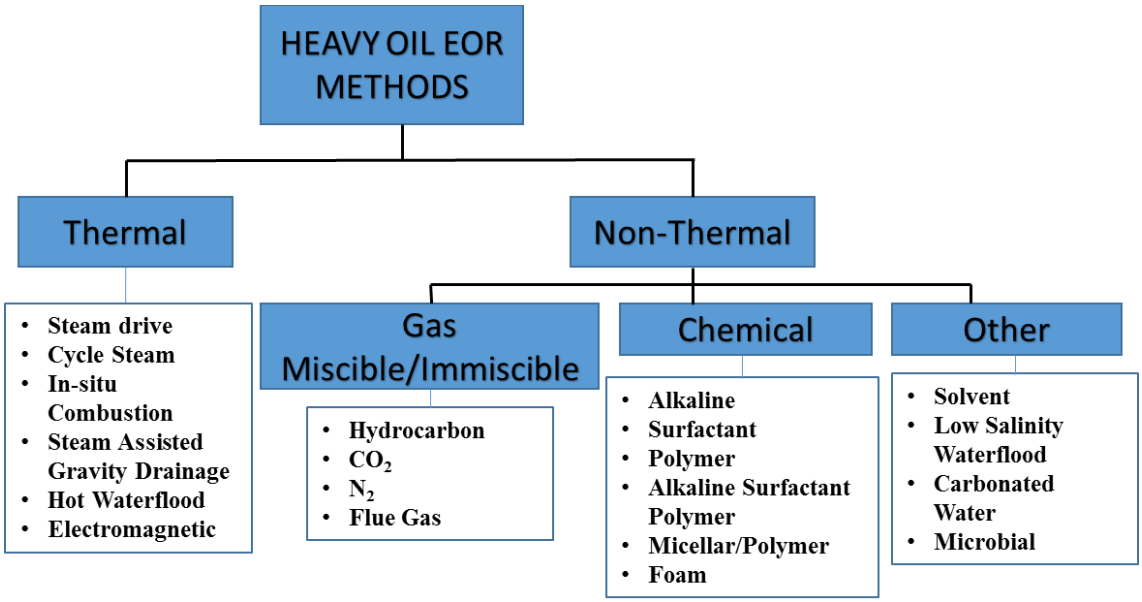

Figure 1-2: Thermal and Non-Thermal methods of Enhanced Heavy Oil Recovery

1.2 NON-THERMAL HEAVY OIL RECOVERY METHODS

As an alternative to thermal methods, waterflooding, has made significant inroads in improving heavy oil recovery (Jennings and Habra, 1966, Smith, 1992, Mai and Kantzas,

2009, Nasehi and Asghari, 2010, Emadi et al., 2011a, Torabi et al., 2012a). This is due in large part to the availability of water, low cost of utilisation as well as benefiting from significant experience in managing field application that is largely borrowed from conventional oil waterflooding technique (Mai and Kantzas, 2009). The performance of waterflooding depends to a large extent on the interplay and competition between viscous (shear) and capillary forces. However, it is less efficient because it suffers from adverse mobility ratio due to large viscosity ratio between the oil and the injected water which leads to a phenomenon known as viscous fingering, resulting in an early water breakthrough during the displacement (Benham and Olson, 1963, M., 1987, Kueper and Frind, 1988, Araktingi and Orr Jr, 1993, Blunt and Christie, 1994, Sharma et al., 2012).

Recently, gas and solvent based injection processes have attracted increased attention as alternative non-thermal techniques. In particular, CO_2 injection has been a subject of wide research and its recovery mechanisms have been well understood for conventional oils. Most of the studies are focussed around its miscibility in hydrocarbon, oil swelling behaviour and its ability to increase oil mass density while in solution (Garcia, 1983, Saner and Patton, 1986, Grogan et al., 1988, Ghoodjani and Bolouri, 2011, Farzaneh et al., 2016). Other desirable effects of CO_2 injection include its ability to extract lighter component from the oil as well as upgrading the produced oil by knocking off heavy components (Farzaneh, 2014).

However, in heavy oil recovery by CO_2 injection, the dominant recovery mechanism is the oil viscosity reduction due to CO_2 high solubility in hydrocarbon. It has been reported that when CO_2 is fully saturated in oil, it can reduce the oil viscosity by up to two magnitudes (Sankur and Emmanuel, 1983, Emadi et al., 2011a). Similar to the waterflooding technique, however, the gas injection also suffers from the debilitating effect of adverse mobility ratio which leads to viscous fingering. The lower density of the gas compared to the oil can also lead to gravity segregation (Terwilliger et al., 1951, Holm, 1982, Garcia, 1983, Glass et al., 1991). Therefore, in heavy/viscous oil recovery using non-thermal techniques such as gas or water injection, adverse mobility ratio, leading to viscous fingering is the crucial factor that affects the performance of the displacement, and can also be further aggravated by mass transfer and fluid-fluid interactions effects (Sankur and Emmanuel, 1983, Spivak, 1984, Mayer et al., 1988, Martin and Taber, 1992, Nasehi and Asghari, 2010, Emadi et al., 2011a).

To improve on the frontal stability of the gas injection methods, other non-thermal techniques for heavy oil recovery have been implemented. These include the combination of gas and water injection such as Water-Alternating-Gas (WAG) and Simultaneous-Water-And-Gas (SWAG) (Farzaneh et al., 2016, Ma et al., 1995, Seyyedsar et al., 2015) injection strategies that are geared toward improving the sweep efficiency. Various chemicals have also been injected in conjunction with water and CO_2 to change the rock wettability or to promote foam and emulsion formation, solely for the purpose of enhancing displacement and sweep efficiency (Thomas et al., 1999, Mai et al., 2009, Torabi et al., 2012b, Farouq Ali, 1976). Furthermore, heavy oils are known for their natural surface-active components that can potentially be used as surfactants or co-surfactants if the governing mechanisms are identified and understood (Farouq Ali, 1976, Farouq Ali, 1974, Rojas et al., 1991).

1.3 SIMULATION OF NON-THERMAL HEAVY OIL RECOVERY PROCESSES

Non-thermal processes are generally capital intensive to implement at reservoir or field scale (with the exception of waterflood), and therefore, prior extensive preliminary studies including pilot scale are initially conducted, followed by systematic simulation studies at larger reservoir scale using the information obtained from the laboratory and pilot scale studies. However, the simulation of these unstable displacement processes for the purpose of performance prediction and forecasting is not a straightforward task. The published data on the numerical simulation of non-thermal heavy oil recovery are quite limited in the literature (Jha, 1986, Pooladi-Darvish and Firoozabadi, 1999, Dauba et al., 2002, Lim et al., 2004, Gerritsen and Durlofsky, 2005, Cuthiel et al., 2006, Wang et al., 2006b, Rahnema et al., 2008, Tripathi and Mohanty, 2008, Yazdani and Maini, 2008, Alkindi et al., 2011, Pei et al., 2011, Pathak et al., 2012, Wan et al., 2014). While some have been reported to be successful, with promising performance prediction using conventional theories based on live oil (Jha, 1986, Dauba et al., 2002), others have indicated that the production performance, sensitive operational parameters and efficient displacement mechanism are not the same as the case of light oil and therefore cannot be fully simulated by the existing theories developed based on the physics of light oils (Pooladi-Darvish and Firoozabadi, 1999, Nasrabadi et al., 2009, Sun and Firoozabadi, 2009, Mutoru et al., 2011, Emadi, 2012, Moortgat et al., 2013). Therefore, it is believed

that the current understanding of simulation in heavy oil displacement and how it differs from the concept of simulation of light oil is limited and inadequate, despite its vital importance in performance prediction and forecasting of heavy oil recovery (Mai et al., 2009, Ortiz-Arango and Kantzas, 2011, Kumar and Okuno, 2012b). It is clear that without the full understanding of how to simulate such processes, the design, optimisation, prediction and forecasting of non-thermal heavy oil recovery is highly impractical.

Among the greatest issues in simulation of non-thermal heavy oil recovery is the limited understanding of the physics of the instability in the displacement. While it is agreed that adverse viscosity ratio and capillary instabilities are the main causes of instability in the displacement, however, there is no clear understanding or approach for modelling them (Benham and Olson, 1963, King, 1987, Araktingi and Orr Jr, 1993, Blunt and Christie, 1994, Cuthiel et al., 2006). Most theories on instability in porous media are empirical formulations that were developed based on the concept of miscible flooding (koval, 1963, Todd and Longstaff, 1972, Fayers and Newley, 1988, Araktingi and Orr Jr, 1993, Blunt et al., 1994, Blunt and Christie, 1994, Barker and Evans, 1995). In immiscible floods, such as heavy oil displacement by water and immiscible solvent, the theories are deficient and require modification in the assumptions (Blunt et al., 1994).

Another important issue is the way the compositional and mass transfer effects associated with solvent injections such as CO_2 are modelled. As miscibility is not a target in heavy oil displacement by gas, solvent gas injection is aimed at improving the oil mobility, the dissolution is gradual and changes in properties of both the injected solvent and the resident oil is a dynamic process (Saner and Patton, 1986, Mayer et al., 1988). However, most compositional simulators that are based on Equation of State (EOS) assume instantaneous equilibrium as soon as the solvent is injected (Coats, 1980, Voskov and Tchelepi, 2012). This can be grossly misleading in a situation where the oil thickness is large and therefore equilibrium hardly achieved, a typical scenario at the reservoir scale. There are however, a few higher order non-equilibrium numerical simulators published in the literature that are thermodynamically consistent with the dynamics of mass transfer taking place in the system (Moortgat et al., 2013, Salehi et al., 2013, Tran et al., 2017). These are also, non-generic, computationally intensive, and currently not fully implemented in commercially available simulation softwares.

The determination of relative permeability for an unstable displacement such as heavy oil displacement is another huge source of uncertainty in simulation (Boukadi et al., 2005). This important flow function which was formulated as a modification of Darcy law to account for multiphase flow in a stable, Buckley-Leverett type displacement, lacks physical meaning when used for unstable displacement(Jerauld et al., 1984, Maini, 1998, Kulkarni and Datta-Gupta, 2000). Maini (1998) has even questioned the futility of its measurement for heavy oil reservoirs because it is the most uncertain parameter in heavy oil simulation and engineers often adjust it in order to history match production data. Nevertheless, it is an essential parameter required in simulation and must be determined. Generally, relative permeability is estimated from experimental data, such as unsteady state displacement experiment, and computed explicitly using methods such as JBN (Johnson et al., 1959). However, the most widely used is the implicit method involving the history matching of unsteady state displacement experiment data to estimate the unknown parameter (Jennings et al., 1988, Li et al., 2009, Shahverdi and Sohrabi, 2011, Zhang et al., 2012, Jahanbakhsh and Sohrabi, 2015, Chardaire-Riviere et al., 1990, Chardaire-Riviere et al., 1992).

Conventionally, a one-dimensional grid model of the displacement is used in the history matching, however, this can lead to erroneous result when used to estimate relative permeability for displacement with instability, since a one-dimensional model cannot capture the instability in the displacement (Christie and Bond, 1987, Christie et al., 1990, Christie et al., 1993). Few literature are available on the estimation of relative permeability from unstable displacement such as immiscible heavy oil displacement (Peters and Khataniar, 1987, Riaz and Tchelepi, 2006, Castillo et al., 2009, Ghoodjani and Bolouri, 2011, Modaresghazani et al., 2015). While Peters and Khataniar (1987) and Castillo et al. (2009) have emphasised on the need to conduct the laboratory displacement experiment at the same degree of instability as the reservoir in order to have a representative relative permeability, others have developed a correction factor for computing pseudo-relative permeability for the unstable displacement (Ghoodjani and Bolouri, 2011, Riaz and Tchelepi, 2006).

Furthermore, simulation studies normally involve lots of uncertainties that require running several what-if scenarios to determine the best or optimal case. Sometimes the studies involve the determination of unknown parameters using inverse techniques like

history matching. In this case, a large number of simulation runs are needed to map the parameter space adequately. In heavy oil displacement by solvent, the instability and slow mass transfer and the resulting dynamic, non-equilibrium compositional and phase properties changes taking place, makes such a history matching even harder to accomplish.

1.4 AIM AND OBJECTIVES OF THE STUDY

The aim of this study is to improve the methodology for the simulation of non-thermal enhanced heavy oil recovery in which instability and compositional effects take place.
The main objectives are to improve on the fluid phase behaviour modelling as well as to develop a computationally efficient methodology for the estimation of flow functions required for the simulation of heavy oil systems in which there is instability and compositional effect. The study benefits graciously from an extensive body of experimental research studies which helps in meeting the set objectives. These include some two-phase and three-phase coreflood experiments involving various injection strategies and a micromodel experiment that described the recovery mechanism and the saturation profiles.

1.5 CHAPTERIZATION

The entire thesis will run into nine chapters. The first introduced the work, brought out the importance of the study and stated the objective of the work.

The second chapter of the thesis introduced the experimental work that was carried out by other PhD studensts; this includes the facilities, procedure, experimental conditions and coreflood preparations as well as how the experiments were performed. It then briefly described the results of the PVT experiments and the two-phase and three-phase coreflood experiments.

The third chapter discussed phase behaviour modelling and gridding effect. The main displacement mechanisms, compositional modelling, phase behaviour modelling using equation of state (EOS), viscosity modelling and effect of model grid size were also discussed. A new methodology for systematic lumping (grouping) of components based

on the behaviour of produced oil components obtained from the GC compositional analysis of the produced oil in the coreflood experiments was proposed. The core modelling approach capable of resolving the finger propagation was also presented.

Chapter four discussed an improved methodology for estimation of flow functions in heavy oil displacement by gas and water. Several approaches for estimation of these important parameters were reviewed; these include the steady state and unsteady state experimental methods as well as explicit and implicit methods of estimation of relative permeability from unsteady-state (dynamic) experiments. Various parametric and non-parametric implicit methods of estimation were also discussed. A methodology for estimation of two-phase gas/oil relative permeability was proposed and verified using real coreflood data.

Chapter five discussed the methods of estimation of three-phase relative permeability. Methodologies for the estimation of three-phase relative permeability from the literature were reviewed. An improved procedure for estimation of three-phase relative permeability using history matching technique was proposed and tested using coreflood data obtained from laboratory experiment.

Chapter six discussed the sensitivity various parameters on the simulation results of heavy oil displacement by injection of gases and water. Sensitivity studies on parameters such as capillary pressure, Fickian diffusion, oil mass density and gas viscosity were carried out to determine their effects on the estimated relative permeability and the stability of heavy oil displacement by enhanced non-thermal recovery techniques.

Chapter seven examined the predictive theory of viscous fingering in heavy/viscous oil displacement. As stated previously, it is often computationally daunting to simulate displacement with significant instability such as viscous fingering or gravity segregation. It is, therefore, expedient to develop a simple, fast, yet theoretically sound tool for predicting the onset of instability in displacements that are prone to instability. The technique should also be able to predict its breakthrough time as well as average saturation distribution within the porous media. Moreover, a tool for benchmarking or verifying simulations of displacements in which instability occurred need to be developed. This chapter considered the use of material balance calculations with tested

empirical equations based on Koval (1963) method to draw up a procedure for predicting average saturation profile in displacements with instability. The main assumption in this theory is that the variation of composition within the fingered region in unstable displacement is linear. The approach was demonstrated with two coreflood experiments as examples.

Chapter eight propsed a multiscale approach to relative permeability estimation in unstable displacement. Commonly, relative permeability is estimated by the history-matching technique using a 1D model. However, for displacements with instability, a fine-scale 2D model would be required to capture the instability propagating at the front of the displacement, as stated earlier; but this comes with attendant consequence on simulation time and resources. In this approach, the versatile three parameters (L.E.T-type) equation and a series of coarse-grid models was used instead of a single fine-grid model for the history-matching. The multiscale methodology has significantly reduced the time required to estimate relative permeability by history matching in displacements with severe instability resulting from viscous fingering by using coarse models that are less time and resource consuming.

Chapter nine discussed the conclusion of the findings and made recommendations. It summarised the key results found on the improved simulation of non-thermal enhanced heavy oil recovery and suggested recommendations for future work.

CHAPTER 2

BACKGROUND MATERIAL AND UNDERPINNING DATA

2.1 INTRODUCTION

This chapter aims to give a brief review of concepts and techniques for modelling of flow functions. These include experimental and numerical techniques and their associated uncertainties and errors. It also highlights the difficulties inherently associated with numerical modelling and simulation of unstable and compositional displacement systems. Many of the ideas introduced in Chapter 1 are expanded here to give a more comprehensive understanding. A summary of underpinning data from physical coreflood experiments that were performed elsewhere but used in this work for the purpose of model validation and prediction were also discussed.

2.2 CONCEPT OF RELATIVE PERMEABILITY

Relative permeability is a concept devised to account for the permeability of phases in multiphase flow in a porous media. The relative permeability of a phase is a dimensionless measure of the effective permeability of that phase to the absolute permeability. It can be viewed as a modification of Darcy's law to account for multiphase flow. Effective permeability measures the ability of flow which is preferential when there is one or more immiscible fluids present and it is affected by the saturations values.

For two-phase or multiphase flow in porous media, the Darcy equation can be written as

$$q_i = \frac{k_i}{\mu_i} \nabla P_i \quad for\ i = 1,23... \qquad 1$$

Where q is the flux, ∇P is the pressure μ is the viscosity. The subscript i denotes the phase, while k is the effective permeability of the phase. The ratio of effective permeability of a given fluid and saturation to the absolute permeability K at total saturation is known as

the relative permeability. Relative permeability values are therefore less than or equal to one, as given by equation (2).

$$k_{ri} = \frac{k_i}{K} \qquad 2$$

2.3 EXPERIMENTAL METHODS FOR MEASURING RELATIVE PERMEABILITY

There are two main experimental methods for estimating two-phase relative permeability of a porous media, these are:

2.3.1.1 The steady state displacement method

In this method, the two phases simultaneously flow at fixed ratio continuously until the saturations in the core and the pressure drop across the sample are constant, which is an indication that the system has achieved steady-state. It is difficult to estimate relative permeability curves using this method because of the inherent experimental artefacts associated with the method. These include capillary end effect, which occurs particularly at low flowrates and local saturation gradients resulting from heterogeneity in the porous media. It is also time-consuming, as it is often necessary to determine 5 to 6 saturation points each for the two relative permeability curves.

2.3.1.2 The unsteady state displacement method:

This is also known as the dynamic displacement method. Here, the porous media is initially saturated with oil at connate water saturation and then displaced by water. The produced volume of water and the produced volume of oil, as well as the pressure drop across the medium, are then used to calculate the relative permeability curves. This method is faster, less expensive and can be designed to mitigate the experimental artefact associated with the steady-state method. This is the most preferred laboratory method and the technique for computing oil/water relative permeability curves from unsteady state displacement data have been fully developed (Honarpour et al., 1986).

2.4 ANALYTICAL METHODS OF ESTIMATION OF TWO-PHASE RELATIVE PERMEABILITY

There are several analytical methods for estimation of relative permeability which mostly based on the analysis of displacement data, typically unsteady displacement data. Here we discussed only the Jonson-Bossler-Naumann (JBN) and briefly the Jones-Roszelle Method.

2.4.1.1 JBN Method

The explicit analytical technique for computing immiscible two-phase (oil/water or gas/oil) relative permeability curves from unsteady state (dynamic) displacement data has been developed by Welge (1949) and Johnson et al. (1959) and is known as the Johnson-Bossler-Naumann (Johnson et al., 1959) method or simply the JBN. It is based on the Buckley and Leverett theory as extended by Welge (1959) and calculates individual relative permeability based on two assumptions: that the flow velocity is high enough to achieve stabilised displacement and that the flow velocity is constant at all the cross-sections of the linear porous body. Stabilised displacement implies that flowing pressure gradient across the porous medium is higher than the capillary pressure difference between the fluid phases. The procedure can be summarised in three steps:

First, the gas or water saturation at the outlet face of the rock is obtained by equation (3) which was proposed by Welge (1959).

$$S_{gL} = \overline{S_g} - Q_{gi} f_{bL} \qquad 1$$

$$f_{bL} = \frac{dQ_{bp}}{dQ_{gi}} \qquad 2$$

Where S_{gL} is the saturation at the outlet end of the rock sample, $\overline{S_g}$ is the average gas saturation, Q_{gi} is the pore volume of injected gas, Q_{bp} is the volume of produced brine, f_{bL} is the Buckley-Leverett fractional flow of brine.

Secondly, the relative permeability at the outlet of the rock sample is obtained by differentiation involving the relative injectivity I_r, which is defined as the ratio of v/ΔP at

a particular time relative to the time at the start of the injection, where v is the injected volume and ΔP is the differential pressure across the porous media.

$$K_{rbL} = K_{rb,max} f_{bL} \frac{d\left(\frac{1}{Q_{gi}}\right)}{d\left(\frac{1}{Q_{gi} I_r}\right)} \quad 3$$

This can be simplified by substituting for f_{bL} in equation (3) as

$$k_{rbL} = k_{rb,max} I_r^2 \frac{dQ_{bp}}{d(Q_{gi} I_r)} \quad 4$$

Where,

$$I_r = \frac{(v/\Delta p)}{(v/\Delta p)_i} \quad 5$$

The $K_{rb,max}$ is the relative permeability of the displaced phase at its initial saturation, measured relative to the intrinsic or total permeability of the rock. Its value is one if the porous medium is initially fully saturated with brine.

In the third step, the relative permeability of the gas or oil at the outlet face of the rock sample is calculated. For gas, it is by equation (6) below.

$$k_{rgL} = k_{rbL} \frac{\mu_g}{\mu_o} \left(\frac{1 - f_{bL}}{f_{bL}}\right) \quad 6$$

For estimation of gas relative permeability, the pressure drop should be small compared to the mean operating pressure for experiments. Christiansen et al. (1997) have found that equation (6) is sensitive to gas expansion effects.

2.4.1.2 Jones-Roszelle Method

The Jones and Roszelle analytical method (Jones and Roszelle, 1978) is similar to the JBN method as it also combines the Welge method and the differentiation of flowrate and pressure drop data. However, it is different in its differentiation method as it uses a graphical data processing approach. This is useful for consistent interpretation of the data. Its derivation is also simpler than that of Welge and JBN methods. The details of

the procedure have been described in Christiansen et al. (1997), and a modification of the method to account for an experimental artefact, the capillary end effect has been proposed by Odeh and Dotson (1985) using an empirical approach.

2.5 RELATIVE PERMEABILITY CORRELATIONS

There are two key ways for determining relative permeability curves. One is the actual estimation of the relative permeability values by analysing measured data as discussed in the previous section. The other method is the representation of the unknown relative permeability curves by a function, which has a sufficient degree of freedom to model the measured data while remaining straightforward and simple to communicate. This is known as an implicit method and is of particular importance in history matching where the relative permeability relationship is represented by a function, and a number of simulation runs are conducted by tuning parameter(s) until a suitable match to the data is found.

2.5.1.1 Parametric Methods

A number of parametric correlations have previously been developed to represent the relative permeability function. These include the Corey method (1954), a relatively simple and straightforward equation that is also a power law with only one empirical parameter which is the power itself. This makes it less flexible in most cases to fully capture the entire saturation range from the high oil saturation such as at connate water saturation (S_{wc}) to residual oil saturation (S_{or}). Sigmund & McCaffery (1979) proposed a simple improvement of the Corey correlation by adding a linear term with an additional empirical coefficient to the power term in the Corey correlation (Equations 7 to 9 for a waterflood displacement of oil). Another correlation which is more flexible was proposed by Chierici (1984) and it uses a two exponential relationship instead of power parameters.

$$S_{wn} = \frac{S_w - S_{wi}}{1 - S_{wi} - S_{or}} \quad (7)$$

$$k_{row} = (1 - S_{wn})^{n_o} \quad (8)$$

$$k_{rw} = K_{rw}(S_{wn})^{nw} \quad (9)$$

Where

S_w is the water saturation

S_{wi} is the initial water saturation

S_{or} is the residual oil saturation

k_{row} is the oil relative permeability

k_{rw} is the water relative permeability

no is the oil relative permeability exponent

nw is the water relative permeability exponent

2.5.1.2 Three Parameter L.E.T correlation

A new versatile 3-parameter correlation was proposed by Lomeland et al. (2005). The idea was to improve on the straightforward parametric method proposed earlier and give it more flexibility and proper curvature for the relative permeability over the entire range of the saturation as compared to the previous parametric methods. This correlation uses both wetting and non-wetting phase saturation in the parametric equation. It can correlate endpoint values correctly for the relative permeability of both phases using non-normalised saturations and can also handle S-behaviour associated with gas-oil relative permeability. Equations (10) and (11) are an LET-type relative permeability correlations for a gas and oil displacement system.

$$k_{ro} = K_{ro}\left(\frac{\left(1 - S_{ge}\right)^{Lo}}{\left(1 - S_{ge}\right)^{Lo} + Eo\left(S_{ge}\right)^{To}}\right) \quad 10$$

$$k_{rg} = K_{rg}\left(\frac{\left(S_{ge}\right)^{Lg}}{\left(S_{ge}\right)^{Lg} + Eg\left(1 - S_{ge}\right)^{Tg}}\right) \quad 11$$

Where

$$S_{ge} = \frac{S_g - S_{gcrit}}{1 - S_{gcrit} - S_{org} - S_{wi}} \quad 12$$

S_{ge}	Effective gas saturation
S_g	Gas saturation
S_{gcrit}	Critical gas saturation above which gas starts to flow
S_{org}	Residual oil saturation after gas flood
S_{wi}	Initial water saturation

K_{rog}	Oil relative permeability in gas table
K_{rg}	Gas relative permeability
K_{ro}	Endpoint oil relative permeability (max k_{rog})
K_{rg}	Endpoint gas relative permeability (max k_{rg})
$L_{o,g}$	Exponent for lower part of kro and k_{rg}
$E_{o,g}$	Coefficient for the elevation of k_{ro} and k_{rg}
$T_{o,g}$	Exponent for top part of k_{ro} and k_{rg}
k_{row}	Oil relative permeability (in water table)
K_{row}	End-point oil relative permeability (max k_{row})

Similar to the Corey exponents, the L.E.T. parameters in equation (10) and (11) do not have any physical meaning. The L is used to describe the upper part of the relative permeability curve and is comparative to the Corey parameter for the particular phase. The parameter E modifies the elevation of the slope in the curve while the parameter T modifies the lower part of the curve in the same fashion L modifies the upper. This method can hence represent flexible S-behaviour associated with some relative permeability curves. Experience has shown that $L \geq 1$, $E > 0$ and $T \geq 0$. This correlation is therefore especially important in implicit history matching for estimation of relative permeability of gas injection displacement processes.

2.5.1.3 Non-Parametric Methods

Non-parametric methods include the B-spline functions, the Neural Network (NN) and the Genetic Algorithms (GA). These are more flexible approaches as no assumptions are made regarding the functional form or the shape of the relative permeability curve. Several forms of this method have been reported in the literature (Kulkarni and Datta-Gupta, 2000). The B-spline function, for example, has an advantage over the power or exponential functions in that any continuous function can be approximated arbitrarily well by polynomial splines, provided that a sufficient number of knots are allowed. However, it also has the significant disadvantage of increased parameter space which can cause the problem to be more ill-conditioned (Kulkarni and Datta-Gupta, 2000). It can also create one or several breaks in the computed relative permeability curves (Lomeland et al., 2005). Other estimation methods include Bayesian methods which use the probabilistic approach in estimating the function (Yang and Watson, 1991).

2.6 HISTORY-MATCHING TECHNIQUE FOR ESTIMATION OF RELATIVE PERMEABILITY

In general, relative permeability curves are estimated explicitly and mainly through the analysis of data obtained from laboratory dynamic displacement coreflood experiment (). The measured data obtained is then analysed analytically using techniques such as the JBN method, which are based on Buckley-Leverett type of flow. However, due to the huge scaling difference between laboratory and the reservoir scale, as well as the difference in operating conditions, it is often not suitable to use the curves generated through this technique at a larger reservoir scale. Also, because of the inherent assumption of Buckley-Leverett diffusive front (Johnson et al., 1959), the approach neglects to take into account the effect of instability in the estimated relative permeability curves.

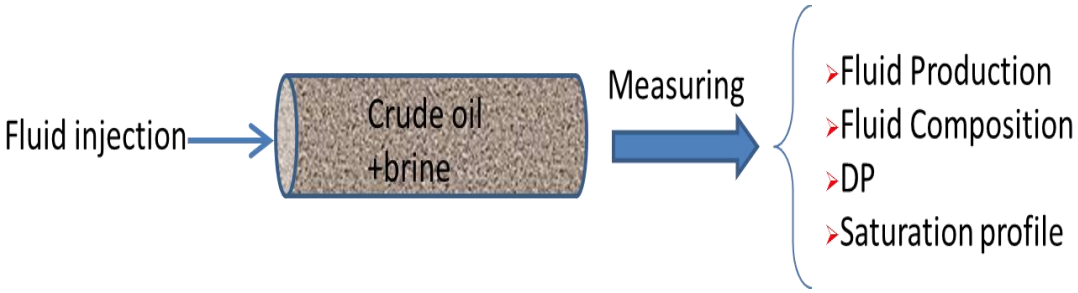

Figure 2-1: Generalised procedure for obtaining unsteady state (dynamic) experimental data for used in estimation of relative permeability.

An inverse process where production data measured from displacement experiments with core or field operations at a set time interval, termed 'history-data' is matched with simulated data and the parameter value is updated; this is known as history-matching. In this process, the parameter values are verified or updated by measuring the misfit between the history data and simulated data. The limited history data available are compared with the simulated data and if there exists an error above the set tolerance, a parameter in the simulation model is adjusted and new simulation data generated; the process is repeated until the tolerance between the history data and simulated data is reached (O'sullivan, 2004).

Relative permeability can be estimated by a history-matching procedure where the curves are represented by a mathematical function through which a parameter can be updated. The mathematical function can be parametric such as the power law as in the case of

Corey (1954), Sigmund and McCaffery (1979) and the more flexible three-parameter correlation by Lomeland et al. (2005) or exponential correlation as in Chierici (1984). It can also be non-parametric such as the B-Spline function (Kulkarni and Datta-Gupta (2000), Li et al. (2009)). They are more flexible since they have more degrees of freedom but can lead to other errors such as non-monotonicity of curves (Li et al., 2009) as described previously.

The implicit estimation of relative permeability by history matching is a non-linear inverse and ill-conditioned problem (Oliver et al., 2008). Some modern non-linear optimisation techniques for solving this type of problem include the Ensemble Kalman Filter (EnKF) optimizer (Li et al., 2009) and the Designed Exploration and Controlled Evolution (DECE) optimizer (Yang et al., 2009), a proprietary optimisation technique developed by Computer modelling group (CMG) and is an integral part of their CMOST optimisation software. It uses an iterative optimisation process that first applies a designed exploration stage to search space in a designed random manner such that maximum information about the solution space can be obtained; this is followed by a controlled evolution stage, which performs statistical analysis of the simulation result obtained in the preceding stage.

Simultaneous Estimation of Relative Permeability and Capillary Pressure

Relative permeability and capillary pressure are two important flow functions required in reservoir simulations. Conventionally, they are obtained separately through explicit analysis of laboratory experimental production data. They can also be obtained implicitly by history matching where the curves are represented by a function as discussed previously. However, several studies have shown that when they are estimated separately, the relative permeability obtained does not correspond to the capillary pressure for flow simulation (Jennings et al., 1988). In the history-matching technique, the relative permeability curve and the capillary pressure can both be estimated simultaneously by assigning the relevant function to each curve. Conventionally, the two functions representing the two curves in history matching are independent. Jahanbakhsh and Sohrabi (2015) proposed a coupled function where the relative permeability was described as a function of the capillary pressure and this significantly improved the relationship between these two important flow parameters.

2.7 GRID SIZE AND NUMERICAL DISPERSION

The predictions of miscible floods are commonly carried out using finite difference numerical simulators in which the coefficients of the convective terms are typically evaluated at the upstream grid blocks. This is termed as single-point upstream weighting or differencing, and is well known that this type of weighing causes truncation error which results from sensitivity to grid size (Stalkup et al., 1990).

In compositional simulation such as heavy oil solvent displacement, aside from the well-known problem of 'numerical dispersion' which causes serious difficulties in simulating the movement of sharp saturation front, there is also the issue of dispersion of composition fronts and saturation fronts (Camy and Emanuel, 1977). Cell or grid size is among the many parameters that control dispersion and mixing error and the smaller the grid size, the smaller the dispersion and mixing error. The most important reasons for model variation in the compositional simulator with respect to grid size are: -

1. Numerical dispersion
2. Non-linear dependence of saturation and total mobility
3. Non-linearity of the flash equation.

The effect of numerical dispersion in compositional finite difference simulator (which is the method available in most commercial simulators) has been extensively discussed in the literature (Jessen et al., 2004). The problem becomes further complicated in a WAG operation where water and gas are injected alternatively. In this case, the smaller the slug size, the smaller grid size that would be required to resolve the slugs effectively. If small slugs and coarse grid size are used, slugs that contain water only, and gas only would be combined as though water and gas were injected together thereby misrepresenting the process. The second source of dispersion is a result of non-linearity of the system total mobility. It occurs when the fluid displacement is represented by a sharp front, which is the case with one-dimensional or coarser grid models. The mobility which is a function of relative permeability is calculated with the values near the high ends of the k_r curves. If a single mobility is however calculated from averaged saturations as in the case of coarse-grid models, the k_r may be picked far away from the high ends of k_r values resulting in lower effective permeability to flow for the coarse grid model. The front would then behave like a dispersed fluids region. The third source of dispersion is associated with the type and solution of the EOS and flash equation. If the solution for the k-values (ratio of the mole in the vapour phase to the moles in the liquid phase) of a

component through EOS for multiple grids at a particular time of the displacement, they would be entirely different from the k-value obtained by combining the grid into a single coarse-grid. This is mainly because of the non-linearity of the flash equation (equation 13).

$$\sum_{i=1}^{NC} \frac{Z_i(1-K_i)}{L+K_i(1-L)} = 0 \qquad 13$$

where: NC is the number of hydrocarbon components
Z_i is the overall mole fraction of component i (total moles in vapour and liquid phases)
K is the k-value of component i and L is the mole fraction of component i in the liquid phase.

In the displacement of heavy oil by solvent or water flooding, viscous fingering or gravitational override may occur due to viscous fingering or gravitational force being the dominant force, respectively. Viscous fingering which results from large viscosity difference between the injected fluid and resident fluid will be discussed in detail in chapter 5. Simulation of these instabilities cannot be achieved with one-dimensional grid using a 'finite-difference' simulator, as this will smear the instability in the front. A high-resolution model would, therefore, be required in order to capture the fingers effectively.

Detailed simulation using fine grid high resolution models have previously been carried out to study viscous fingering. These include the work of Christie and Bond (1987) who simulated an unstable miscible flow on an extremely fine (130x130) two-dimensional (2D) finite-difference grid model based on an experiment conducted by Blackwell (1959). They obtained good agreement with the experiments for the simulations with mobility ratios between 5 and 86. Christie (1989) extended the work to coupled miscible and immiscible flow in which both water and solvent flow simultaneously and thus mimicked the stabilising effect of a WAG scheme. In all the cases, the optimum fine grid size for the model was obtained based on the fact that beyond a certain grid size, results from the model simulation are not affected by the increase in grid size. This sensitivity on grid size is typically carried out on changes in oil recovery and pressure drop.

2.8 COREFLOOD EXPERIMENTS

Experimental results are fundamental part of any numerical studies as they provide reliable data for comparison with the numerical predictions thereby reducing the uncertainty in the model and enhancing its reliability for predictions. In this numerical study, six physical coreflood experiments conducted by other PhD students (Farzaneh, 2014, Emadi, 2012) were considered. The core used in the experiments was a high permeability Fife silica-sand (carboniferous) sandstone that was taken from Burrowine Moor quarry in central Scotland. The sandstone was chosen because of its relatively high permeability, typical of a heavy oil reservoir, which is shallow, unconsolidated and high permeability sand. The core sample is also of high quality with feldspar and clay content of less than 2 percent. Table 2-1 summarises the properties of the core sample used in the studies. The crude oil sample used in the experiments termed here as "Crude-J", was a (medium) heavy crude oil with a viscosity of 617cp at standard condition, an API gravity of 16 and an asphaltene content of 2.6%. Table 2-2 shows the experiments that were utilised, as well as the experimental conditions, injected and resident fluids, and the core orientation. A brief discussion on the experiments are subsequently presented.

Experiment-1: In this experiment, CO_2 was injected into dead heavy oil (crude J) in a horizontal core at a temperature of 28^0C, the outlet of the core during the injection was kept constant at approximately 1500psig. The CO_2 at this experimental condition was in the liquid state with a kinematic viscosity of 0.089cp and density of 0.779g/cm^3, while the dead oil has a viscosity of about 617cp and density of 16API at the same experimental condition. Injection rate was kept constant at 7cc/hr, which is equivalent to 1ft/day, a typical injection rate in a heavy oil field. This rate was enough to mitigate some experimental artefacts such as capillary end effect. The experiment recorded an early breakthrough of the gas as expected, resulting from the adverse mobility ratio, which leads to the occurrence of viscous fingering. An appreciable amount of the oil was produced after the breakthrough, which is typical of severely unstable floods. There was also evidence of significant mass transfer occurring within the core during the displacement as a result of the CO_2 dissolving in the oil and reducing its viscosity. The GC compositional analysis of the produced oil has proved this fact and as well indicated the possibility of the CO_2 upgrading the oil by knocking down the heavier components and some heavy metals in the oil. The injected gas was later chased by water in order to

investigate the effect of three-phase water relative permeability, this was termed "Tertiary Water Injection" in the subsequent numerical simulation.

Experiment-2: In this experiment, N_2 was injected into heavy oil (crude J) in a vertical core at a temperature of 38^0C while the outlet of the core during the injection period was also kept relatively constant at 1500psig. The injection was from the top of the core with a rate of 7cc/hr. The oil was pre-saturated with N_2 at 1500psig before injection into the core. This was done to mitigate any compositional exchange between the N_2 and the oil. The N_2 was in gaseous state with a viscosity of 0.187cp and density of 0.111g/cm^3 at the experimental condition. In contrast to Experiment-1, here, the viscosity of the oil when it was fully saturated with the N_2 was not measured but estimated using an equation of state to be approximately 250cp, a significant reduction from its dead oil value of 617cp. Even though the viscosity ratio was still high (250:0.187), the displacement benefited from gravity stability since the gas was lighter and the injection was from the top, making the displacement more stable. Hence, the breakthrough was delayed compared to Experiment-1. The compositional analysis of the produced oil from this experiment indicated no significant compositional exchange.

Experiment-3: Here, the heavy oil (Crude J) was initially saturated with methane to depict the true subsurface oil composition. CO_2 was then injected into the saturated oil in a horizontal core. Same experimental condition and injection rate was adopted as in the previous experiments, however, in contrast to the dead oil used in Experiment-1, in this case, the methane gas in solution was expected to compete with the CO_2 and therefore interfere in the exchange of mass between the CO_2 and the oil. As CO_2 had to expel the methane from the oil solution before it could dissolve, this lead to its reduced solubility. On the other hand, the ejected methane may evolve and form a homogenous solution with the CO_2 phase or may form a separate phase as dictated by the thermodynamics of the displacement process. For the purpose of numerical simulation, the viscosity of the fully saturated oil was estimated using an equation of state as 100cp. As expected, the adverse mobility ratio led to the early breakthrough of the gas while the differential pressure across the core showed an initial spike up to a maximum of 2psi before the breakthrough occurred, and was followed by a very gradual decline up to the end of the injection period. The compositional analysis indicated a significant variation of the composition, underlying the effect of mass transfer across the phases.

Experiment-4: This is similar to Experiment-1 except that the orientation of the core was in vertical. CO_2 was injected into the core to displace dead crude J under the same experimental conditions of temperature and pressure. The purpose here is to compare the recovery from vertical and horizontal injection strategies and understand any difference in recovery mechanism as a result of the gravity effect. An early breakthrough was also observed here resulting from viscous fingering but more oil was recovered after the breakthrough compared to the horizontal injection. This could be attributed to gravity drainage mechanism similar to that seen in vapour extraction (VAPEX) of heavy oil by solvent (James et al., 2008, Torabi et al., 2012b).

Experiment-5: In this experiment, oil recovery by secondary waterflood of dead heavy oil (crude J) in a horizontal core was investigated. The experimental conditions, as well as the injection rate, were similar to that of the previous experiments. Since water is heavier than oil and the injected water has the same composition with the connate water established in the core, the flood was relatively stable and more piston-like compared to the secondary gas injections and the recovery after breakthrough was not as continuous as in the case of gas injection. This experiment in addition to Experiment-1 was employed to highlight the effect of injection mode (secondary and tertiary injection modes) on the shape of the relative permeability.

Experimet-6: In this experiment, CO_2 and water were simultaneously injected at the same rate to displace the resident heavy oil (Crude-J). Experimental conditions and injection rate were similarly maintained as in previous experiments. Since the CO_2 is more mobile compared to the water, its breakthrough was observed earlier than the water. However, the injection of water led to an increase in the recovery because it followed the path which has been opened up by the CO_2, as indicated by the micromodel experiment. This is as a result of the CO_2 lowering the viscosity of the oil as it dissolved in it.

Table 2-1 Basic properties of the core samples used in these studies

Parameter	Size	Unit
Weight	1299.9	g
Diameter	5.12	cm
Length	32	cm
Core Pore Volume (PV)	163.02	cm^3
Porosity (φ)	24.74	%
Permeability to Brine (K)	2.5	Darcy

Table 2-2: Coreflood experiment investigated in this study

Exp.	Description	Fluids	Core Orientation	Test Conditions
1	Secondary CO_2 injection into Dead Crude-J Tertiary chase water injection	Injection fluid: CO_2 Resident oil: dead Crude-J Resident brine: 20000 ppm Injected brine: 20000 ppm	Horizontal	T=28°C, P=1500 psig
2	Secondary N_2 injection into pre-equilibrated Crude-J	Injection fluid: N_2 Resident oil: Saturated Crude-J with N_2 Resident brine: 20000 ppm	Vertical	T=38°C, P=1500 psig
3	Secondary CO_2 injection into Live Crude-J	Injection fluid: CO_2 Resident oil: live Crude-J (saturated with methane) Resident brine: 20000 ppm	Horizontal	T=28°C, P=1500 psig
4	Secondary CO_2 injection into Dead Crude-J	Injection fluid: CO_2 Resident oil: dead Crude-J Resident brine: 20000 ppm	Vertical	T=28°C, P=1500 psig
5	Secondary Water injection into Dead Crude-J	Injection fluid: brine Resident oil: dead Crude-J Resident brine: 20000 ppm	Horizontal	T=28°C, P=1500 psig
6	Simultaneous Water and CO_2 injection into dead Crude-J	Injection fluid: brine, CO_2 Resident oil: dead Crude-J Resident brine: 20000 ppm	Horizontal	T=28°C, P=1500 psig

2.9 CORE MODELLING

The details of the core properties used in the experiments have been described in section (2.8) and for convenience the core was modelled using a two-dimensional (2D) rectangular block. This approach did not affect the total core volume since the area of the rectangle was equated to that of the cylindrical core through equation (14). The two

directions considered were the x-axis, along the core length and the k-axis representing the core diameter in the horizontal core. The porosity was assumed homogenous based on the core analysis, and the permeability was stochastically populated using a normal Gaussian distribution with a small variability (standard deviation of 50) for the purpose of triggering the fingers. This was the method adopted by Christie and Bond (1987) and Christie (1989, 1993). Another method of triggering the fingers that was tested used a finite-amplitude perturbation of the front at t equals to 0, but with a homogeneous permeability field. The two approaches were similar for small values of the variance, and hence the former method was adopted. Figure 2-2 shows the core transformed to Cartesian core model by equating their cross-sectional areas while keeping the core length the same in the model. Figure 2-3 shows the core model generated using CMG-builder where the permeability field was randomly populated.

$$A = \pi r^2 = L^2 \qquad 14$$

Where r is the radius of the core and L the width or thickness (y and k axes in a horizontal core) of the cross-section of the Cartesian core model. Table 2-1 presents the core properties while Table 2-3 summarises the core model properties, the parameter values and the approach used.

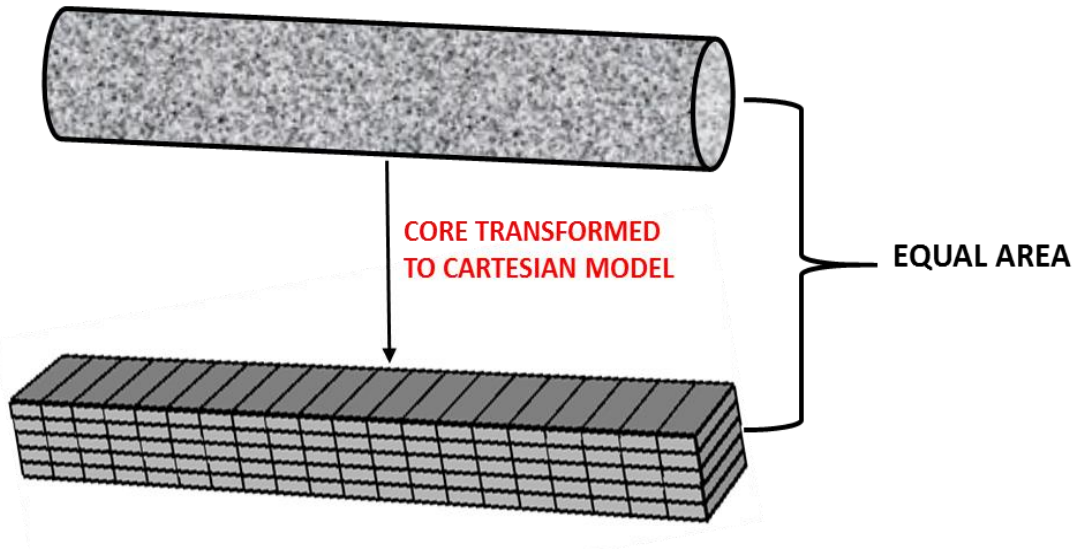

Figure 2-2: A 2D Cartesian model transformed from core measurement

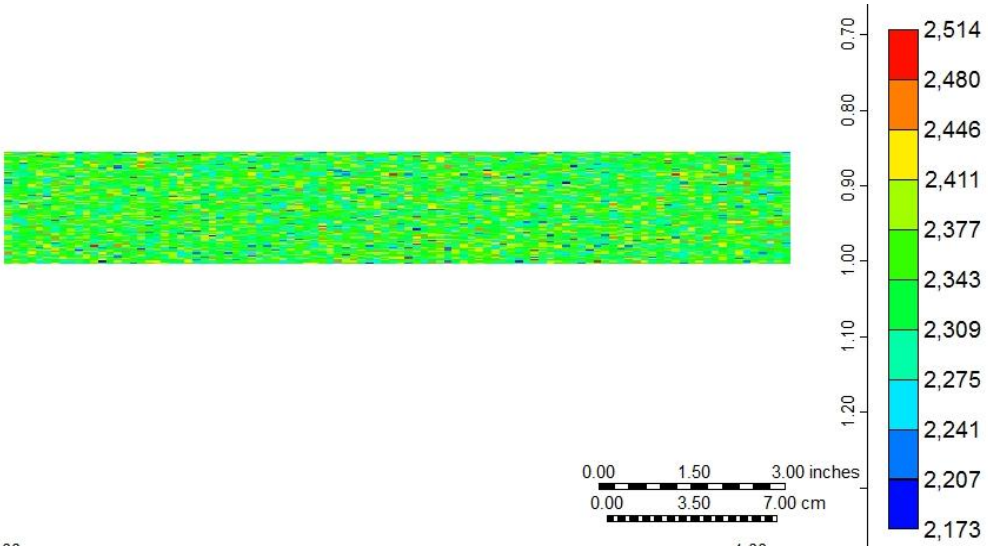

Figure 2-3 Random Permeability Distribution (mD) in the core to trigger the instability.

Table 2-3 Summary of the core modelling approach and the parameter values

Core Model Property	Method	Value
Porosity	Homogenous	0.24
Permeability	Normal Distribution Variance	2500mD 200mD
Finger Triggering	Permeability Heterogeneity	

Core Model Optimum Grid Size

To determine the appropriate grid size for the study, the most unstable injection process, which is 'CO_2 injection into horizontal core saturated with dead crude oil (Experiment 1) was considered. The grid-size obtained was then used as the basis for the simulations of all the other experiments considered in this study. The criteria for selecting the appropriate or optimum grid size has been discussed in the previous section. The change in oil recovery and differential pressure (DP) across the core was considered as the criteria for choosing the optimum grid. The grid size variation was also considered in both the longitudinal flow direction (horizontal direction along the core) and normal to the flow direction (along the vertical cross-section of the core). The variations considered are as follows:

1. Normal to the flow direction: 20, 40 80, and 160 grids
2. Along the flow direction: 100 and 200 grids.

Figure 2-4 shows the effect of the grid refinement in two directions. As discussed above, if the system is prone to frontal instabilities, the number of grids especially normal to flow

direction plays a crucial role. As can be seen in (A), refining the gridding from 20 to 80 affected the simulation results significantly, however dividing the medium into 80 or more grid cells affected the oil recovery minimally and hence 80 grids sufficiently captured the instabilities. For other direction of gridding, i.e. along the injection direction, (B) depicts the simulation results of two cases; 80×100 and 80×200. No difference can be seen in the simulation results, which makes 100 grids adequate for the simulation of the coreflood experiments. Consequently, for the subsequent simulations, 80×100 gridding configuration was chosen as the optimum grid size.

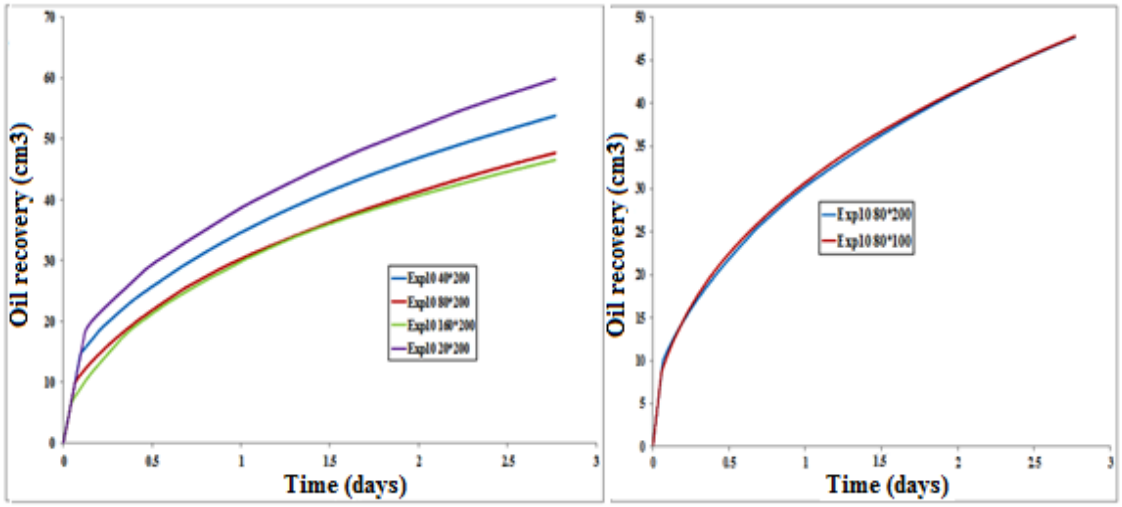

Figure 2-4 Effect of grid numbers on the oil recovery profile; the left image shows the sensitivity analysis in the direction normal to core orientation, which indicates high sensitive to this direction. The right image highlights less sensitivity in a direction along the core orientation.

2.10 SUMMARY AND CONCLUSION

The chapter begins by defining the concept of relative permeability and explains the experimental and analytical approaches for the estimation of this important flow function. The procedure for estimation of relative permeability by history matching was discussed and the inadequacy of the conventional method of history matching using one-dimensional model was highlighted. Numerical dispersion error resulting from the choice of grid size and other sources were then discussed. The injection strategy, the fluid types and the displacement mechanisms of the experiments considered in this work were then presented and finally the core modelling approach was discussed and the optimum grid size of the 2D model of the most unstable displacement experiment was then determined for use in all subsequent simulations.

CHAPTER 3

HEAVY OIL CHARACTERIZATION AND PVT MODELLING

3.1 INTRODUCTION

Solvent methods for enhancing heavy oil recovery such as CO_2 have been studied at laboratory scale (Emadi et al., 2013, Emadi et al., 2011b, Sohrabi and Emadi, 2012, Seyyedsar et al., 2015), and at the field scale (Desch et al., 1984, Kantar et al., 1985, Saner and Patton, 1986, Mohanty et al., 1995). Among gas injection displacement processes, CO_2 is one of the most widely used injection gases. This is because, besides issues related to global warming, it also has high solubility in crude oil making it attractive for enhancing oil recovery. When dissolved in oil, CO_2 increases the density of the oil (Simon et al., 1978) which may have a profound effect on the flow path (Nasrabadi et al., 2009) as well as instigating convective mixing (Foroozesh and Moghaddam, 2015). Another property of CO_2, which is even more significant in heavy oil recovery, is its ability to lower oil viscosity when it is in solution. Conversely, it has been reported that CO_2 can cause up to two magnitudes of viscosity reduction when fully saturated in heavy oil (Emadi et al., 2013). It can also lead to increase in the viscosity of the gas when there is substantial vaporisation of lighter liquid components from the oil into the gas phase (Emadi et al., 2011b).

This chapter discussed the procedure for modelling fluid phase behaviour using equation of state and how current conventional approaches are deficient in modelling the behaviour of heavy oil system. A new improved methodology was therefore proposed for effective modelling of heavy oil system using equation of state. It also described the gridding mechanism and the choice of the optimum grid size for use as a base case in subsequent simulations.

3.2 COMPOSITIONAL DISPLACEMENT

In gas injection, such as lean gas, CO_2 or N_2 gas, there is significant mass transfer between the bulk gas phase and the displaced crude oil. The gas component can diffuse into the oil phase and or extract lighter components from the oil phase into the gaseous phase, thereby changing the compositional and physical properties of the phases. These types of displacements are termed compositional displacements as opposed to black oil displacements where the oil or gas phase is considered as a single component. This exchange of mass occurs at the interphase between the two fluids. The region in which this mass transfer or exchange take place can be small or large, depending on the rate of mass transfer between the phases. The rate of this mass transfer is controlled by the thermodynamic and convective forces. Figure 3-1 shows a clear example of a compositional displacement (Nasrabadi et al., 2009) indicating a transition zone where exchange of components between the displacing fluid and the displaced fluid takes place.

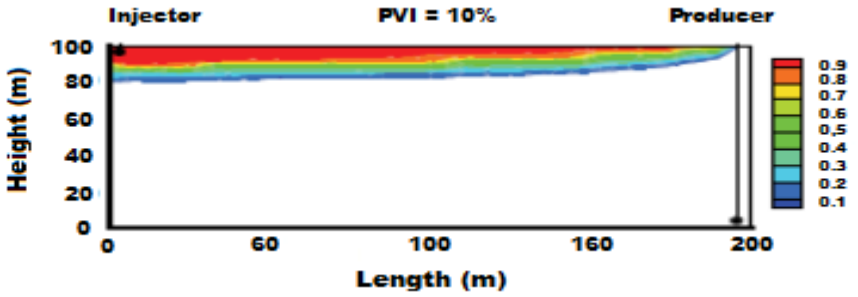

Figure 3-1: CO_2 saturation profile after 0.1PV injection into a core saturated with oil indicating a mixing region(red and blue area) where mass transfer takes place (Nasrabadi et al., 2009)

Therefore, to take into account all physical changes that may occur in the simulation of the displacement processes studied, an equation of state is required to handle the thermodynamic aspect such as density and viscosity changes resulting from, composition, volume, or pressure variations. The molecular (Fickian) diffusion and dispersion also need to be addressed. Moreover, as stated earlier, because of the mass transfer leading to significant compositional changes, a compositional simulator that is capable of handling the dynamics of the variations, with the right physics and without it being masked by numerical diffusion was required.

3.3 HEAVY OIL CHARACTERIZATION USING AN EQUATION OF STATE

Characterization of heavy oil using equation of state (EOS) is more complex than conventional oil because much more uncertainties are associated with its composition and PVT data (Sancet, 2007). This is because compositions of heavy oils are highly uncertain in terms of the fraction of each Single Carbon Number (SCN) and the Paraffins-Naphthalene-Aromatics (PNA) within each SCN (Kumar and Okuno, 2012a). Secondly, critical parameter values, required in EOS calculations, are not known for SCN above C_{24} and are only estimated (Ambrose and Tsonopoulos, 1995). Thirdly, it is difficult to obtain a reliable downhole sample. and even in the rare situation where it can be obtained, it is not practicable to determine all the components, because it would contain a high concentration of various isomers of heavy hydrocarbon components that are not identifiable. Even when more exhaustive tests are conducted, it is still futile because, only a few number of pseudo-components are needed for a practical simulation and would, therefore, end up lumping the detailed components. This uncertainty in its composition also creeps into the experimental PVT data, which are typically carried out under the condition of high viscosity. For these reasons, quite often, only simple measurements such as saturation pressure (P_{sat}), densities and viscosities that are reliable and available (Kumar and Okuno, 2012b). Hence, Constant Composition Expansion (CCE) and Differential Liberation Expansion experiments are more difficult to carry out or highly unreliable because of the afore-mentioned problems.

3.3.1 Equation of State (EOS)

An equation of state is required to characterise the phase behaviour of the reservoir fluids in compositional displacements of hydrocarbons. These are mainly Cubic Equations of State (EOS) that are based on Van der Waals equation of state. The most widely used cubic EOSs include the Soave-Redlich-Kwong (Soave, 1972) and the Peng and Robinson (1976, 1978). These popular EOSs have been implemented in commercial software (Pedersen and Christensen, 2007) and the procedure for modelling a fluid behaviour using EOS can be summarised in four main steps as follows (Kumar and Okuno, 2012b):

Step 1 *Plus Fraction Splitting (e.g. C6+) into more detailed components to obtain an estimate of the molar distribution of the components with respect to single carbon number (SCN) or Molecular Weight* (MW).

It has been stated in various works of literature that using Plus Fraction as a single carbon group in the PVT calculations often gives inaccurate results (Elsharkawy, 2001). In this stage, therefore, the plus fraction obtained from the compositional analysis such as gas chromatography (GC) is split into a number of components to fit a distribution function spanning all the components in the fluid phase. A number of distribution functions have been proposed for both conventional and heavy oils; these include the chi-square (Quiñones-Cisneros et al., 2003), the gamma distribution which is a three-parameter distribution function (Whitson, 1983, Whitson, 1984) and the logarithmic distribution (Pedersen et al., 1984b). The latter is the most widely used for conventional oils because quite often, their composition consists of a broad spectrum of well-defined components that range from light components to heavy components and a small amount of plus-fraction component. In heavy oils, however, the well-defined components make only a small fraction of the composition while the undefined plus-fraction makes the bulk of the composition, this is the reason more flexible distributions like the gamma-distribution are often utilised for heavy oil plus-fraction splitting (Kumar and Okuno, 2012b). Rodriguez and Hamouda (2008) have also proposed a method that is based on gamma-distribution for splitting heavy plus-fraction components into single carbon numbers (SCN). The method integrates the experimental mole fractions using a fitting parameter called alpha (α) to characterise the limiting components.

Step 2 *Estimation of properties for the split fraction components*

In this step, the properties of the plus fraction that was split in step 1 are estimated. For components with SCN 45, the critical properties are available in the literature (Wakeham et al., 2002). For hydrocarbons with SCN greater than 45, the properties are estimated using correlations. A number of correlations have been proposed, and the widely used which have so far been deployed into commercial software packages include the Lee and Kesler (1975), Whitson (1983), Goossens (1996) the Twu (1985) and the Riazi and Al-Sahhaf (1996) correlations. The first three are recommended for conventional oils while the Twu (1985) correlation method generally yields consistent results for heavy oils (Whitson and Brulé, 2000). The Riazi (1996) correlation, a modification of the Whitson (1983) correlation, is relatively straightforward and easy to implement but often gives a far inaccurate estimate of the critical properties, a modification of the Riazi method was proposed by Sancet (2007).

Moreover, it must be emphasised here that the accuracy of the correlation methods depends on the reliability of the compositional information available, which is often not the case for heavy oils. This can be attributed to the difficulty in fluid sampling, the technique for component elucidation and the experimental procedure due to the nature of the oil viscosity and density that result in inaccurate data measurement and hence a high degree of uncertainty in the composition. Therefore, using EOS with these correlations to estimate properties such as phase density would require the use of volume shift parameter in order to tune the EOS. However, when the volume-shift parameter is used compositional behaviour predictions of the resulting fluid would depend heavily on the parameter and this is thermodynamically inaccurate since it would lead to compositional and volumetric phase behaviours being modelled separately (Kumar and Okuno, 2012b). To mitigate the effect, Kumar and Okuno (2012a) proposed a correlation using a perturbation factor for critical parameters and predicted liquid densities and vapour pressures for n-alkanes from C_7 to C_{100} without utilising the volume-shift parameter.

Step 3 *Pseudo-ization (Lumping) of components*

Compositional simulators using an EOS to describe the phase behaviour of multicomponent fluid mixtures are expensive to use because of a large number of iterative phase calculations (Hong, 1982). It is therefore of fundamental and practical importance to reduce the dimensionality of the composition space. In this step, the number of SCN components is reduced by grouping (or lumping) them into fewer pseudo-components whose properties are calculated by averaging the properties of group member components. Widely accepted lumping or pseudo-ization procedure in the literature and which have been deployed into commercial software packages include the Whitson (1984) and the Pedersen et al. (1983). The former is based on 'equal mole' grouping with mole weighted averaging while the latter is based on 'equal mass' grouping and the averaging of properties is mass-weighted. Because of the uncertainty in experimental data for heavy oil solvent systems, it is common practice to have more pseudo-components compared to lumping of conventional oils as that would ensure reliable representation of phase behaviour at a wide range of composition conditions (Díaz et al., 2011). The method of averaging can, however, introduce bias leading to incorrect result, this is especially the case with heavy oil because at higher SCN, even though the constituent Paraffin, Naphthalene, Aromatics (PNA) have the same carbon number, they may exhibit a markedly different behaviour (Rodriguez and Hamouda, 2008). Again, the accuracy of

the properties of the lumped components, especially for heavy oils, depends on the accuracy of the estimated properties of the split components in Step 2 above.

Step 4 *Regression procedure to match properties of (Lumped) Pseudo-components to available experimental data.*

This step is required because each step 1 to 3 above makes some assumptions, which result in bias in the prediction of the actual phase behaviour. Regression is used here to tune the equation of state to match the available experimental data. Component properties (such as critical Properties P_c and T_c and ω), binary interaction coefficients and occasionally volume shift are used as the regression parameters. Several regression procedures for oil characterization have been proposed in the literature (Pedersen and Christensen, 2007). These include Agarwal et al. (1991) and Li and Nghiem (1982). These methods order the parameters from the list specified by the user in such a way that the most sensitive parameters are used first. For computational efficiency, this procedure initially starts with a small number of parameters at a time. Once a parameter reaches its maximum or minimum values or does not contribute to the tuning, it is replaced by another parameter that has not been tested, and the procedure is repeated until the error is minimised. It is pertinent to note here that the regression procedure is not an attempt to correct deficiencies of the equation of state (EOS).

The accuracy of the prediction using EOS depends entirely on the amount, type and reliability of the data employed in the regression procedure. It is also equally important to choose meaningful regression parameters as well as reasonable physical limits for the parameters to ensure that a representative model is generated. This is the main reason why different EOS fluid models result from the same data, and extra care needs to be attached to this (Lolley and Richardson, 1997). Moreover, as described above, this procedure is even more challenging and with more tendency to fail because of the inherent uncertainties associated with the compositional data, estimated component properties and phase behaviour. Figure 3-2 obtained from Winprop (2015) shows a typical flowchart of a computer program for tuning an EOS to match a PVT data.

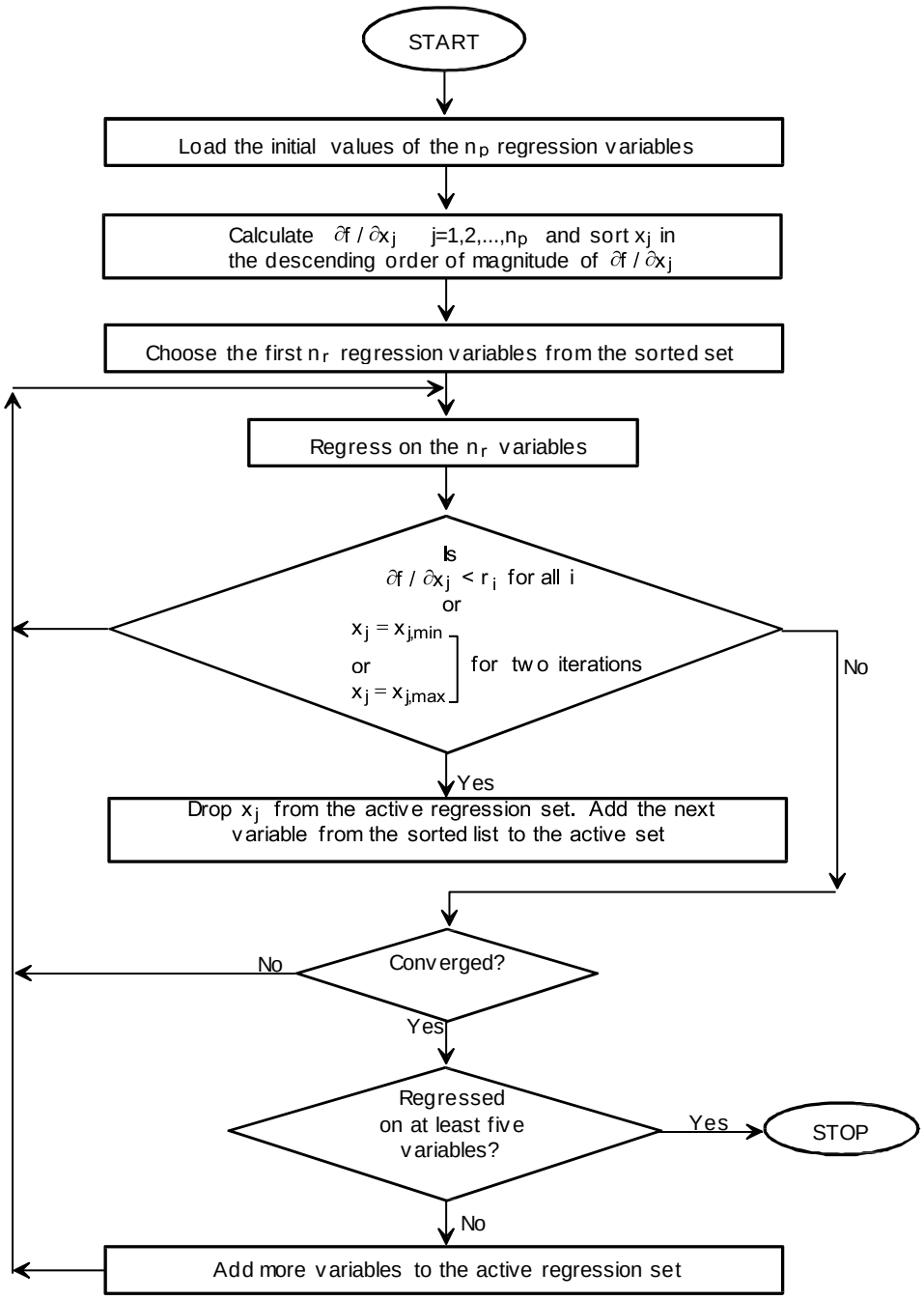

Figure 3-2 Flow chart for regressing EOS equation based on five parameters at a time.

3.3.2 Viscosity Modelling

The viscosity of the oil at different composition is also modelled using a correlation. Several models have been proposed in the literature. These include the Pedersen corresponding state model (Pedersen and Fredenslund, 1987, Pedersen et al., 1984a) which is based on the corresponding state of methane, the Lohrenz-Bray-Clark (LBC) model (Lohrenz et al., 1964), which is a function of composition of the components and the Jossi-Stiel-Thodos model (Jossi et al., 1962), which also relies on properties of the composition. However, in viscosity modelling of heavy oils, due to the high uncertainty

in the oil composition and the estimated properties, the modified Pedersen correlation method is the most preferred. This is because it does not depend on having accurate density predictions and is based on a unified approach to both oil and gas phases and therefore gives a better correlation for the viscosity of heavy oil than the other two (Lindeloff et al., 2004).

3.4 PHASE BEHAVIOUR MODELLING OF CRUDE J

3.4.1 Oil Properties

Crude J (dead oil) is the base fluid used in the studies and was provided by the sponsors of the project. It is a medium heavy oil with a viscosity of about 600cp at ambient temperature. Rheological analysis of the oil revealed that it was a non-Newtonian fluid, meaning viscosity is independent of the applied shear rates. To simulate the enhanced displacement of the oil by gas (CO_2, N_2) injection, the PVT phase behaviour of the fluids was modelled using an EOS, the Peng-Robinson equation (Peng and Robinson, 1978), which is designed for characterising heptane and heavier fractions (equations 15 to 18) and was deemed the most suitable for this type of fluid (Shokri and Babadagli, 2012).

$$p = \frac{RT}{v-b} - \frac{a_c \propto (T)}{v^2 + 2bv - b^2} \quad (15)$$

Where $a_c = 0.457235529 \frac{(RT_c)^2}{P_c}$ (16)

$$m = 0.37464 + 1.54226\omega - 0.26992\omega^2 \ \ for\ \omega < 0.49 \quad (17)$$

$$m = 0.379642 + 1.4850\omega - 0.164423\omega^2 + 0.016666\omega^3 \ for\ \omega > 0.49 \quad (18)$$

Table 3-1 shows the compositional analysis of crude-J obtained using gas chromatography (GC) indicating a small weight percent of light components up to C_7 and a high weight percent of heavy components with the C_{26}+ accounting for up to 62.14 percent. Table 3-2 shows a more detailed analysis using high-temperature column GC analyser which is more useful and more reliable since it gives representative components within a range of carbon number (CN). For 'Crude J' the range of carbon number was from C_6 to C_{42} as shown in the table and reduces the uncertainty in the characterization associated with the plus-fraction, a huge source of uncertainty in phase behaviour

modelling using EOS. A swelling test experiment was carried out on 'crude J' and its mixture with CO_2 to generate information for input as experimental data in the tuning of EOS to fully characterise the phase behaviour of the fluids. The experiment was carried out at the experimental condition of temperature (28^0C) and pressure (1500psig). The data obtained include the solubility of CO_2 at different pressure, the viscosity and the swelling factor of the oil at various CO_2 solubility. The result is summarised in Table 3-3. The density of the dead oil, the density of the fully saturated oil with CO_2 and the asphaltene content of the oil are presented in Table 3-4 below.

Table 3-1 GC Compositional analysis for Crude J obtained from GC analysis of the oil

Oil "J" Composition (Whitson's Generalised MWs)			
Comp	MWs	Weight%	Mole%
C1	16.04	0.00	0.00
C2	30.07	0.00	0.00
C3	44.10	0.00	0.00
iC4	58.12	0.00	0.00
nC4	58.12	0.00	0.02
iC5	72.15	0.02	0.10
nC5	72.15	0.01	0.06
C6s	84	0.07	0.32
C7s	96	0.14	0.56
C8s	107	0.37	1.29
C9s	121	0.72	2.23
C10s	134	1.12	3.13
C11s	147	1.39	3.54
C12s	161	1.87	4.37
C13s	175	2.23	4.78
C14s	190	2.28	4.50
C15s	206	2.89	5.27
C16s	222	2.92	4.93
C17s	237	2.61	4.13
C18s	251	2.87	4.29
C19s	263	2.68	3.81
C20s	275	2.74	3.73
C21s	291	2.27	2.92
C22s	300	2.36	2.95
C23s	312	2.26	2.71
C24s	324	2.05	2.37
C25s	337	1.98	2.21
C26+	652	62.14	35.76
NB MW measured by Cryette		100.00	100.00
		MW	375

Table 3-2 A detailed compositional analysis of Crude J using high-temperature column GC analysis

Compound	Composition	Compound	Composition	Compound	Composition	Compound	Composition
C6-C7	0.2225	**C16**	5.2868	**C25**	3.4866	**C34**	1.5278
C8	0.6637	**C17**	5.2063	**C26**	3.563	**C35**	1.0143
C9	0.9366	**C18**	5.6315	**C27**	3.3891	**C36**	0.7832
C10	1.85	**C19**	5.5987	**C28**	3.327	**C37**	0.6057
C11	2.5	**C20**	5.2472	**C29**	2.7444	**C38**	0.472
C12	3.4877	**C21**	5.1449	**C30**	2.7684	**C39**	0.3448
C13	4.4035	**C22**	4.5179	**C31**	2.2533	**C40**	0.2648
C14	5.1517	**C23**	4.4986	**C32**	1.9625	**C41**	0.1047
C15	5.3934	**C24**	4.2363	**C33**	1.4111	**C42**	0

Table 3-3: Result of swelling test experiment of Crude J and CO2

Pressure (psia)	**GOR (cm^3/ cm^3)**	**CO_2 Saturation (%)**	**Swelling Factor**	**Oil viscosity (cp)**
15	0	0	1	617
100	0.065274856	0.076797008	1.000128281	615.2990025
200	3.383705346	3.980988401	1.006649827	528.8240224
300	12.35891167	14.5404753	1.024288351	294.9391209
400	23.02865706	27.09361698	1.045257068	137.8639267
500	32.98040347	38.80202034	1.064814738	78.21216357
700	49.06741587	57.72867122	1.096429739	47.70041326
1000	66.04795244	77.70656889	1.129800739	26.7918627
1200	74.48783015	87.63623233	1.146387208	21.62834551
1400	81	95.29791383	1.159	17.8
1515	84.99661404	100	1.167039596	15.2

Table 3-4 Density and asphaltene content of crude J

Density of dead oil (g/cm^3)	Density of fully saturated Oil (g/cm^3)	Asphaltene content Wt.%
0.9592	0.9732	**11.6**

3.4.2 Novelty in the Lumping of Crude J

It has previously been stated that one of the sources of error and huge uncertainty in modelling of fluid behaviour using EOS is the lumping of components. The conventional method for lumping of components into pseudo-components has been described in detail in the previous section. Since only a few experimental data are available, using the conventional method would lead to an unreliable model for the fluid phase behaviour.

To ensure that the fluid behaviour in the model equation obeys the actual behaviour of the fluid components during the experiment, in this approach, the produced oil from a CO_2 coreflood experiment was considered and the behaviour of the produced components was analysed. This formed the basis of the lumping scheme. Figure 3-3 shows the compositional behaviour of the components at different times during the injection process. The variation of the components composition in the oil from the start to the end of the injection process reveals interesting traits in the behaviour of the components. Components with similar behaviour can be classified as a group and hence can be lumped as one pseudo-component. It can be inferred from the figure that "crude-J" with respect to CO_2 injection can be lumped into a number of pseudo-components. For instance, C_{10} to C_{13} have exhibited a similar non-monotonic behaviour with regard to compositional change, and hence, they can be grouped. On the other hand, the compositions of C_{34} to C_{41} were monotonically reducing during the coreflood experiment. Therefore, six hydrocarbon groups can be defined based on the compositional information; these are C_6-C_9, C_{10}-C_{13}, C_{14}-C_{19}, C_{20}-C_{26}, C_{27}-C_{33}, and C_{34}-C_{41}.

This lumping method has significantly improved the tuning procedure and reduced over-reliance on the volume-shift parameter in matching volumetric (density) behaviour of the fluids as used in the conventional method. The most sensitive parameters utilised in the regression of the EOS are the Omega-A, Omega-B as well as the P_c and the T_c of the heaviest groups. Table 3-5 shows the EOS parameter values obtained after matching the experimental data in the tuning process while Table 3-6 shows the matched experimental volumetric parameters (gas solubility and oil swelling factor).

Table 3-5 EOS parameters after matching the experimental information.

Component	Pc (atm)	Tc (K)	Acentric factor	MW	Volume shift	Omega-A	Omega-B
CO2	84.01255	335.41666	0.225	44.01	-0.098115572	0.37410703	0.078294989
C6toC9	28.38951	577.45917	0.36127107	111.3383	0.044529339	0.45723553	0.077796074
C10toC13	21.94748	660.87381	0.51467154	159.0965	0.087402687	0.45723553	0.093355
C14toC19	19.261	740.71102	0.70424522	227.006	0.16367505	0.44868762	0.088942742
C20toC26	13.53984	810.80518	0.90158172	288.466	0.237328	0.4408193	0.074417041
C27toC33	10.25708	868.73386	1.0712376	387.702	0.27887367	0.45366209	0.066429189
C34toC41	8.684999	911.89462	1.1954503	455.6924	0.28852207	0.45723553	0.070318743

Table 3-6 CO2 solubilities and formation volume factor of the saturated Crude-J.

Gas Solubility (ccCO2/ccOil)	Value	Bo (ccOil @ Res.) / (ccOil @ ambient)	Value
Exp	85	**Exp**	1.81
Model	85.8	**Model**	1.803

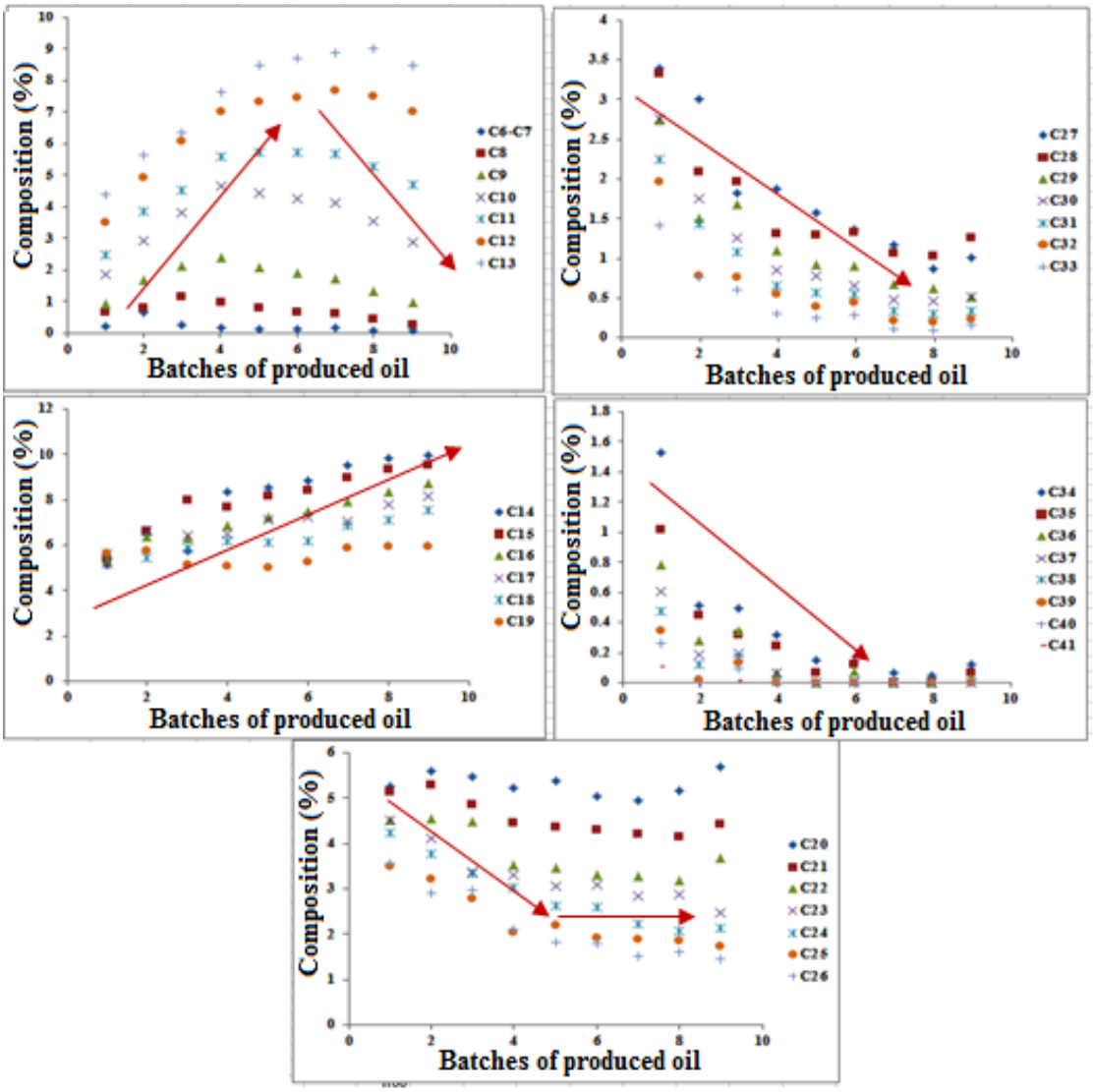

Figure 3-3 Composition of the produced oil during CO2 injection. Each Figure shows a group of components that behaved in a similar fashion and were lumped as a pseudo-component

3.4.3 "Crude J" Viscosity Modelling

After matching the volumetric behaviour of the fluid, the next important step is to match the viscosity behaviour of the phases with respect to temperature, pressure and composition. The Pedersen viscosity correlation for component liquid and vapour viscosities was used for estimating the viscosities of the mixture and pseudo-components.

This is because it uses the principle of corresponding states to calculate the viscosity of a component or mixture when the viscosity of a reference substance at the same conditions of reduced pressure and temperature is known. The Jossi-Stiel-Thodos (JST) or Lohrenz-Bray-Clark (LBC) viscosity correlations were not used because the methods have a strong dependency on the density of the mixture predicted by the equation of state and since this is highly uncertain for heavy oil it may result in errors in its prediction of viscosity values for the components. For the low-pressure condition, Lee and Eakin (1964) correlation was used, and two main parameters were considered for tuning the main viscosity correlation; the coefficients of the viscosity correlation and the critical volume (V_c). Figure 3-4 illustrates the experimental data and the modelling results after tuning the relevant viscosity parameters. The agreement between the model and experimental data is good, which indicates the ability of the model to estimate the interactions between CO_2 and Crude-J. The matched EOS equation was subsequently used to describe the behaviour of fluids in the heavy oil solvent injection processes studied.

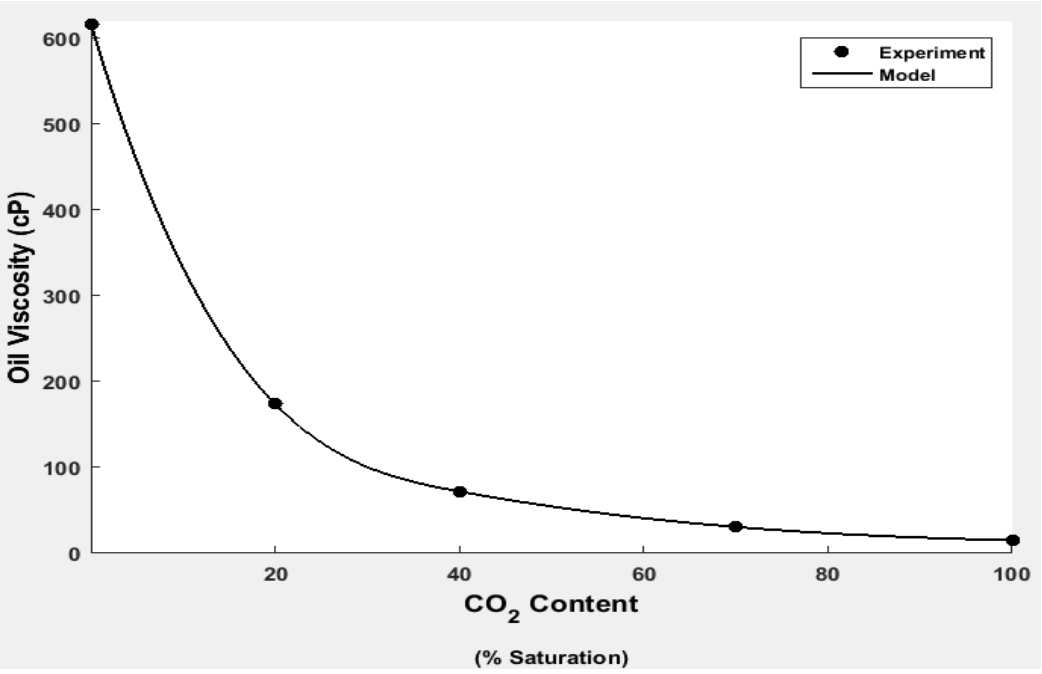

Figure 3-4: Result of matching oil viscosity based on the experimental data.

3.5 SUMMARY AND CONCLUSION

In this chapter, compositional displacement processes involving CO_2 and other gases were first reviewed, and the use of the equation of state (EOS) in the characterization of

heavy oil for simulation of compositional displacement was highlighted. In the procedure for tuning the EOS, a new methodology for lumping the heavy oil components into pseud-components was proposed. The methodology was based on the behaviour of produced fluid components rather than the arbitrary scheme of lumping components in conventional methods. The new procedure showed a better matching of the fluid properties and components behaviour during simulation. One-dimensional core model was also shown to be incapable of simulating compositional displacement where there is instability at the front due to viscous fingering or gravity drainage. Grid sensitivity study was therefore carried out on a two-dimensional model of the core to determine the optimum grid size that would sufficiently resolve the fingers in such displacements. The sensitivity study was based on the difference in cumulative oil recovered and differential pressure across the core, and it was observed that the gridding is more sensitive in the direction perpendicular to the flow. The optimum model for the horizontal core was found to be 100 grids in the horizontal direction and 80 grids in the vertical direction. The modelling approach was capable of capturing the fingers and their behaviour.

CHAPTER 4

ESTIMATION OF TWO-PHASE RELATIVE PERMEABILITY FROM UNSTEADY STATE HEAVY OIL COREFLOOD EXPERIMENT WITH INSTABILITY

4.1 INTRODUCTION

The ability for two or more immiscible fluids to flow through a porous medium depends on their saturation and the absolute permeability of the rock. The term absolute permeability as described by Darcy Law was originally formulated to account for the resistivity of the porous medium to the flow of a single fluid. When two or more fluids are flowing through the medium, however, the concept of relative permeability and effective permeability are used to convert the single-phase Darcy equation into multiphase estimations at a given saturation. Relative permeability is, therefore, an essential flow parameter and is routinely measured for input into the simulation of fluid flow in porous media such as waterflood or gas injection. Most of the analytical methods for estimating this important parameter were formulated based on the assumption of stable Buckley-Leverett displacement, which is characterised by the advancement of encroaching fluid as a diffusive front consisting of a shock wave that is immediately followed by a rarefaction (Buckley and Leverett, 1942). This is not the case in heavy oil displacement by gas/solvent where the displacing phase is advancing through the porous media in the form of well-defined channels known as viscous fingers or a gravity override resulting from density difference or both.

The objectives of this chapter are to investigate the effect of instability on gas/oil or water/oil two-phase relative permeability curves computed from measurements based on

the dynamic displacement (unsteady-state) method and to develop a methodology for accurate estimation of this important parameter in displacements with instability.

4.2 INVESTIGATING THE BEHAVIOUR OF FLOW FUNCTIONS IN HEAVY OIL GAS DISPLACEMENT

To study the behaviour of the flow functions (k_r and Pc) with respect to composition, core orientation and initial oil viscosity, three coreflood experiments (Farzaneh, 2014) were considered.

1) Experiment-1, CO_2 injection into a horizontal core saturated with dead crude oil (Crude-J)
2) Experiment-2, Nitrogen injection into the top of a vertical core saturated with Crude-J pre-equilibrated with nitrogen (experiment 2).
3) Experiment-3, CO2 injection into a horizontal core saturated with live crude oil (Crude J saturated with methane)

These experiments were chosen based on the differences in their compositional behaviour. While mass transfer occurred in the first and the third experiments, the second was pre-equilibrated with the injection gas (N_2) to mitigate any compositional exchange that may take place. This was to allow for observation of any change in the flow functions resulting from the mass transfer effect and hence the dependency of relative permeability on compositional effect. Table 4-1 lists the test conditions and fluids used in the selected coreflood experiments.

Table 4-1 Description of the coreflood experiment selected for this simulation study

Exp.	Description	Fluids	Core Orientation	Test Conditions
1	Secondary CO_2 injection into Dead Crude-J	Injection fluid: CO_2 Resident oil: dead Crude-J Resident brine: 20000 ppm	Horizontal	T=28°C, P=1500 psig
2	Secondary N_2 injection into pre-equilibrated Crude-J	Injection fluid: N_2 Resident oil: Saturated Crude-J with N_2 Resident brine: 20000 ppm	Vertical	T=38°C, P=1500 psig
3	Secondary CO_2 injection into Live Crude-J	Injection fluid: CO_2 Resident oil: dead Crude-J saturated with methane Resident brine: 20000 ppm	Horizontal	T=28°C, P=1500 psig

An implicit history matching technique was used to obtain the flow functions by representing the relative permeability curves with a versatile parametric correlation known as the L.E.T correlation (equations 10 to 11). Its flexibility and ability to honour the so-called gas S-behaviour makes it suitable for estimating the gas/oil relative permeability. An exponential function was also chosen for the capillary pressure (Pc) and presented in equation (19) below. The parameters in the two correlations were used for tuning the relative permeability and the capillary pressure in the history matching process.

$$Pc = Po\frac{(S_{ge})^{\beta}}{1-(S_{ge})^{\beta}} \qquad 19$$

Where, Po is oil pressure and β is the capillary pressure exponent.

In Experiment-1, CO_2 was injected into a horizontally oriented core saturated with dead Crude-J. Viscosities of the displacing (CO_2) and displaced (crude oil) fluids are 0.077cp and 617cp, respectively, which makes the displacement prone to viscous instabilities. On the other hand, compared to the resident crude oil, the injected fluid has a lower density, resulting in the possibility of gravitational instabilities (Fayers and Newley, 1988). These phenomena cannot be modelled in conventional one-dimensional model simulation as stated in the previous section since it does not take into account component and phase dispersion, as well as fingering and overrides and therefore another dimension needs to be considered (Christie et al., 1990).

For this experiment, two modelling approaches were compared and analysed to investigate the applicability of 1D and 2D models and the impact of these assumptions on the estimated relative permeability. A compositional simulator (CMG-GEM) capable of capturing the dynamic behaviour of the components and the fluid phases was used for the investigation.

4.2.1 One Dimensional (1D) Model History-Matching Approach

In the first approach, a one-dimensional model of the experiment (Experiment-1) was history matched. As stated earlier, the use of a 1D model will not allow for the onset and propagation of any finger that would have emanated as a result of unfavourable mobility ratio. However, the results enabled an understanding of the contribution of instability on

the estimation of the flow function. In order to estimate the 1D relative permeability by history matching, an L.E.T correlation was used to represent the relative permeability function while gas/oil phase behaviour was modelled using PR-EOS (see Chapter 3), CMG-GEM compositional simulator and DECE optimiser in CMG-CMOST optimisation software were utilised for tunning the L.E.T parameters in order to match the history data, which are produced gas, produced oil and the differential pressure (DP) across the core.

Figure 4-1 shows a match of the simulation on the experimental data for produced oil and the differential pressure (DP) across the core obtained at the end of the optimisation process. It can be seen that a good match was obtained for the produced oil but the simulated DP was up to 2psi higher than the experiment before breakthrough. The DP at the breakthrough was also not matched. This mismatch is the result of the 1D model not being able to account for the instability which has resulted in lowering the DP before the breakthrough in the actual experiment. Figure 4-2 also shows the gas saturation profile along the core, it can be observed that the flow is a typical Buckley-Leverett type of flow with a diffusive front that is typically sharp at the front. Figure 4-3 shows the relative permeability obtained from the 1D model history matching. The oil relative permeability has an S-shape characteristic while the gas relative permeability indicated a very low critical gas saturation of 0.02. In addition, the gas relative permeability jumped from 0 to 0.13 for a relatively small increase in gas saturation from 0.02 to 0.03. This behaviour of the relative permeability curves is due to the small gas saturation that formed in the displacement front reaching its critical flow velocity. The estimated 1D relative permeability curves was used in subsequent sections for analysing the impact of viscous fingering or gravity tongue on the shape of the curves.

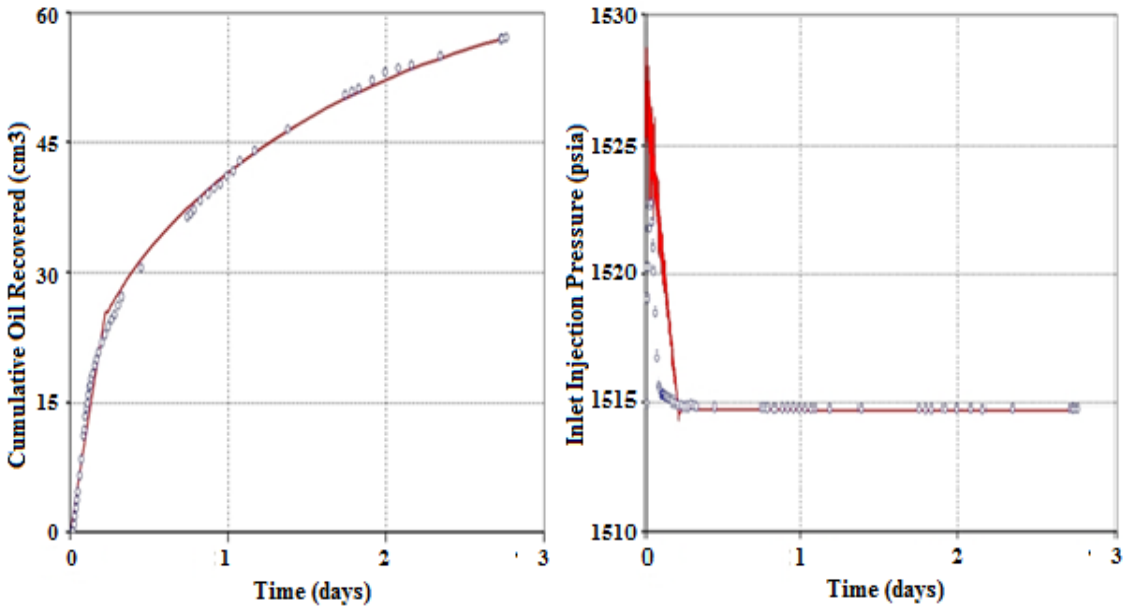

Figure 4-1 Results of the history matching of experimental cumulative oil production (left graph) and the pressure at the inlet of the core (right graph) obtained from Experiment-1 using 1D model.

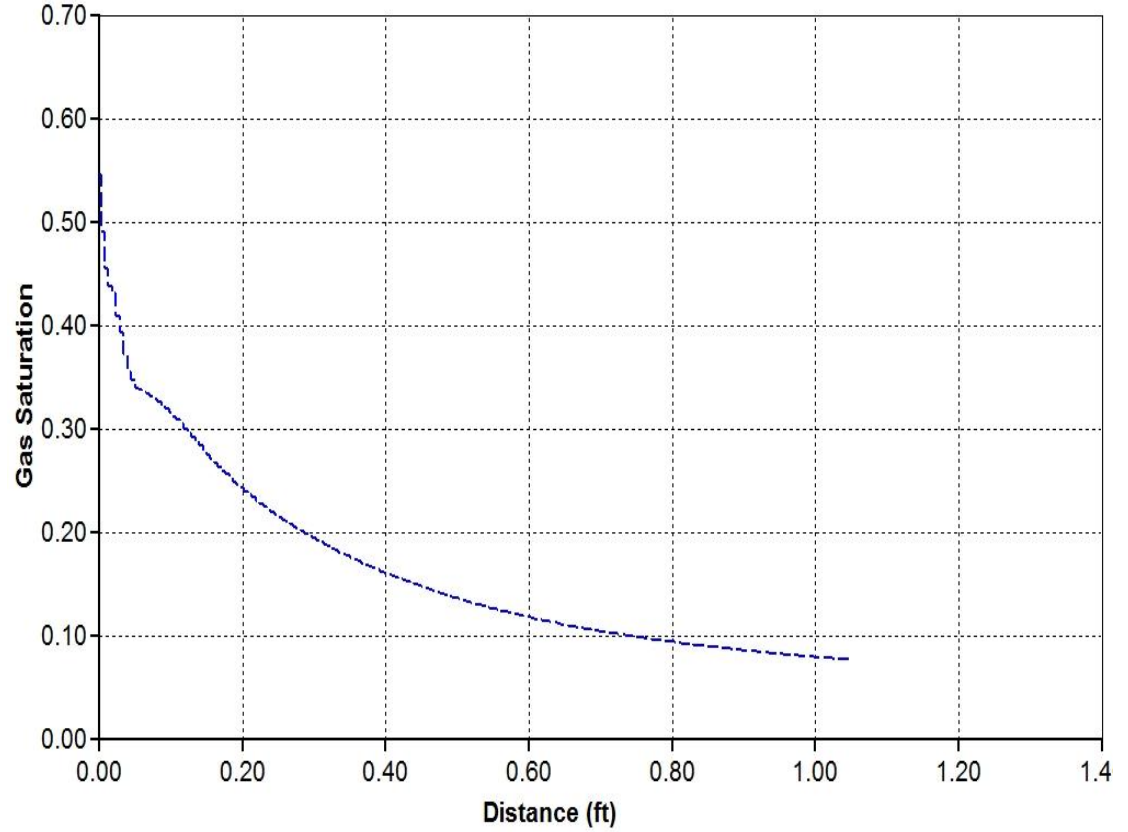

Figure 4-2 Simulation of gas saturation along the core using 1D model. Gradual change in gas saturation can be linked to fingering development

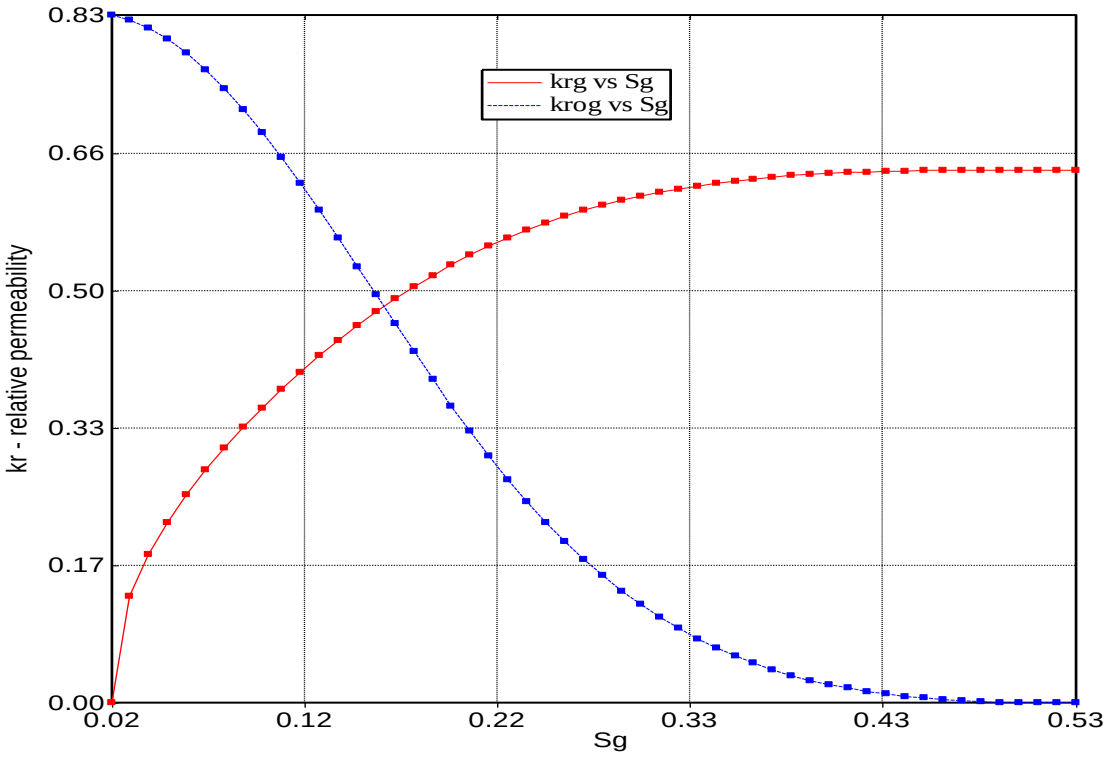

Figure 4-3 Two-phase gas and oil relative permeability curves as a function of gas saturation estimated from the 1D model history matching Experiment-1

4.2.2 Analysis of Viscous and Gravity Forces

Displacement of heavy (viscous) oil by gas is a complex process that requires special considerations in the simulation. A number of sources of instability that may result in the displacement need to be taken into account in the model. Along with the adverse mobility ratio between the CO_2 and viscous oil, the density contrast may lead to gravitational segregation. While the former leads to viscous fingering, the latter results in a gravitational tongue. One of the easiest ways to determine if a simulation will lead to viscous fingering is from the analysis of one-dimensional model displacement simulation of the process. If the ratio of the total mobility at the interface is greater than one, then the injection process would be unstable if simulated using a two or three dimensional model of the process (Blunt and Christie, 1994). A review and analysis of displacement with viscous fingering is the subject of Chapter 7. Additionally, in the presence of an adverse mobility ratio and effective density contrast, the competition between the viscous and gravitational forces can bring about transitional behaviours between severe viscous fingering and a sharp gravitational tongue. To analyse the dominance of the forces, Fayers extended Dietz theory (Fayers and Newley, 1988) and proposed a dimensionless viscous-to-gravity parameter (N_G) as expressed by equation (20)

$$N_G = 2\left[\frac{\left(1-\frac{\lambda_o}{\lambda_g}\right)q}{\lambda_o \Delta\rho g} - \theta\right] \times \left(\frac{H}{L}\right) \quad (20)$$

Where q is superficial velocity (flow rate per unit area), $\Delta\rho$ is density difference, θ is the inclination of the core, H and L are core thickness and length respectively. Figure 4-4 illustrates how viscous-to-gravity forces can control instabilities. As can be noted, the model in is tilted, which reduces the impact of gravitational forces on the instability development. It has been determined that an N_G value of 1 is the transition point from gravity to viscous force, i.e. gravitational instabilities (tongue) are dominant when N_G <1. Conversely, N_G > 20 has been reported as the point where viscous fingering becomes dominant over the gravitational tongue.

In the case of CO_2 injection into horizontal core saturated with dead crude-J (Experiment-1), using the relevant parameter values in equation (20) resulted in N_G value of approximately 0.05 and hence gravitational instabilities dominated viscous fingering in the displacement. Therefore, positioning the core horizontally in the experiment facilitated the formation of the gravitational tongue. However, in contrast to the uncertainty involved in the simulation of viscous fingering such as the number of fingers and the differing behaviour of each finger (Todd and Longstaff, 1972), the formation of a gravitational tongue mainly depends on the thickness of a single tongue and speed of its advancement.

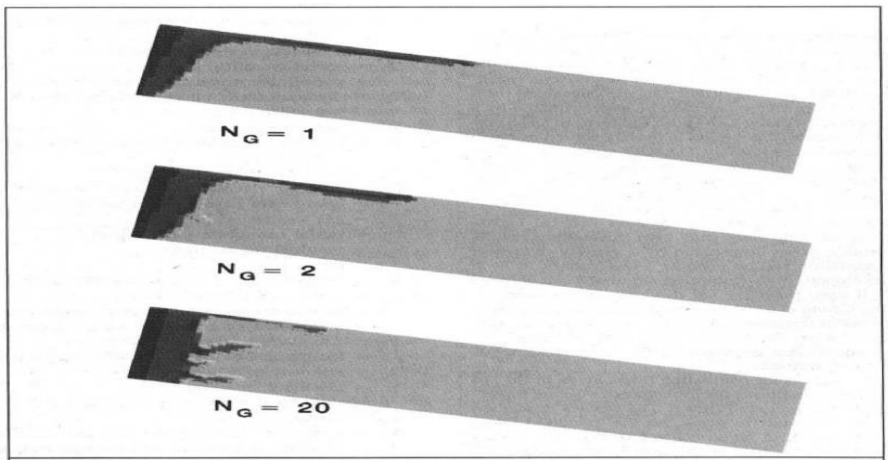

Figure 4-4 Impact of N_G (viscous-to-gravity number) on the type of instability developed in an unstable displacement. Top image (N_G=1) shows the formation of a gravitational tongue whereas the bottom image (N_G=20) exhibited a dominant viscous fingering. In the middle image (N_G=2), the transitional behaviour from a tongue toward viscous fingering can be seen (Fayers and Newley, 1988)

4.2.3 Effect of relative permeability on flow stability (2D model Approach)

It is imperative at this point to investigate the impact of the choice of relative permeability function on the development and propagation of instability. Therefore, before embarking on the history-matching studies, which is known to be resource and time consuming, a preliminary study was carried out to give an idea on which parameter in the correlation for the relative permeability curves needs to be tuned to adequately match the production history data.

For this purpose, a relatively refined 40x100-grid cells core model was generated to investigate the impact of relative permeability on development and propagation of instability. The L, E and T parameters (Lomeland et al., 2005) in the relative permeability function (equation 13-15) were varied to generate two distinct sets. Figure 4-5 shows the relative permeability curves and their normalised forms (normalisation in terms of end-point saturation). The two curves have same end point relative permeability for comparison, but the shapes are markedly different. The impact of the change in the shape of the curves on saturation pattern and the stability of the displacement was investigated.

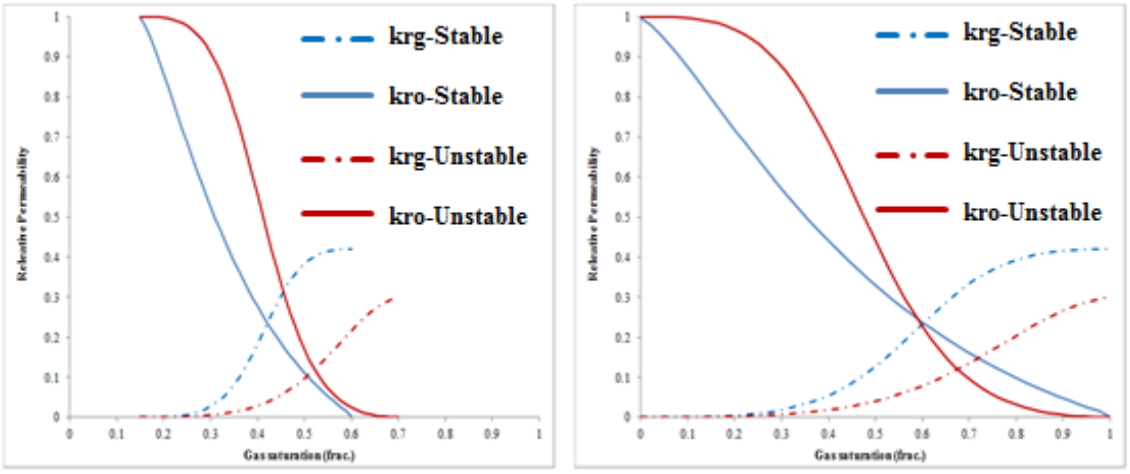

Figure 4-5: The left image shows gas/oil relative permeability defined for sensitivity analysis. The right image illustrates the normalised relative permeability based on the end-point saturations

Figure 4-6 and Figure 4-7 depict the cumulative oil recovered and the pressure drop across the inlet and outlet of the core, respectively, using the two sets of relative permeability curves described previously. shows that they have equal maximum pressure at the inlet of the core, which agrees with the inputted identical k_{ro} at critical gas saturation values in the relative permeability functions. However, the rate of pressure decline was notably different in the two cases. The simulation of the displacement performed with

the blue relative permeability curve was unstable and had an abrupt drop in the inlet pressure, whereas the simulation using the red relative permeability was more stable and exhibited a more gradual decline in the inlet pressure. In terms of the cumulative oil production (Figure 4-7), the blue curve with unstable relative permeability showed an early breakthrough with a gradual and continuous oil production after the breakthrough.

Figure 4-8 also illustrates the sequence of the gas saturation profile as the front advances at different times for the two simulations. It is clear that the simulation on the left-hand side was relatively stable while the one on the right was highly unstable. The difference here was clearly the choice of relative permeability curves, which can result in piston-like displacement or highly unstable flow displacement. We can therefore conclude that relative permeability can be used to alter the stability of a displacement.

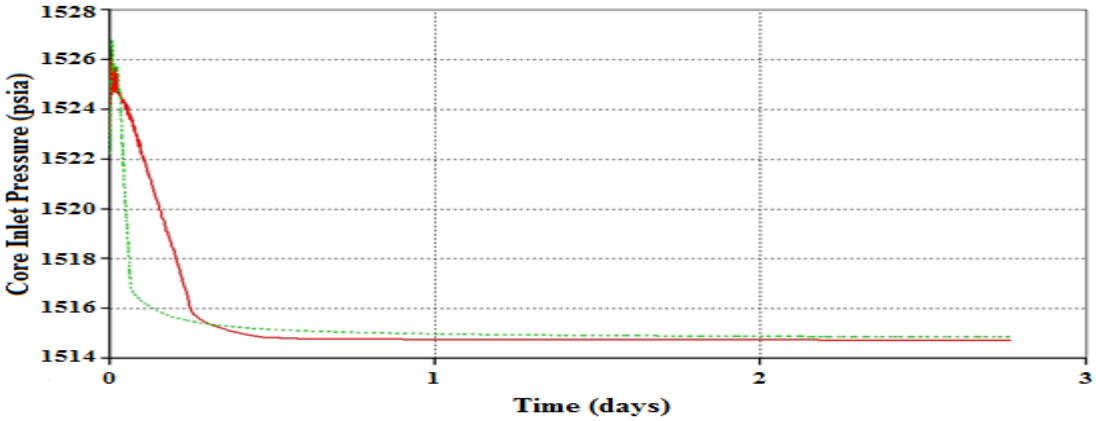

Figure 4-6 Pressure at the inlet of the core for the two relative permeability curves defined in sensitivity analysis. The green dashed curve shows the pressure for the unstable kr while the red line indicates the pressure for semi-stable relative permeability.

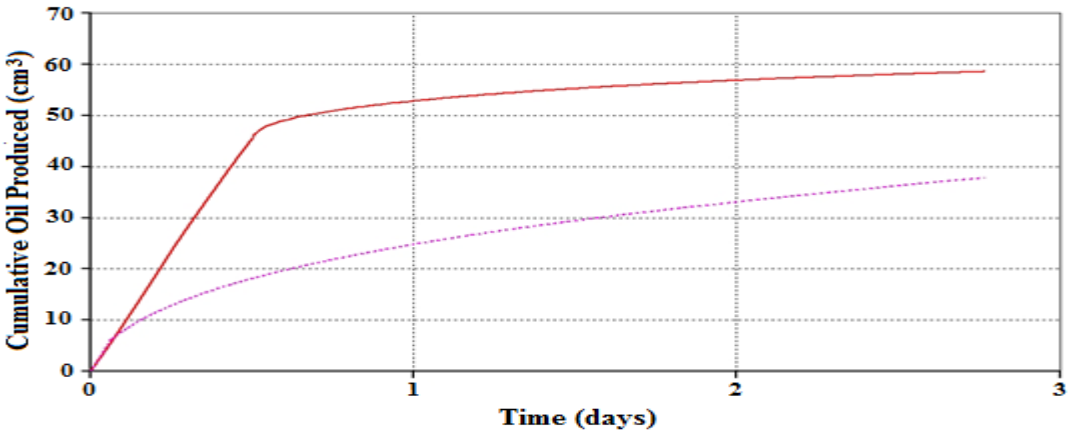

Figure 4-7 Cumulative oil production for two cases: semi-stable kr (red line) and unstable kr (dashed purple curve). An early breakthrough in the purple curve indicates the development of an unstable front in the simulation.

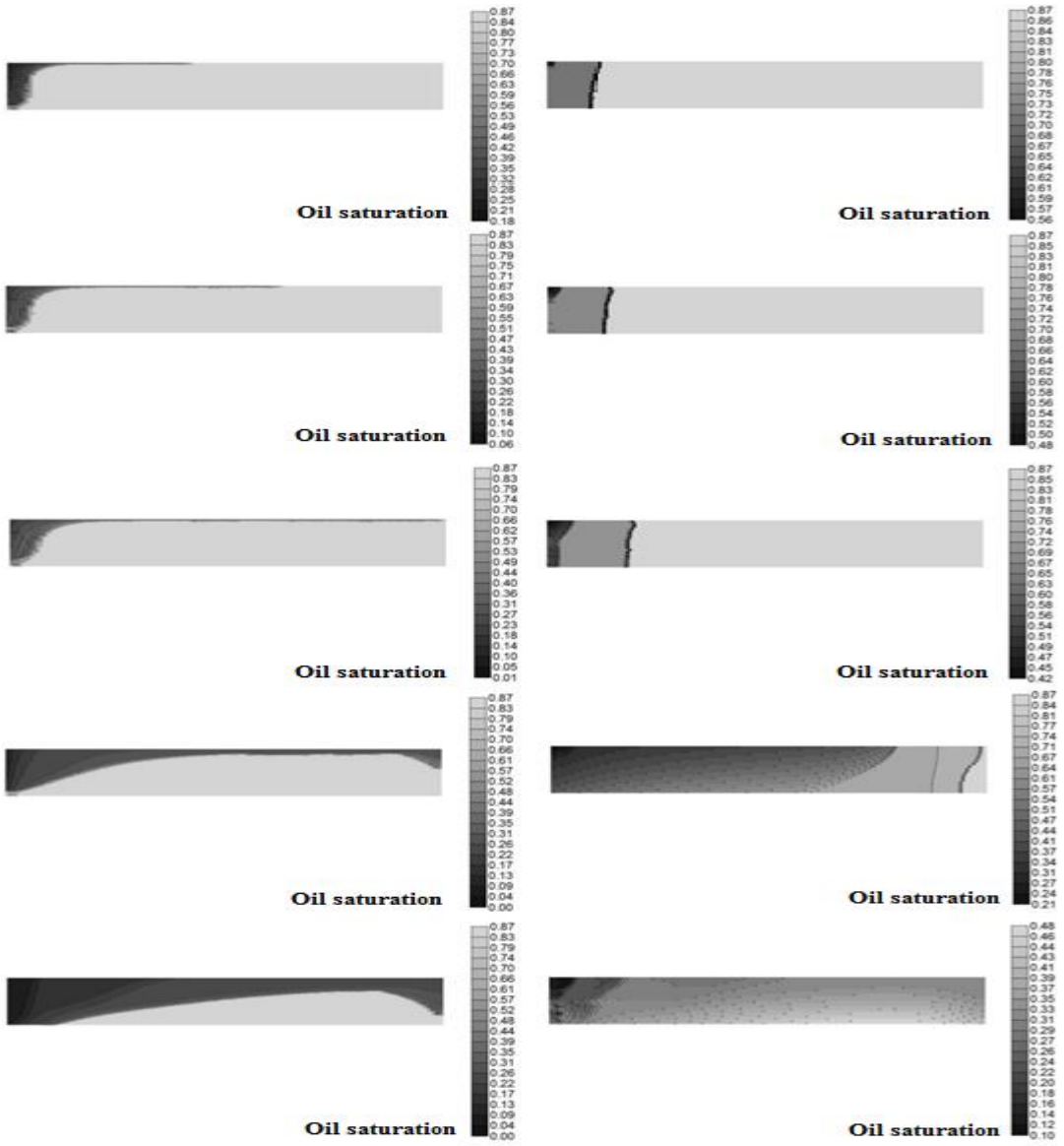

Figure 4-8 Oil saturation distributions for the two relative permeability curves used in the preliminary studies at different pore volumes injected (PVI). The left images were obtained from simulation using the unstable relative permeability curve while the ones on the right were obtained using the relatively stable one.

The preliminary studies also looked at the effect of relative permeability on compositional (CO_2/Oil) interactions. The choice of relative permeability can significantly affect the rate of mass transfer by convection as seen in Figure 4-9 where the transition zone (mixing zone) for the unstable relative permeability was larger than that of the stable relative permeability. If molecular mass transfer was the only mechanism or the main mechanism for mixing, the two models would have had same transition area since they have same molecular diffusion coefficient. This was not the case due to the convective effect of

relative permeability and underscores the importance of relative permeability in compositional displacement.

Therefore, it can be concluded that the parameters used for generation of relative permeability curves were directly related to the effective mobility ratio. Consequently, the instabilities across the front in a displacement can either be enhanced or suppressed by manipulating the relative permeability parameters. Another information from this preliminary investigation is that even though numerical issues (numerical dispersions or truncation errors) are known to cause instability in displacement, in this case, it can be concluded that it is mainly as a result of the choice of relative permeability curves, as seen in the two simulations (one stable, the other unstable). Hence, relative permeability curve can be modified in 2D grid model to simulate displacement with instability.

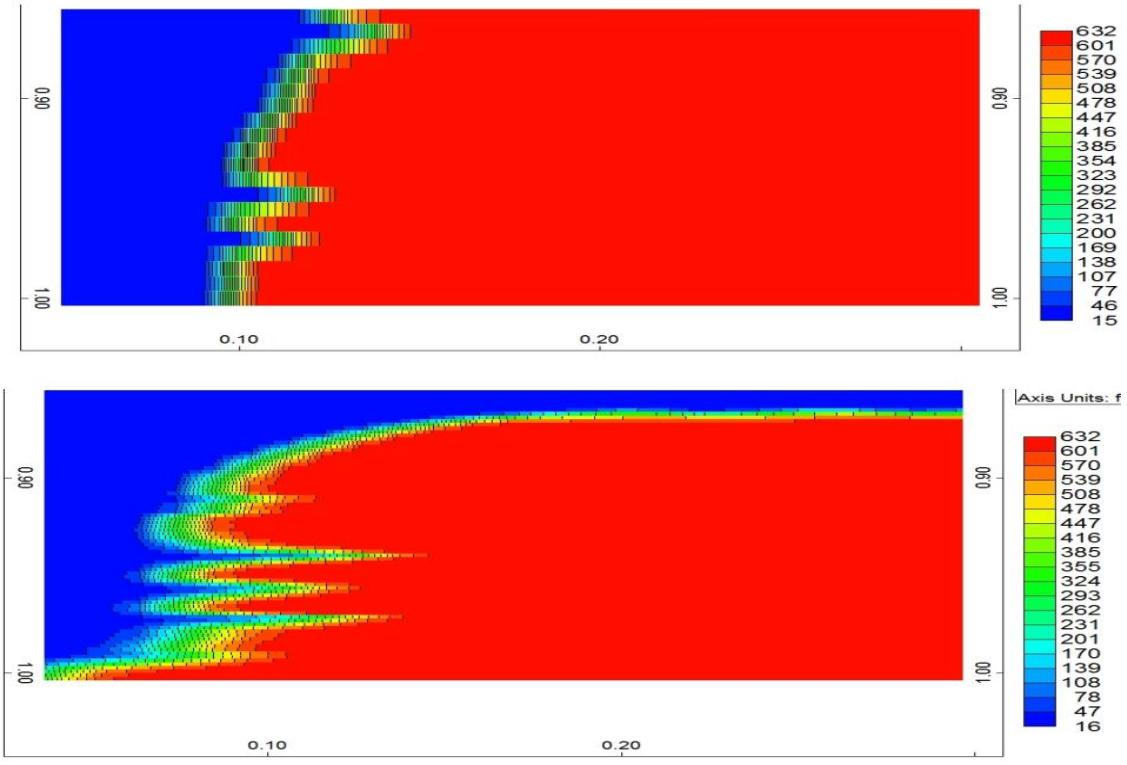

Figure 4-9: Result of simulation of oil viscosity variation indicating the transition zones for the two cases; a semi-stable kr (top image) and an unstable kr (bottom image). The width of the transition zone where mass transfer took place was notably affected by the stability of the front advancement and hence the shape of the relative permeability.

.

4.3 ESTIMATION OF RELATIVE PERMEABILITY FOR EXPERIMENT 1 (CO_2 INJECTION INTO DEAD CRUDE OIL IN HORIZONTAL CORE)

In this experiment, CO_2 was injected into dead heavy (viscous oil) in a horizontal core. The relative permeability curve obtained by history matching using one–dimensional (1D) model of the core, which did not take into account the instability propagating at the front has been presented in section (4.2.1). This section considered the estimation of the CO_2/Oil relative permeability using two-dimensional (2D) model. The grid sensitivity has also been carried out for the 2D model and reported in section (2.9). It showed that the optimum grid cells size for the core model was 100x80. Where the direction normal to flow has the highest refinement with 80 grid cells. Though the core length is larger than the diameter of the core, discretization of the axis into 100 grid cells was sufficient. The permeability of the core was populated randomly using Gaussian distribution with a mean of 2340mD and a standard deviation of 50mD. The details of the core model and the equation of state (EOS) that modelled the phase behaviour have been described in depth in Chapter three.

For the history-matching, a parametric approach was considered using the versatile L.E.T-type correlation (Lomeland et al., 2005) and setting the capillary pressure zero. Therefore, the estimated relative permeability combined capillary pressure effect. In the subsequent section, the effect of capillary pressure was sensitised. A compositional simulator (CMG-GEM) and CMG-CMOST, similar to the 1D model case, were used for the simulation and the optimisation, respectively. Figure 4-10 and Figure 4-11 show the comparison between the optimum case and the history data for cumulative oil production and the pressure across the core respectively. The match between the experimental results and simulation is satisfactory. Figure 4-12 shows the tuned relative permeability curve obtained from the history-matching process. Therefore, it is the estimated 2D relative permeability curve, which honoured the instability that occurred in the CO_2-heavy oil displacement process. It can be seen from the figure that the gas relative permeability had a strong gas related S-behaviour while the oil relative permeability has a relatively linear shape. The oil relative permeability at critical gas saturation is 0.988 while the gas end-point k_r is 0.36. This means that the non-wetting phase, against the usual convention, has lower relative permeability value than that of the wetting phase. Therefore, in unstable displacements, it is not always true to infer the wetting characteristics from relative permeability curves. Furthermore, critical gas saturation is estimated to be

around 0.13 indicating that gas remains immobile from 0 to 0.13 saturations for this unstable displacement. This is more than the acceptable range in stable Buckley-Leverett type displacement where the critical gas saturation is generally believed to be less than 0.1. Thus, the relative permeability of an unstable gas/oil two-phase flow have unique characteristics that are not in line with the accepted rule of thumbs for relative permeability.

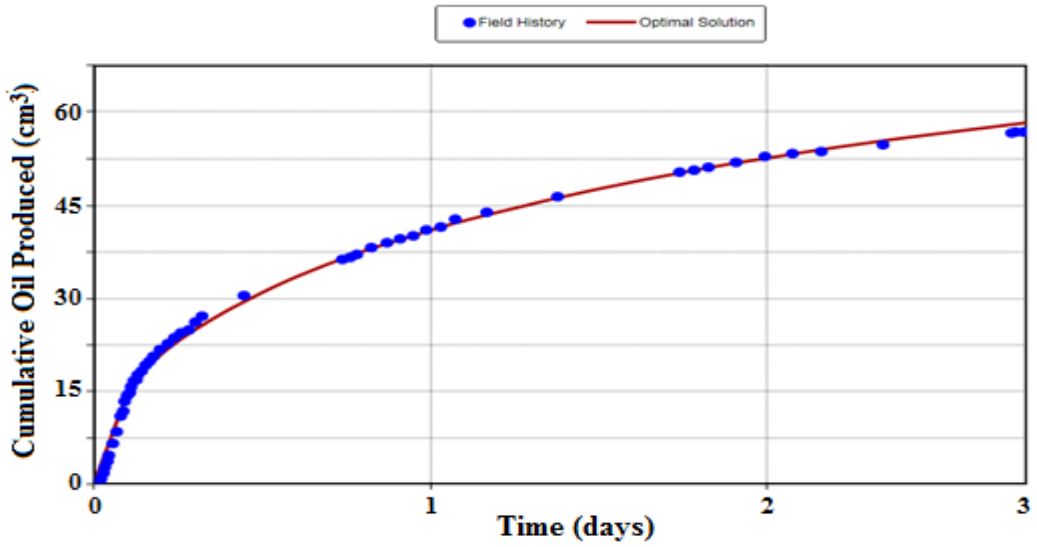

Figure 4-10: Matched (red lines) cumulative oil production against the experimental data (blue dots) obtained from the history matching of Experiment-1 using 2D model approach.

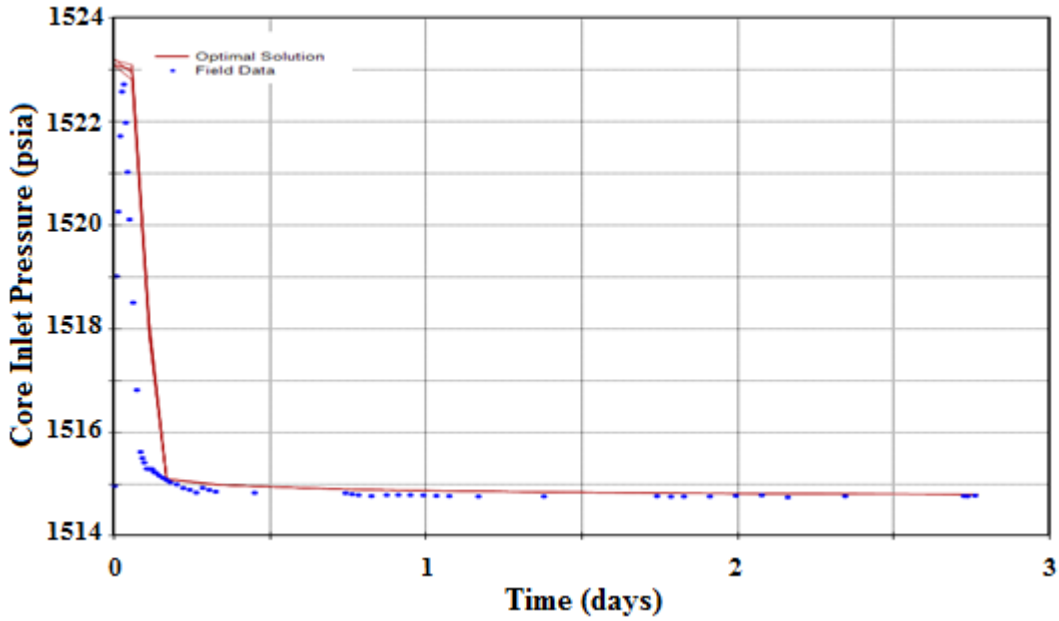

Figure 4-11 Matched (red lines) pressure at the inlet of the core against the experimental data (blue dots) obtained from the history matching of Experiment-1 using the 2D model approach.

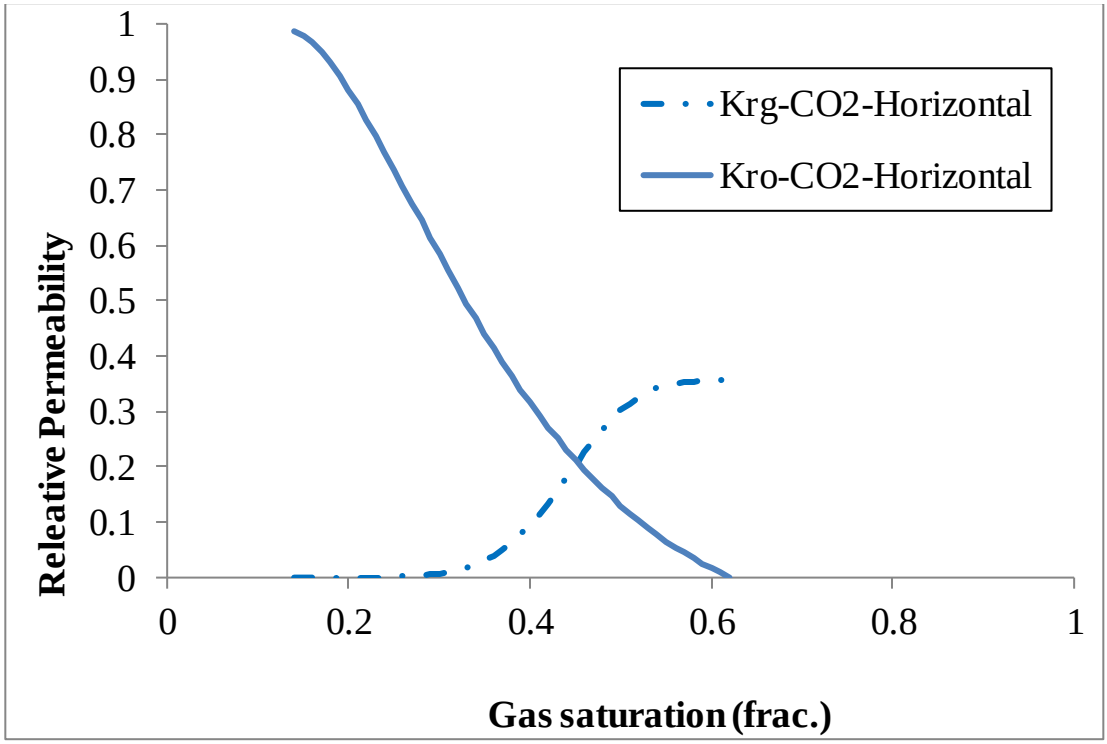

Figure 4-12: 2D tuned gas/oil relative permeability estimated by history matching of Experiment-1 indicating a critical gas saturation of 0.13 and an S-behaving gas relative permeability curve

Figure 4-13 shows the oil saturation distribution in the core at different time steps, indicating the formation of a sharp gravitational tongue at the top part of the core. This is true because of an analysis of the viscous/gravitational force using equation (20), which shows that the value of N_G <<1 and hence verified that the gravitational force in the CO_2 injection into heavy oil (crude J) in a horizontal resulted in severe gravity override.

Additionally, to verify the simulation of the compositional behaviour of the oil phase components and the injected CO_2, the simulated results were compared with the laboratory compositional analysis of the produced oil obtained from GC analyser. The composition (mole fraction) of each component in the oil phase at different times in the simulation was plotted. Figure 4-14 to Figure 4-19 show the behaviour of the various components obtained from the simulation compared with their actual behaviour in the experiment. The conclusion from the figures is that though the simulator was able to capture the general behaviour of the components as can be seen by comparing the shapes of the images on the left (simulations) to those on the right (experiments); however, it was deficient in matching the magnitude of the compositional changes. For instance, C_6-C_9 has a non-monotonic behaviour (right image Figure 4-14) with an increase in early stages, and this trend was replicated in the simulation results. Likewise, the general behaviour of C_{10}-C_{13} has been successfully simulated. For the monotonic compositional

trends, i.e. C_{14}-C_{19} and C_{20}-C_{26} and C_{27}-C_{33} and C_{34}-C_{41}, a reasonable consistency exists between the simulation results and the general trend of the experimental information. The mismatch in the magnitude of the composition can be attributed to two main reasons.

1. The assumption by the simulator of instantaneous thermodynamic equilibrium: This is not the case in the experiment because the earlier breakthrough of the CO_2 through the sharp finger did not allow enough time for mixing fluids to reach thermodynamic equilibrium.
2. The use of volume shift in the tuning of the EOS equation for phase behaviour modelling may lead to conflict between phase component behaviour and its volumetric behaviour making it difficult to match these two properties at the same time (Kumar and Okuno, 2012b). It could also result from other uncertainties related to the EOS such as in the prediction of properties of lumped components.

Nevertheless, the simulation results exhibited a good agreement with the actual experimental trends and behaviour. Therefore, it can be concluded that the history matching approach coupled with the improved tuning of EOS has reproduced the general behaviour of the components with regards to dissolution and vaporisation characteristics.

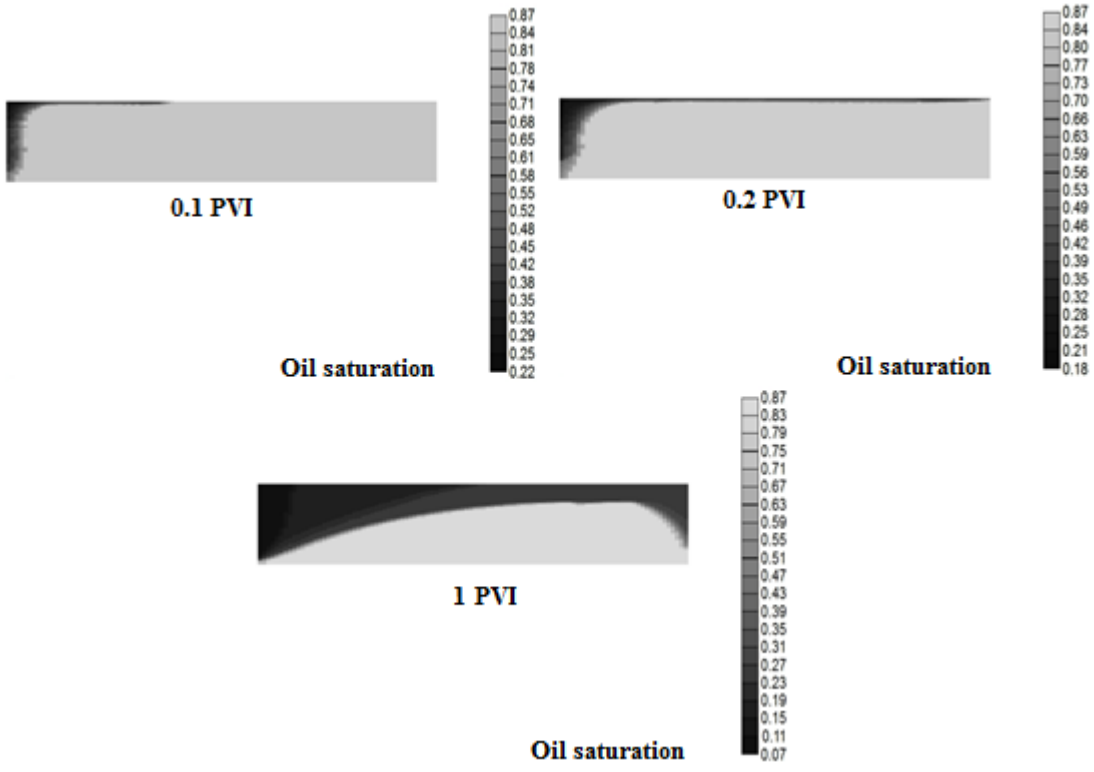

Figure 4-13: Gas saturation profile along the core at different pore volume injected (PVI) showing the propagation of the gravitational finger.

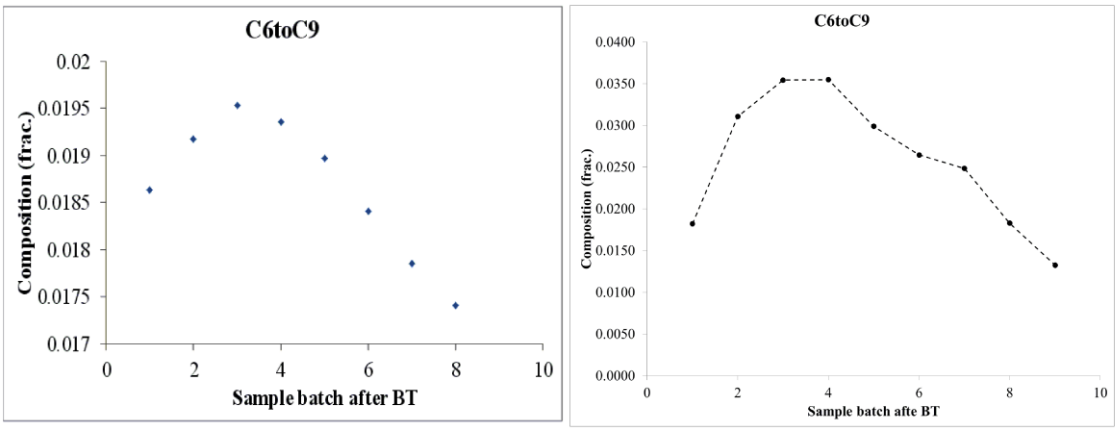

Figure 4-14: Composition of produced oil after breakthrough; Simulated (left image) versus the experimental data (right image) for C6 C9.

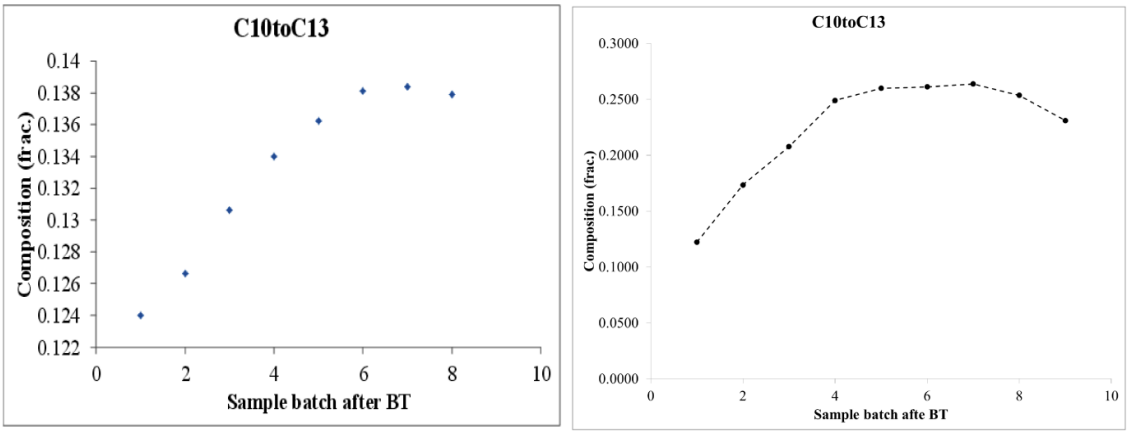

Figure 4-15: Composition of produced oil after breakthrough; Simulated (left image) versus the experimental results (right image) for C10 C13.

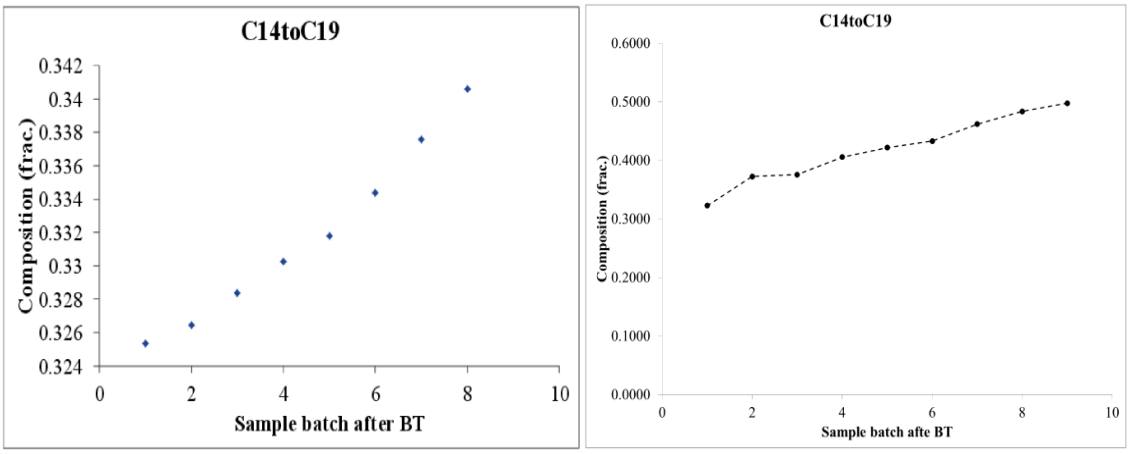

Figure 4-16: Composition of produced oil after breakthrough; Simulated (left image) versus the experimental results (right image) for C14 C19.

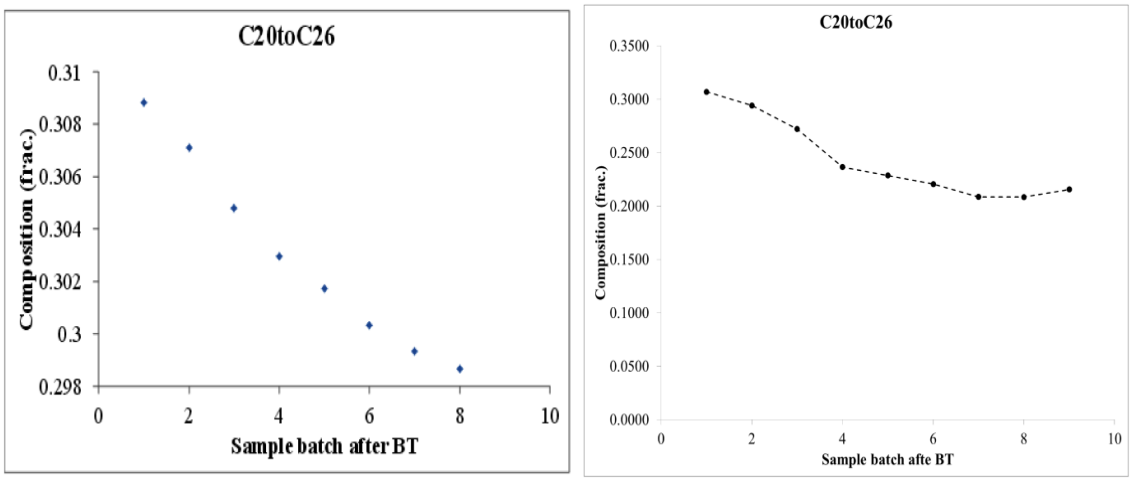

Figure 4-17: Composition of produced oil after breakthrough; Simulated (left image) versus the experimental results (right image) for C20 C26.

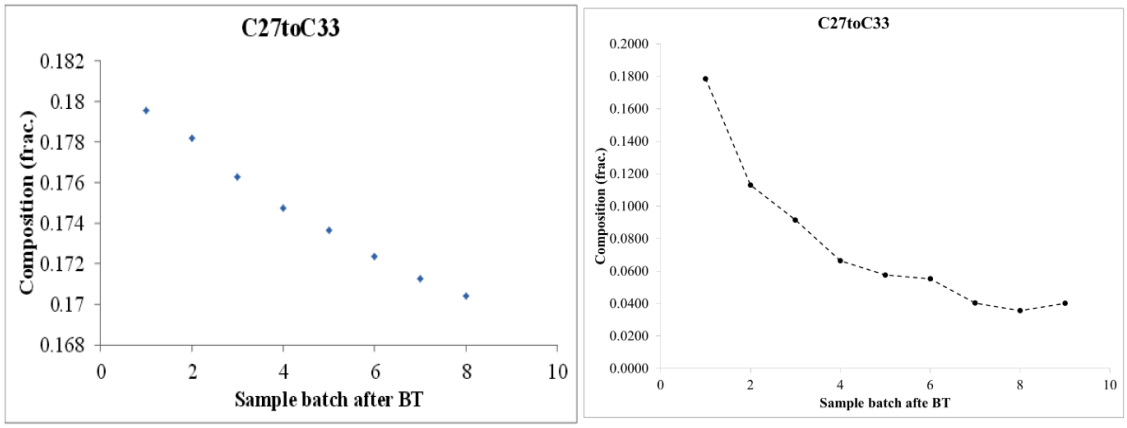

Figure 4-18: Composition of produced oil after breakthrough; Simulated (left image) versus the experimental results (right image) for C27 C33.

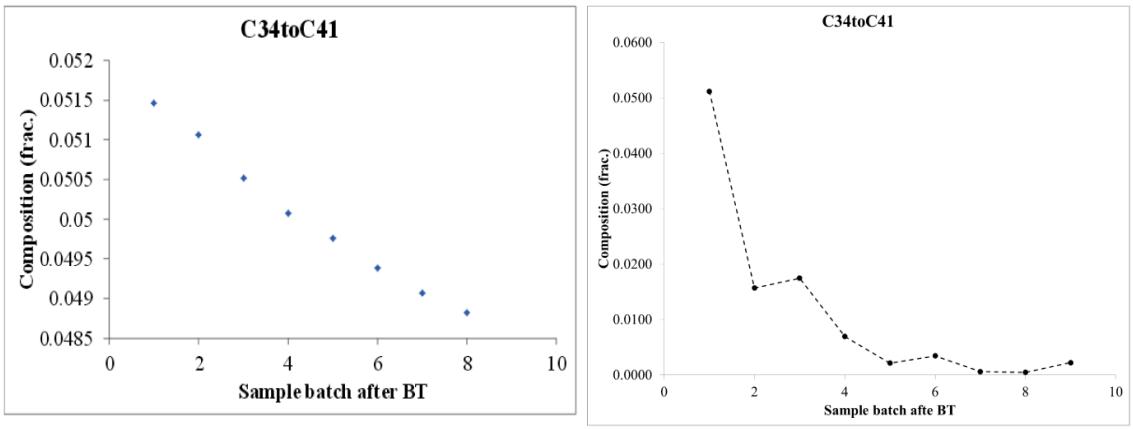

Figure 4-19: Composition of produced oil after breakthrough; Simulated (left image) versus the experimental results (right image) for C34 C41

4.4 ESTIMATION OF RELATIVE PERMEABILITY FROM EXPERIMENT-2 (N_2 INJECTION INTO PRE-EQUILIBRATED CRUDE-J IN VERTICAL CORE)

In this experiment, Nitrogen (N_2) was injected into crude-J using the same core mounted in Experiment-1 but was orientated in the vertical direction to investigate the effect of gravity on the displacement efficiency and the shape of the relative permeability. Also, the crude has been pre-equilibrated (saturated) with N_2 to mitigate any mass transfer that may occur between the oil and the N_2 during the injection. The results of the simulation of this experiment was compared to that of Experiment-1 in which mass transfer took place to sensitize the effect of mass transfer on the shape of the estimated relative permeability curve.

Laboratory experimental compositional analysis for matching the phase behaviour was not conducted for this experiment and only one data point was available, the gas-oil-ratio (GOR) of the saturated oil (7 ccN_2/ccOil) at the experimental condition of temperature and pressure (28^0C and 1500psi respectively). The data was considered sufficient since the oil has been pre-equilibrated and therefore, significant compositional exchange between the phases that may lead to changes in the oil composition during the displacement process was not expected. Therefore, based on the available information the EOS was tuned by adjusting the binary interaction coefficients between the N_2 and crude oil components to match the experimental data. Specifically, the interaction coefficients between N_2 and the lighter components were adjusted to match GOR. One of the critical parameters that needed to be predicted was the oil viscosity variation due to the dissolution of N_2, and the tuned EOS was therefore employed for its estimation. With a N_2 viscosity of 0.02cp and density of 0.111g/cc, the viscosity of the saturated oil was estimated to be 261cp, a reduction from the original value of 617cp for the dead oil before N_2 the injection.

This tuned EOS was fed into the 2D (CMG-GEM) simulation model for history matching and the same L.E.T-type parametric equation used in the CO_2 injection (Experiment-1) was employed to represent the relative permeability function in the history-matching process. An analysis of the gravitational/viscous forces (equation 20), which describes the dominant displacement mechanism and hence the type of instability that occurred in the displacement has indicated an N_G value of 1.5 (which is greater than 1), suggesting

that the displacement is within the transition zone from gravitational to viscous force dominance. Therefore, it was expected in this case to see a slightly more viscous fingering type of displacement.

Figure 4-20 and Figure 4-21 show the cumulative oil production and the pressure across the core respectively for the optimum simulation model from the history-matching process. A good match between the experimental data and the simulation result was obtained. Figure 4-22 shows the oil saturation profile in the core at different time steps indicating the shape of the unstable displacement front, as well as how the instability propagated over the injection period. Figure 4-23 shows the tuned relative permeability curves obtained from the history matching process of Experiment-2 plotted together with the previously obtained relative permeability from Experiment-1 (CO_2 injection into dead heavy oil). The two relative permeability curves are comparable in shape with only the end-point gas relative permeability at residual oil saturation and the critical gas saturation being mainly different. It can therefore be concluded that mass transfer or gas type do not affect the shape of the relative permeability but rather the magnitude of the viscosity ratio.

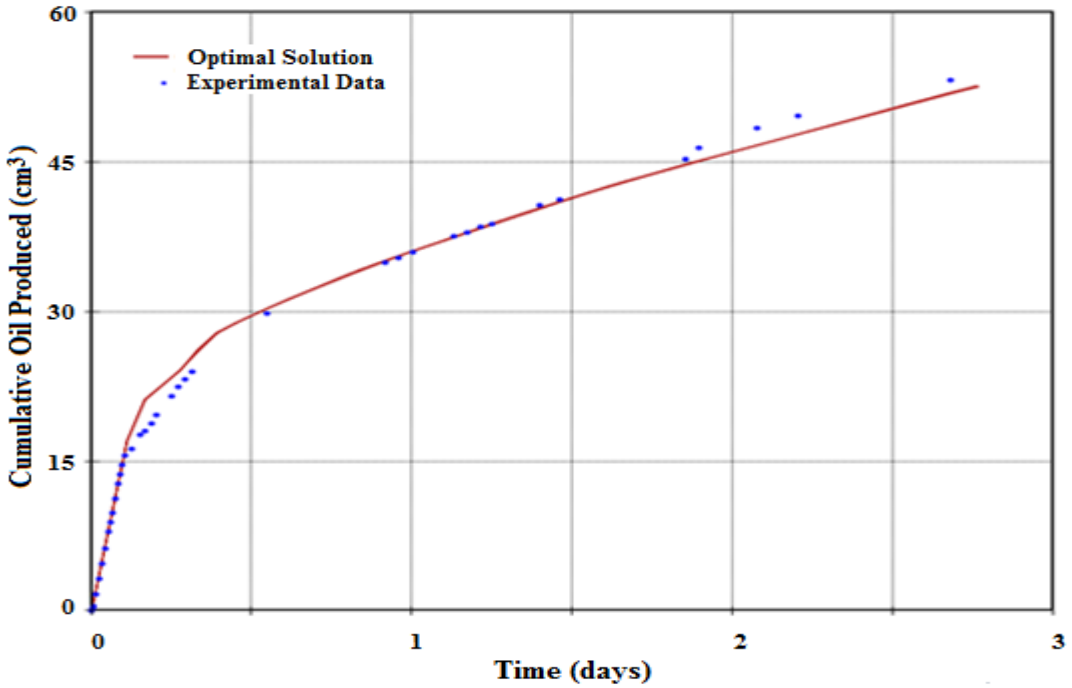

Figure 4-20: Matched (red lines) cumulative oil production against the experimental data (blue dots) obtained from the history matching of Experiment-2 (N_2 injection) using the 2D model approach.

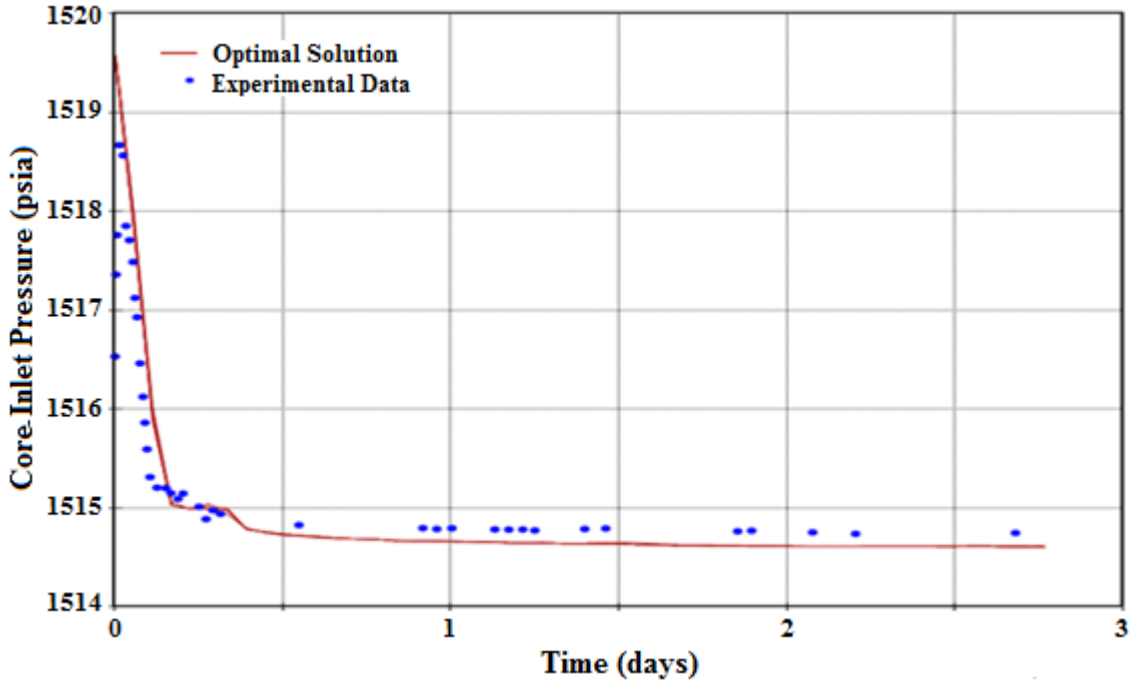

Figure 4-21: Matched (red lines) pressure at the inlet of the core against the experimental data (blue dots) obtained from the history matching of Experiment-2 (N_2 injection) using the 2D model approach.

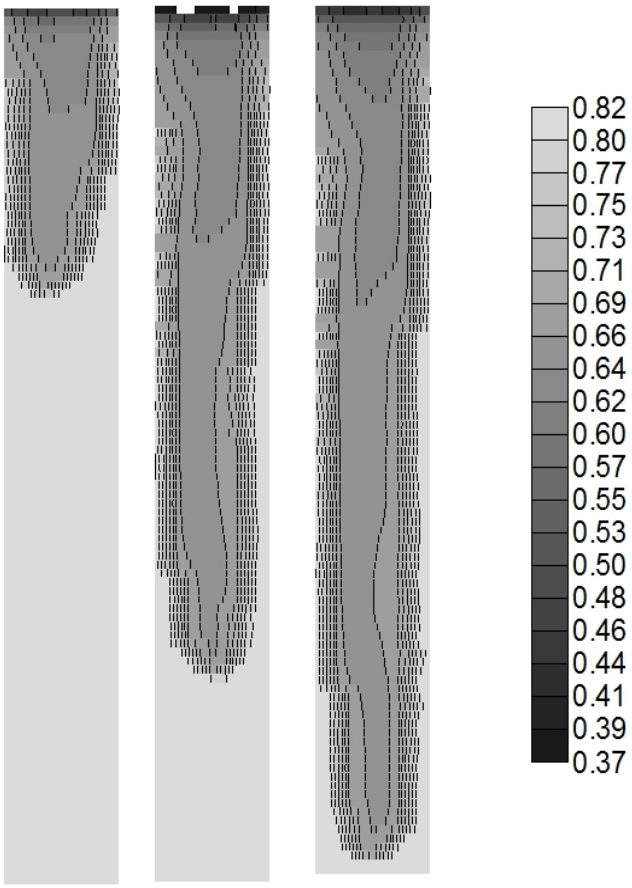

Figure 4-22: Oil saturation profile obtained from the simulation at different pore volume injected. Showing the unstable displacement front and how front propagated over the injection period

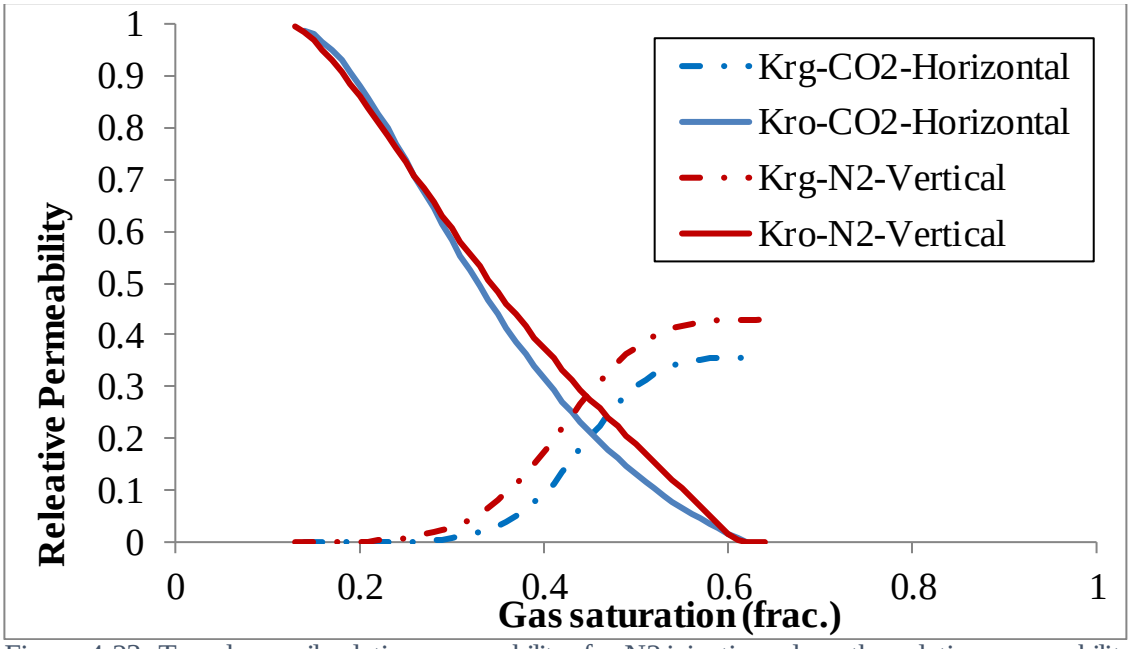

Figure 4-23: Tuned gas-oil relative permeability for N2 injection along the relative permeability estimated for CO2 injection. A fair similarity can be seen between the curves indicating the role of adverse mobility ratio in the estimated relative permeability curves

4.5 SUMMARY AND CONCLUSION

In this chapter, the deficiency of conventional approach of using a one-dimensional (1D) model in order to history match for relative permeability was highlighted. A parametric implicit history matching method was therefore proposed for estimating an unstable relative permeability using a 2D model (as against the conventional 1D) and a versatile parametric correlation to represent the unknown relative permeability function in the history matching. A number of parameters, which can affect the shape of the curves were investigated. The key conclusions on the sensitivities are: that the estimated relative permeability curves were solely controlled by the type of instability and viscosity ratio; and the transition zone where the exchange of mass takes place does not have a significant effect on the shape of the curves.

The two-phase gas/oil relative permeability curves estimated from the CO_2 and the N_2 injections into heavy oil were basically similar, an indication that the shape of the curves does not depend on the gas type but rather on the viscosity ratio and the instability. A one-dimensional model simulation and analysis of the displacements also showed that in such displacements there is competition between gravitational and viscous forces. However, the analysis did not take into account the effect of capillary pressure. It also showed that gravity force was the dorminant mechanism during the CO_2 injection into a

horizontally mounted core saturated with dead crude-J and the type of instability in the displacement was gravity tonguing. However, for the N_2 injection into the vertically mounted core saturated with pre-equilibrated crude-J, viscous force was the dominant displacement mechanism and the type of instability in the displacement was a viscous fingering.

Conclusively, the history-matching procedure using 2D model and a versatile function to represent the relative permeability curve was able to estimate these important flow functions. The key issues observed during the displacement include (i) the numerical dispersion problem that is inherently associated with finite difference, which is the method in commercial simulators and was minimised using a fully implicit compositional simulator. (ii) The time required to simulate the 2D models was high, a new method for reducing the simulation time is the subject of chapter eight. (iii) Non-uniqueness is an issue with most optimisation procedure; for this procedure, a semi-analytical approach where the saturation distribution in the displacement, which has the greatest impact on the shape of saturation profile was verified and presented in chapter seven.

CHAPTER 5

ESTIMATION OF THREE-PHASE RELATIVE PERMEABILITY FROM UNSTEADY STATE HEAVY OIL COREFLOOD EXPERIMENTS WITH INSTABILITY

5.1 INTRODUCTION

The recovery of heavy (viscous) oil by gas or water injection can lead to viscous fingering, a well-known instability phenomenon in porous media that results from adverse mobility ratio between the displaced fluid (oil) and the displacing fluid (gas or water). The consequence of this phenomenon is the bypassing of a significant amount of oil as residual oil with attendant adverse effect on overall recovery factor. The effect of viscous fingering on heavy oil recovery by gas and water has been studied extensively in the laboratory (Sankur and Emmanuel, 1983, Araktingi and Orr Jr, 1993, Cuthiel et al., 2006, Emadi, 2011, Sohrabi and Emadi, 2012) and at the field scale (Garcia, 1983, Mai et al., 2009). Additionally, the stability of heavy oil displacement by gas can be significantly affected by capillary pressure which can lead to exacerbating or dampening of viscous fingers, as the case may be, in the displacement (Outmans, 1962, Peters and Flock, 1981, Jerauld et al., 1984, Kueper and Frind, 1988, Jerauld and Salter, 1990, Riaz et al., 2004).

In order to improve the stability of the displacement front and consequently the sweep efficiency, a number of techniques have been investigated which often involve the simultaneous flow of three or more immiscible fluids, including oil, water and gas. To fully understand how these techniques, improve reservoir production, and for the purposes of performance prediction and forecasting, numerical simulation models are now increasingly being utilised, due mainly to the constant enhancement of computer speed and memory. Hence, by imploring a typical reservoir simulator, several recovery methods can be evaluated for feasibility and efficiency in order to determine the recovery method that is most efficient in terms of economy, practicality and environmental impact.

A number of these simulators including most commercial simulators are Darcy-type, based on the concept of relative permeability. For the recovery methods involving the simultaneous flow of three fluids, a three-phase relative permeability would be required to simulate the process. Inaccurate measurement of this important flow function has been identified as one of the major sources of uncertainty in performance prediction (Boukadi et al., 2005).

Three-phase relative permeability has been widely investigated for immiscible gas injections (Kokal and Maini, 1990, Muqeem et al., 1993) and for Water Alternating Gas (Land, 1968, Shahverdi and Sohrabi, 2011, Shahverdi and Sohrabi, 2013, Akhlaginia et al., 2013). Two major experimental techniques are available for the estimation of three-phase relative permeability, the steady state and the unsteady state method (Honarpour et al., 1986). In the steady state displacement method, the two phases simultaneous flow at fixed ratio continuously until the saturations in the core and the pressure drop across the sample is constant, an indication that the system has achieved steady-state. It is difficult to estimate relative permeability curves using this method because of the inherent experimental artefacts associated with the method. The more common approach is the unsteady-state method, which is also known as the dynamic displacement method (section 1.1) where the porous media is initially saturated with oil at connate water saturation and then displaced by a second fluid. The produced volume of the injected fluid and the produced volume of oil, as well as the pressure drop across the medium, are then used to calculate the relative permeability curves using analytical techniques that are based on methods developed by Welge (1949) and Johnson et al (1959). These include the Johnson-Bossler-Naumann (Johnson et al., 1959), popularly known as the JBN method and the Jones and Roszelle analytical method (Jones and Roszelle, 1978). Additionally, history matching technique is also used to determine three-phase relative permeability by representing the curves with parametric equation and matching the production history data.

Although the importance of reliable experimental data in numerical analysis is well recognised, laboratory measurements of three-phase relative permeability are usually not attempted. The reason for this appears to be the time and expense involved as well as the poor reliability of available experimental data (Muqeem et al., 1993). Quite often, relative permeability values are estimated from correlations such as Stone I and II models (1970,

1973) and the Baker model (1988). The Stone models are probabilistic methods that use two sets of two-phase relative permeability data to predict the relative permeability of the intermediate wet phase in a three-phase system. Both Stone models were based on water-wet systems in which gas and water relative permeability depend on the gas and water saturations respectively. The Baker model is a simplistic three-phase relative permeability correlation that is based on Saturation-Weighted Interpolation (SWI) between two-phase relative permeability data in which the three-phase relative permeability of each phase is assumed to be a function of two saturations. Relative permeability has also been examined to strongly depend on saturation history in cyclic processes otherwise known as hysteresis. This phenomenon has been extensively investigated experimentally and numerically (Land, 1968, Carlson, 1981, Jerauld and Salter, 1990, Braun and Holland, 1995, Spiteri et al., 2008). A few three-phase relative permeability models have been proposed which incorporated hysteresis, compositional and interfacial tension (IFT) effect. These include the Jerauld (1997) model which attempts to predict three-phase, gas, oil and water hysteresis as well as the dependence of relative permeability on composition and gas/oil IFT. Blunt (2000) empirical model also accounts for hysteresis, changes in hydrocarbon composition as well as trapping of gas, oil and water.

Since all these correlations utilise two-phase relative permeability data as input in the estimation of three-phase relative permeability, their accuracy can, therefore, be complicated7 by uncertainty in the two-phase relative permeability data. More so, when the two-phase relative permeability for a heavy oil displacement by gas or water is determined by history matching technique, it is important to ensure that an appropriate model which mimics the instability in the system is utilised. For example, using a one-dimensional model to represent a displacement with an unstable front in a history matching process would subdue the instability in the front and hence any obtained relative permeability from the process would not be a representative of the actual system. An additional dimension(s) would, therefore, be required to effectively capture the instability occurring in the front. It is important for any numerical studies of the motion of unstable front to faithfully follow the development of the instabilities. This indicates that a relative permeability obtained from a stable displacement when used in the simulation of an unstable displacement may lead to erroneous result (Sherwood, 1987, Taura et al., 2016).

In heavy oil displacement by gas or water, the displacement is highly unstable due to the adverse viscosity ratio between the displacing fluid and the heavy oil. Also, during gas injection, such as CO_2, significant mass transfer take place that contributes to the displacement mechanism. These benefits include oil swelling, viscosity reduction, increase in oil density and vapour extraction (Farouq Ali, 1976, Mayer et al., 1988, Chung et al., 1998, Thomas et al., 1999). Therefore, it is important to investigate the effect of these mechanisms on the estimated three-phase relative permeability. Although several investigators have questioned the futility of estimating relative permeability in unstable systems arguing that it is the parameter which is normally varied to match history data in field simulation (Maini, 1998), however, it can be shown that the choice of relative permeability curves can have a significant effect on the fluids saturation distribution and hence the long-term performance prediction of the displacement method.

The objective of this chapter is to investigate three-phase relative permeability in heavy oil systems in which instability occurs. A history matching approach using a compositional simulator, and a 2D model would be adopted to determine two-phase relative permeability data and a modified Stone empirical model would be employed to estimate the corresponding three-phase relative permeability.

5.2 METHODOLOGY

The approach adopted for the estimation of gas, oil and water, three-phase relative permeability from heavy oil dynamic displacement experiment, was based on empirical correlation, where the three-phase flow function was estimated from two sets of two-phase data, the gas/oil and the oil/water relative permeability data (Honarpour et al., 1986, Modaresghazani et al., 2015). Two different relative permeability functions were used to represent the two sets of two-phase flows. The gas/oil relative permeability was represented by a flexible three-parameter correlation known as the L.E.T-type correlation (Lomeland et al., 2005) due to its versatility in honouring the so-called "S-behaviour" of gas relative permeability (equations 13-15), while the water/oil relative permeability was represented by a simple Corey (1954) correlation (equations 12a & 12b). For the three-phase relative permeability, the Stone II (1973) model was chosen because of its simplicity and bivariate nature, where both gas and water relative permeability can affect oil relative permeability in the three-phase flow (equation 18). A two-dimensional (2D) high-resolution model (100x80) which has been sensitised for grid size effect (Section

1.1) was used to account for the displacement instability and a compositional simulator (CGM-GEM) was utilised for the mass transfer effect. The history matching optimisation process was carried out using CMG-CMOST software. Table 5-1 presents the experiments used in this study.

Table 5-1: Experiments used in the investigation of three-phase relative permeability

Exp. No.	Description	Fluids	Core Orientation	Test conditions
. 1	Secondary CO_2 injection into Dead Crude-J Tertiary Water Injection into Dead Crude J and CO_2	Injection fluid: CO_2, Water Resident oil: dead Crude-J Resident brine: 20000 ppm	Horizontal	T=28°C, P=1500 psig
5	Secondary Water injection into Dead Crude-J	Injection fluid: brine Resident oil: dead Crude-J Resident brine: 20000 ppm	Horizontal	T=28°C, P=1500 psig
6	Simultaneous Water and CO_2 injection into dead Crude-J	Injection fluid: brine, CO_2 Resident oil: dead Crude-J Resident brine: 20000 ppm	Horizontal	T=28°C, P=1500 psig

5.3 ESTIMATION OF TWO-PHASE OIL/WATER RELATIVE PERMEABILITY (EXPERIMENT-5)

In Experiment-5, water was injected in secondary mode into Crude-J in a horizontal core at the experimental pressure and temperature (1500psi and 28^0C). The injection rate was 7cc/hr similar to the gas injection. The details of the experiment can be found in Emadi (2012). To history match the experiment, a simple Corey (1954) correlation was used to represent the relative permeability function in the optimisation process. Furthermore, drainage capillary pressure data obtained from mercury intrusion test was included in the estimation for the relative permeability. Although the Pc curve shown in Figure 5-1 does not fully represent the capillary forces in the system, it is, however, the closest available information. Similarly, a compositional simulator was employed for the flow simulation even though the oil has been pre-equilibrated with the brine in the experiment to mitigate any mass transfer. In addition, the injected brine was also of the same composition (20000 ppm) with the established connate water in the core. Therefore, the purpose of using the compositional simulator was purely for comparative purposes. Hence, comparison of the estimated relative permeability curves with that obtained for gas injection (section

4.3) can indicate the impact of the type of injection fluid and viscosity ratio on relative permeability and displacement efficiency.

Prior to the start of the history matching studies, sensitivity on grid size was carried out using four different grid size models. Figure 5-2 shows that the displacement is relatively stable and corroborates what was observed in the experiment. This is mainly due to the stabilising effect of the capillary pressure (Civan and Donaldson, 1989), as seen in Chapter 6. Also, Figure 5-3 shows that the cumulative oil recovered for all the models were exactly on top of each other, an indication of a stable front. Hence, the 100x80-grid size model was adopted for easy comparison with the gas injection experiment. Figure 5-4 and Figure 5-5 illustrate the matched oil recovery and the pressure at the inlet of the core for Experiment-5 with capillary pressure included while Figure 5-6 shows the estimated relative permeability with the Pc included.

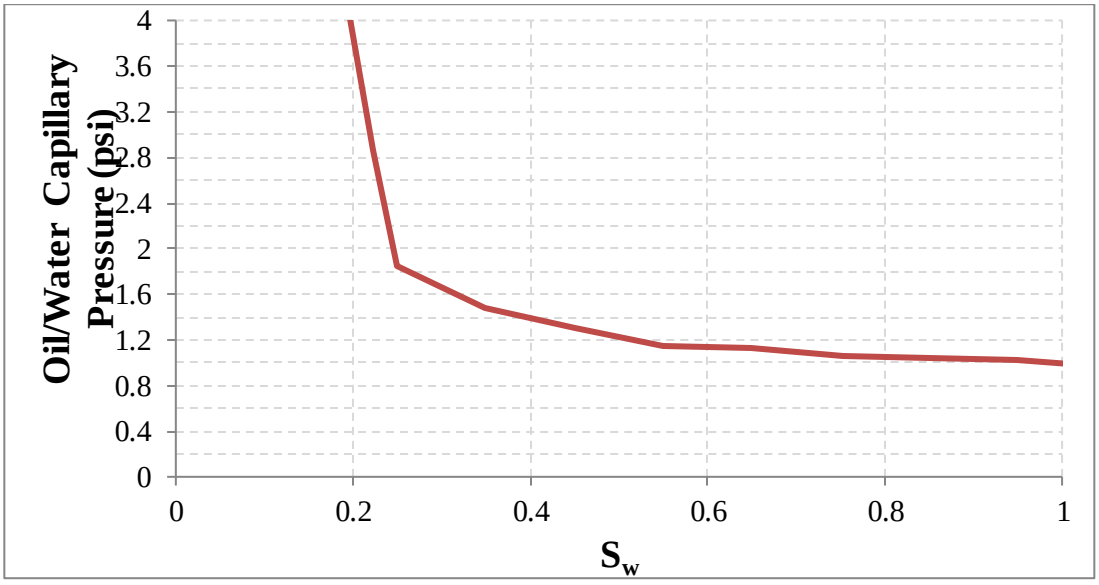

Figure 5-1: Water/Oil Capillary Pressure obtained from mercury intrusion test

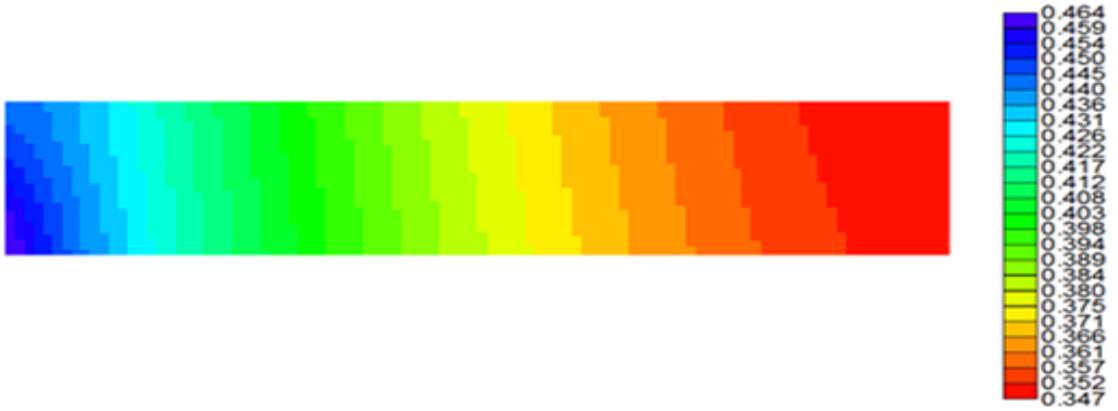

Figure 5-2: Water saturation distribution before breakthrough obtained from the simulation, highlighting high degree of stability in the water-front as a result of capillary pressure inclusion

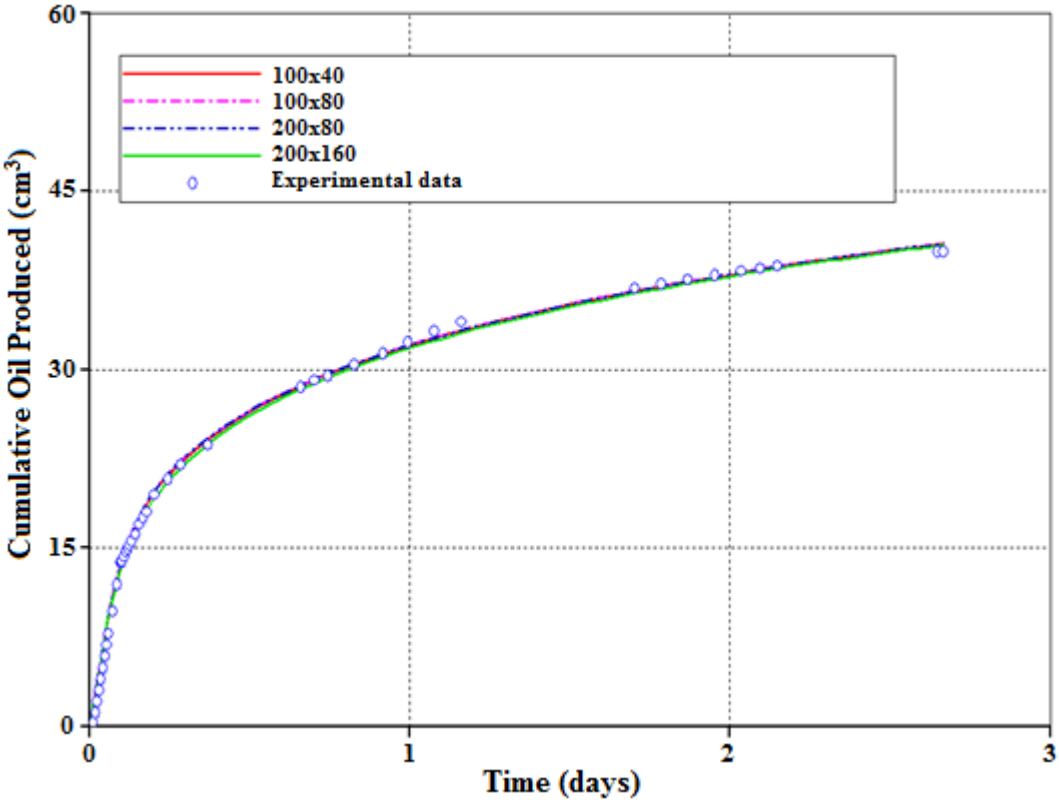

Figure 5-3: Experiment-5 Cumulative oil produced, simulated using different grid size models (100x40, 100×80, 200×80, and 200×160), showing curves lying on top of each other, an indication of independence of the results on the model grid size.

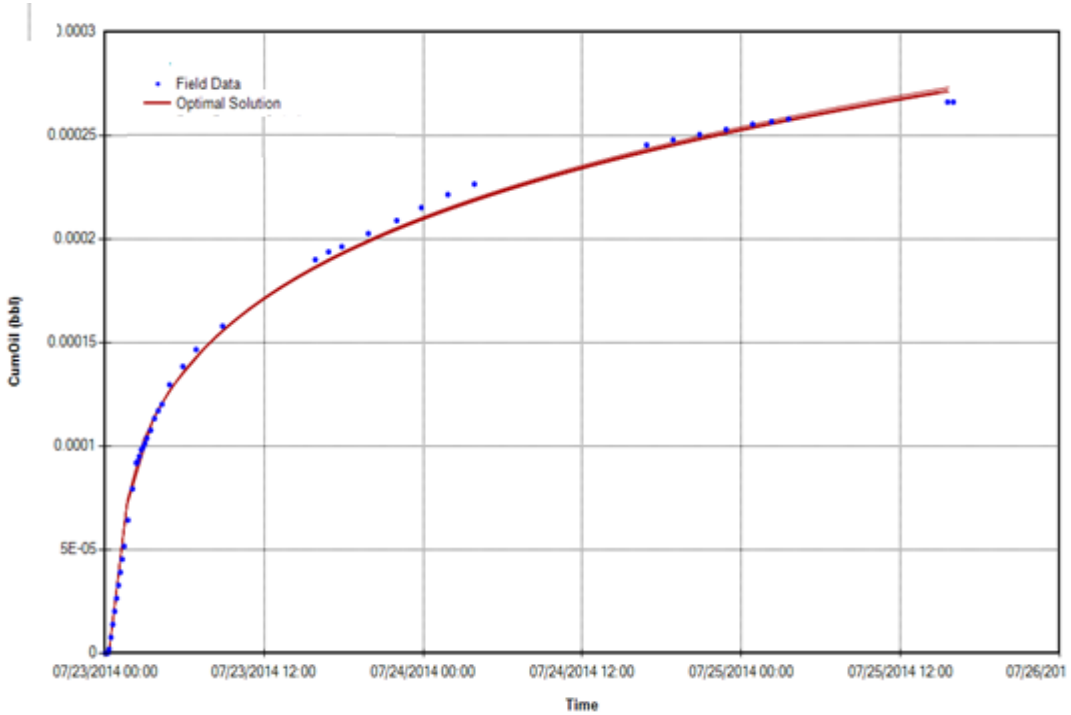

Figure 5-4: Matched cumulative oil production against the experimental data for the Experiment-5 with Pc included.

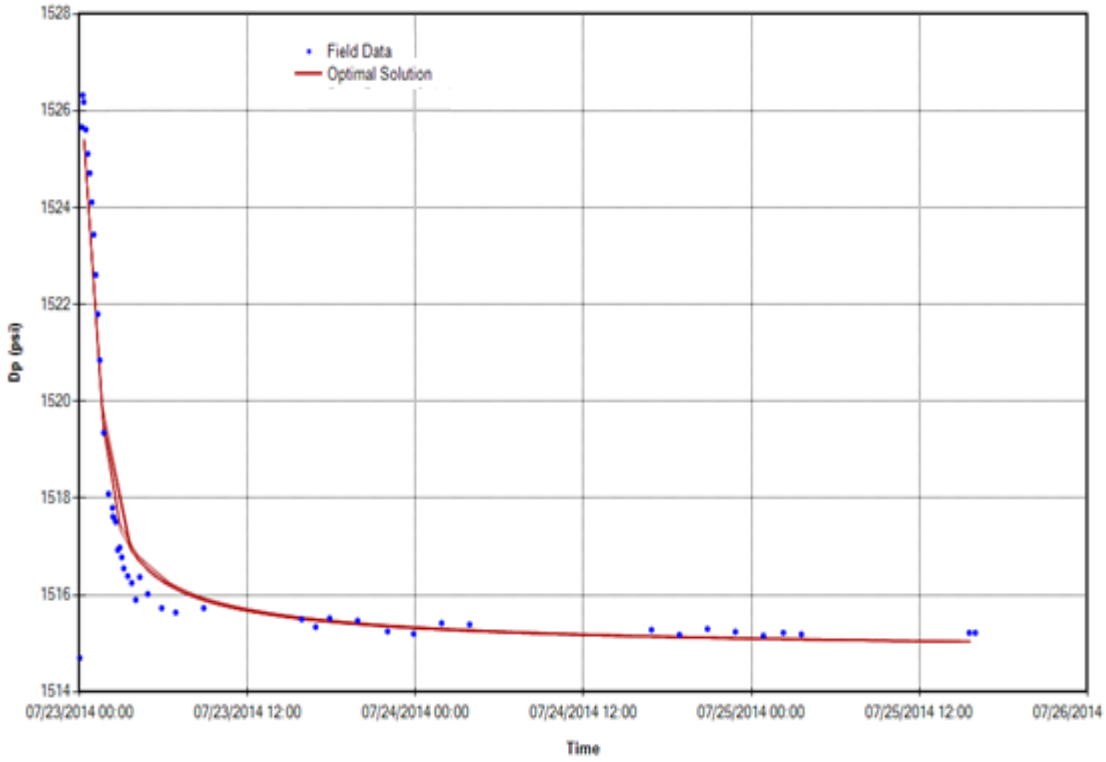

Figure 5-5: Matched pressure at the inlet of the core against the experimental data for the Experiment-5 with Pc included.

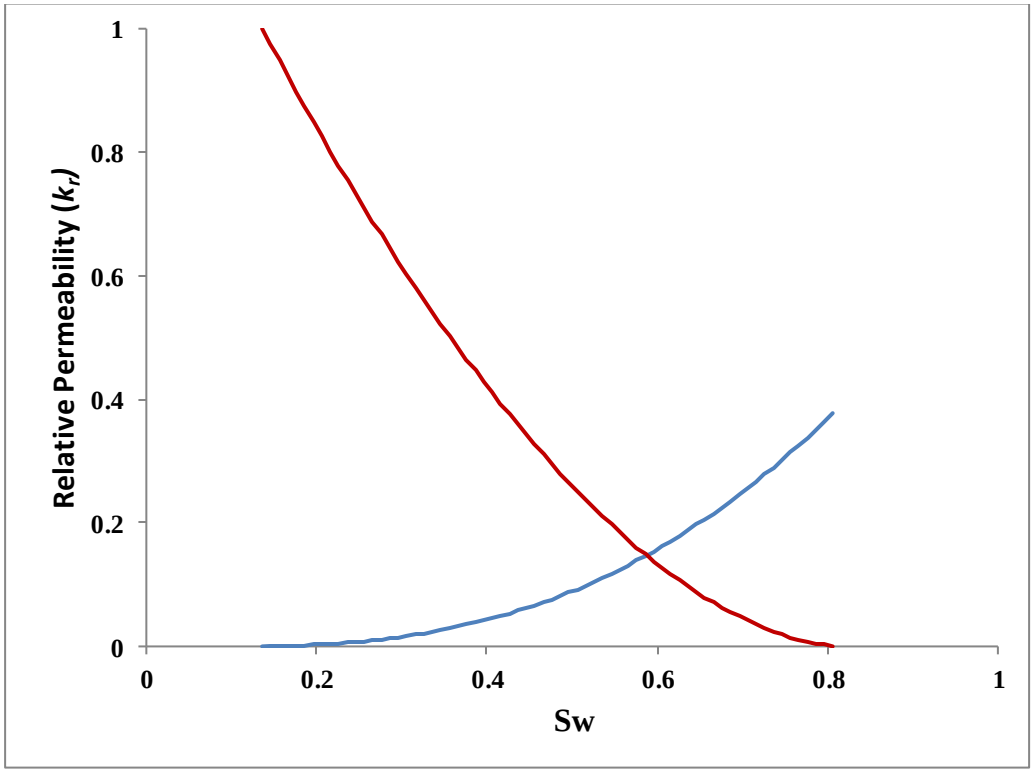

Figure 5-6: History matched oil/water relative permeability curves estimated for experiment-5 with Pc included.

In summary, the grid sensitivity study has shown that the displacement was not sensitive to grid size when Pc was included because the displacement was stable. The shape of oil/water relative permeability curves is not similar to that of CO2/Oil (section 4.3) because the mechanisms of displacement are different. The inclusion of Pc has helped in stabilising the displacement front. A case with zero capillary pressure was sensitised in Chapter 6. The relative permeability obtained from the secondary water injection was later used for simulating water-alternating-gas injection scenarios.

5.4 SIMULATION OF TERTIARY WATER INJECTION

The tertiary water injection experiment was conducted as a chase flood of the secondary CO_2 injection in Experiment-1. Like in conventional WAG processes, the chase waterflood encounters two regions of trapped oil, the capillary trapped oil in the swept area in which CO_2 dissolution has occurred and significantly reduced the oil viscosity, and a bypassed region whose oil retains original viscosity value. Based on the findings from the coreflood experiment, water-alternating-CO_2 is potentially the most efficient displacement process compared to only water or CO2 injection (Emadi, 2012, Emadi et al., 2011a). This is due to the method benefiting from better pore-scale and sweep efficiencies of CO2 and water, respectively. Current knowledge of WAG modelling is based on the hysteresis formulations in which relative permeability functions of water/oil/gas are adjusted in successive injections of water and gas. In this method, based on the adjustment of estimated three-phase relative permeability of water/oil/gas in previous cycles, the saturation functions (kr, Pc) of subsequent cycles are predicted accordingly. Therefore, because of the influential CO_2-oil interactions, there are several peculiar issues in tertiary water injection that need to be taken care of in the simulation. These are listed as follows:

1 viscosity and density of the oil in the swept region,
2 viscosity and density of the bypassed oil,
3 viscosity of the remaining CO_2 in the core at the end of the secondary CO_2 injection,
4 different capillary forces between CO_2/oil/water in the swept and bypassed areas.

These flow phenomena can all affect the simultaneous flow of water, oil, and CO_2. It is important therefore to determine the properties of oil in the swept area at the end of each CO_2 injection cycle. Figure 5-7 illustrates CO_2 and oil viscosities at the end of secondary CO_2 injection with the swept area having a lower viscosity (16cp) and the bypassed area

retaining the original oil viscosity of 617cp. The transition zone between the two residual oil regions (pink layer) is a huge source of uncertainty because measurement of the effective diffusion coefficient that controls transfer at the interface is highly unreliable (Weissberg, 1963). The diffusion coefficient is also dynamic and time dependent (Kavousi et al., 2013), therefore, to reduce the uncertainty in the parameter, extensive PVT experiments need to be performed. However, it must be emphasised that these experiments are not easy to conduct and are highly unreliable especially for heavy oil systems and no attempt was made in this work to determine effective diffusion coefficient and its dynamic nature.

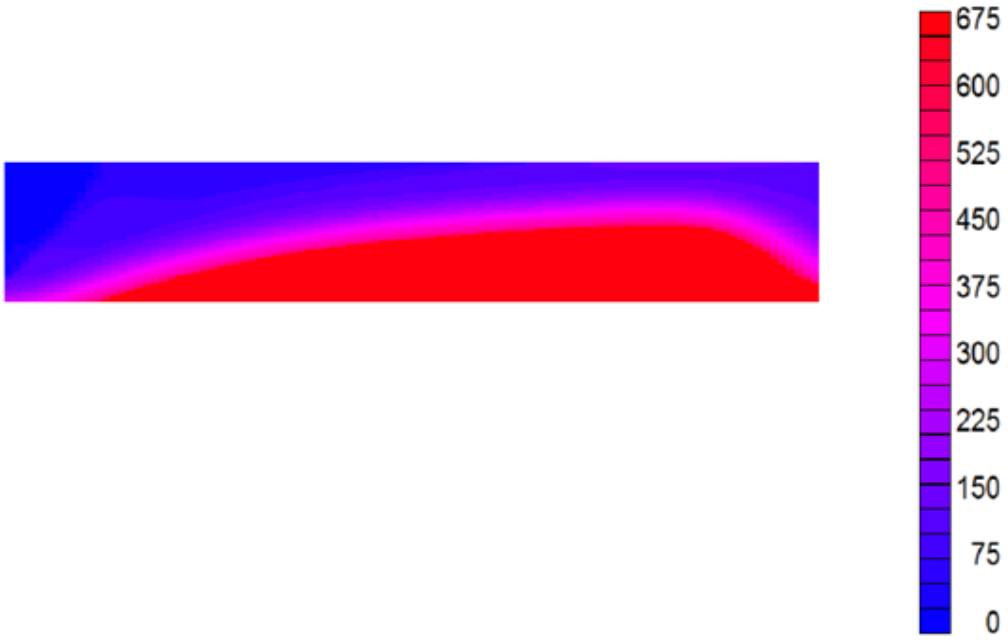

Figure 5-7: Oil viscosity at the end of the tertiary water injection indicating the trapped oil (blue area), the bypassed oil (red area) and the transition zone (pink)

5.5 ESTIMATION OF THREE PHASE RELATIVE PERMEABILITY FUNCTIONS FOR HEAVY OIL SYSTEM

To estimate three-phase relative permeability for heavy oil system in which instability occurs, Experiment-1 where CO_2 was first injected to displace the oil followed by water injection was considered. During the water injection, which was at tertiary mode, three fluids, water, oil and gas flowed, leading to three-phase flow phenomenon. To estimate the three-phase relative permeability for the displacement, an implicit parametric

approach was used, similar to the two-phase flow. L.E.T-type and Corey correlations were used to represent the two-phase gas/liquid and oil/water relative permeability respectively in the history matching process. Stone II model (equation 21) in which gas and water relative permeability can affect three phase oil relative permeability was employed for the three-phase flow of gas, oil and water. Having established the oil viscosities of swept and bypassed regions as 16cp and 617cp, in the prior gas injection respectively (section 4.2), the three-phase relative permeability was history matched. Figure 5-8 shows the simulation results in comparison with experimental data for the cumulative oil recovered, cumulative gas produced, the differential pressure across the core and the cumulative water production. The estimated tertiary relative permeability are shown in Figure 5-9. It can be observed that not only did the end-point saturations were affected by cyclic injection but also, the relative permeability have changed.

Additionally, the hysteresis in the oil/water relative permeability is much smaller compared to that of gas/liquid relative permeability. This can be as a result of the large variation in viscosity ratios at the different cycles. For instance, in the secondary CO_2 injection, pure CO_2 with a viscosity of 0.072cp displaced the resident oil with a viscosity of 617cp, whereas in the tertiary water injection, CO_2 in place (CO_2 mixed with light hydrocarbon components) with a viscosity of 0.8cp was displaced by water with a viscosity of 0.9cp (which is more viscous than the CO_2). Therefore, viscosity pairs are critical in the estimation of relative permeability, which in turn can be linked to the occurrence of frontal instabilities. Also, a pronounced change in endpoint saturation of water/oil relative permeability was also observed, indicating a shift in the residual oil saturation in the waterflooding scenario. This improvement in endpoint saturations can be attributed to the lower oil viscosity in the area previously swept by CO_2 (oil with viscosity of 16cp), making the oil more mobile. Additionally, based on this simulation result, it can be concluded that CO2-WAG can perform more efficiently in the case where CO2 initially dissolves in the oil, reduces its viscosity, and is subsequently followed by water injection, which then readily recovers more mobile oil.

$$K_{ro} = K_{rocw} * \left\{ \left(\frac{K_{row}}{K_{rocw}} + K_{rw} \right) \left(\frac{K_{rog}}{K_{rocw}} + K_{rg} \right) - K_{rw} - K_{rg} \right\} \qquad 21$$

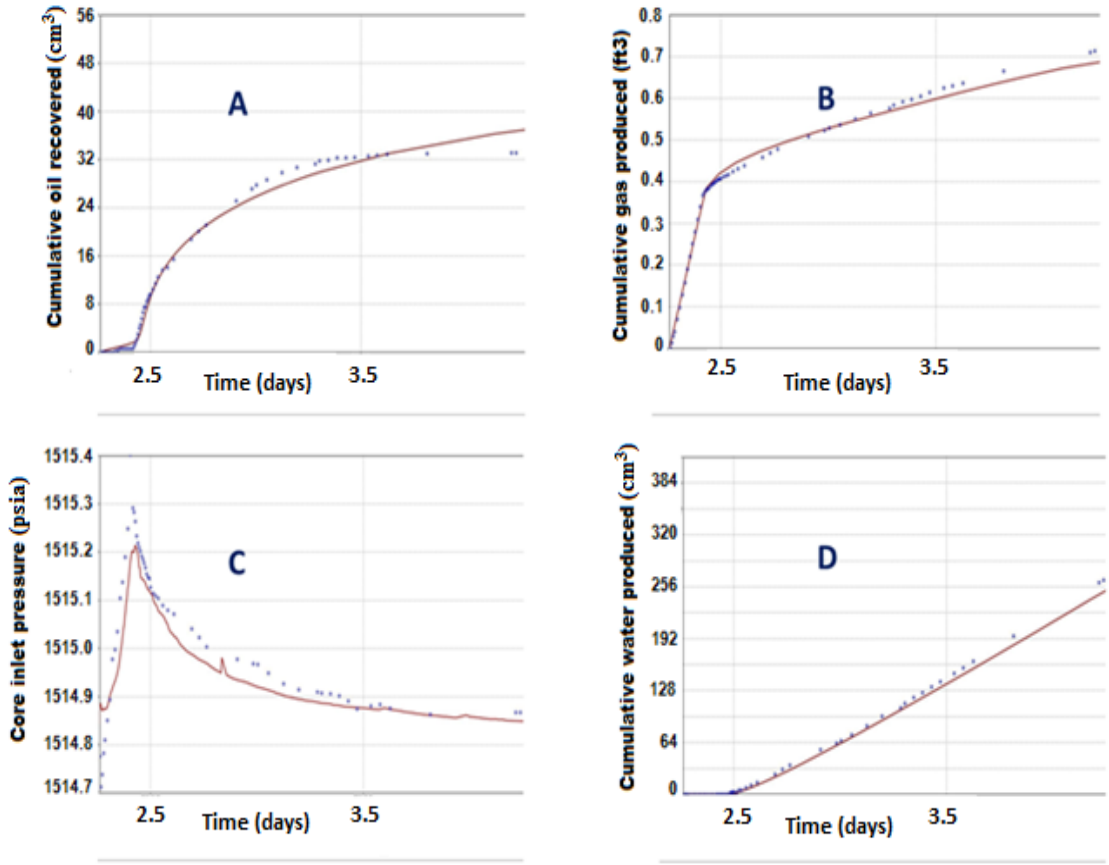

Figure 5-8: Simulation results obtained through history matching (red line) against the experimental data (blue dots) for (A) oil production, (B) gas (CO_2) production, (C) differential pressure across the core, and (D) water production for the tertiary water injection of Experiment-1 (note: time continuous after the secondary CO_2 injection)

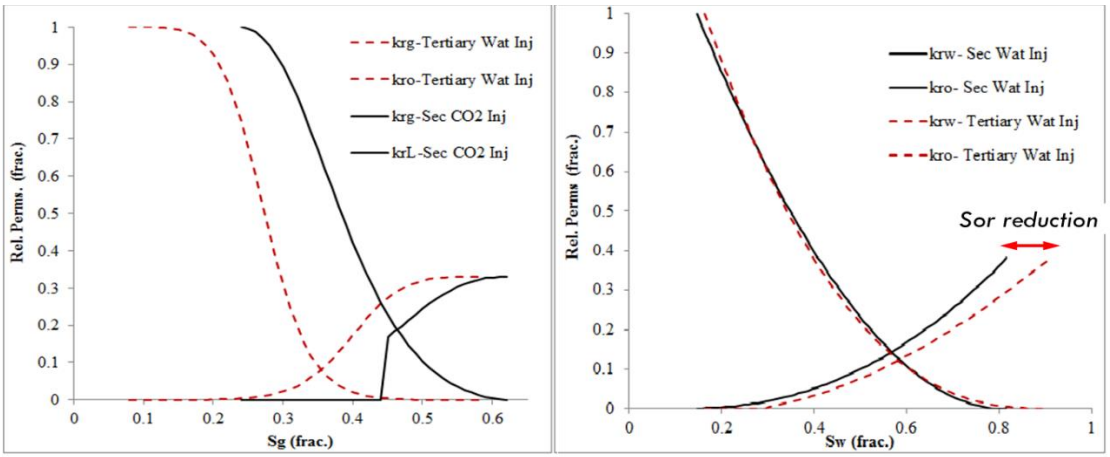

Figure 5-9: Water-oil (right image) and oil-CO2 (left image) relative permeability obtained by history matching the corresponding coreflood experiments. The sequence of displacements, i.e. Secondary or tertiary, can affect the relative permeability functions

Figure 5-10 shows the simulation results of the water saturation distribution, which highlights the sweeping pattern of the tertiary water advancement. In the early stage of water injection, water tended to underride the resident CO2 and oil. However, as shown

in the middle image, the water-front exhibited a more stable shape when it encountered the bypassed oil with high viscosity (617cp). As the water advanced, the front flowed through the pre-swept area easier than the bypassed oil, which brought about another type of instabilities controlled by contrast in viscosities of oil in different areas. The main finding here was the preference of water to displace the resident gas compared to the residual oil.

In conventional WAG injection (light to medium oils), it is believed that water and gas would invade different paths based on the competition of capillary forces (wettability)(Sohrabi and Fatemi, 2013). However, as seen in the simulation of this experiment, the large contrast in viscosities of displacing and displaced fluids dictated the selection criterion for the water and gas paths. This process has another implication; most of the hysteresis models have been derived based on the change in wettability characteristics, e.g. Land's model (Land, 1968). However, in this case, the viscosity ratio changes both pore-scale and sweep efficiencies, necessitating a thorough investigation on the validity of hysteresis models in adverse mobility conditions.

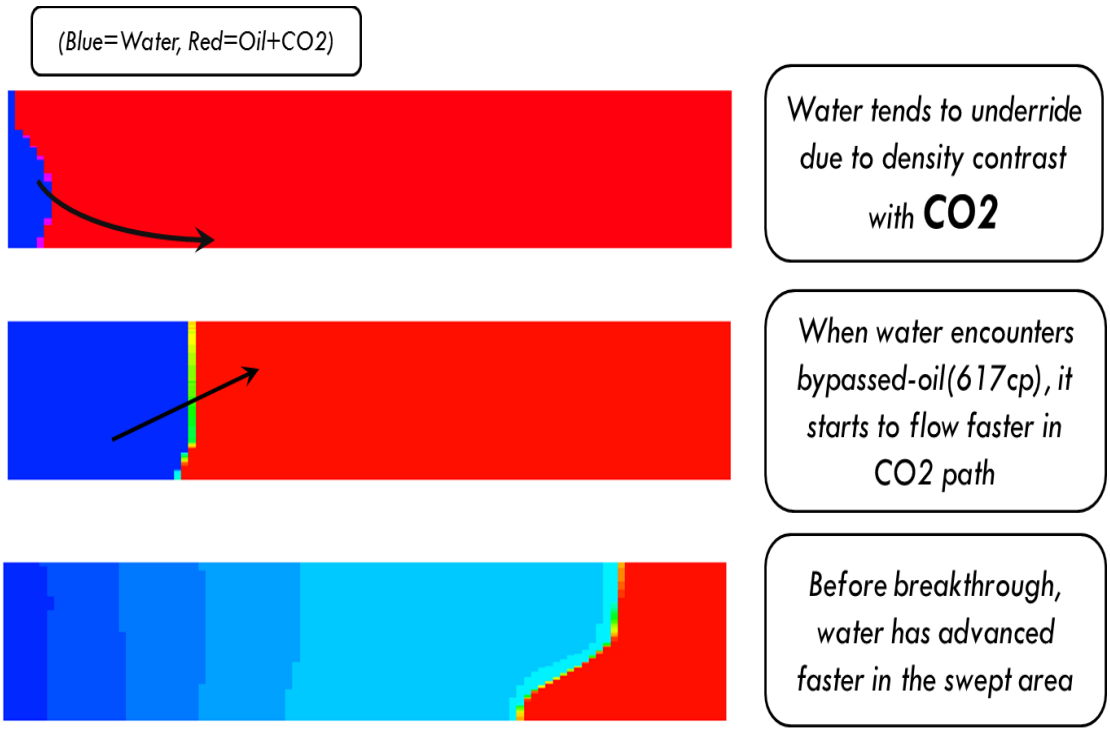

Figure 5-10: Water saturation profile at different injection times indicating the preferred path by water resulting from the effect of preceding gas (CO_2) injection.

5.6 SIMULTANEOUS WATER ALTERNATING GAS INJECTION INTO HEAVY OIL (EXPERIMENT-6)

Experiment-6 is a coreflood experiment where water and CO_2 were simultaneously injected at equal rates and the process is known as Simultaneous Water and Gas (SWAG) injection. In conventional light oil displacement using this method, capillary forces play a crucial part in the preference for pore occupancy by the fluids (Ma et al., 1995). However, in heavy oil displacement using SWAG, where the gas is soluble in the oil leading to its viscosity reduction, viscous forces are dominant over capillary forces in preference for pore occupancy by the fluids (Farzaneh et al., 2016). Consequently, from flow functions point of view, a reliable set of relative permeability functions coupled with a consistent viscosity reduction correlation suffices to simulate the coreflood experiment.

In this section, the SWAG coreflood experiment was simulated where the two-phase gas/liquid and oil/water relative permeability functions obtained in the previous section were used in a three-phase relative permeability correlation since the experimental condition as well as rock and fluid properties are similar. Considering that CO_2 has notably higher mobility compared to water during the simultaneous injection, evident from the different breakthrough times of secondary CO_2 (Experiment-1) and water (Experiment-5) injections (where the breakthrough time of CO_2 was significantly earlier), it would be a reasonable assumption, therefore, that CO_2 flow can be controlled by the relative permeability obtained from the secondary CO_2 injection process (Figure 5-9). However, two choices exist for the water relative permeability based on the water injection modes, either secondary or tertiary relative permeability. To determine the appropriate curves to use, two corresponding simulations were ran, Figure 5-11 shows the results of the simulations compared with the experimental data. The fluid production profiles highlighted that a reasonably good match can be achieved when the tertiary oil/water relative permeability was employed.

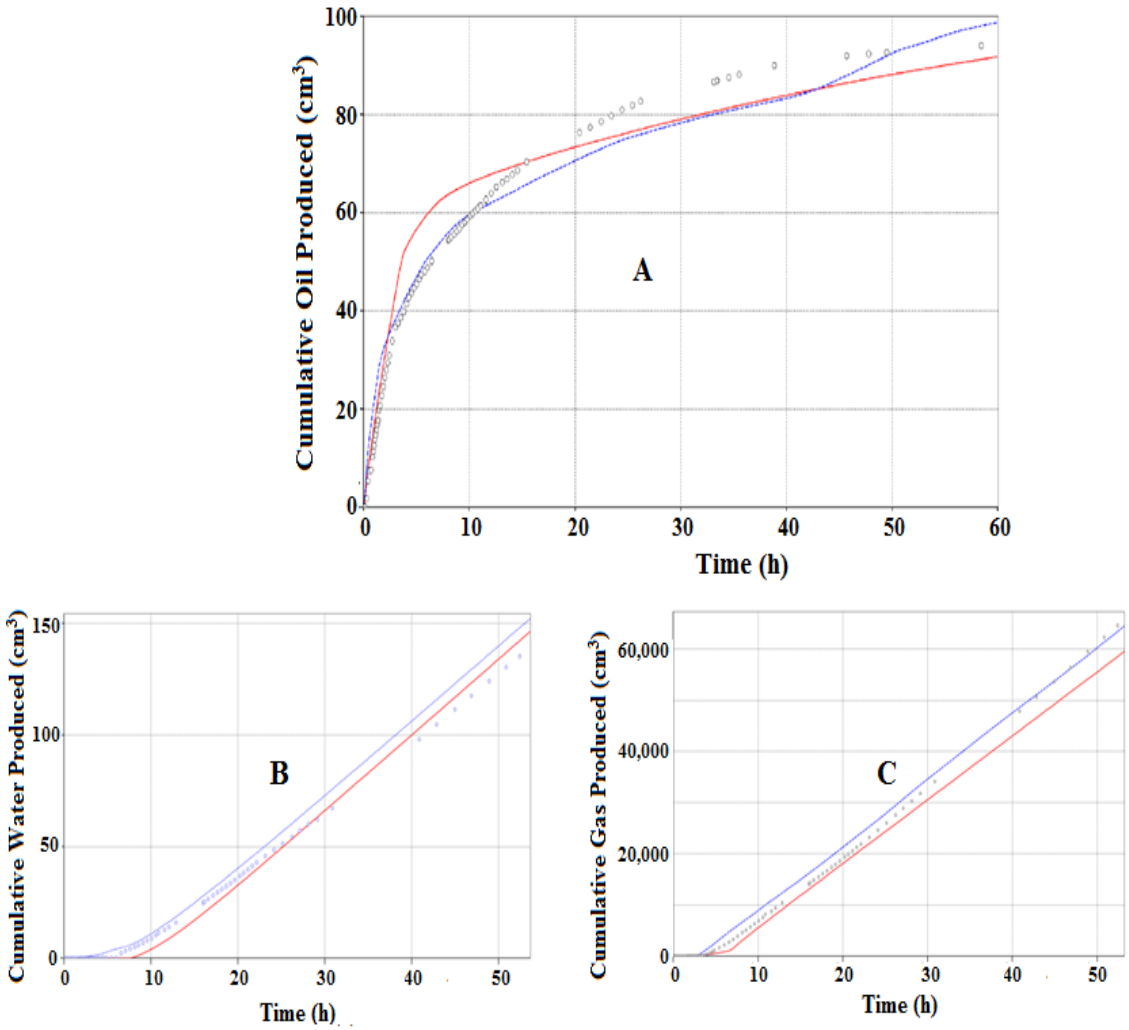

Figure 5-11: Results of the fluid productions ((A) oil, (B) water, and (C) CO2) obtained from simulation runs using secondary (red curves) and tertiary (blue curves) water-oil relative permeability curves. Comparison of simulation against experimental data (dots) indicating a better estimation for the case using tertiary water-oil relative permeability.

Although the simulations did not match the experimental data perfectly, the mismatch is reasonable for this highly complex system. In particular, the blue curve in Figure 5-11 (tertiary water-oil relative permeability case) has demonstrated a better match in the early stages in which viscous forces were dominant. However, after two pore volumes of injection, a slight degree of deviation between the simulation and experimental data was observed. This slight difference can be attributed to the competition between the viscous and capillary forces. Moreover, there was also a notably high discrepancy in the predicted differential pressure by the two simulations (Figure 5-12). Although the blue curve (tertiary water-oil relative permeability) had a better estimate with regards to the experimental data compared to the red (secondary water-oil relative permeability), the difference during the early stage of the injection is large. Nonetheless, it should be

mentioned here that, apart from the mismatch on the maximum differential pressure, the match between the blue curve and experimental data is within an acceptable limit for preliminary studies. In oil displacement, the maximum differential pressure is mainly controlled by oil flow characteristics, whereas the declining and the constant DP section are related to the finger before breakthrough and displaced fluids' movements after the breakthrough, respectively. However, the discrepancy in maximum DP can also be as a result of the diffusive flow of CO_2, which was not included in the simulation. Diffusion of CO_2 into the oil facilitates the mixing of the oil and CO_2, which in turn reduces the oil viscosity and hence better movement of the resident oil. This process can reduce the oil resistance to flow and hence reduce the maximum DP. It should be pointed out that this discrepancy in DP was also observed in the secondary CO_2 injection simulations but not in the secondary water injection. Therefore, considering the diffusive flow of CO_2 can be helpful in reducing the discrepancy, sensitivity on rate of diffusion was carried out in Chapter 6.

Figure 5-13 shows the result of simulation of the gas saturation distribution before the breakthrough, indicating the injected CO_2 tending to segregate gravitationally. This implies that CO_2 injection would be more efficient if injected in a gravitationally stable approach. On the other hand, Figure 5-14 illustrates the pattern of water frontal advancement. It can be observed that water started to flow downwards near the inlet but then suddenly tended to advance upward and followed the CO_2 path, similar to the WAG displacement. Therefore, the efficiency of the SWAG displacement is mainly controlled by the extent of CO_2 penetration into the oil, which reduces the oil viscosity. Figure 5-15 shows the viscosity of the resident oil at two stages, the CO_2 breakthrough and the end of SWAG injection. The poor CO_2 sweep efficiency has resulted in a relatively large volume of bypassed oil (red area in Figure 5-15). Figure 5-16 illustrates the oil saturation distribution at the end of the simulation and shows the distinct characteristic of the displacement. It indicates that the residual oil saturation at the top of the core has a relatively low value, approaching less than 5%, whereas the residual oil saturation at the bottom of the core, which has only been partly swept by water, has a relatively high residual oil saturation that was up to about 60 percent.

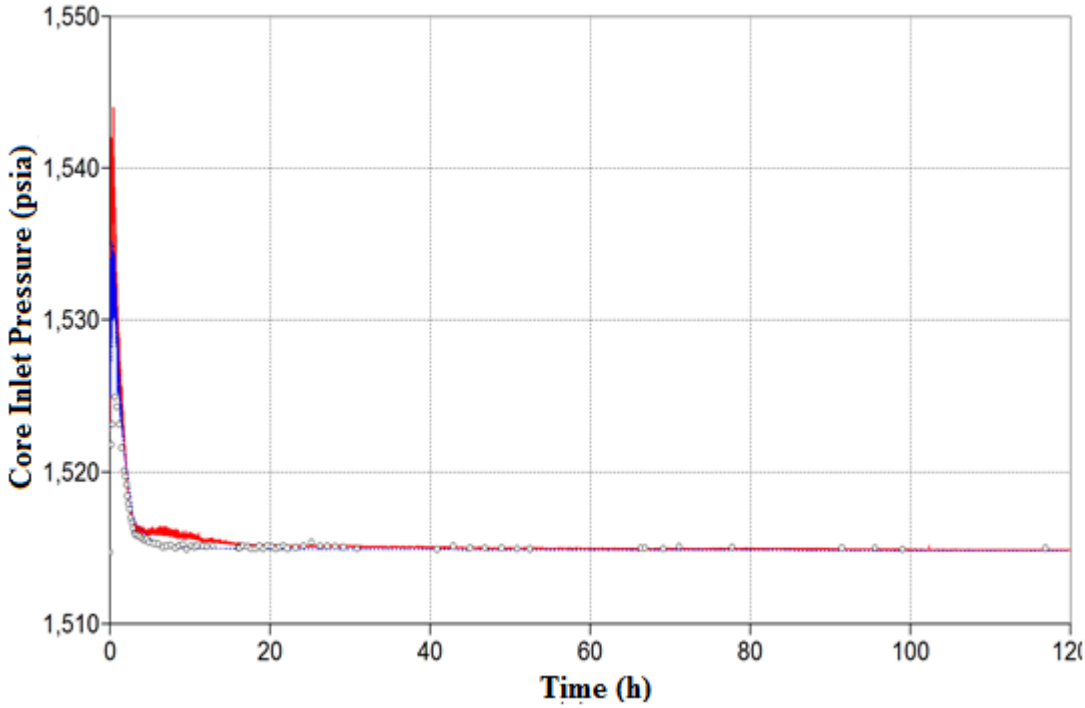

Figure 5-12: Recorded pressure at the inlet of the core (outlet pressure was constant at 1514.7 psia) obtained by simulation (blue and red curves for tertiary and secondary water-oil relative permeability curves) and experimental data (dots). A better match was achieved when tertiary water-oil relative permeability was used in the simulation.

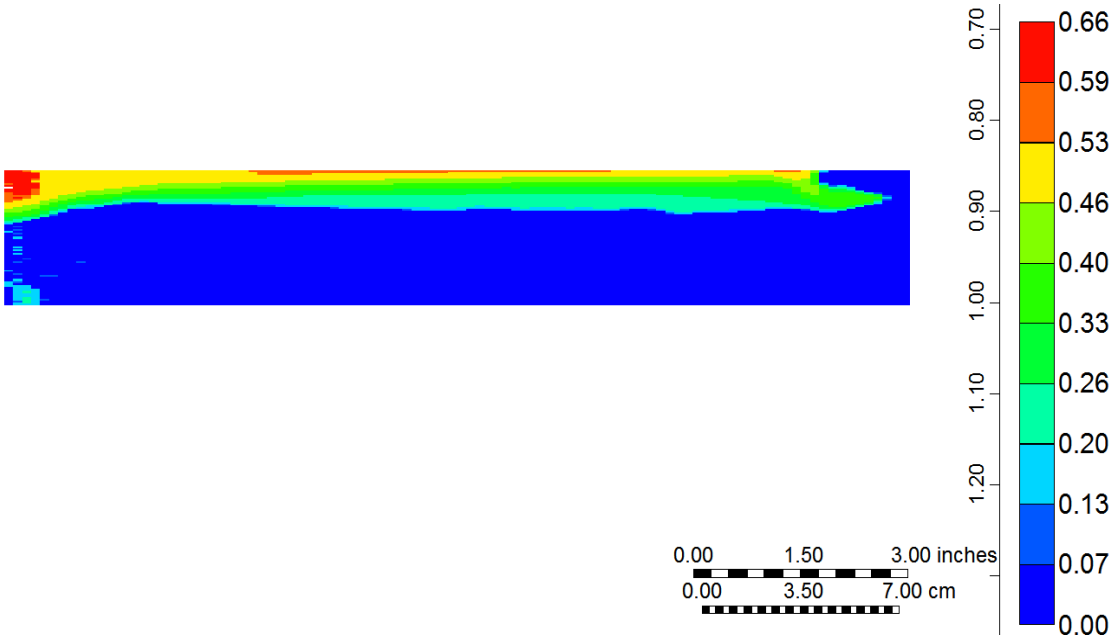

Figure 5-13: Gas saturation distribution before CO2 breakthrough indicating the CO2 tendency to segregate.

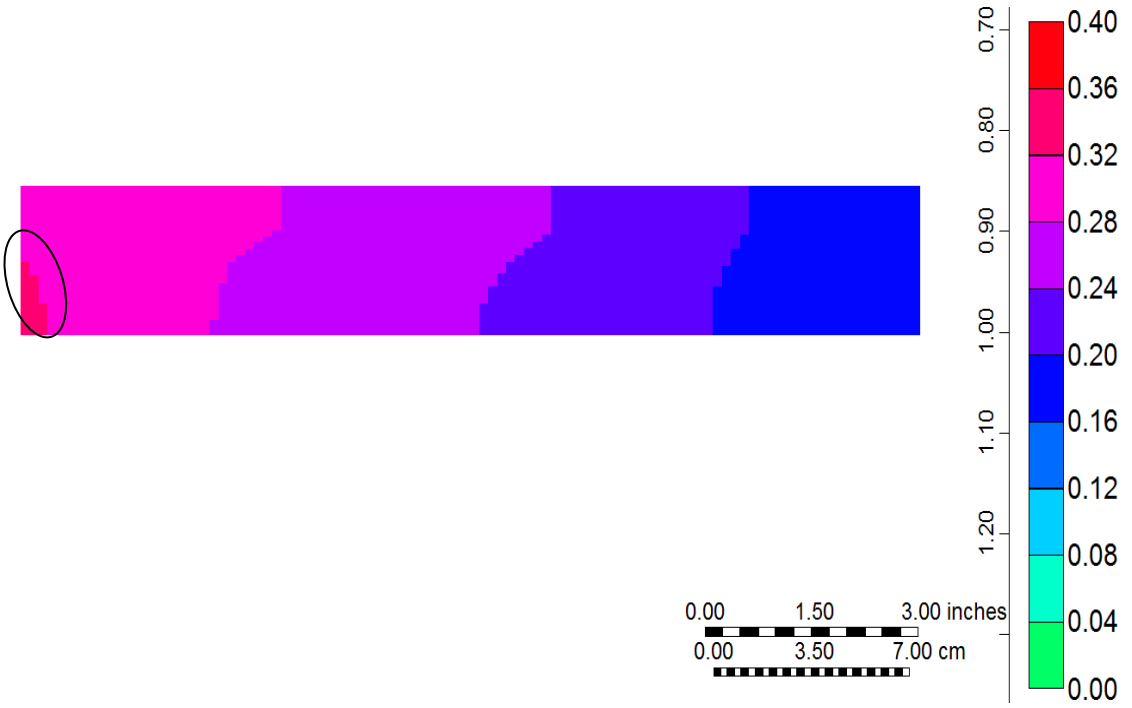

Figure 5-14: Water saturation distribution at breakthrough of water. The accumulation of water highlighted with a black circle in the core inlet indicates the tendency of water to flow downwards.

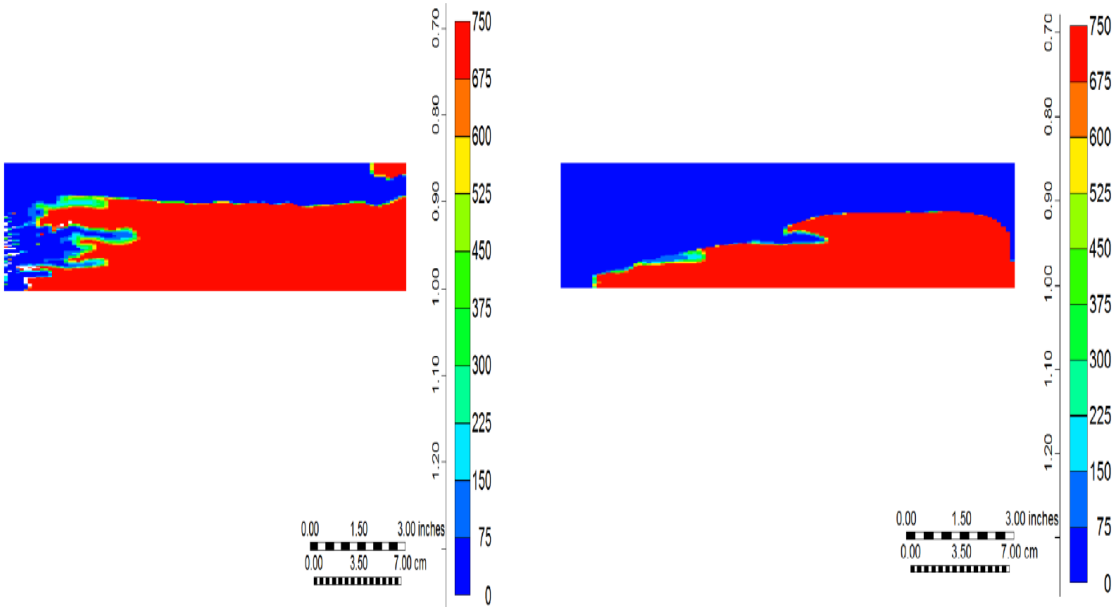

Figure 5-15: Viscosity of the resident oil in the core at two simulation times; at CO_2 breakthrough (left image) and end of coreflood experiment (right image).

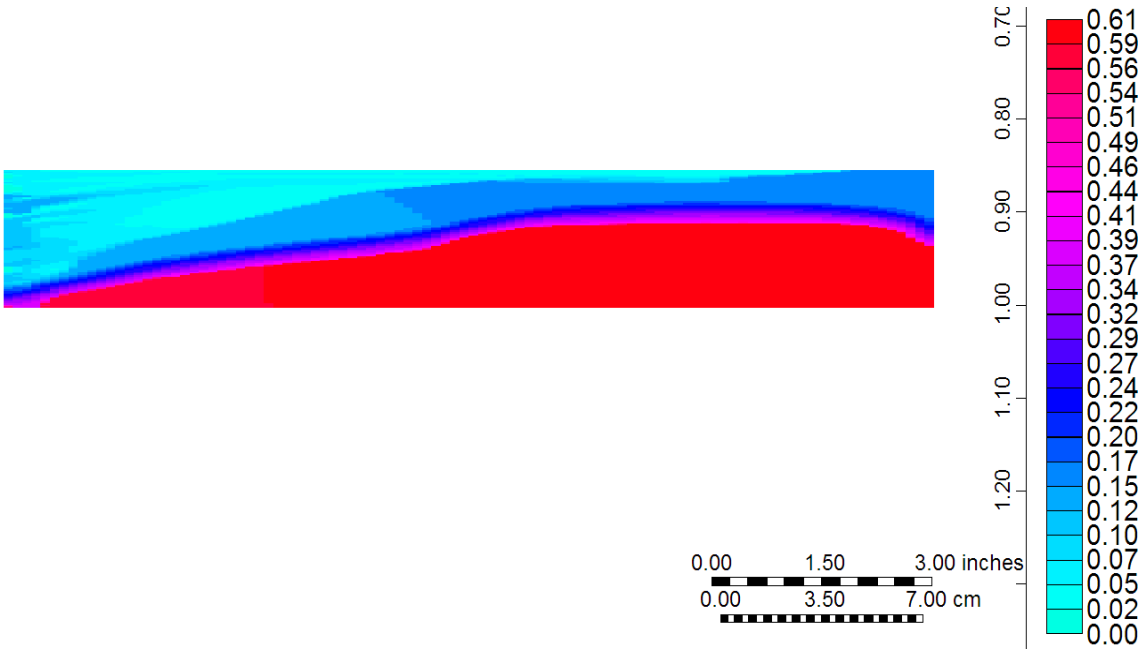

Figure 5-16: Oil saturation distribution throughout the core at the end of SWAG injection indicating very low residual oil saturation at the top of the core where CO_2 could invade and reduce the oil viscosity.

5.7 SUMMARY AND CONCLUSIONS

The mechanism of tertiary waterflood preceded by CO_2 injection was investigated in this chapter. Tertiary oil/water relative permeability was estimated by history matching an experiment in which water was used to chase a CO_2 flood. The estimated tertiary water-oil relative permeability together with secondary gas/oil relative permeability was used in stone's three-phase relative permeability model to simulate a three-phase Simultaneous Water and Gas injection (SWAG). The following conclusions can be drawn from the simulations performed on the coreflood experiments:

The simulation of the tertiary water injection shows that water preferred to follow the path already opened by the previously injected CO_2. However, this mechanism is different from conventional Water Alternating Gas Injection (WAG) where water, because of its higher density than both gas and oil was expected to open up a new path different from that of the gas. In here, the water preferred to follow the CO_2 path because the dissolution of the gas in the oil has significantly reduced the viscosity of the trapped oil in the path. Hence, the lower resistance in the CO_2 path compared to that in the bypassed oil makes it more preferable for the tertiary water to follow.

History matching studies of a tertiary water injection experiment in which three-phase flow of CO_2/oil/water existed was also carried out to estimate tertiary oil/water relative permeability curves. Two simulation runs were performed to reproduce a three-phase flow experiment in which CO_2 and water were injected simultaneously (SWAG). In one, a secondary gas-oil and secondary oil/water relative permeability curves that have been estimated previously were used while in the second, a secondary gas/oil and a tertiary oil/water relative permeability curves were used instead. The results showed that the experimental fluid production data could be adequately matched using the secondary gas/oil and tertiary oil/water relative permeability curves. This can be explained by the notably higher tendency of CO_2 to flow ahead of water creating a situation where the secondary CO_2 injection was replicated with the injected water chasing the CO_2. However, in these simulations, there are discrepancies in the results of differential pressure profiles, which could be attributed to the diffusive flow of CO_2 that was not considered in the simulation due to substantially high associated computational costs. As a recommendation, it would be worthwhile to include the diffusive flow of CO_2 into the simulations to sensitise its impact.

CHAPTER 6

SENSITIVITY STUDIES ON ESTIMATED HEAVY OIL RELATIVE PERMEABILITY

6.1 INTRODUCTION

The implicit estimation of unknown parameters such as relative permeability by history matching is an ill-conditioned and nonlinear inverse problem (O'sullivan, 2004, Oliver et al., 2008, Li et al., 2009), meaning a relatively small change in input parameter value can result in a disproportionate change in the result of the estimated relative permeability. It is, therefore, important where possible to reduce the uncertainty in the input parameter and to quantify the effect of such parameter or a combination of parameters on the estimated relative permeability. Additionally, the implicit method of parameter estimation which uses a functional form for the relative permeability cannot guarantee the monotonicity of the estimated relative permeability and the higher the degree of freedom of the functional form the greater the risk of non-uniqueness (Li et al., 2009). Therefore, measures need to be adopted for the verification of the estimated relative permeability. One expensive way of achieving that is by verifying the dynamic saturation in the simulation with experimental saturation data since relative permeability is a strong function of saturation, saturation history and initial saturation (van Dijke et al., 2001a, van Dijke et al., 2001b, Piri and Blunt, 2005, Spiteri and Juanes, 2006). However, in some cases, laboratory based measurement of saturation distribution is not feasible due to the nature of the fluid or the experimental condition.

Other important parameters in non-thermal enhanced recovery process that can affect the shape of the estimated relative permeability include capillary pressure (Chardaire-Riviere et al., 1992, Theodoropoulou et al., 2005), which can also affect the flood stability (Kueper and Frind, 1988), core orientation and gravity effect (Sherwood, 1987, Sahni et

al., 1998), flow rate (Sandberg et al., 1958, Honarpour et al., 1986, Skauge and Poulsen, 2000), fluids viscosity ratio (Odeh, 1959, Downie and Crane, 1961, Wang et al., 2006a) and solution gas (Blunt, 2000). Another important issue is the way most simulators including all commercial compositional simulators handle the physics of the displacement. For example, the dissolution of solvent into oil is a gradual process controlled by the rate of diffusion (Nghiem and Sammon, 1997, Kechut et al., 2011, Zubov et al.), however, these simulators assume instantaneous phase equilibrium as soon as the solvent is injected. Mutual insolubility between water and hydrocarbon is also assumed by these simulators (Coats, 1980). The objective of this chapter is therefore to sensitize the effect of various parameters on relative permeability and displacement stability. Table 6-1 presents the physical experiments considered for the sensitivity study. Note: that the sensitivity study is not in the order of the experiments as presented.

Table 6-1: Experiments simulated for sensitivity studies

Exp. no	Description	Fluids	Core Orientation	Test Conditions
1	Secondary CO_2 injection into Dead Crude-J Tertiary Water Injection	Injection fluid: CO_2, Water Resident oil: dead Crude-J Resident brine: 20000 ppm	Horizontal	T=28°C, P=1500 psig
3	Secondary CO_2 injection into Live Crude-J	Injection fluid: CO_2 Resident oil: live Crude-J (saturated with methane) Resident brine: 20000 ppm	Horizontal	T=28°C, P=1500 psig
4	Secondary CO_2 injection into Dead Crude-J	Injection fluid: CO_2 Resident oil: dead Crude-J Resident brine: 20000 ppm	Vertical	T=28°C, P=1500 psig
5	Secondary Water injection into Dead Crude-J	Injection fluid: brine Resident oil: dead Crude-J Resident brine: 20000 ppm	Horizontal	T=28°C, P=1500 psig

6.2 EFFECT OF ORIENTATION ON GAS/OIL RELATIVE PERMEABILITY

Compositional displacement such as CO_2 injection into heavy oil is a complex process where nonlinear coupling of thermodynamics, which describes how components partition across the multiple phases (gas and oil) in space and time, and the transport of multiple components under the influence of gravity and viscous forces occurs (Voskov and Tchelepi, 2012). Appropriate modelling of the displacement would require consistent

resolution of the coupled compositional interactions and the instability in the displacement process.

One source of such instabilities is gravity and for that reason the effect of core orientation on the shape of relative permeability estimated from an unstable displacement was investigated in this section. Two experiments were considered, secondary CO_2 injection into heavy oil in a horizontal core (Experiment-1) and secondary CO_2 injection into heavy oil in a vertical core (Experiment-4), which were similar in all respect except in the core orientation. The horizontal injection experiment (Experiment-1) has been simulated in Chapter 4 (section 4.3) and the corresponding relative permeability estimated. Experiment-4, where the gas was injected from the top of the core was simulated in this section and the results compared with that of Experiment-1.

In simulating Experiment-4, similar modelling approach to that in experiment-1 was followed for consistency, where the porosity was assumed to be homogenous and the permeability was stochastically distributed using a Gaussian random distribution with a mean of 2340mD and a standard deviation of 50mD. The permeability perturbation served as the methodology for triggering fingers in the displacement model (Christie, 1989). In addition, even though the displacement was in the vertical direction, similar grid size was maintained as in Experiment-1 (80x100-grid size), because similar magnitude of instability was expected with respect to the width of the main fingers. This is evident from their similar breakthrough time and same amount of produced oil at breakthrough (Figure 6-1). Table 6-2 shows the parameter values used in the model and Table 6-3 summarises the modelling approach, while Figure 6-2 shows the random permeability field in the model.

Firstly, a direct simulation of the experiment using the relative permeability obtained from the history matching of the horizontal injection (Figure 6-3) was carried out. This was to highlight any effect of orientation on the estimated relative permeability. Figure 6-4 shows the result of the simulation of cumulative oil recovered obtained from the direct use of the relative permeability obtained from the horizontal injection. Given that no history matching exercise was carried out, an excellent degree of agreement between the simulation results and experimental (production) data was obtained, which agrees with literature for the case where vertical permeability (K_v) is the same as horizontal

permeability (Meaney and Paterson, 1996) and reflects the consistency of the simulation approach and the accuracy of the previously estimated relative permeability curves from the history matching procedure. The breakthrough time was also predicted accurately, reflecting a representative simulation of the finger onset, propagation and growth. Figure 6-5 illustrates the gas saturation distribution, indicating how CO_2 finger propagated in the core. It also shows that between 0.2 and 0.4 days, CO_2 interaction with in-situ oil resulted in gravity drainage type of flow where the oil saturation of the bypassed area gradually decreased as a result of the CO_2 extracting the lighter components (black arrow pointing right in the figure). This phenomenon exhibited a constant rate of oil flow from the oil/CO_2 interface as evidenced in the experiment, where there was a constant oil production rate of 1cc/hr between 0.5 to 2 days (highlighted with a dashed blue oval in Figure 6-4) and confirmed the occurrence of the behaviour observed in the simulation results. This is the principal mechanism exploited in Vapour Extraction (VAPEX) processes (Alkindi et al., 2008, James et al., 2008, Torabi et al., 2012b) and highlights the capability of CO_2 to act like solvents such as propane in vapour extraction processes.

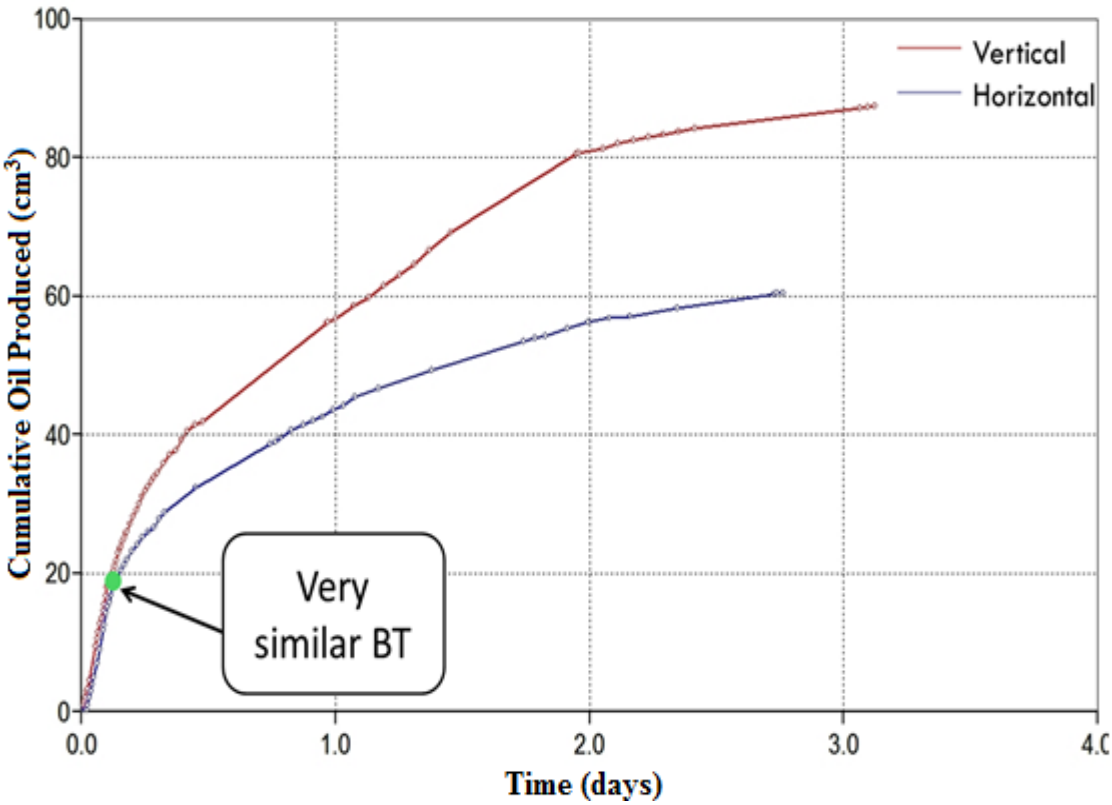

Figure 6-1: Cumulative oil recoveries for experiment-1 (horizontal) and experiment-4 (vertical) showing similar breakthrough times.

Table 6-2 Core model properties

Core Parameters	Value
Diameter	5.12 cm
Length	32 cm
Core Pore Volume (PV)	163.02 cm^3
Porosity (□)	24.74
Permeability to Brine (K)	2500mD

Table 6-3 Summary of the core modelling approach and values

Core Model Property	Method	Value
Porosity	Homogenous	0.24
Permeability	Normal Distribution (mean) Standard deviation	2340mD 50mD
Finger Triggering	Permeability Heterogeneity	

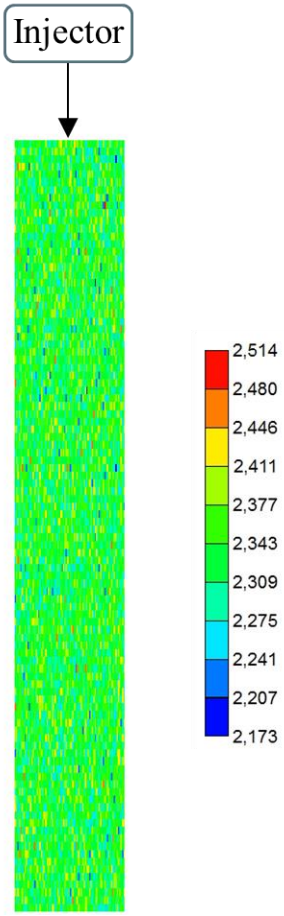

Figure 6-2: 2D model used for simulation of experiment-4 showing the random permeability field generated to trigger the finger

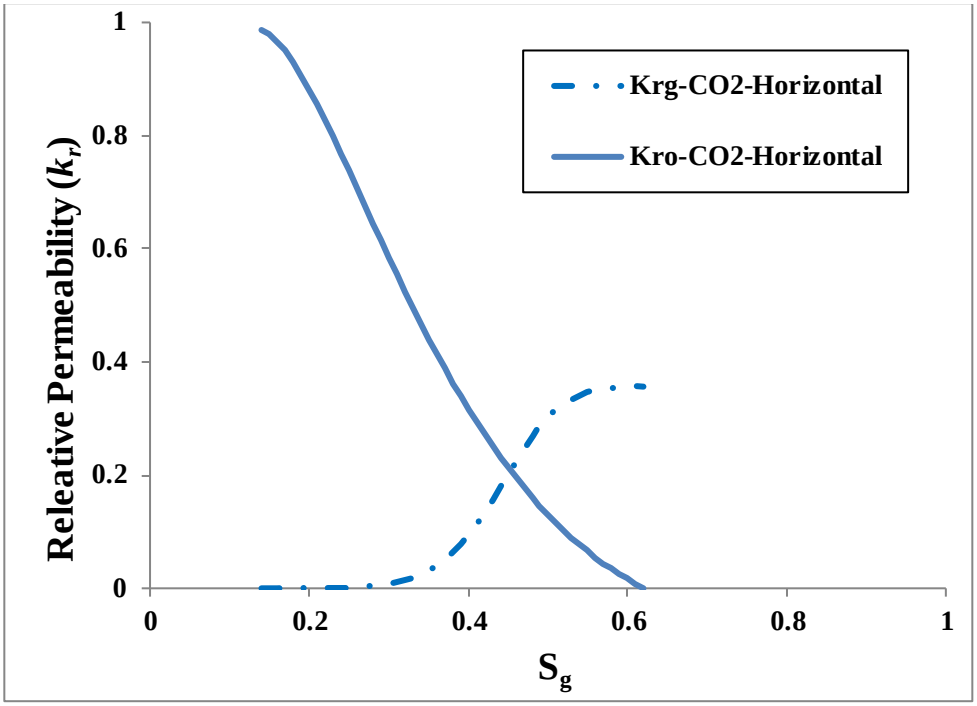

Figure 6-3: Gas-Oil Relative Permeability estimated from experiment-1 for use in the simulation of experiment 4.

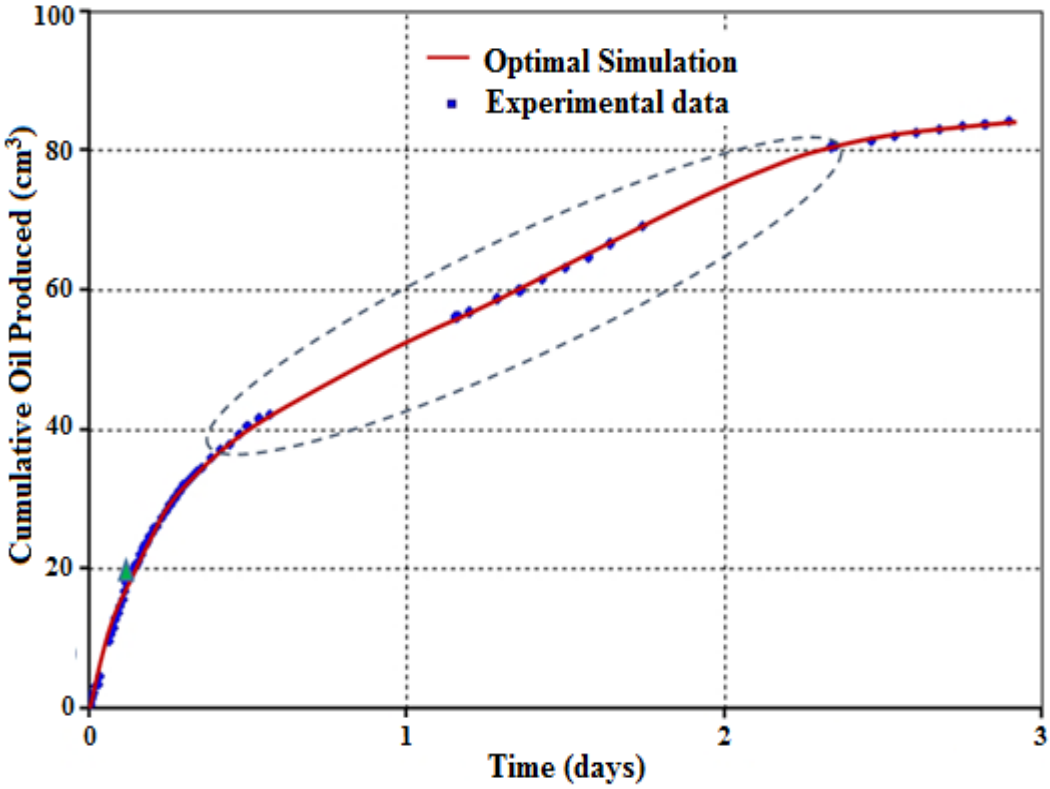

Figure 6-4: Oil recovery profiles obtained from coreflood experiment (blue dots) and simulation (red line). The green triangle shows the breakthrough time indicating a good agreement with simulation results. The blue dashed points represent the period of constant oil rate of 1cc/hr due to gravity drainage.

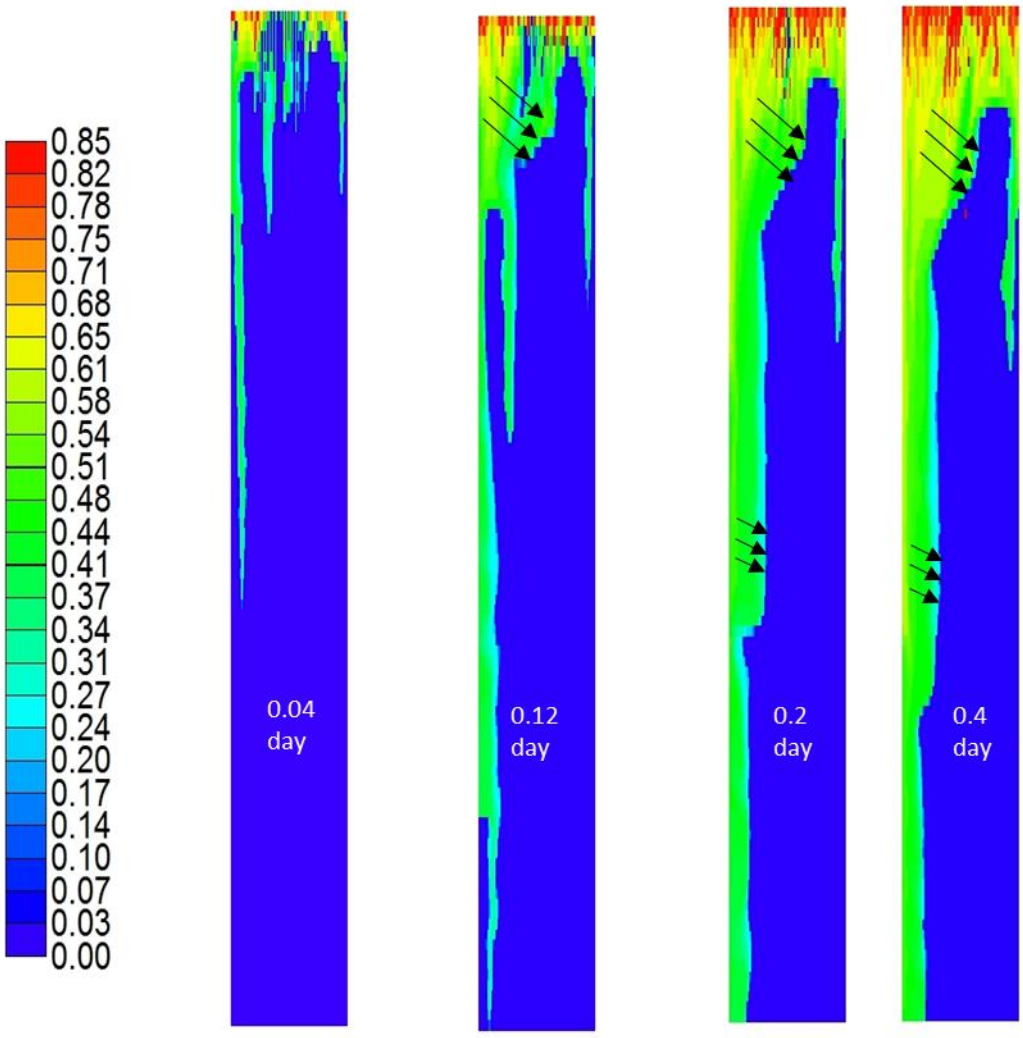

Figure 6-5: Gas saturation distributions in core obtained from simulation results, which are sorted chronologically (white note shows the time of the simulation). The formation of finger and growth of the instability can be seen in the images. In last two right images, the drainage of the bypassed oil can be seen.

6.3 EFFECT OF CAPILLARY PRESSURE ON SIMULATION RESULT

In this section, the sensitivity of capillary pressure on relative permeability and displacement stability was examined. These two flow functions (relative permeability and capillary pressure) are difficult to determine by experimental techniques and especially for heavy oil systems due to the high viscosity of the fluid and the unconsolidated nature of the porous medium in most heavy oil reservoirs. Quite often, the flow functions are simultaneously estimated by history matching technique (Chardaire-Riviere et al., 1992, Nordtvedt et al., 1993, Zhang et al., 2012). However, the method suffers from increased non-uniqueness due to increase in the degree of freedom with more parameters.

Jahanbakhsh and Sohrabi (2015) and Papatzacos and Skjæveland (2002) have modified the method by conditioning the relative permeability as a function of capillary pressure, which reduced the non-uniqueness. Because of this inherent non-uniqueness in the simultaneous estimations, engineers often use zero capillary pressure in the history matching process and estimate relative permeability that integrates the capillary pressure effect in it, thus changing its true meaning. The biggest drawback of this approach is that the beneficial stabilising effect of capillary forces is neglected and that affects the true nature of the stability of the displacement process (Fayers and Sheldon, 1959, Peters and Flock, 1981, Jerauld et al., 1984, Li et al., 1994, Bachu and Bennion, 2008).

Here, the effect of capillary pressure on the shape of relative permeability estimated from an unstable displacement was investigated. The effect of capillary pressure on displacement stability was also sensitised.

6.3.1 Effect of Pc on Estimation of Relative Permeability and Residual Oil Saturation

The experimental studies on the injection of CO_2 into dead Crude-J (Emadi et al, 2012) has shown that a significant degree of mass transfer took that lead to changes in interfacial tension that markedly varied the capillary pressure curve. In other words, the dynamics of CO_2/Crude-J interactions is expected to vary the capillary pressure dynamically from the one estimated from the converted mercury intrusion test presented in chapter 5.

Therefore, in order to history match for the two flow functions, the same modelling approach as in section (4.3) was followed except that here the two flow functions were simultaneously estimated; the unknown relative permeability curve was estimated using the L.E.T-type function (as in section 4.3) while the capillary pressure (Pc) was represented by an exponential function. The converted mercury intrusion test was used to condition the Pc so as to mitigate the effect of non-uniqueness in the optimisation process.

Figure 6-6 shows the result of simulation of the cumulative oil recovered that was obtained from the history matching process compared with the experimental data. Similarly, Figure 6-7 shows a comparison of the simulation result with experimental data for the core inlet pressure. It can be observed that the matches between the experiment and the simulations are acceptable for this highly complex system. Figure 6-8 also shows

the estimated capillary pressure (Pc) curve obtained from the history matching, while Figure 6-9 illustrates the tuned gas/oil relative permeability curves for Experiment-1 for the two cases; (i) with zero capillary pressure (from section 4.4), and (ii) simultaneous estimation with the conditioned Pc included. In both cases, the gas relative permeability has characteristic S-shape behaviour while the oil relative permeability has a linear shape. However, the inclusion of capillary pressure in the process has brought about significant change in the gas relative permeability curve. It can be seen that the estimated gas relative permeability for the case where Pc was included in the history matching had higher critical gas saturation and lower relative permeability value at irreducible oil saturation. Thus, the relative permeability of an unstable gas/oil two-phase flow has unique characteristics, which are not in line with the accepted rule of thumbs for conventional oil.

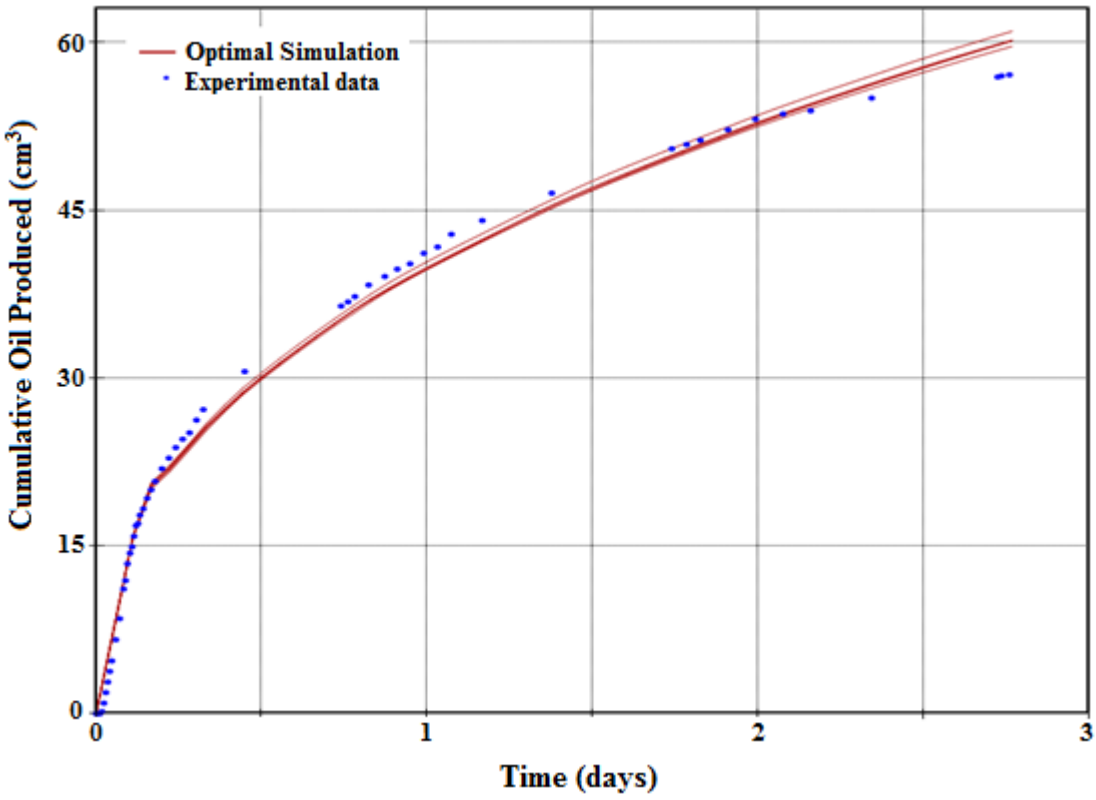

Figure 6-6: Matched (red lines) cumulative oil production against the experimental data (blue dots) obtained from the simultaneous estimation of kr and Pc by history matching of Experiment-1 . Multiple red lines show the five best matches that were obtained through the process of the optimisation.

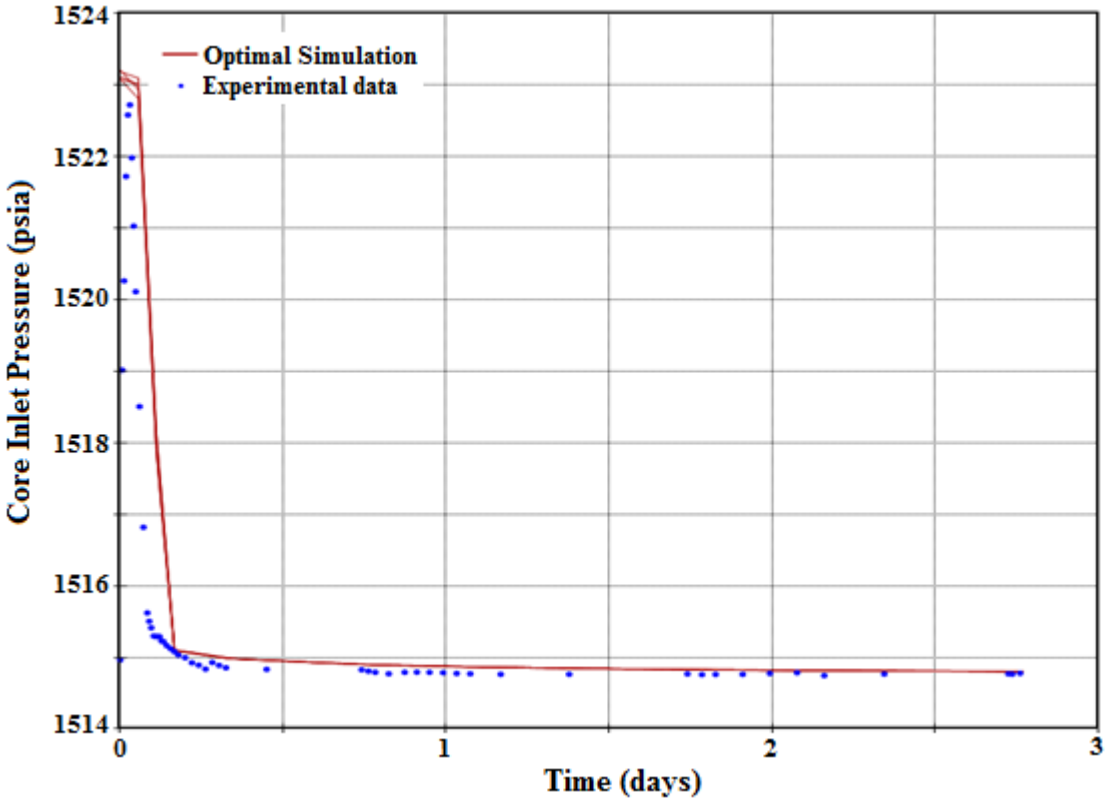

Figure 6-7: Matched (red lines) pressure at the inlet of the core against the experimental data (blue dots) for the Experiment-10. Multiple red lines show the five best matches that were obtained through the process of the optimisation.

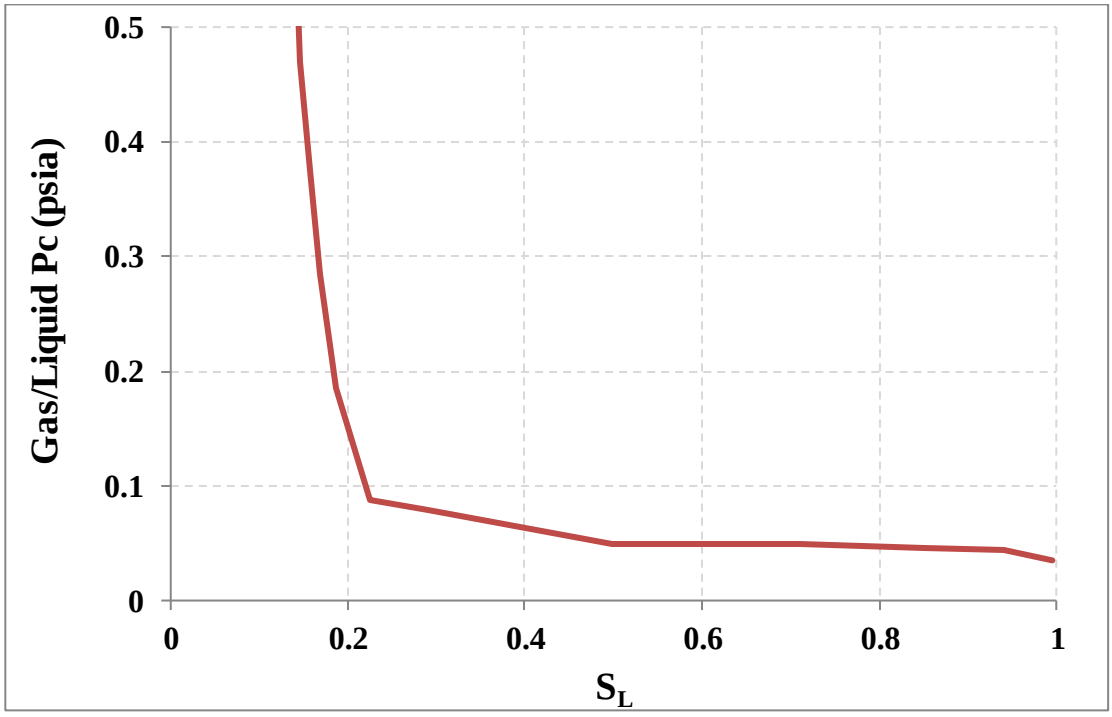

Figure 6-8: Capillary pressure versus liquid saturation obtained by converting mercury intrusion results.

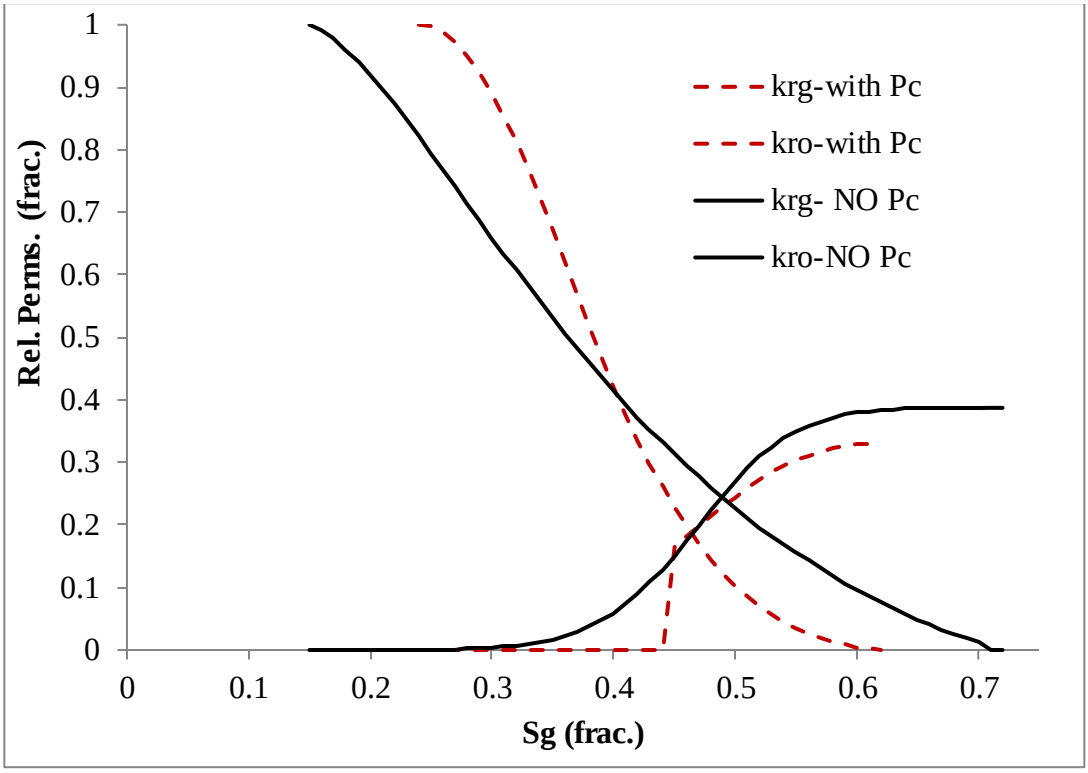

Figure 6-9: History matched gas/oil relative permeability function with respect to gas saturation for two cases; with Pc (red dashed line) and without Pc (black line).

Another implication of including capillary pressure in the history matching process can manifest in the sweeping pattern which results in the variation of the end-point saturations in the relative permeability curves. In an unstable displacement, residual oil saturation can be trapped in two forms; pore-scale trapping and bypassed oil. Sweep efficiency mainly controls the latter form of trapping. Given that the total residual oil saturation is known from the oil production data (coreflood experiment), the change in sweep pattern caused by the inclusion of capillary pressure can vary the amount of bypassed oil. Figure 6-10 demonstrates the sweep patterns extracted from the simulations of Experiment-1 for the cases with and without capillary pressure included. It is evident from Figure 6-9 that by including capillary pressure, the sweep efficiency of CO_2 displacement was improved at core scale and consequently, the end-point saturation was impacted. This highlights the significance of using the right Pc curve in simulation of displacements as well as in the estimation of flow parameters such as relative permeability.

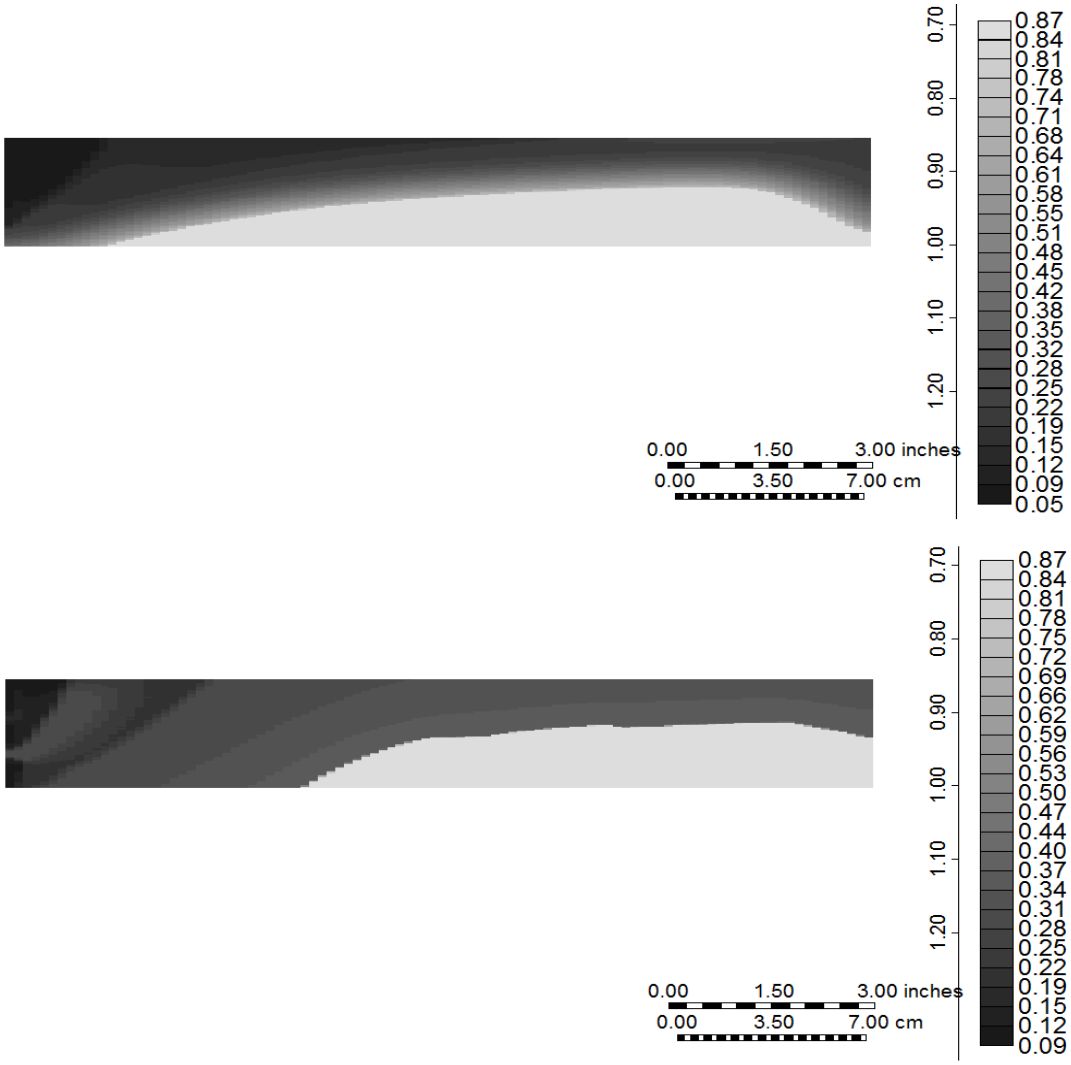

Figure 6-10: Oil saturation distribution at the end of CO2 injection in two cases; no Pc (above image) and with Pc (bottom image). The brighter the colour, the higher oil saturation exists in the grid block. The inclusion of capillary pressure has slowed down the onset of the gravity tongue and hence better sweep efficiency near core inlet.

6.3.2 Effect of inclusion of Pc on Frontal Stability

The impact of capillary pressure on the stability of front needs also to be investigated since instability has been described as the main issue militating against the efficiency of heavy oil displacement by non-thermal methods (Thomas et al., 1999). The difficulty in determining a reliable experimental capillary pressure measurement especially for heavy oil systems is a huge source of uncertainty in the simulation of such process. For example, the centrifugal force available in centrifuge cups during the determination of capillary pressure for a heavy oil system by the centrifugal method can easily be overwhelmed by the viscosity of the oil if measured at the reservoir condition. Moreover, when heat is

added in order to reduce the viscosity so as to facilitate the measurement, the IFT of the fluid changes for which conversion cannot guarantee the reliability of the measurement.

Also, the mercury intrusion test capillary pressure used in the simulation of the secondary water injection (Experiment-5) was obtained from a mercury/air test and converted to water/oil using their IFT values, hence introducing uncertainty in the parameter. Therefore, sensitivity on the curve needs to be carried out in order to quantify the magnitude of this uncertainty. To demonstrate this, another history matching optimisation for the estimation of relative permeability was performed on Experiment-5 (secondary water injection into heavy oil in a horizontal direction) with the assumption of zero capillary pressure in order to sensitise the effect of Pc on the displacement stability. Figure 6-11 and Figure 6-12 illustrate the matched cumulative oil recovered and the pressure at the inlet of the core obtained from the history matching of the experiment with the assumption of zero capillary pressure. Figure 6-13 shows the relative permeability curves estimated with the assumption of zero capillary pressure along with the relative permeability obtained earlier where capillary pressure was included. Comparison of the two curves indicated only a slight shift in the curves. Therefore, it can be concluded that for the oil/water system, the capillary pressure did not have a significant effect on the shape of the estimated relative permeability curves.

However, the same conclusion cannot be made on the stability of the displacement front, the saturation profile obtained from the simulation of the displacement with zero capillary pressure shows that the displacement was prone to instability due to viscous fingers. Figure 6-14 shows a comparison of the water saturation profile before breakthrough for the displacement with and without capillary pressure indicating the occurrence of viscous instability for the case with zero Pc. Therefore, the presence of capillary force has dampened the fingers and helped stabilise the flow front highlighting the significance of Pc on displacement stability.

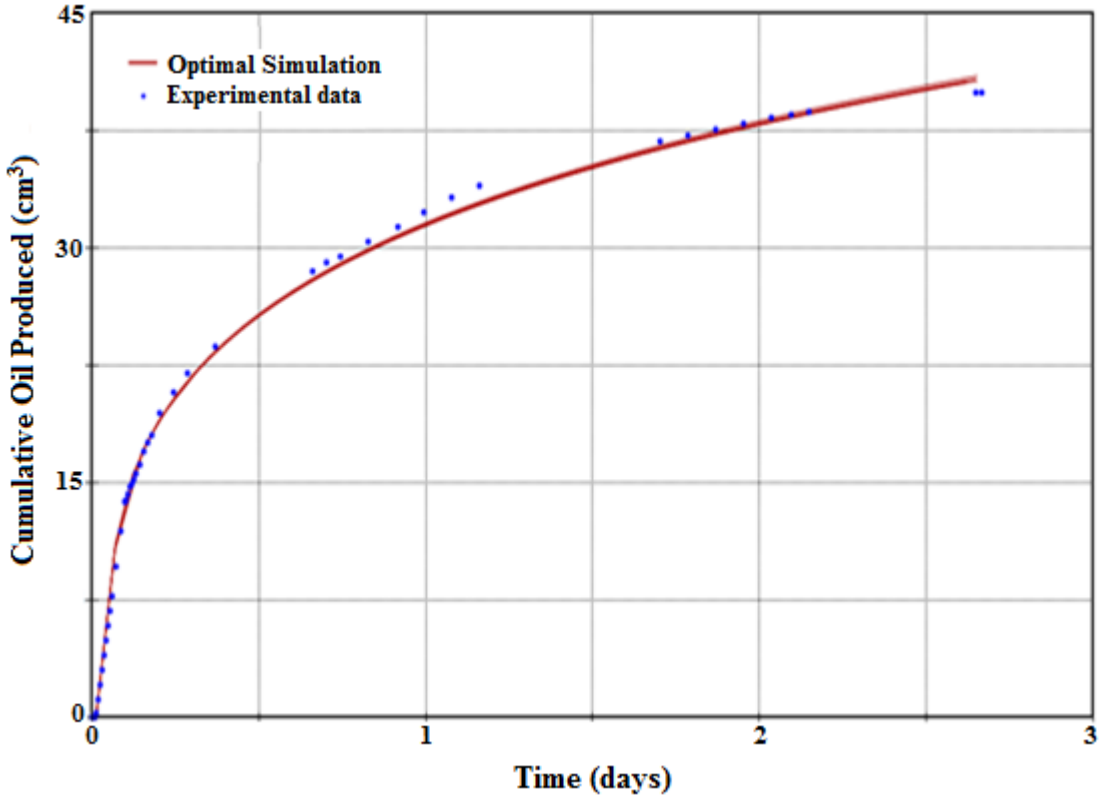

Figure 6-11: Matched (red lines) cumulative oil production against the experimental results (blue dots) for the Experiment-5 (no capillary pressure included).

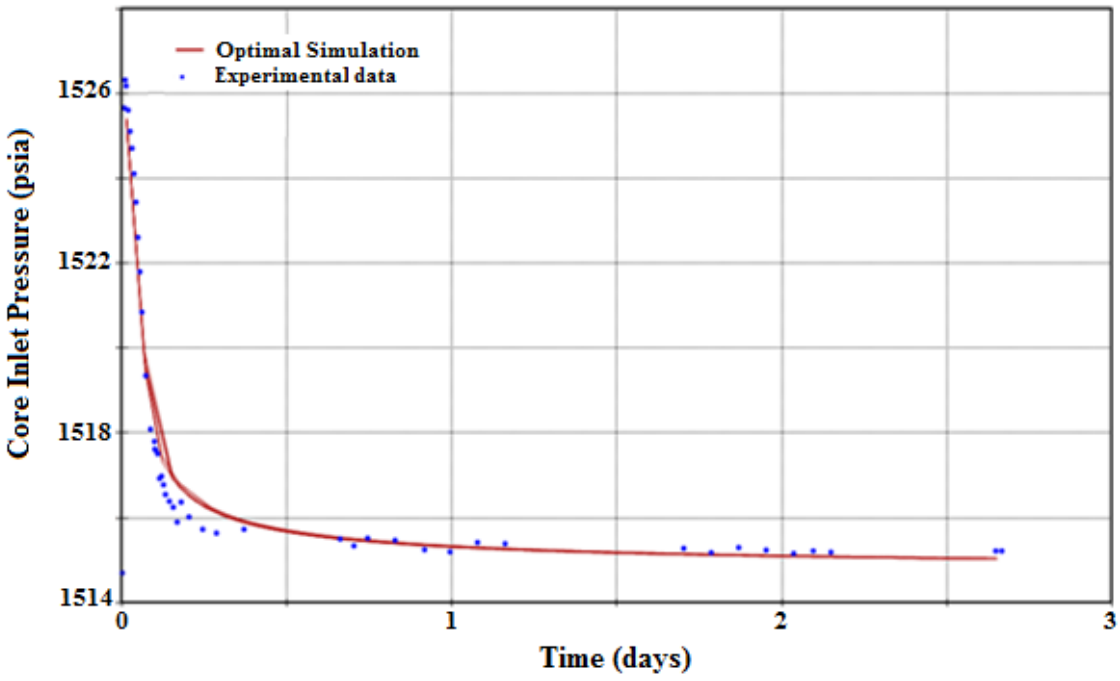

Figure 6-12: Matched (red lines) pressure at the inlet of the core against the experimental data (blue dots) for the Experiment-5 (no capillary pressure included).

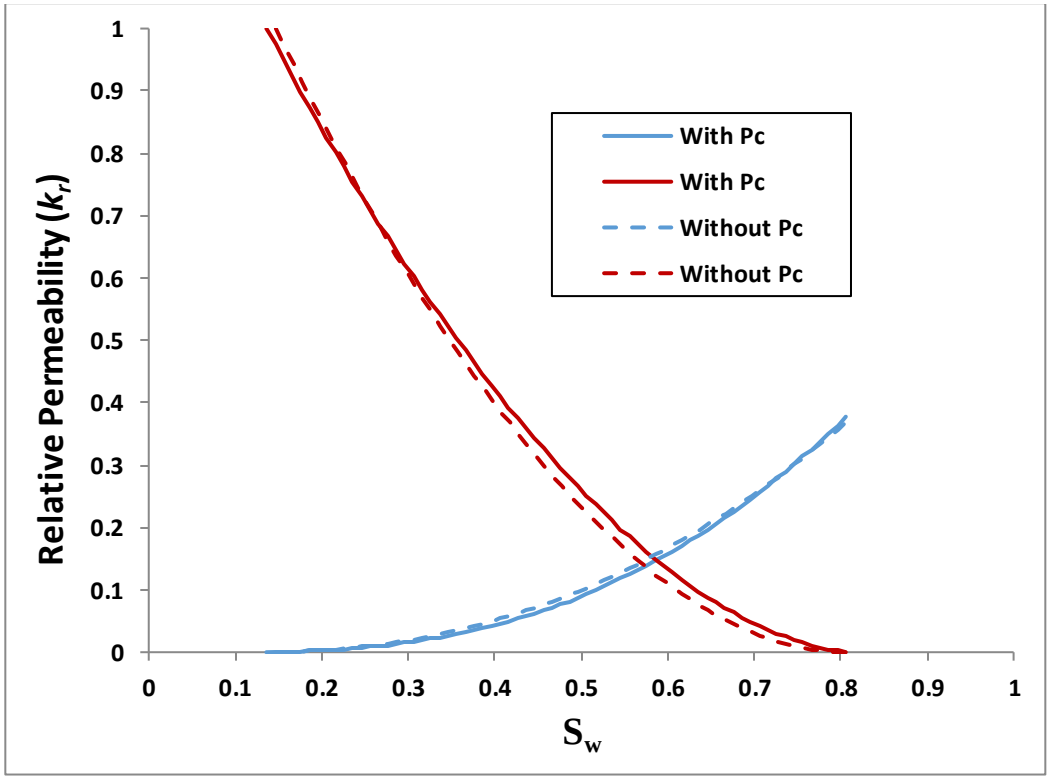

Figure 6-13: Tuned water-oil relative permeability curves estimated with two assumptions; with Pc (solid lines) and without Pc (dashed lines).

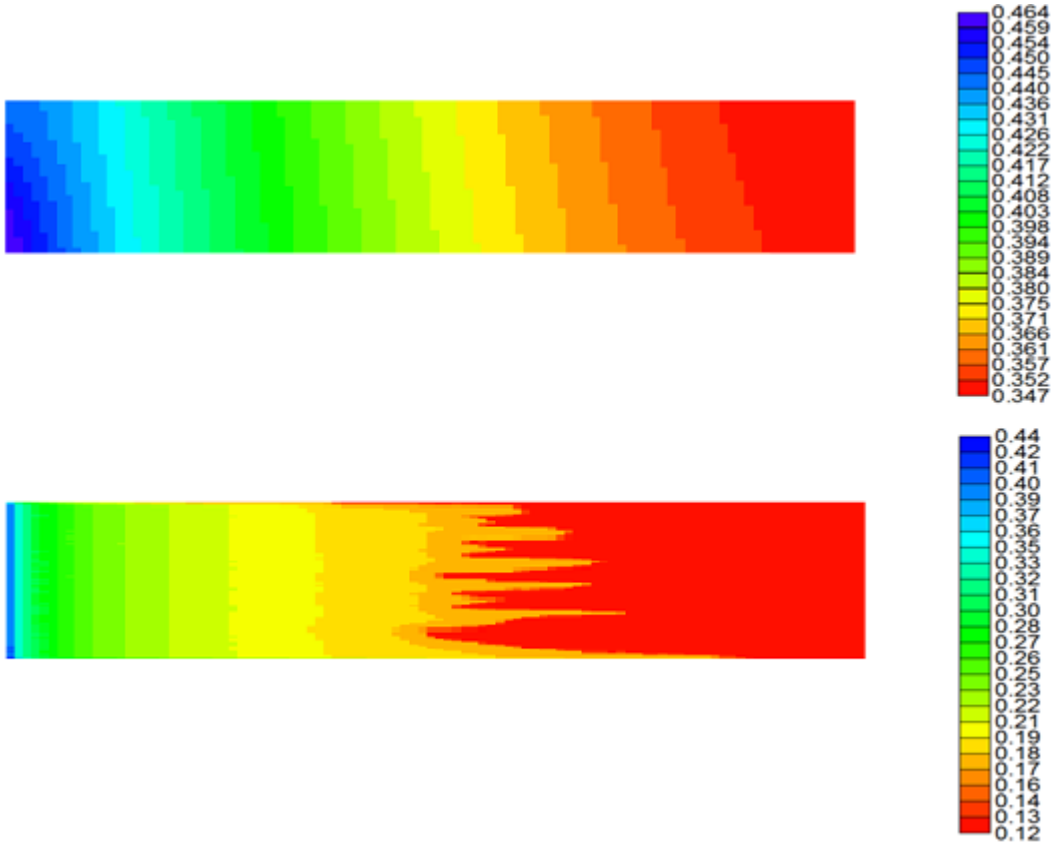

Figure 6-14: Water saturation distribution in the core before breakthrough of water for two cases; Top: with capillary pressure included. Bottom: with the assumption of zero capillary pressure, which shows the occurrence of viscous fingers in the absence of stabilising capillary force.

In summary, to ascertain the influence of Pc on the displacement pattern and displacement front stability of heavy oil recovery by water injection, two sets of relative permeability curves were estimated considering two cases, with Pc and without Pc. It was observed that in the case with zero Pc, viscous fingering occurred which impacted the sweeping pattern, whereas when Pc was included, the displacement front was stable, indicating the cushioning effect of capillary forces on the propagation of viscous fingers. Therefore, this indicates the importance of including the appropriate capillary pressure curve in the simulation of heavy oil displacement by water. This important parameter should always be meticulously investigated when viscous force is not large enough to suppress its influence. It should also be re-emphasized here that when the displacement is prone to fingering, a thorough grid sensitivity needs to be carried out. For example, Figure 6-15 shows the simulation results of cumulative oil recovered and the pressure at the inlet of the core for Experiment-5 (water injection into heavy oil in a horizontal core) in a 160x200 grid model but using the relative permeability obtained from the history matching of an 80x100 grid model. By increasing the grid size, a significant change in the cumulative oil recovered was observed, an indication of the sensitivity of the result to grid size due to viscous fingering. However, for the case where the capillary pressure was included, further gridding was not required since the displacement was stable.

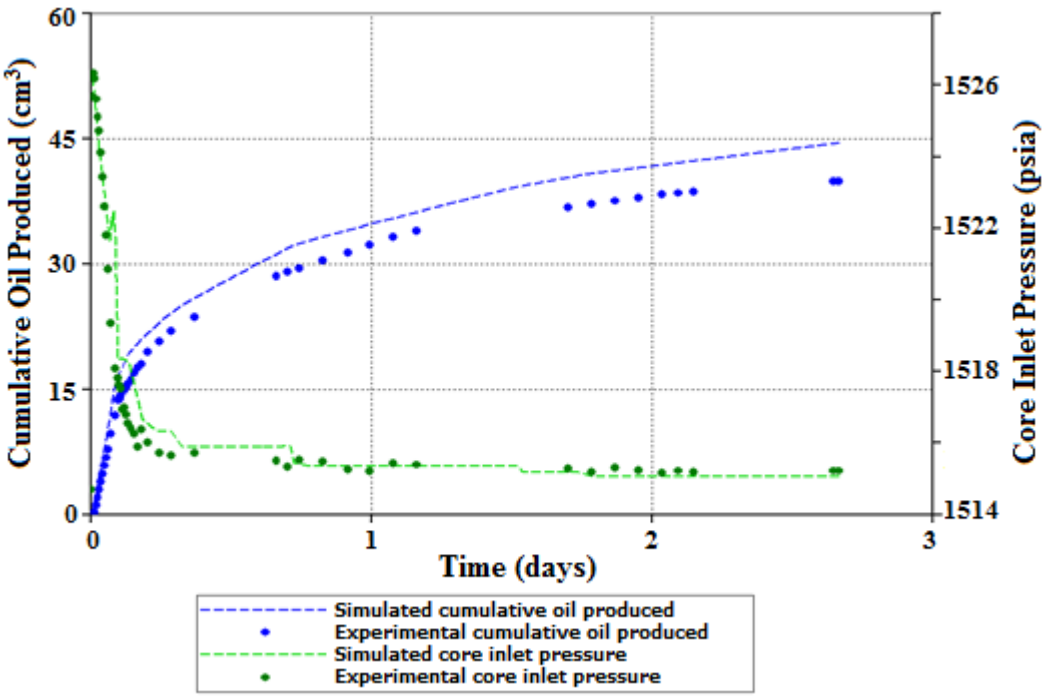

Figure 6-15: Simulation of cumulative oil recovered and pressure at the inlet of the core for Experiment-5 with (160x200) grid model using relative permeability obtained from (80x100) model showing a change with the experimental data.

6.4 EFFECT OF MOLECULAR DIFFUSION RECOVERY

During the injection of solvent such as CO_2 into heavy oil, diffusion is one of the several complex processes that occur within the system. Diffusion mechanism can lead to mixing and dissipation of plug in WAG injection thereby reducing the efficiency of the displacement process, on the other hand, the dissipation effect of the mechanism may tend to damp out viscous fingers (Perkins and Johnston, 1963). Hence, diffusion can be detrimental or beneficial. The measurement of effective diffusion coefficient in porous media is based on the apparent diffusion coefficient of the component in air (Weissberg, 1963), a huge source of uncertainty in the measurement of the parameter. Diffusion coefficient is also known to exhibit short time behaviour and is, therefore, a time dependent parameter (Mitra et al., 1993). In displacement where miscibility is not achievable, such as in heavy oil system, molecular diffusion is the most influential mechanism for the solvent dissolution in the oil, a process that can lead to significant reduction in the oil viscosity. For CO_2/heavy oil system up to 90% viscosity reduction has been reported (Jha, 1986, Emadi, 2011). The mechanism also helps in the upgrading of oil by extracting lighter components from the oil and knocking off the heavier components (Boustani and Maini, 2001). This is evident in the produced oil of Experiment-1 where the compositional analysis of the produced oil after breakthrough indicated a higher percentage of the lighter component than in the original oil. It is therefore, important for the purpose of simulation to determine the right viscosity values and other properties of the upgraded oil and the residual oil, which comprises of the trapped and the bypassed oil in order to properly model the system. This can only be achieved by proper modelling and tracking of the mass transfer of components between the phases.

Therefore, to sensitise the impact of molecular diffusion on the result of the simulation, a simple static Fickian diffusion analysis was performed on Experiment-1, in which the depth of CO_2 penetration and resultant viscosity reduction were calculated using equations (22 and 23).

$$n(x,t) = n_o erfc\left(\frac{x}{2\sqrt{Dt}}\right) \quad 22$$

$$D_{effective} = \frac{D \times \phi}{\tau} \quad 23$$

Where n_0 and D, are CO_2 solubility and apparent diffusion coefficient in oil, respectively, ϕ is the porosity and τ is the tortosity constant. For the sake of simplifying the analysis, since experimental data for the diffusion coefficient was not available, an apparent diffusion coefficient of 5×10^{-8} cm^2/s was assumed on the basis of the oil viscosity. The effective diffusion coefficient of the porous media was then calculated using equation (23). A diffusion time of one day and a tortuosity value of 2 were considered in the analysis. Figure 6-16 shows the profiles of CO_2 composition and oil viscosity with respect to the thickness of oil layer, indicating the oil region penetrated by the gas and changing its viscosity value. Based on this Fickian analysis, the oil thickness affected by CO_2 diffusion was about 1 mm. Even though this indicates only about 10% penetration of the total oil thickness, it can be quite significant when allowed for longer time, which is the case at field scale. Additionally, the value can be significantly higher if the analysis was done for a dynamic diffusion which include dispersion resulting from mixing of fluids caused by diffusion, local velocity gradients, locally heterogeneous streamline lengths, and mechanical mixing (Lake, 1989, Kavousi et al., 2013).

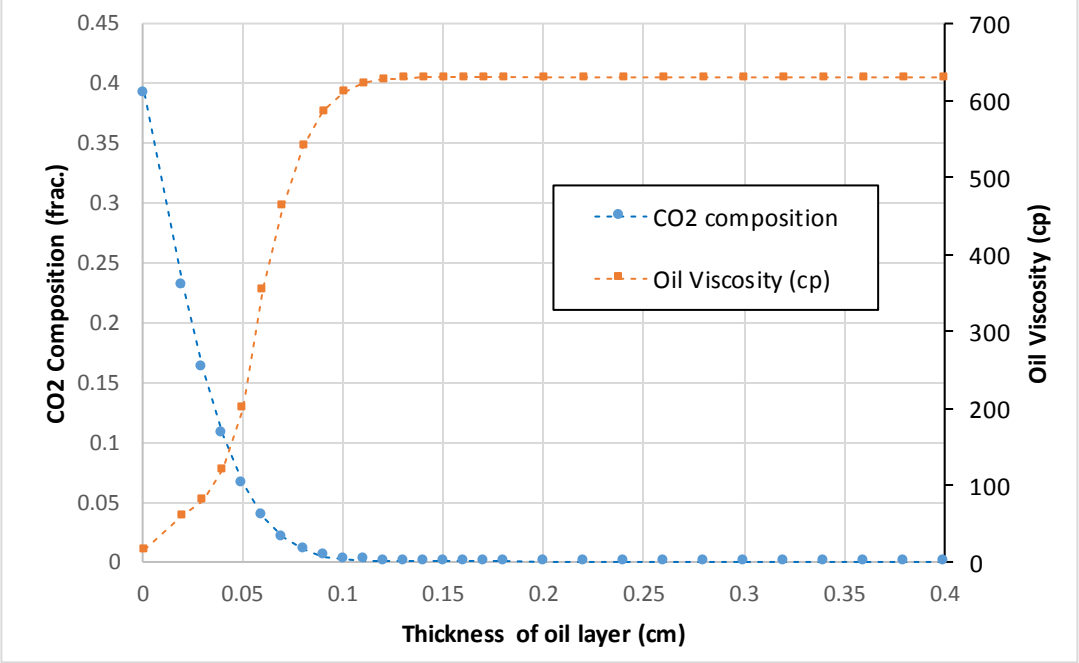

Figure 6-16: CO_2 composition in oil layer and the resultant viscosity reduction calculated using Fickian diffusion assumption.

In addition, several types of correlations have been proposed for effective diffusion coefficient based on experiments carried out on the diffusion of several types of molecules in paraffin. The most widely used are the Sigmund (1976) and the Wilke and Chang

(1955) correlations. The Sigmund correlation method for calculating molecular diffusion (unit is cm^2/s) is based on the binary diffusion coefficient between Component i and j in the mixture and is given by

$$D_{ij} = \frac{\rho_k^0 D_{ij}^0}{\rho_k}.(0.99589 + 0.096016\rho_{kr} - 0.22035\rho_{kr}^2 + 0.032874\rho_{kr}^3) \quad 24$$

Where:

$$\rho_{kr} = \rho_k.\left[\frac{\sum_{i=1}^{n_c} y_{ik} V_{ci}^{5/3}}{\sum_{i=1}^{n_c} y_{ik} V_{ci}^{2/3}}\right] and \quad 25$$

$$\rho_k^0 D_{ij}^0 = \frac{0.0018583 T^{1/2}}{\sigma_{ij}^2 \Omega_{ij} R}.\left[\frac{1}{M_i} + \frac{1}{M_j}\right]^{1/2} \quad 26$$

The binary diffusion of component i in the mixture is therefore given by

$$D_{ik} = \frac{1 - y_{ik}}{\sum_{j=1} y_{ik} D_{ij}^{-1}} \quad 27$$

In the above equations, the collision diameter σij and the collision integral Ωij of the Lennard-Jones potential are related to the component critical properties through the following equations described by Reid et al. (1977).

$$\sigma_i = (2.3551 - 0.087\omega_i).\left[\frac{T_{ci}}{P_{ci}}\right]^{1/3} \quad \varepsilon_i = k_B(0.7915 + 0.1963 w_i) T_{ci} \quad 28$$

$$\sigma_{ij} = \frac{\sigma_i + \sigma_j}{2} \quad \varepsilon_{ij} = \sqrt{\varepsilon_i\, \varepsilon_j} \quad T_{ij}^* = \frac{k_B}{\varepsilon_{ij}} \quad 29$$

$$\Omega_{ij} = 1.06306\left(T_{ij}^*\right)^{-0.15610} + 0.19300\exp\left(-0.47635\, T_{ij}^*\right) + 1.03587\, exp\left(-1.52996\, T_{ij}^*\right) + 1.76474 exp\left(-3.89411\, T_{ij}^*\right) \quad 30$$

Where k_B is the Boltzmann's constant (=1.3805E-16 ergs/K)

The Wilke-Chang molecular diffusion coefficient (cm^2/s) correlation, on the other hand, is given by equation (31)

$$D_{ik} = \frac{7.40E-8(M_{ik}^{'})^{1/2}T}{\mu_k v_{bi}^{0.6}} \; with \; M_{ik} = \frac{\sum_{j=1} y_{jk} M_j}{1-y_{ik}} \qquad 31$$

The viscosity μ_k (cp) is calculated from the Lorentz, Bray, and Clark correlation (Lohrenz et al., 1964), and the partial molar volume of Component i at the boiling point, v_{bi} (cm^3/mol), is estimated from the Tyn and Calus method (Reid et al., 1977):
$v_{bi} = 0.285 v_c^{1.048}$ Where v_c is the critical volume (cm^3/mol)

To demonstrate the effect of the correlations on 1D and 2D displacement models, Experiment-3 where CO_2 was injected into heavy oil in a vertical core was considered. Figure 6-17 shows the CO_2 saturation profiles of the 1D model with and without molecular diffusion while Figure 6-18 shows the results of the cumulative oil recovered for the two cases. It can be seen that for the 1D model, the molecular diffusion did not change the CO_2 saturation profile. Also, the cumulative oil recovered for the two cases using Sigmund and Wilke correlations and the case without molecular diffusion were exactly on top of each other. However, for the 2D simulation, Figure 6-19 shows that both correlations affected the CO_2 saturation profile with different magnitudes in terms of the sweeping pattern. Figure 6-20 presents the cumulative oil recovered from the 2D simulation, indicating significant incremental oil recovery when molecular diffusion correlations were employed. This has demonstrated the beneficial effect of molecular diffusion in heavy oil displacement by CO_2 even at laboratory scale, where the contact time is quite low. Therefore, a comprehensive experimental study involving molecular diffusion, known to be the limiting mechanism in CO_2/heavy oil systems needs to be carried out in any simulation studies in order to reduce the uncertainty related to mass transfer.

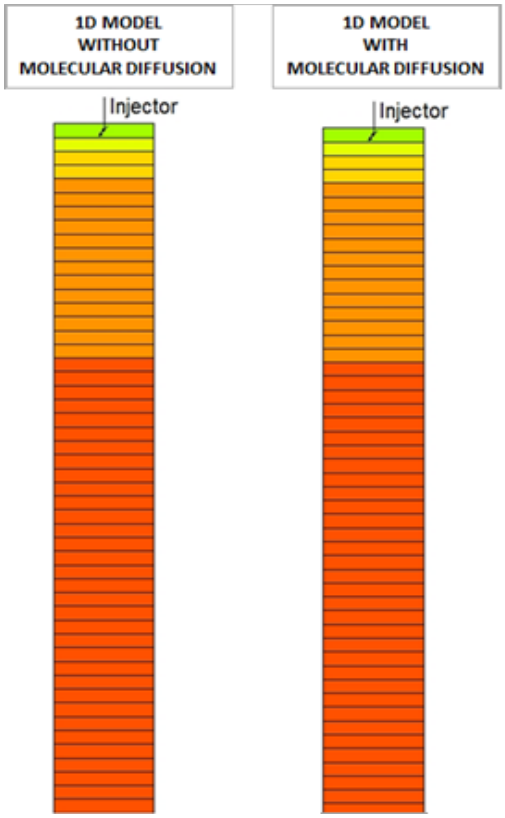

Figure 6-17 Comparison of CO_2 Saturation profiles from a 1D model after 2 hours of injection for simulations with and without molecular diffusion indicating no difference in the saturation profile.

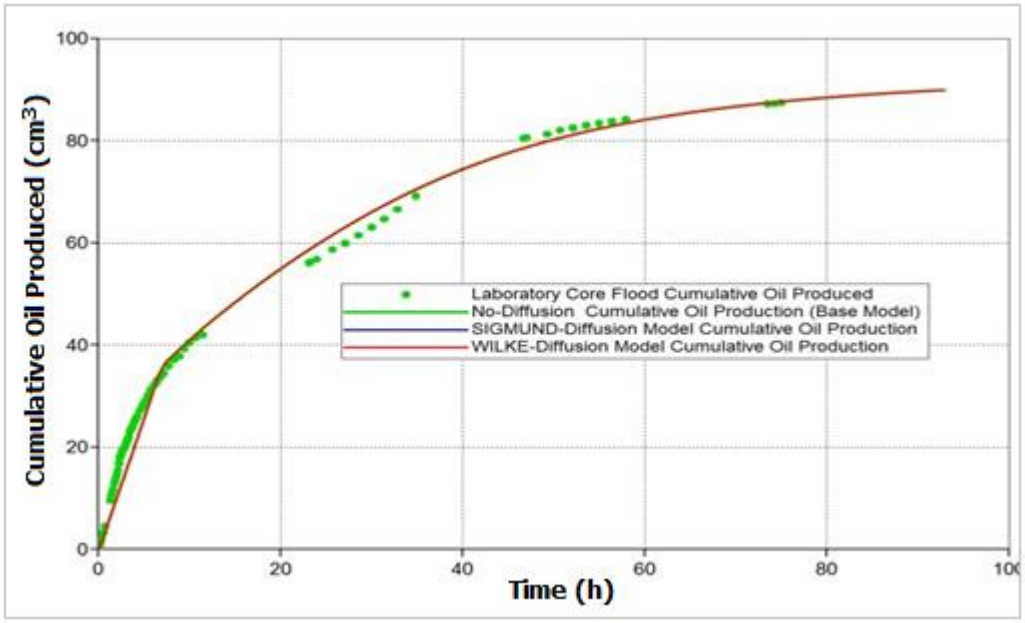

Figure 6-18 Comparison of simulation of cumulative oil recovery using a 1D model with different correlation models for molecular diffusion and the case without diffusion, showing all the models are exactly on top of each other.

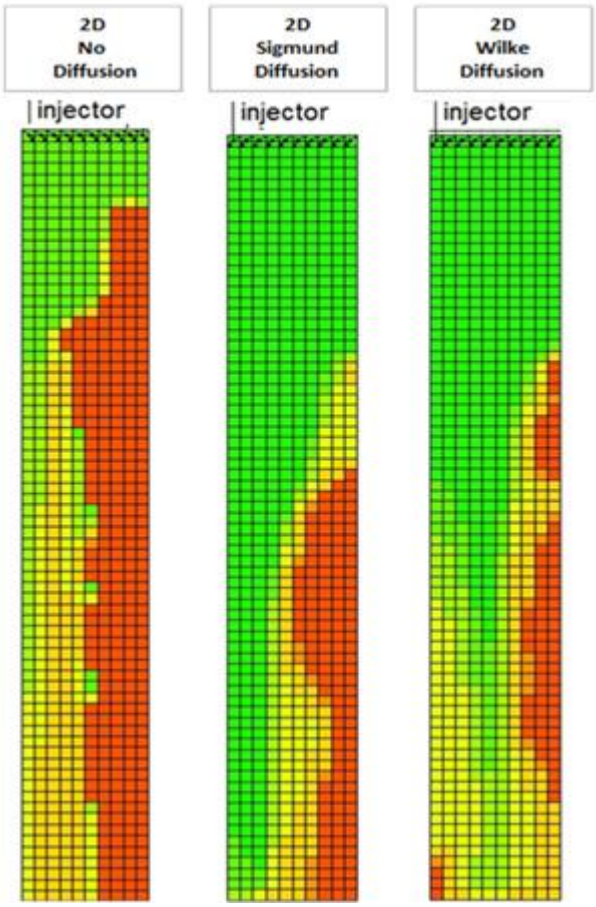

Figure 6-19 Comparison of CO_2 saturation profiles from simulations using 2D model with Sigmund and Wilke molecular diffusion correlations and a case without molecular diffusion in the simulation.

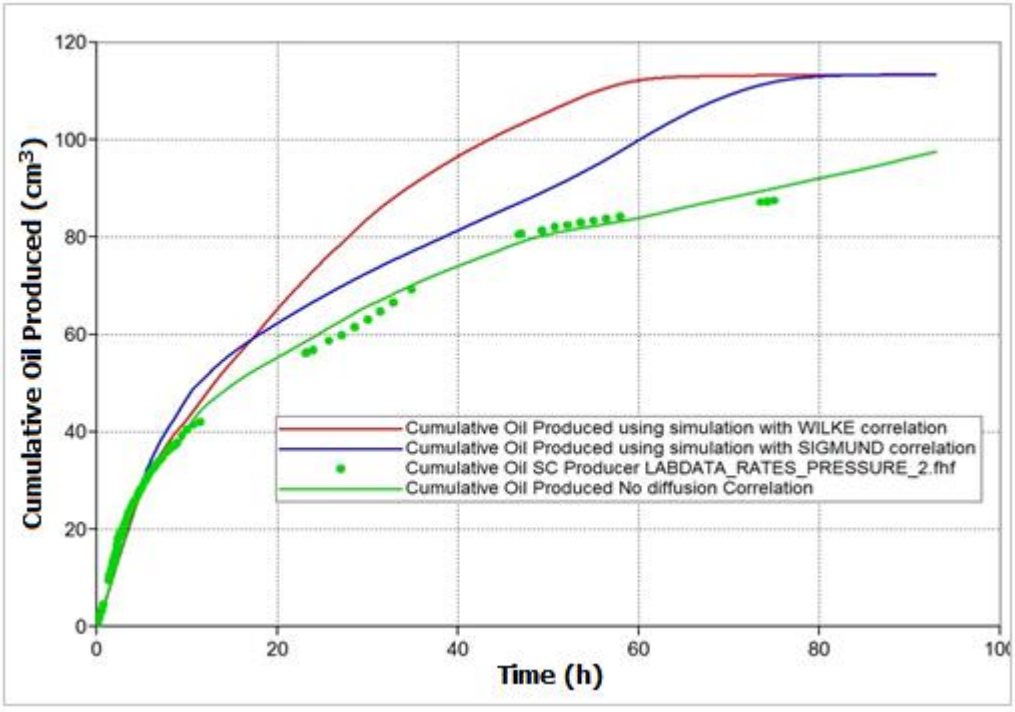

Figure 6-20 effects of different diffusion correlations on cumulative oil produced using a 2D coarse model (10 x 1 x 70)

6.5 EFFECT OF GAS VISCOSITY ON RECOVERY

The viscosity of the contacted gas is another huge source of uncertainty that requires to be investigated. In Experiment-4, when the pure CO_2 with a viscosity of 0.07cp was injected into the heavy oil, it immediately contacted with the oil by molecular diffusion, dispersion and mixing which resulted in the transfer of components between the CO_2 phase and oil phase. Even though the heavy oil has fewer light components, the interaction can affect the thermodynamic equilibrium, leading to some oil components flashing into the vapour phase (Farouq Ali, 1974, Mai et al., 2009). The resulting mixture of the CO_2 and the flashed oil components has therefore changed the composition and property of the gas phase, which was originally CO_2 only. This mass transfer and the consequential property changes are dynamic processes. However, this dynamic change in composition and properties of the phases is not captured in simulation because of the inherent assumption of instantaneous equilibrium by the compositional simulators. Typically, the simulator will compute an average value for the properties using an EOS and assign the values uniformly throughout the phase, ignoring the spatial and temporal variations that are actually taking place in the porous medium.

To examine the effect of this apparent overlook on recovery by these simulators, three cases were considered by varying the viscosity of the gas phase after the CO_2 contacted with the oil; these were 0.7cp, 0.8cp and 0.9cp. Figure 6-21 shows the results of the simulation of cumulative oil recovered in Experiment-4 for the three cases. It can be seen clearly that they all have the same breakthrough time, however, an increase of 0.1cp in gas viscosity resulted in 4% increase in ultimate oil recovery. The increase in oil recovery with increase in gas viscosity was mainly due to extracted components which were produced from the continuous gas phase as well as improvement in the mobility ratio due to the gas having a higher viscosity as a result of extracting lighter oil components. However, the contribution to recovery from the continuous gas phase cannot be distinguished from that produced in the continuous oil phase after flashing the produced fluids in the separator. Figure 6-22 also shows the differential pressure across the core. A significant difference in the differential pressure across the core was observed at the beginning of the injection and before the breakthrough. The reduction in DP with an increase in gas viscosity can also be related to the higher viscous force associated with higher gas viscosity, which reduces the maximum DP. The study therefore highlights the

importance of using a consistent EOS that can adequately reproduce the dynamic changes in the viscosity of the injected fluid after mixing and vaporising lighter components.

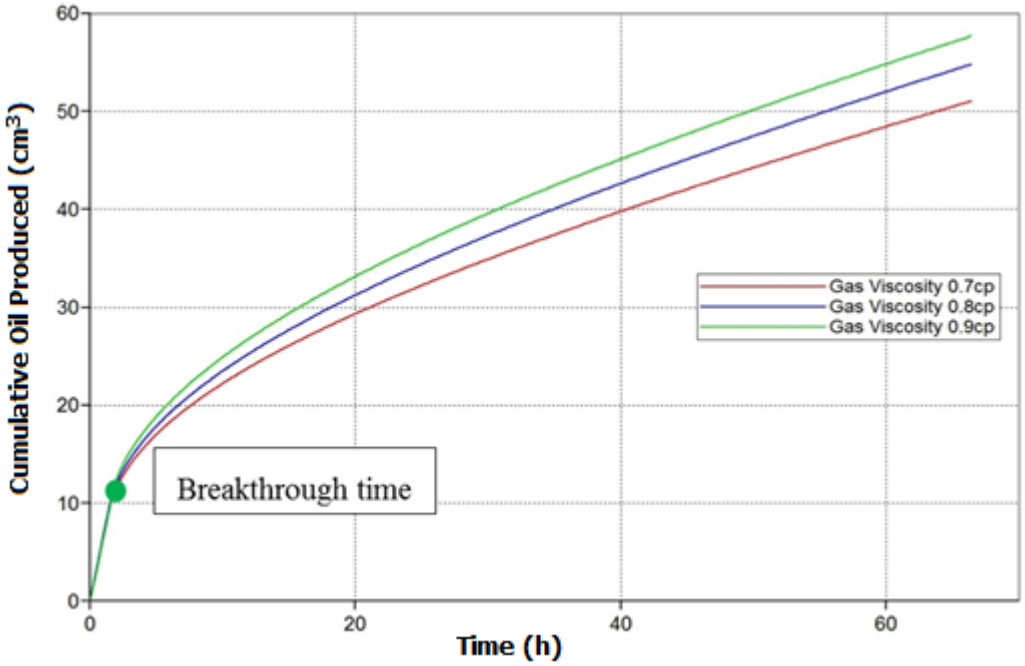

Figure 6-21: Simulation of cumulative Oil Recovered for experiment-1 using 0.7cp, 0.8cp and 0.9cp for contacted gas viscosity. Green dot indicates the same breakthrough time.

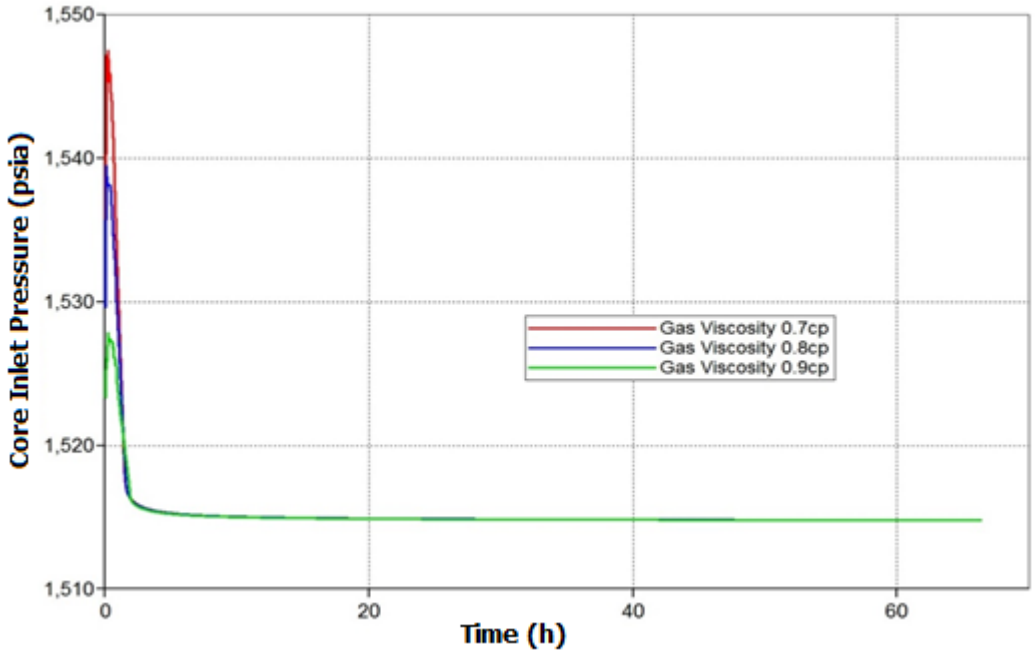

Figure 6-22: Simulation of pressure across the core for Experiment-1using 0.7cp, 0.8cp and 0.9cp for contacted gas viscosity.

6.6 EFFECT OF CO_2 DISSOLUTION ON OIL DENSITY

In most studies involving CO_2 injection into heavy oil for improving recovery, the emphasis is around improving the viscosity reduction ability of CO_2 with dissolution in the oil. However, other associated benefits include density-driven current. The injection of CO_2 into oil has been known to induce the mass transfer of CO_2/Oil systems resulting from the isothermal free convective mass transfer (Nasrabadi et al., 2009, Rongy et al., 2012). This behaviour is brought about by the density behaviour of CO_2-hydrocarbon mixture, which shows an abnormal viscosity behaviour dependence on density. While the viscosity monotonically decreases, the density is found to increase with continued dilution of oil with CO_2 (Lansangan and Smith, 1993).

The increase in density resulting from CO_2 dissolution in oil resulting in change in the flow pattern in this type of displacement has been corroborated by Nasrabadi et al. (2009). For example, Figure 6-23 from Nasrabadi, (2009) shows CO_2 injection into a horizontal homogenous core saturated with light oil at 0.05, 0.1, 0.3 and 0.7 PV, the injection was from the top of the core while production was from the bottom. It shows that an increase of 5% in density resulting from 60% saturation of CO_2 in the oil led to downward trend and formed density fingers (left-hand figures). In comparison, the default case, where there is no variation in density (right-hand side figures), the CO_2 remained at the top and did not reach the producer until later.

To investigate the effect of dynamic change in oil mass density on heavy oil recovery by CO_2 injection, we considered two cases, where instantaneous equilibrium was employed in one case and spatial and temporal density variation in the other. Figure 6-24 shows the results of simulations of Experiment-1 (injection of CO_2 into heavy Oil) where Figure 6-24 (A) shows the oil mass density profile at the end of the injection for the case of instantaneous equilibrium where CO_2 dissolved in the oil instantaneously and hence no density gradient was created. In this case, the CO_2 could only penetrate a certain depth where it was in contact with the oil. However, in Figure 6-24 (B), the CO_2 gradually dissolved in the oil as against the instantaneous equilibrium. This was achieved by allowing the CO_2 to diffuse into the oil using a small mass transfer coefficient. The result was the formation of density gradient in the system that led to the occurrence of density current which manifested into better recovery with smaller bypassed oil region

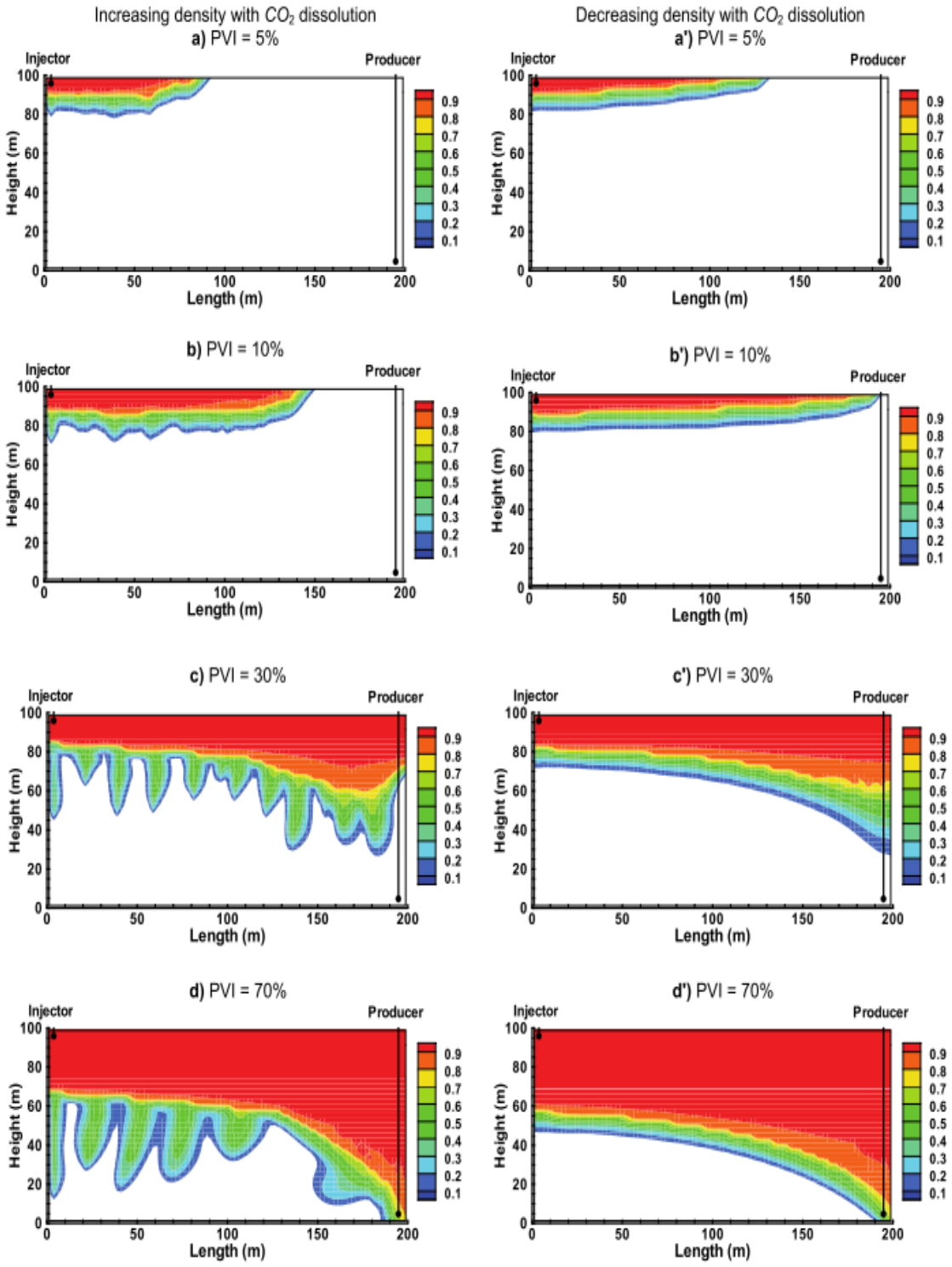

Figure 6-23: Overall CO_2 composition (mole fraction) at different times for (a, b, c, d, on left hand side) increasing density with CO2 dissolution (5% increase at 60% CO2 mole fraction) and (a', b', c', d' on right hand side) decreasing density with CO_2 dissolution: top injection, homogeneous media, k=1000 md (Nasrabadi et al., 2009).

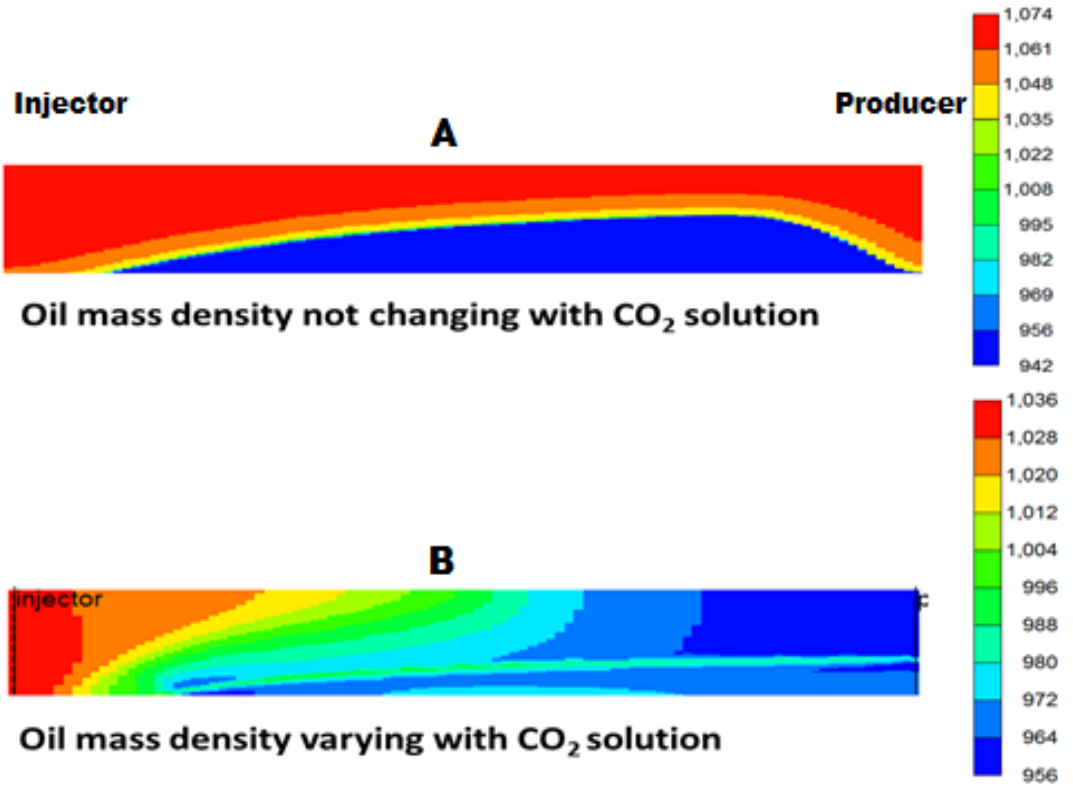

.

Figure 6-24: Shows the results of simulations of oil mass density profile for experiment-1. Where A: shows the profile when the CO_2 instantaneously dissolved in the oil leading to CO_2 penetrating a certain region of the oil, whereas B: shows the oil mass density profile when the CO_2 gradually dissolved in the oil leading to density current and the CO_2 interacting with a larger oil region.

6.7 EFFECT OF HYDROCARBON SOLUTION GAS RECOVERY AND RELATIVE PERMEABILITY (EXPERIMENT 3)

The most significant benefit of CO_2 injection in heavy oil reservoirs for the purpose of enhancing recovery comes from the reduction in oil viscosity as a result of the dissolution of CO_2 in the oil. However, crude oil always contains some dissolved gas, which can affect the rate and amount of dissolution of CO_2 that can dissolve in the oil. To investigate the effect of solution gas, Experiment-3 where CO_2 was injected into live crude-J (crude saturated with methane) in a horizontal core was considered. The results showed that the main oil recovery mechanisms during the displacement (direct displacement, dissolution, and extraction) were similar (but with varying magnitude) to those operating in secondary CO_2 flooding in the dead crude oils. However, before the CO_2 breakthrough (BT), direct displacement of oil by CO_2 was the dominant recovery mechanism, after the CO_2 BT, the recovery of the (continuous) oil phase continued due to the pressure gradient across the core. Other mechanisms which assisted oil recovery were CO_2 dissolution, oil swelling, viscosity reduction and hydrocarbon extraction by CO_2.

Figure 6-25 compares the oil recovery curves obtained during the secondary CO_2 flooding in saturated oil system (Experiment-3) and the secondary CO_2 flooding in dead oil test (Experiment-1). It shows a reduction in oil recovery when the oil was saturated with gas. This is attributed to the adverse effect of dissolved hydrocarbon gas on the rate of CO_2 dissolution in oil. The dissolved hydrocarbon gas had to be dislodged first from the oil before the CO_2 could dissolve in it. This competition significantly reduced the potential of CO_2 dissolution and hence the reason for the lower viscosity reduction and displacement efficiency. As can be seen, this difference in oil recovery is more profound at early times, and ultimately the amount of oil recovery in the saturated (live) oil approaches that of the dead oil. This means that the injection of CO_2 would be more beneficial for undersaturated reservoirs compared to saturated ones and that the sooner the CO_2 injection begins, the better, since the degree of undersaturation would be higher in the reservoir at early time after the start of oil production when the reservoir pressure is more likely to be still high and above the bubble point pressure.

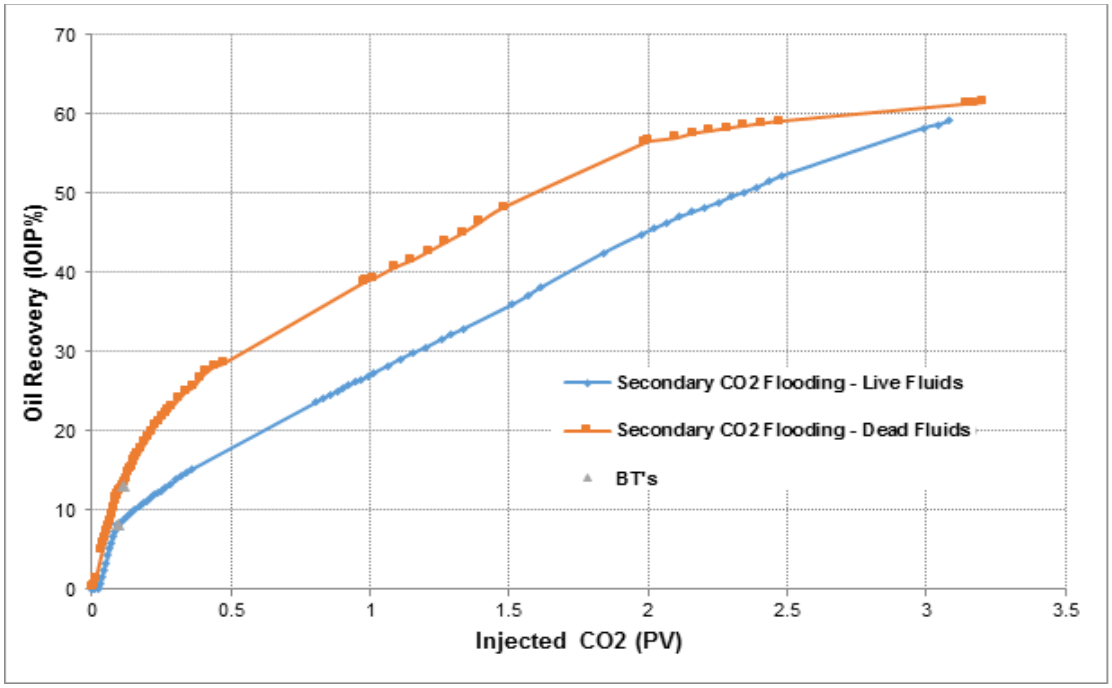

Figure 6-25: Comparison of the oil recovery versus injected pore volumes during secondary CO2 flooding with fully saturated oil (Experiment 3) and secondary CO2 flooding in dead oil (Experiment 1)

To simulate the experiment, the live oil viscosity was estimated using EOS since laboratory based viscosity measurement was not available. This was achieved by re-

combination of the dead oil with methane and computing the viscosity of the mixture using Pedersen (1984a) viscosity correlation for crude oil mixture. A viscosity of about 100cp was achieved which was much lower than that of the dead oil (617cp). The CO_2 viscosity at the experimental pressure and temperature (1500psi 28^0C respectively) was 0.007cp. It was therefore expected that instability due to unfavourable mobility ratio would also occur similar to the dead oil case. An analysis of the instability using equation 17 indicates that $N_G \approx 0.07$ which is less than 1, an indication that gravitational finger similar to that observed in the dead oil displacement would be formed. In addition, it was also expected that the CO_2 having a higher potential would displace methane from the solution thereby evolving it into the gaseous phase. The released methane then dynamically alters the composition and the properties of the bulk gas phase since it has a much lower density (0.078g/cc) and viscosity (0.014cp) compared to the dense CO_2 phase (0.79g/cc and 0.07cp respectively) at the experimental condition. It can also form a separate phase after evolving from the oil since the CO_2 is in dense phase and the methane would be in gaseous phase at the experimental condition, hence leading to a three-phase flow. The latter hypothesis is not a subject of this research.

Therefore, to investigate these mechanisms and to determine the effect of solution gas on the unstable relative permeability, firstly the relative permeability curves obtained from the dead oil displacement in which there was no solution gas in the oil (Experiment-1) was used. The result of the cumulative oil produced from the simulation shows that the relative permeability could not match the experiment. Hence, to determine the appropriate set of relative permeability curves, history matching of Experiment-3 using a high-resolution model that was determined after prior grid sensitivity studies, similar to that described in section 1.1 was conducted. The grid size for the high-resolution model was 100x80, which agrees to that used in Experiment-1 (section 4.3). Accordingly, the same modelling approach was implemented to account for the compositional effect and instability in the displacement process. This was achieved using the CMG-GEM simulator. The history matching was carried out by optimising the match on production data, produced oil and gas and the core inlet pressure (DP) using CMG-CMOST software.

Figure 6-26 shows the result of the match on the cumulative oil recovered from the simulation compared with the experimental data. A good match was obtained before the breakthrough and an acceptable match after. Figure 6-27 shows the result of the pressure

at the inlet of the core for the optimised simulation while Figure 6-28 shows the match on produced gas in comparison with the experimental data. A good match was obtained especially after the breakthrough for all the simulation results. Similarly, as in the case of the dead oil displacement (Experiment-1), the matching before the breakthrough cannot be improved, due to the limitation of the simulator, which assumes instantaneous equilibrium and hence not able to properly account for viscosity variation with CO_2 dissolution in the oil.

Moreover, Figure 6-29 shows the relative permeability curve obtained from the history matching procedure in comparison with that obtained from the dead oil displacement. It can be observed from the curves that the oil relative permeability at the irreducible water saturation (Kro) for the live oil was 0.861, which is lower than the Kro for the dead oil displacement (0.988). This may be as a result of change in contact angle or wettability of the rock to more oil-wet due to the change in the oil composition. Also, the gas/oil relative permeability at the irreducible oil saturation (Krg) for the live oil was 0.459, which is higher than that of the dead oil. This may be due to the mixture of the CO_2 and methane in the bulk gas phase having a lower viscosity than the pure CO_2 that was in the bulk gas phase during the dead oil displacement (methane has a lower viscosity than CO_2 at the experimental condition). Similarly, even though both gas curves indicated strong S-shape behaviour, the curve for the live oil rises earlier and has lower critical saturation because the mixture of methane and CO_2 that formed the bulk gas phase was less viscous and therefore easier to flow. It is quite noteworthy, however, that the estimated relative permeability for the live oil is based on a 'crude' estimation of the oil viscosity since no measured data is available and is therefore not very reliable.

Figure 6-30 shows the oil saturation profile of the CO_2 injection after 0.1PV injected and at the end of the injection period for the dead oil (top) and live oil (bottom) displacements. It indicated that, at the beginning of the injection (0.1PV), both displacements indicated a tendency to form a gravity finger. This is commensurate with the earlier analysis of the instability which showed N_G to be lower than 1 for both cases. The live oil displacement also developed more than one finger at the beginning of the injection (due to lower viscosity of the oil compared to that of the oil) which later coalesced to form a single finger. At the end of the injection, both displacements left behind a bypassed region at the bottom of the core and a swept region at the top of the core, a typical evidence of

gravity tonguing. However, the swept areas for the two displacements are different, at the end of the injections, due to the different mechanisms involved. The dead oil saturation profile showed a smaller bypassed oil compared to the live oil displacement. This can be due to CO_2 dissolving more in the oil and reducing the oil viscosity, making it easier to flow. Additionally, it can also be caused by the CO_2 gravitationally extracting lighter component from the bulk oil region that is at the bottom. A compositional analysis of both oils would verify any evidence of these mechanisms.

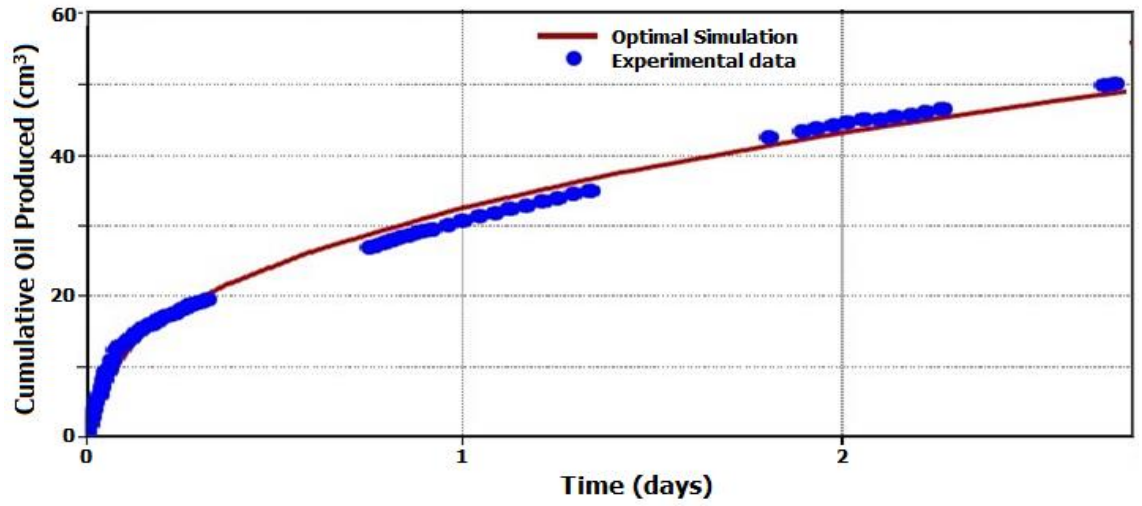

Figure 6-26: Shows the result of the history matching of cumulative oil recovered during the secondary CO_2 injection into live oil in a horizontal core compared with production data.

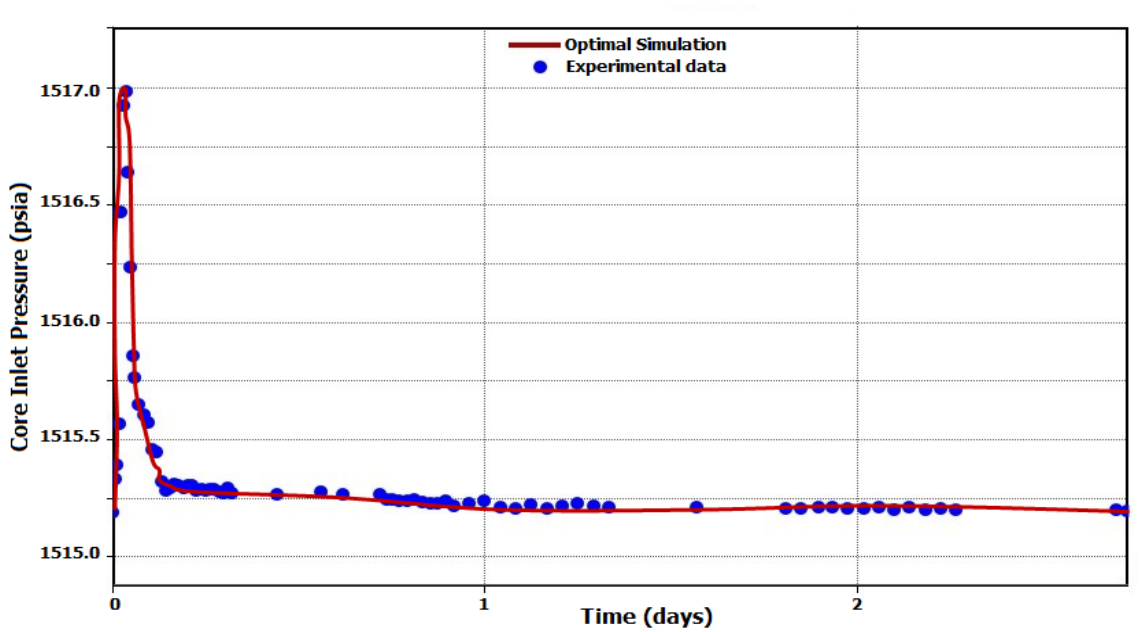

Figure 6-27: Shows the result of the history matching of pressure at the core inlet during the secondary CO2 injection into live oil in a horizontal core compared with production data.

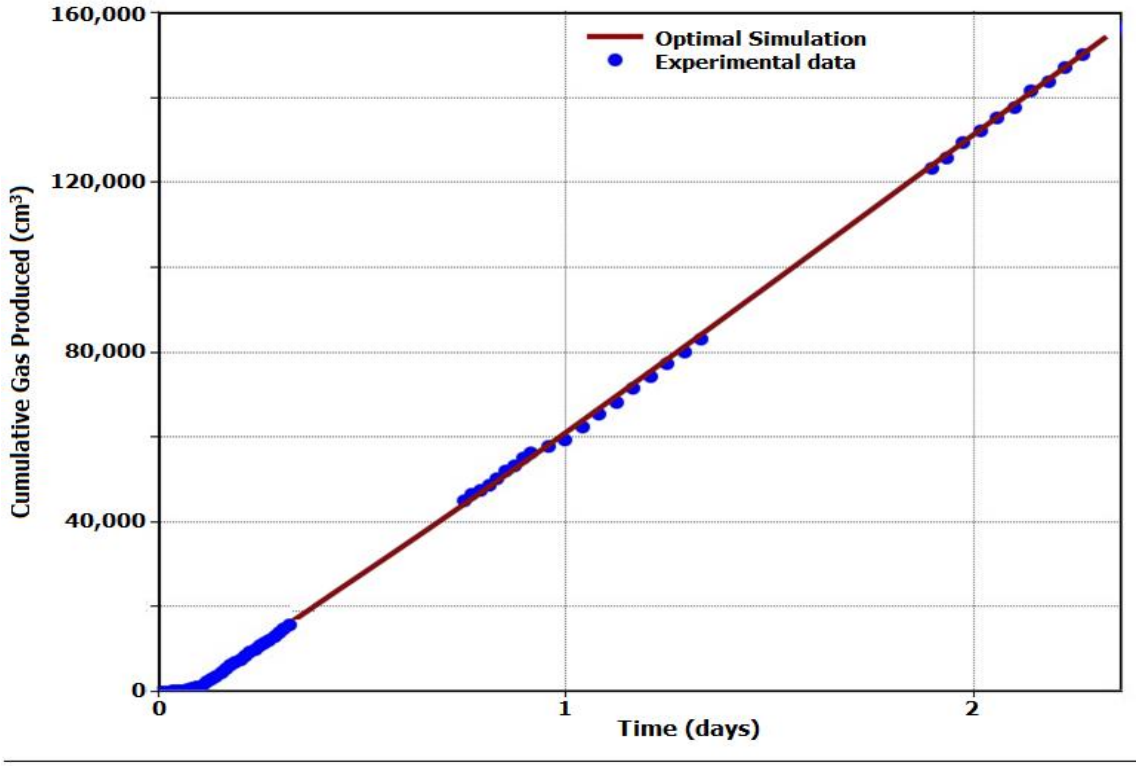

Figure 6-28: Shows the result of the history matching of cumulative gas produced during the secondary CO2 injection into live oil in a horizontal core compared with production data.

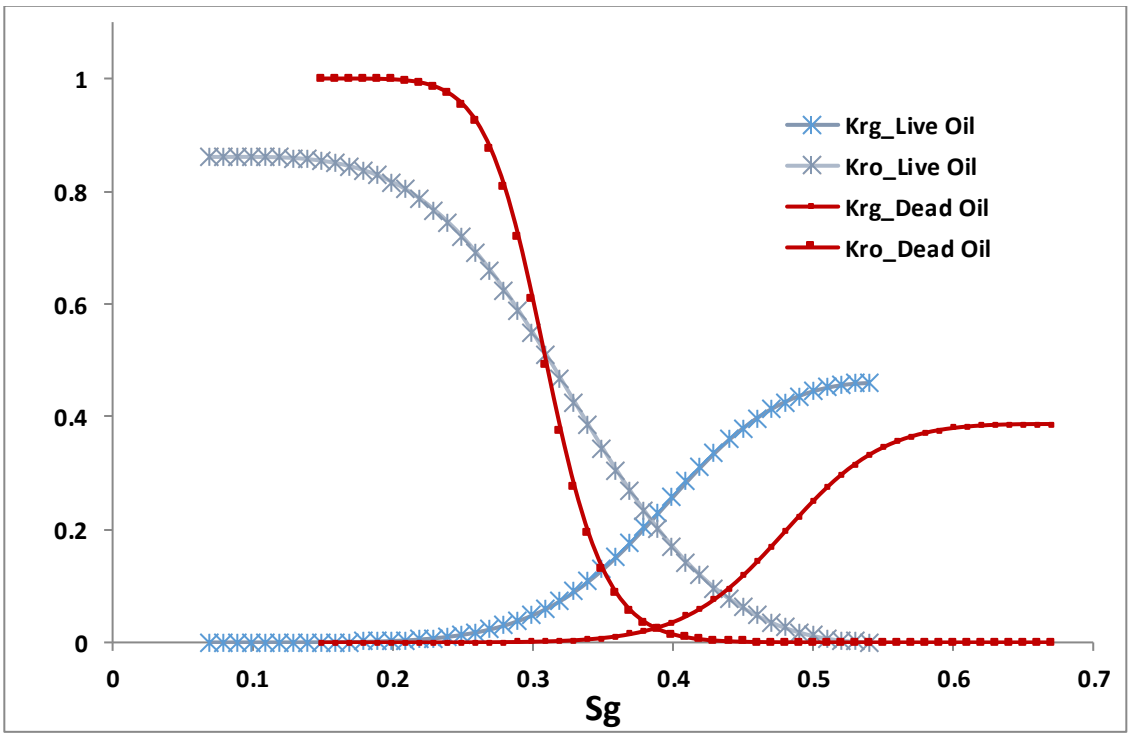

Figure 6-29: A comparison of history matched relative permeability obtained from the secondary injection of CO2 into live oil in a horizontal core and secondary injection of CO2 into dead oil in a horizontal core.

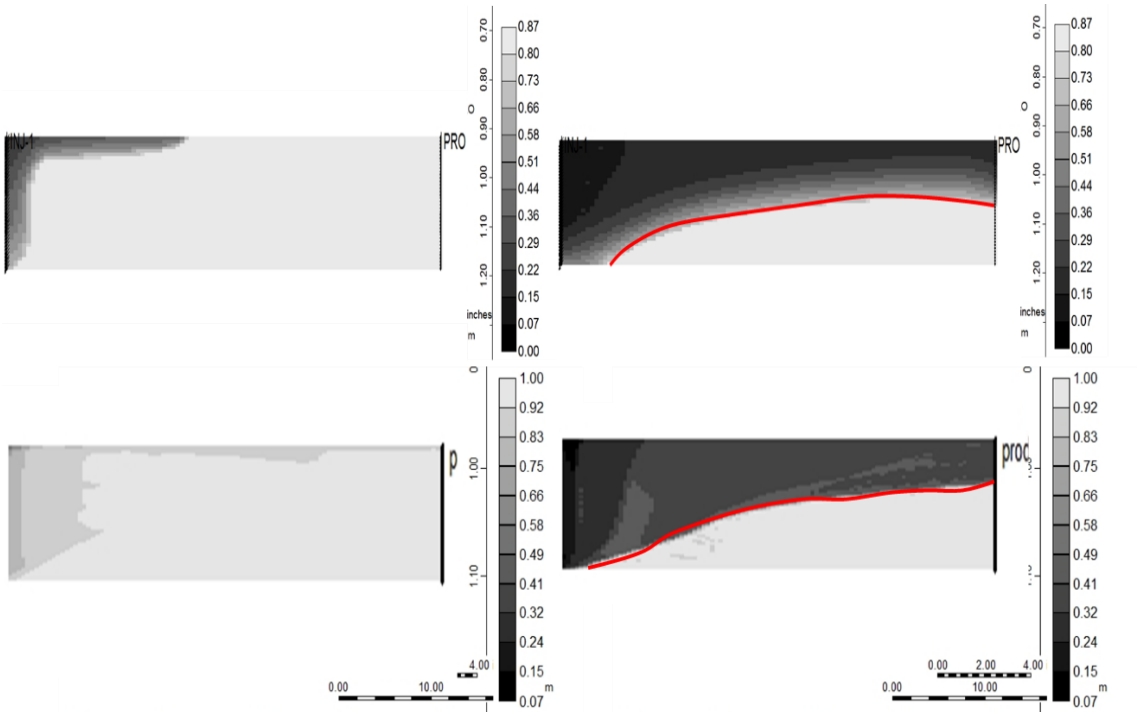

Figure 6-30: Shows the oil saturation profiles of the dead oil (top) and the live oil (bottom) displacements at the beginning of the injection (0.1PV) and the end of the injection. The red line divides the swept area and the bypassed oil region.

6.8 CONCLUSION

In the displacement of heavy oil by water, gas or solvent, several processes which gradually occur can dynamically change the overall fluid and the rock properties, making the modelling of such displacement an onerous task. These properties include the mass transfer between phases, which can lead to a dynamic change in fluid composition and properties, as well as capillary pressure and rock wettability alterations due to the change in interfacial tension. In addition, there is also the issue of viscous fingering resulting from the large mobility ratio and the adverse effect of hydrocarbon solution gas on oil recovery. These are complex processes that require a tremendous amount of experimental and theoretical information to adequately model and simulate. It is for these reasons that it is important to gauge the model against their effect. To this end, the effect of some of these processes on the estimation of flow parameters for the simulation of heavy oil displacement was sensitised.

The following conclusions are drawn from the work in this chapter:

1. The two-phase gas/oil relative permeability obtained from the history matching of secondary CO_2 injection into a horizontal core saturated with heavy oil (Experiment-1) was used directly to simulate similar experiment, which was in the vertical orientation (Experiment-5). The results showed a perfect match with the experimental data obtained from the vertical injection experiment, indicating that the estimated relative permeability was not affected by the orientation.

2. The results of the simulation also showed that the gravity drainage displacement mechanism similar to that in vapour extraction (VAPEX) process occurred in the vertical CO_2 injection (Experiment-5), indicating the ability of CO_2 to extract component under the influence of gravity through density current.

3. The shape of the relative permeability estimated by history matching when capillary pressure curve was included is different from that estimated when capillary pressure was not included. They have significantly different critical saturation values and residual oil saturation even though the core was homogenous with relatively high permeability. This understates the importance of including capillary pressure in estimating relative permeability in heavy oil displacement.

4. The simulation of the secondary waterflood in which converted experimental drainage capillary pressure curve was included during the estimation of relative permeability, showed a stable, Buckley-type front, while the simulation of the same experiment, without capillary pressure inclusion in the estimation of relative permeability showed an unstable front with multiple viscous fingers. This highlights the importance of capillary pressure in the stability of fronts in the simulation of heavy oil displacement processes.

5. Effect of Fickian (molecular) diffusion on the residual oil and the recovery was investigated. The analysis showed that only about 10% of the bypassed oil can be penetrated. However, this can be significantly higher when

convective and dispersive effects are considered and also when injection time is longer such as in a reservoir.

6. The viscosity of the CO_2 gas phase can dynamically change during injection into the heavy oil as it gradually extracts lighter components from the oil. This would have a significant effect on the amount of trapped oil in the pores and hence, the recovery. Since most commercial simulators use assume instantaneous equilibrium as the gas is injected as it comes in contact with the oil, this effect was sensitised by varying the viscosity of the contacted gas. An increase of about 10% in the contacted viscosity led to about 5% increase in ultimate oil recovery.

7. A unique property of CO_2 is its ability to increase oil density when it dissolves in oil. This phenomenon can lead to density current which can significantly affect recovery. The simulation result showed that the dynamic density change developed into density current and eddies which resulted in lower bypassed oil compared to the displacement with constant oil density.

8. Hydrocarbon solution gas dissolved in heavy oil can limit the amount of CO_2 that can dissolve in the oil thereby hampering the viscosity reduction effect of CO_2. This can adversely affect the rate of oil recovery in heavy oil displacement by CO_2

9. The relative permeability curves of live oil were markedly different from that of the dead oil due to change in fluid viscosity and possibly as a result of changes in rock properties such as wettability and contact angle.

CHAPTER 7

THEORETICAL PREDICTIVE MODEL FOR VISCOUS FINGERING IN HEAVY OIL COMPOSITIONAL DISPLACEMENT

7.1 INTRODUCTION

Solvent injections such as CO_2, N_2 and hydrocarbon gases are common non-thermal processes of enhancing oil recovery. In conventional oil, the aim of these injection processes is to achieve miscibility, a concept where two or more fluids can form a single homogeneous phase when mixed in all proportions, as opposed to solubility which is defined as the ability of a limited amount of one substance to mix with another substance to form a single homogeneous phase (Holm, 1986). Miscibility improves the recovery by eliminating the interfacial tension between the oil and the solvent (Stern, 1991). However, in heavy oil displacement systems, miscibility is not practically achievable, and the aim of solvent injection in such systems is mainly to reduce the oil viscosity when the solvent dissolves in the oil. But the solvent injection leads to another adverse effect known as viscous fingering, which occurs due to the adverse mobility ratio between the solvent and the oil. The physics of occurrence of this phenomenon is not entirely understood, and current techniques of modelling processes that involve viscous fingering require considerable resolution to be able to capture the instability (Christie and Bond, 1987, Christie et al., 1990, Blunt and Christie, 1994).

The previous chapters tackled the first objective of this research, which is how to simulate displacement processes in which viscous fingering occurs as well as how to estimate relative permeability in such displacement processes. However, no laboratory based measurement such as saturation distribution were used to verify the simulation and the estimated relative permeability. The reason is because in heavy oil displacement by water for example, in-situ saturation measurement is not usually attempted due to the similar densities of the two fluids. Visual saturation monitoring (like transparent sand packs) is

also not convenient due to the associated high experimental pressure. Therefore, this chapter looks at an alternative methodology for verifying the results of simulation of saturation distribution in displacement with instability and compositional effect. The objective, is to analytically or otherwise verify the results obtained in the previous chapters, which include saturation profile and gas/oil relative permeability obtained from the history matching technique of the displacement involving viscous fingering and compositional effect.

7.2 VISCOUS FINGERING

Viscous fingering as a form of instability is common to miscible and compositional injection scenarios and has been investigated at both laboratory and field scales extensively (Cuthiel et al., 2006). Several attempts have also been made to establish a theoretical basis for its occurrence (Araktingi and Orr Jr, 1993). Viscous fingers in these types of injections manifest themselves early, propagate and lead to an early breakthrough. Four major factors have been identified which bring about and or exacerbate the effect of instability. These are mobility ratio, gravity effect, channelling and longitudinal dispersion. Other factors whose effect can be controlled to some certain limit include injection rate and diffusion.

7.2.1 Viscous Fingering Theory

Earlier theoretical works on viscous fingering were based on miscible displacement and included the famous works of Koval (1963) and Todd and Longstaff (1972) that form the basis of most of the empirical studies and approaches in modelling viscous fingering.

7.2.1.1 Miscible displacement Scenario

Koval's (1963) model was developed based on First Contact Miscible (FCM) floods with the inherent assumption that the solvent fractional flow is proportional to the volume fraction of the solvent in the porous medium. This hypothesis is analogous to immiscible displacement case where the injection fluid and the oil relative permeability are assumed proportional to the volume fractions of the injection fluid and the oil respectively. Another assumption in this approach is the existence of an effective average solvent viscosity, which is independent of the solvent local concentrations that can be used in the mobility equation. The modified fractional flow F_{sk} by Koval is given by equation (32)

$$F_{sk} = \frac{1}{1+\frac{\overline{\mu_s}}{\mu_o}\frac{(1-C)}{C}} \quad 32$$

Where C is the concentration of the solvent and μ_s and μ_o are the solvent and oil viscosities respectively.

Using the one-quarter power mixing rule and a number of miscible experiments, Koval determined the effective average concentration as C=0.22 by fitting the effluent concentration behaviour from the experiments. The effective average solvent viscosity ($\overline{\mu}_s$) was given by equation (33)

$$\overline{\mu}_s = \left(\frac{0.22}{{\mu_s}^{1/4}} + \frac{0.78}{{\mu_o}^{1/4}}\right)^{-4} \quad 33$$

The limitation of this method is that it does not provide for the total effective mobility of the combined flow, which is required in numerical simulation. It also does not state if the effective density of the solvent would be based on the effective average concentration C=0.22 in cases where gravitational segregation is to be considered.

Todd and Longstaff (1972) approach, which is also based on FCM, is an improvement over the Koval's method. It uses the similar assumption of relative permeability being proportional to the components volume fractions, but both the effective average viscosities of solvent and that of oil are modified using the mixing rule. The modified equations in Todd and Longstaff are given by (34) and (35) for solvent and oil respectively.

$$\mu_{se} = {\mu_s}^{1-\omega}{\mu_m}^{\omega} \quad 34$$

$$\mu_{oe} = {\mu_o}^{1-\omega}{\mu_m}^{\omega} \quad 35$$

$$\mu_m = \left(\frac{C}{{\mu_s}^{1/4}} + \frac{1-C}{{\mu_o}^{1/4}}\right)^{-4} \quad 36$$

Where ω is a mixing parameter and μ_{se} and μ_{oe} are effective solvent and oil viscosities respectively.

Therefore, the modified fractional flow for the Todd and Longstaff model can, be given as equation (37)

$$F_{sTL} = \frac{1}{1+\frac{\mu_{se}}{\mu_{oe}}\frac{(1-C)}{C}} \quad 37$$

7.2.1.2 Immiscible Displacement Scenario

For immiscible displacement and compositional gas floods in which viscous fingering occurs, the work of Blunt and Christie (1994) is the most famous. It is a modification of the empirical model proposed earlier by Todd and Longstaff, which was based on FCM. In their approach, the viscosity ratio in the famous Koval's equation was replaced with total mobility ratio across the finger. This is a good assumption, and their equation will be similar to that of Koval's for a fully miscible case. Additionally, for compositional displacement where there is a partial dissolution of components or evaporation/extraction, they considered a multicomponent material balance of the hydrocarbon phase flow in a 1D porous medium to track the position of the front. This is given by equation (38).

$$(\partial m_i/\partial t) + (\partial u_i/\partial x) = 0 \quad 38$$

Where m_i is the mass of component i per unit volume and u_i is the mass flux of component i per unit area.

For a system with only oil and gas phase, the equation can simply be written as equations (39) and (40).

$$m_i = \emptyset\left(\rho_o S_o x_i + \rho_g S_g y_i\right) \quad 39$$

$$u_i = v_t\left(\rho_o f_o x_i + \rho_g f_g y_i\right) \quad 40$$

$$\text{Where} \quad v_t = v_0 + v_g \quad 41$$

The parameters f_o and f_g are volumetric fractional flows of the oil and gas phases respectively, and v_t is the total Darcy velocity.

The solution to these set of equations is a function of a single variable (v=x/t) and can be solved numerically or analytically for simple cases (Dumore, 1964). Accordingly, in compositional displacement, another important parameter is the total mobility, which is the sum of the ratio of relative permeability to the viscosity of the displaced and the displacing fluid in a porous medium. This ratio gives the condition for instability and in particular viscous fingering. For a system with oil and gas only, the total mobility is given by equation (42)

$$\lambda_t = \lambda_o + \lambda_g = (k_{ro}/\mu_o) + (k_{rg}/\mu_g) \qquad 42$$

Where λ is mobility, k_r is relative permeability, and μ is viscosity. The subscripts t, o and g, represent total, oil and gas respectively.

In 1D displacement, the ratio of total mobility at the Buckley-Leverett shock front is called M_{shock} (equation 43). It specifies the condition for instability in a multi-dimensional simulation of the displacement.

$$M_{shock} = \lambda_t^L/\lambda_t^R \qquad 43$$

Where L denotes "behind the front" and R denotes "ahead of the front".

The flow will essentially be stable when this value of M_{shock} is less than 1 and essentially unstable when it is greater than 1 (see equation 44)

$$stable\ when\ M_{shock} \leq 1 \qquad 44$$
$$\text{and unstable when } M_{shock} > 1$$

However, in 2D displacements with instability, the sharp profile observed in the 1D Buckley-Leverett type front is smoothed out as a result of viscous fingering. Here the total mobility, in contrast to the 1D displacement, is the total mobility across the fingered region. Blunt et al, (1994) proposed a flux function form of an empirical model, which can predict the average flow behaviour for the 2D compositional displacement with instability assuming the average composition is a linear combination of the compositions of the leading edge and the trailing edge of the finger. The average composition of any component within the fingered region $\bar{m}_i$ is given by equation (45).

$$\bar{m}_i = C_i m_i^{left} + (1 - C_i) m_i^{right} \quad (45)$$

Where "left" indicates the trailing edge and "right" indicates the leading edge, Ci is a parameter varying from 0 to 1 as the composition varies from the trailing to the leading edge. The flux function for the average composition $\bar{u}_i$ has the same functional form as used in Todd and Longstaff model (1963) and is given by equations (46) and (47). Where g_i is a function of C_i similar to the one used by Todd and Longstaff.

$$\bar{u}_i = g_i(C_i) u_i^{left} + [1 - g_i(C_i)] u_i^{right} \quad (46)$$

$$g_i(C_i) = C_i / [C_i + (1 - C_i)] / M_i \quad (47)$$

Where M_i is a parameter, which depends on the composition of the trailing edge and must be determined. It is related to the Koval's number (M_e) through equating the speed of the leading edge given by equation (48) where v^s is the speed of the component at the leading edge of the finger in 2D simulation and M_e is the modified Koval's effective mobility given by equation (49).

$$v_i^s = v^{shock} M_e \quad (48)$$

$$M_e = (0.22 + 0.78 M_t^{0.25})^4 \quad (49)$$

Where M_t is the total mobility given by the ratio of the total mobility at the trailing edge of the finger termed as left (L), to that ahead of the finger termed as right (R) and can be written as equation (50).

$$M_t = \lambda_t^L / \lambda_t^R \quad (50)$$

7.3 EFFECT OF SATURATION DISTRIBUTION ON RELATIVE PERMEABILITY

The saturation distribution of fluids in porous media has the largest impact on the shape of relative permeability curves because relative permeability is a strong function of saturation. This necessitates verifying saturation distribution obtained from history matching process where non-uniqueness is an issue, in order to have a representative system. To achieve this, physical techniques such as x-ray and other theoretical means

are employed to obtain experimental data that is used to verify the results of history matching. However, the experimental results are often not reliable especially for heavy oil waterflood where the viscosity of oil is similar to that of water. Visual saturation monitoring (like transparent sand packs) methods are also not attempted due to the high pressure condition of the experiments. For unsteady state flow experiments, material balance, which is relatively easier, is often utilised.

The dynamic saturation distribution in the simulation is controlled by factors such as mobility ratio, the density of fluids and the wettability of the porous medium (Sandberg et al., 1958). In heavy oil displacement by a gas such as CO_2, the saturation profile is controlled by the adverse mobility ratio between the two fluids. In this case, in addition to honouring the physics of the flow, it is essential to ensure the right resolution is used to capture the fine fingers effectively. To illustrate this, Figure 7-1 shows the saturation profiles of four different models of Experiment-1 after 0.1PVI. The models were differentiated by varying the number of grids in the direction perpendicular to the flow (z-direction); the models are 100x10, 100x20, 100x40 and 100x80. Although all the four models were history-matched with the same experimental production data, namely, cumulative oil recovered, differential pressure and cumulative gas, however, they vary significantly in the saturation distribution of the fluids after the same period of injection. This underscores the importance of obtaining the right resolution for the simulations.

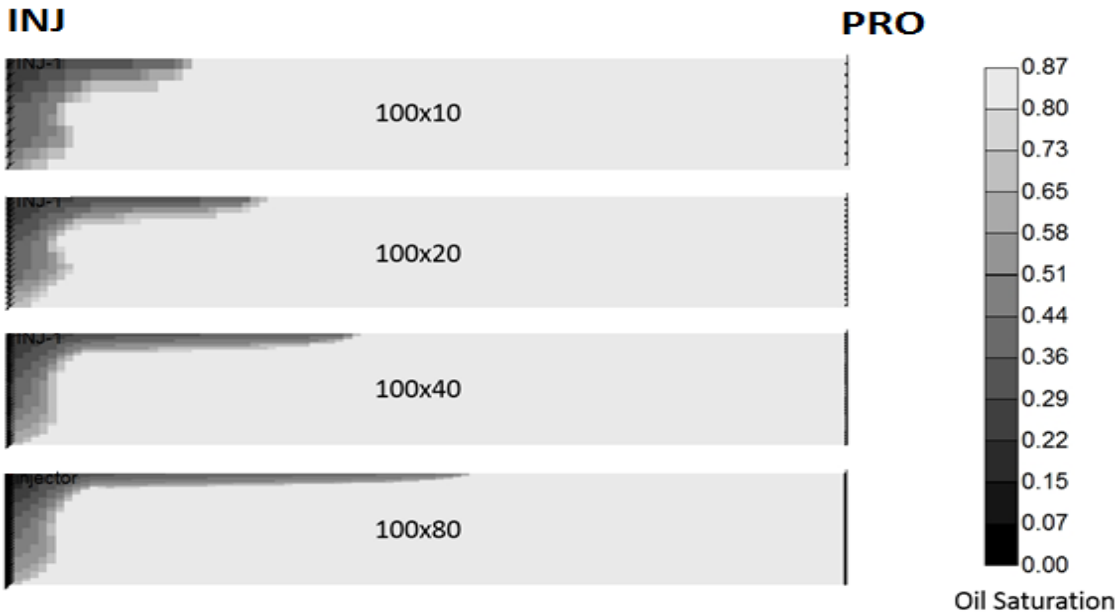

Figure 7-1: Oil saturation distribution after 0.1PV injection for four different models

7.4 PREDICTING AVERAGE SATURATION IN GAS/HEAVY OIL DISPLACEMENT

Simple theoretical models are useful and quick tools for predicting average properties such as saturation distribution or breakthrough time. This is because, quite often, an engineer is confronted with having to run a large number of simulations to determine unknown parameter such as relative permeability curve. For stable displacements, these studies can be carried out using simple one-dimensional models since the front will be more or less be sharp and can therefore be represented by a Buckley-Leverett type of flow. However, for unstable cases, as seen previously, it requires a multi-dimensional simulation model with a considerably higher resolution to effectively capture the instability at the front. Such studies involving a large number of fine-scale high-resolution models will attract higher computational requirement and time and may lead the engineer to make a compromise in the grid resolution thereby creating bias in the estimated unknown parameter. If the resolution were compromised in history matching studies for the estimation of relative permeability, for example, it would significantly affect the saturation distribution of the fluids as seen previously, thereby leading to bias in the estimated relative permeability curve.

For this purpose, Semi-empirical models have previously been proposed for immiscible conventional displacement by gas in which compositional changes may occur, Blunt et al. (1994) and Blunt and Christie (1994) have used this approach to predict saturation front in immiscible and compositional displacement up to a maximum viscosity ratio of 86. This forms the basis for the approach in heavy oil displacement, where the viscosity ratio is much higher. The similar assumption would be used as that of the Blunt and Christie where they proposed that the diffusion and dispersion effects are small and therefore the composition within the fingered region varies linearly from the trailing end of the finger to the leading edge based on fractional flow formulation. Therefore, the proposed procedure for predicting compositional profile in heavy oil displacement with viscous fingering is as follows.

1 Conduct a preliminary 1D-model simulation of the experiment. This is required to determine if the displacement would be unstable in real 2D or 3D displacement. Instability can be calculated by satisfying the condition of equation (44) after matching the 1D simulation with experimental production data.

1 Determine the composition at the trailing end of the finger from the 1D simulation. In the Blunt and Christie approach for conventional oil, their method for determining the trailing edge of the finger is a trial and error approach. However, in heavy oil displacement, the large viscosity difference makes the finger very sharp and trailing edge can mostly be easily picked close to the injector. Hence, the parameters M_t and M_e can then be calculated.

2 Using the assumption that the composition within the fingered region varies linearly from the trailing edge to the leading edge of the finger. The compositional profile of the displacement can be constructed.

Two physical coreflood experiments simulated in chapter 4 were considered to demonstrate the methodology by verifying the estimated relative permeability obtained from the history matching process. This was achieved by comparing the average gas saturation obtained from the semi-analytical technique and the gas saturation obtained from the fine-scale simulation of the experiments. Table 7-1 describes the details of the physical coreflood experiments.

Table 7-1: Experiments considered for verification of estimated relative permeability.

Exp.	Description	Fluids	Core Orientation	Test Conditions
1	Secondary CO_2 injection into Dead Crude-J	Injection fluid: CO_2 Resident oil: dead Crude-J Resident brine: 20000 ppm	Horizontal	T=28°C, P=1500 psig
2	Secondary N_2 injection into pre-equilibrated Crude-J	Injection fluid: N_2 Resident oil: Saturated Crude-J with N_2 Resident brine: 20000 ppm	Vertical	T=38°C, P=1500 psig

7.5 EXAMPLE 1: HORIZONTAL CO2 INJECTION INTO DEAD HEAVY OIL (EXPERIMENT-1)

In this example, the simulation result of Experiment-1 presented in section (4.4) where CO_2 was injected into heavy oil in a horizontal core and in which compositional and instability occurred was verified. The viscosity of the oil and the CO_2 at the experimental

condition were 617cp and 0.077cp, respectively, while the viscosity of the oil when it was fully saturated with CO_2 was 16cp. The adverse viscosity ratio has caused instability in the displacement through viscous fingering. To predict the saturation (compositional) profile of this coreflood experiment a one-dimensional model of the experiment was firstly generated. The model was history matched with production data (produced oil, produced gas and differential pressure across the core) to estimate relative permeability by varying the parameters in the chosen L.E.T-type parametric function. The detail of the history-matching procedure has been described in section (4.4). Figure 7-2 shows the history-matched cumulative oil recovered and the differential pressure across the core while Figure 7-3 shows the relative permeability obtained from the history-matching procedure.

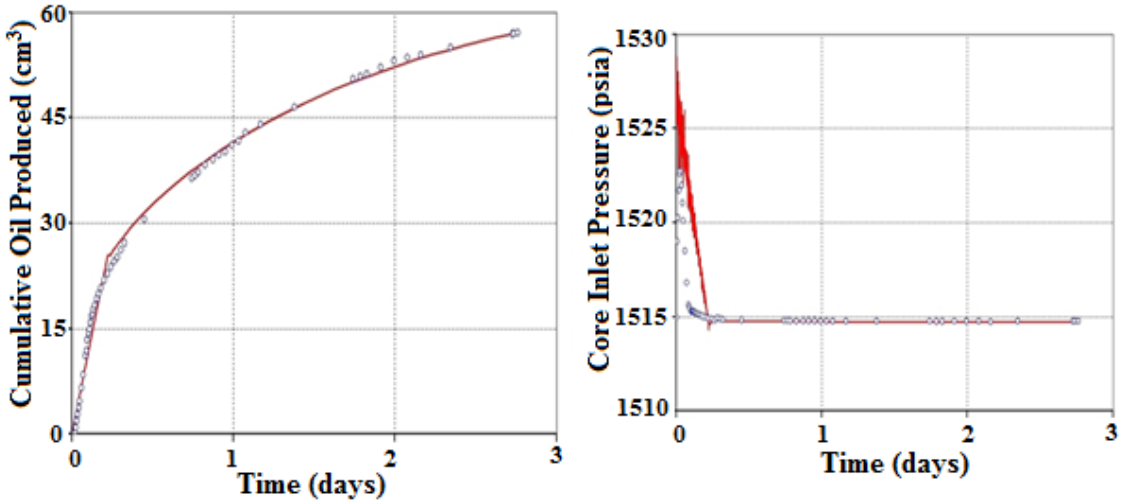

Figure 7-2: History-matched cumulative oil recovered and Differential Pressure of experiment using 1D model.

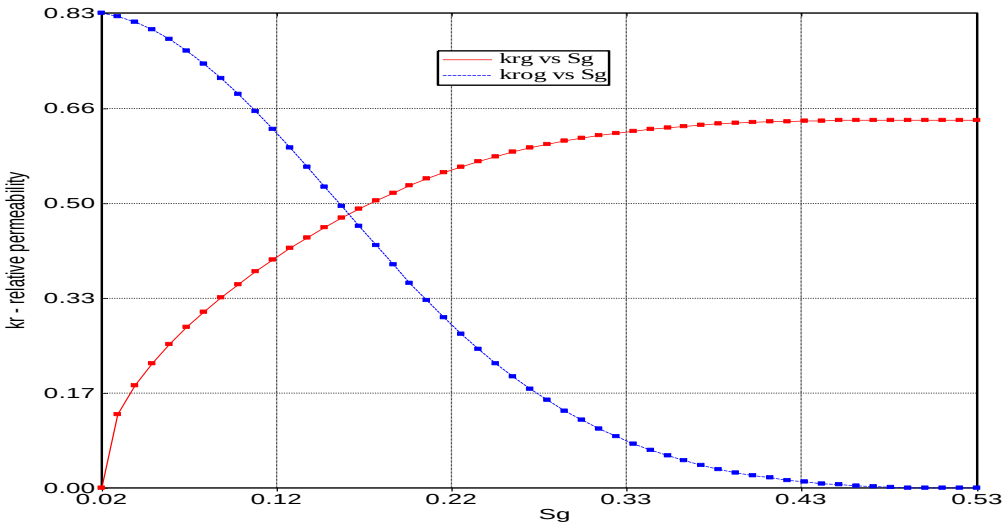

Figure 7-3: History-matched 1D relative permeability for Experiment-1

An analysis of the total mobility along the core, which is an indicator of instability in multi-dimensional displacement simulation, was carried out and showed that the total mobility ratio across the front (M_{shock}) is greater than one, an indication that instability will occur in a multi-dimensional flow simulation of the same experiment. Figure 7-4 shows the calculated total mobility along the core from the 1D simulation.

Figure 7-5 shows the gas saturation along the core plotted against the gas flow velocity (distance/time) after an injection time of 0.1PV for the one-dimensional simulation. The saturation profile has an initial sharp slope representing the saturation close to the injector and then flattens out as it moves away from the injector to the producer. The first steep region in the profile represents the rear end of the finger while the later part, the flat section, would represent the saturation within the fingered region in a multi-dimensional flow simulation of the same experiment. The empirical parameters required for the prediction, which is given by equations 46-50 given by Blunt et al. (1994) can be computed from the saturation curve. As a result of the distinct nature of the 1D saturation profile, where you have two separate sections, a very steep slope at the beginning of the curve followed by a flat section up to the shock front, it is easier to pick up the composition at the trailing edge of the finger. It is the point of intersection between the steep section and the relatively flat section as shown in Figure 7-5. Accordingly, Table 7-2 shows the parameter values determined from the analysis of the one-dimensional gas saturation profile that were used for the prediction of the compositional displacement with a viscous finger.

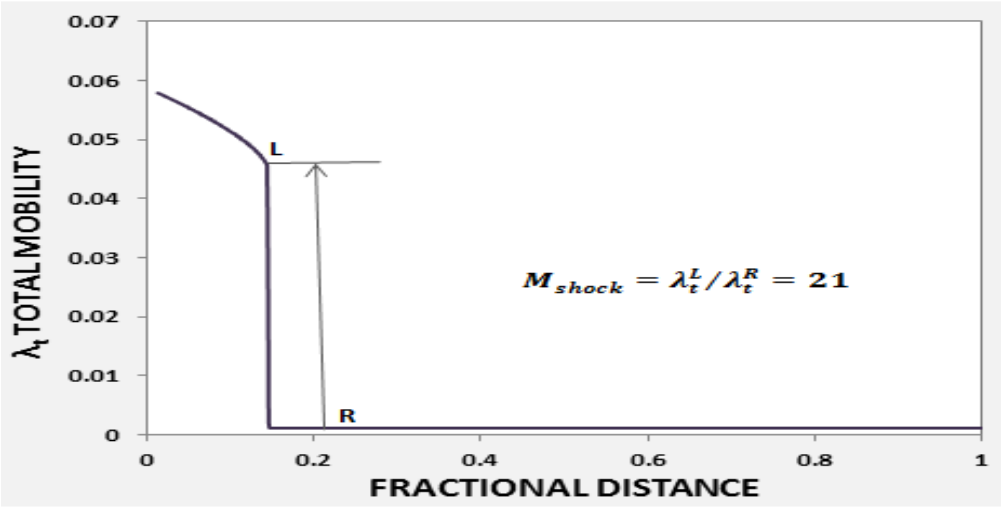

Figure 7-4: A plot 1D model total mobility against the fractional distance for Experiment-1 showing the M_{shock} value at the shock front

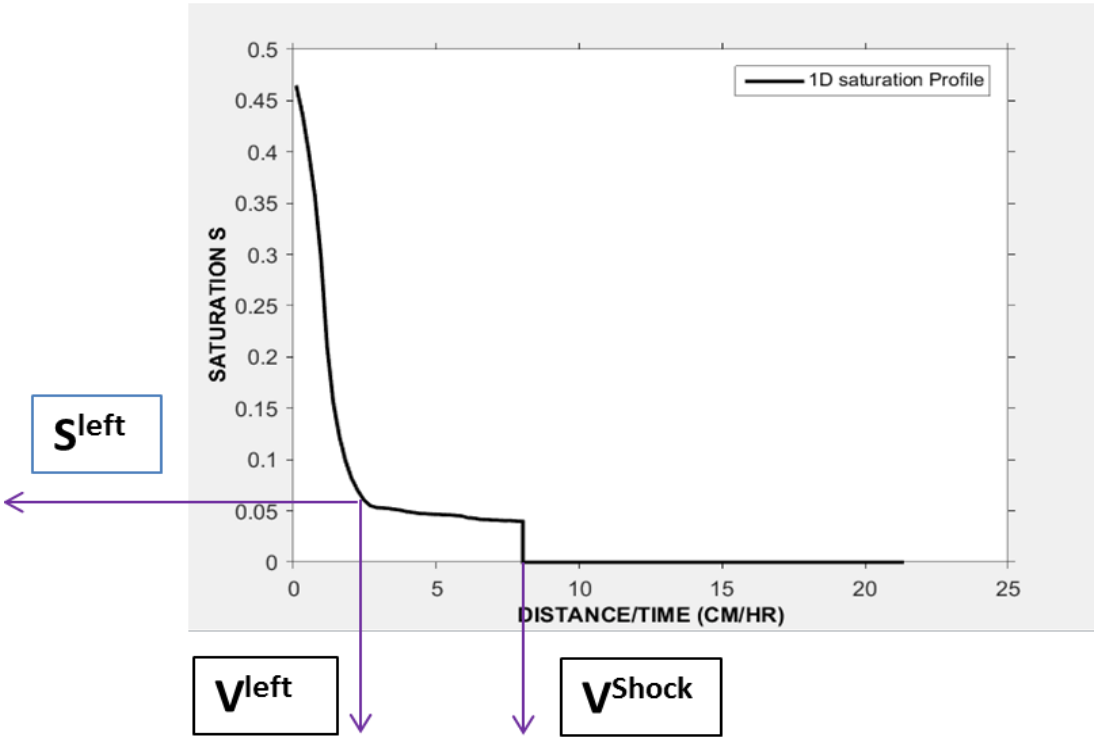

Figure 7-5: 1D model saturation profile of experiment 10 plotted against the gas velocity indicating the parameter values.

Table 7-2: Parameter value computed from the 1D model simulation that would be used in the prediction

Parameter	**Exp. 1**	**Exp. 2**
S^{left}	0.06	0.13
V^{left}	2.46	1.37
V^{shock}	8.02	2.56
M_e	1.87	1.87

As stated earlier, in multi-dimensional flow simulation the sharp front observed in the one-dimensional simulation as seen in Figure 7-5 would be smeared out. Consequently, following previous assumptions for immiscible displacement with viscous fingering, it can be assumed that within the fingered region, the composition varies linearly from the composition at the trailing edge of the finger, which is given by m^{left}, to the composition at the leading edge of the finger given by m^{right}. Therefore, the average gas saturation within the fingered region can be calculated from the following equation (51).

$$S_{av} = [C/[C + (1 - C)]/M_e]S^{left} \quad (51)$$

Where C is a value varying between 1 and 0 and is given by equation 52. It is self-consistent in nature since the saturation would be equal to the trailing edge saturation of the finger at a value of C equals to 1 and equals to the saturation of the leading edge at a value of C equals to zero.

$$C = \frac{V^{i} - V^{front}}{V^{left} - V^{right}} \qquad 52$$

Where V^{front} is the speed of the leading finger and can be estimated from M_e and V^{shock} from the equation given by Blunt et al. (1994) below (equation 53).

$$V^{front} = M_e V^{shock} \qquad 53$$

Therefore, using equations 40-42, the saturation profile within the fingered region in Experiment-1 can be predicted. Conversely, the saturation of the whole core (including the stable region) can be constructed by coupling the saturation profile before the trailing edge of the finger, which can be obtained from the one-dimensional saturation profile (Figure 7-5), together with that of the predicted fingered region. The predicted gas saturation profile is shown in Figure 7-6.

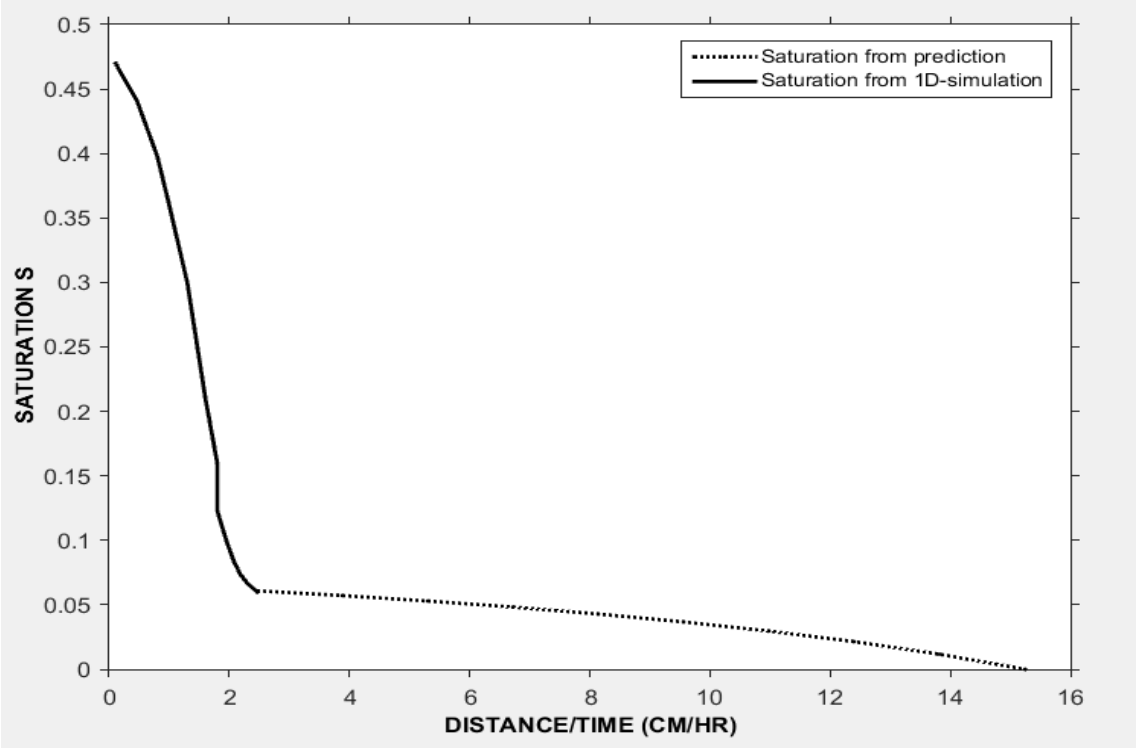

Figure 7-6: Predicted saturation profile for experiment 10 using the semi-empirical theoretical method

The simulated saturated profile obtained from the history matching of Experiment-1 using 2D model in section (4.4) can now be verified with the result of this semi-analytical approach. Figure 7-7 shows the match of the cumulative oil recovered and the differential pressure across the core obtained from the history-matching process while Figure 7-8 shows the relative permeability curve obtained from the history matching (obtained from section 4.4). Figure 7-9 shows the simulated saturation profile obtained from the same 2D high-resolution model simulation of the experiment after 0.1PV injection. Similarly, the saturation value for each grid within the 2D model simulation was averaged along a direction perpendicular to the direction of the flow. The averaged simulated gas saturation values were then plotted against the velocity (cm/hr) and compared with the predicted values. There was an excellent match between the prediction of the saturation and the computed average from the simulation as shown in Figure 7-10 below. This approach therefore verifies the simulated saturation profile obtained from the history matching and since relative permeability is a strong function of saturation profile and its value used in determining the M_e parameter, by implication, it has also been verified.

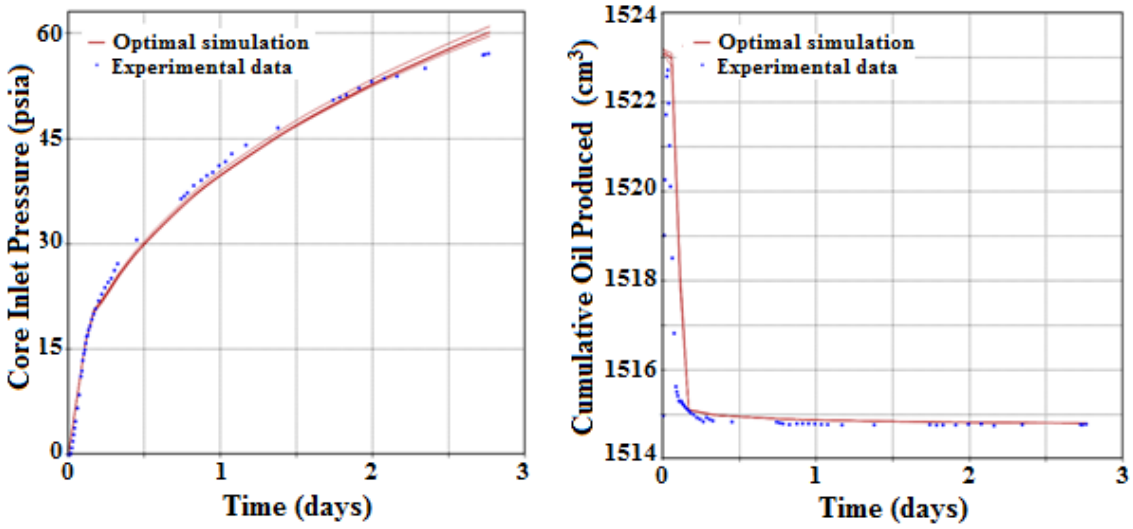

Figure 7-7: History-matched cumulative oil recovered and Differential Pressure of experiment using 2D high-resolution (100x80) model.

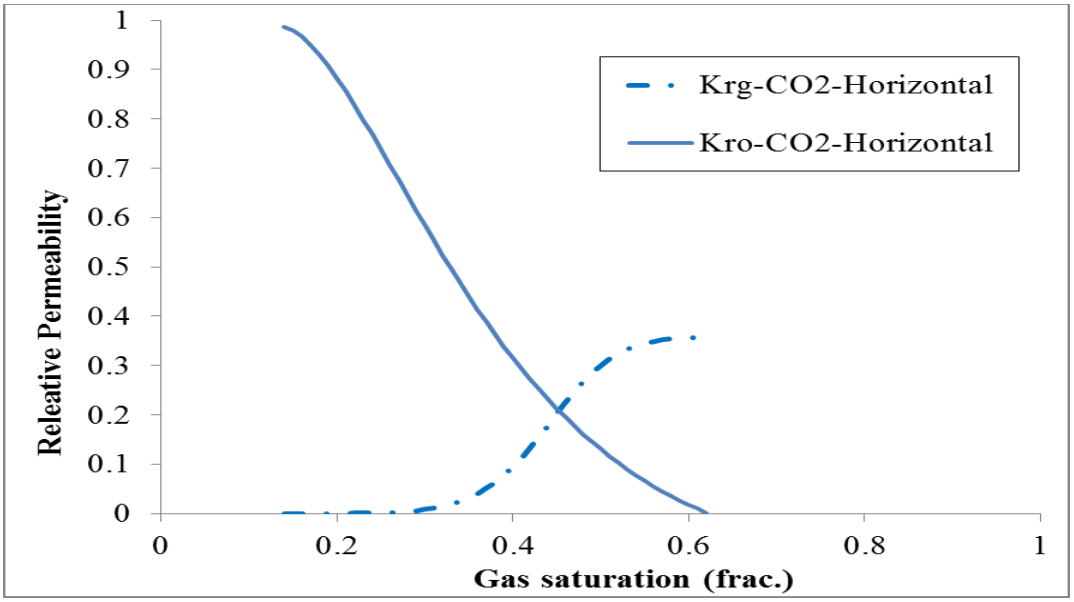

Figure 7-8: Experiment 10 gas-oil relative permeability curve obtained from 2D (100x80) model history matching.

Figure 7-9: A cross-section of saturation profile along the core from a 2D high-resolution (100x80) model.

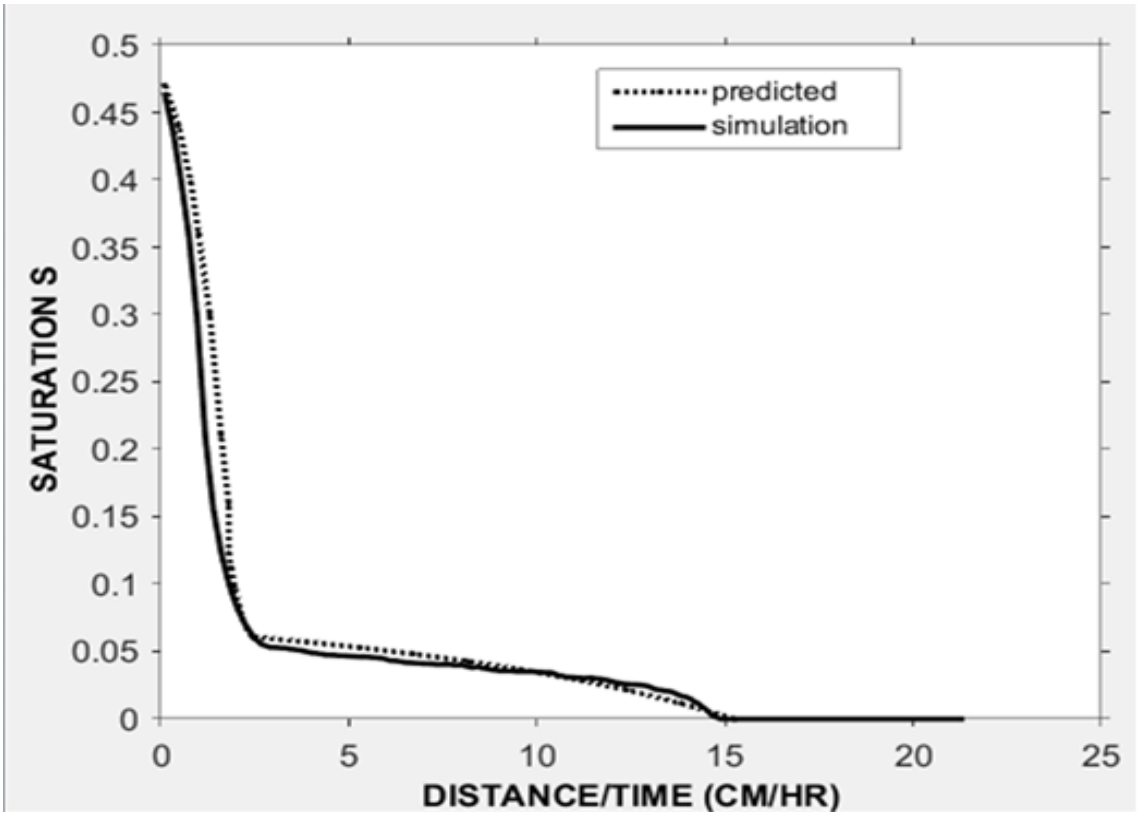

Figure 7-10: Comparison between the saturation profile from prediction and the averaged saturation from the fine-scale high-resolution simulation.

7.6 EXAMPLE 2: VERTICAL CO_2 INJECTION INTO HEAVY OIL (EXPERIMENT-4)

In this case, the experiment was carried out under the same condition as in example one. However, the orientation of the core here was in vertical as against the horizontal in the previous example. The injection was also from the top (Table 7-1**)**. Since the same core was used and the experimental conditions of temperature, pressure and injection rate are the same, the relative permeability curve obtained from the history matching of the previous experiment (horizontal injection) was directly used in the fine-scale simulation of this experiment, and it effectively matched the experimental data obtained, the details of the fine scale model simulation have been presented in section (6.2)

A preliminary one-dimensional model simulation of the experiment was required to determine the prediction parameters in order to predict the saturation profile of this experiment. A 1D model with grid-size 1x1x200 was used for history-matching the experimental data to determine the 1D relative permeability and the capillary pressure curves. A Corey type relative permeability function was used for the water/oil relative

permeability and L.E.T-type correlation for the gas/oil relative permeability function since it provides greater flexibility with the shape of the curve as against the Corey-type that was used for the oil-water relative permeability. The two relative permeability functions or values are required as input by the simulator, even though no three-phase flow was expected. Figure 7-11 shows the cumulative oil recovered and the differential pressure across the core from the one-dimensional history matching process. The relative permeability obtained is shown in Figure 7-12, which indicates similar shape pattern for both gas and oil relative permeability as that achieved in the 1D simulation of horizontal injection (Experiment-1).

Similarly, Figure 7-13 which is a plot of the total mobility along the core obtained from the 1D simulation indicates that the total mobility ratio at the front is 53, which is greater than one, an indication that the displacement would be unstable if simulated with a multidimensional model. Figure 7-14 shows the one-dimensional model gas saturation profile plotted against gas velocity (cm/hr) after 4 hours of injection. The prediction parameters were determined from the plot and the values indicate that the front is moving slower than the one predicted in the horizontal injection. Table 7-2 gives the values of the prediction parameters while Figure 7-15 shows the prediction using the values determined from the 1D simulation.

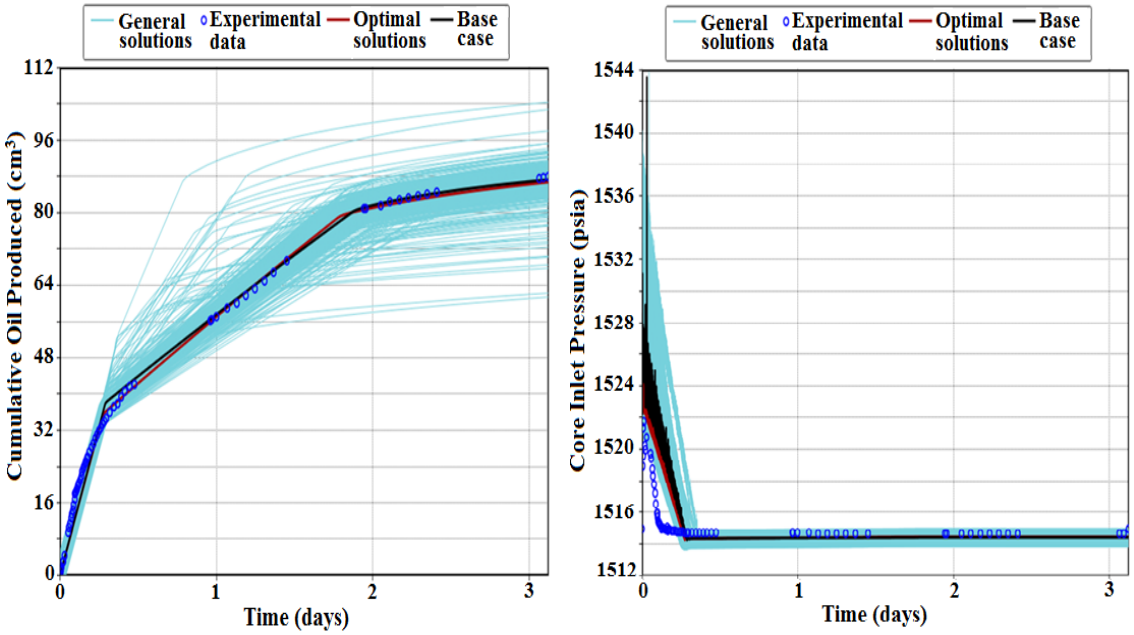

Figure 7-11: History-matched cumulative oil recovered and the differential pressure across the core for Experiment-4 using a 1D model. The multiple blue lines (general solutions) indicate other solutions of different realisations that are not optimum.

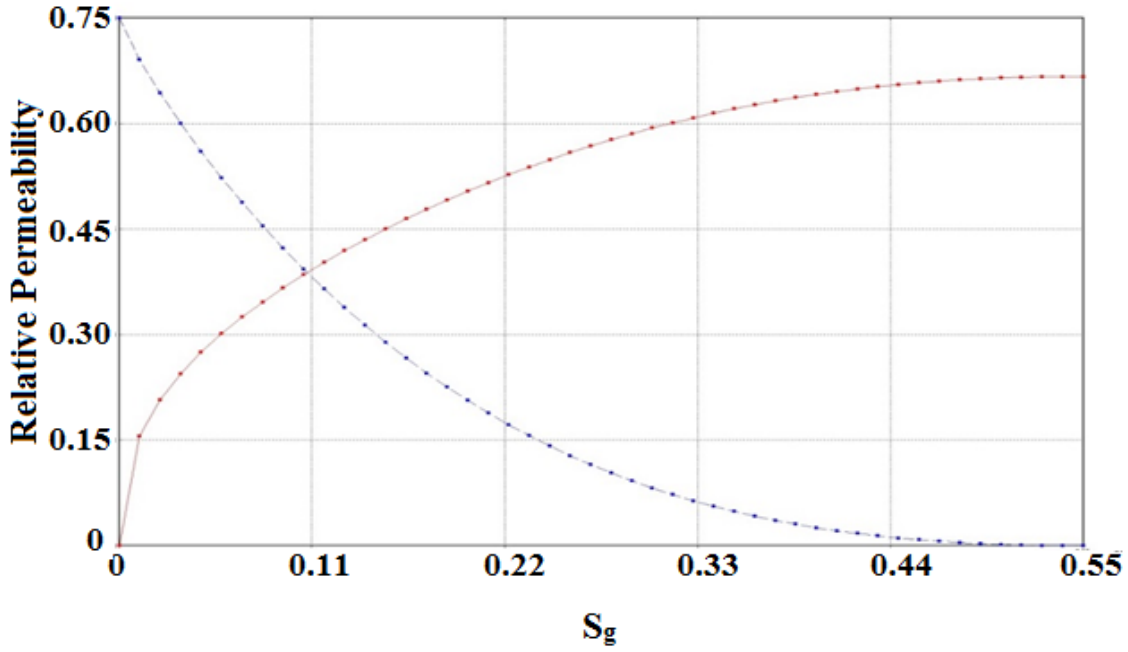

Figure 7-12: Gas/oil relative permeability curves obtained from the 1D model history-matching of Experiment-4

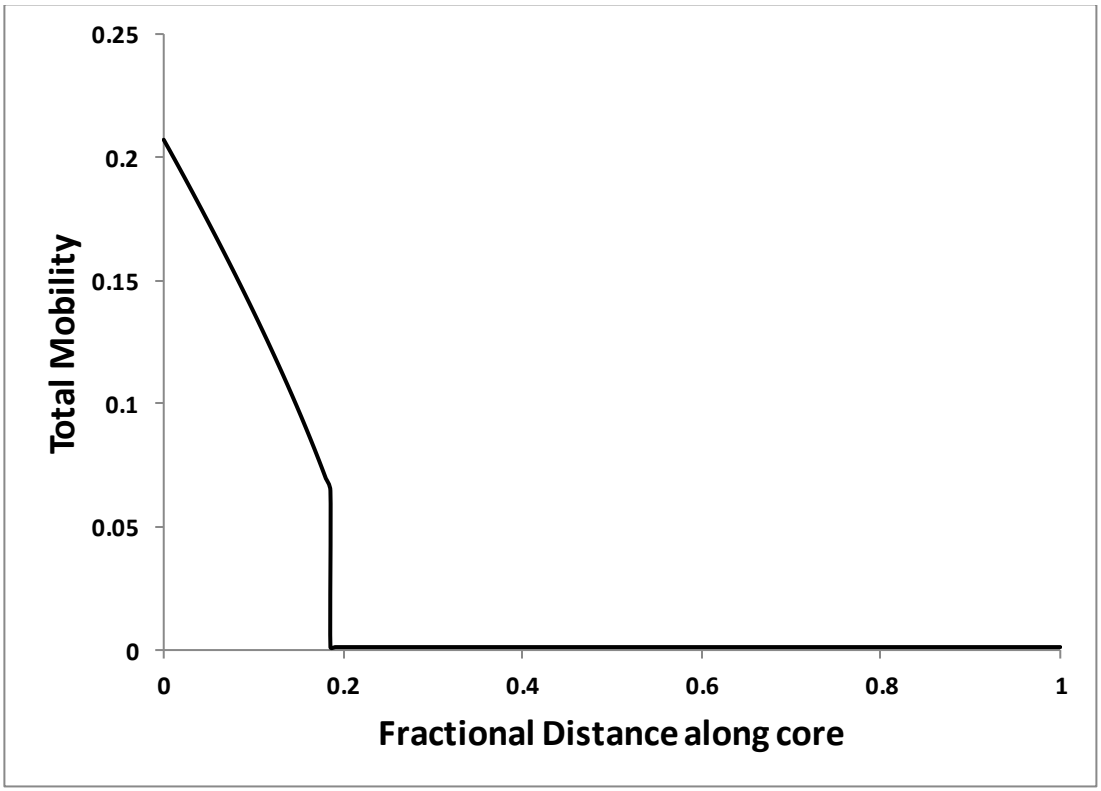

Figure 7-13: Total mobility along the fractional length of the core from the one-dimensional model simulation.

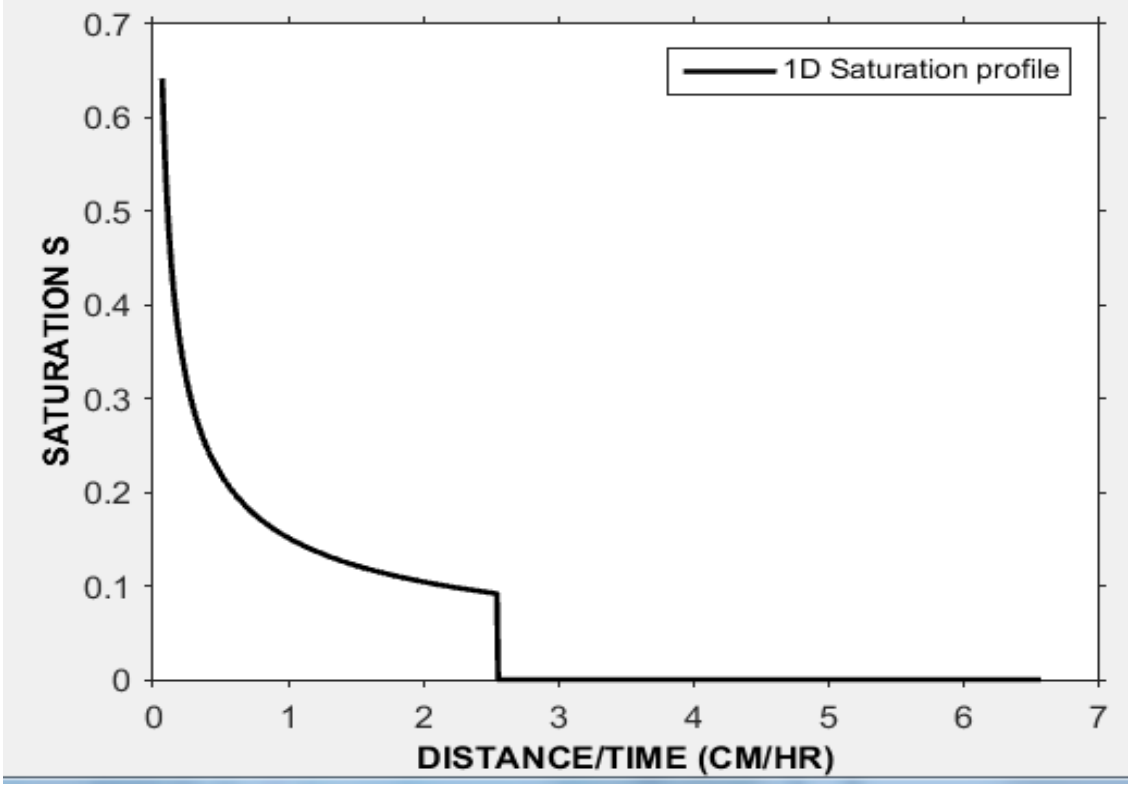

Figure 7-14: Gas saturation from the 1D model of Experiment-4 plotted against the gas velocity, indicating Buckley-Leveret sharp front and the trailing edge.

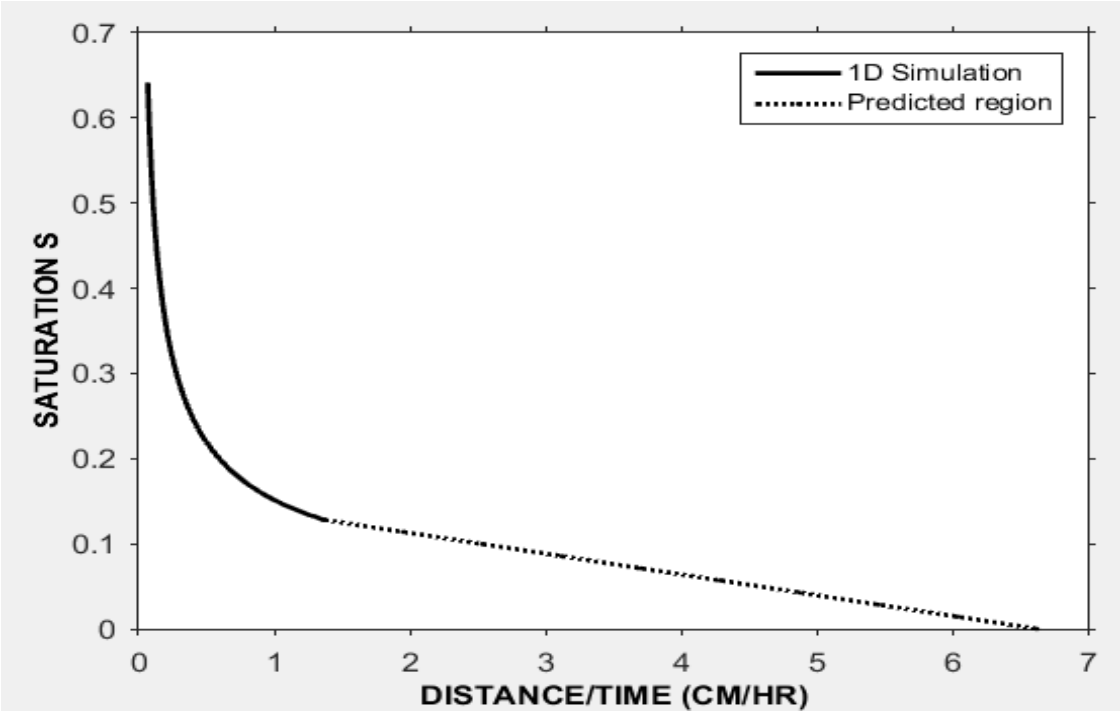

Figure 7-15: Prediction of saturation profile along the core; a combination of 1D saturation profile before the finger and the predicted saturation profile within the fingered region (experiment-4).

Accordingly, as in example 1, the simulated saturation profile obtained using the 2D high-resolution model (80x100) of the experiment was verified with this semi-analytical prediction. Figure 7-16 shows the saturation profile obtained from the high-resolution simulation after 4 hours of injection and just before the breakthrough. It showed far greater instability within the fingered region compared to the horizontal injection, as predicted by the total mobility plot. The instability was due to a strong gravity drainage in addition to viscous fingering. The gravity drainage was synonymous to vapour extraction (VAPEX) process, which has also been confirmed in the experiment.

For the purpose of comparison, the saturation values across the core in the model was similarly averaged and plotted against the gas velocity. Figure 7-17 shows the averaged gas saturation along the core plotted against the velocity of the gas. Since there is considerable variation within the fingered region, the prediction, which is based on the assumption of linear variability within the fingered region, cannot honour this behaviour. However, it can predict the breakthrough time and the averaged saturation within this fingered region by smoothening the saturation profile obtained from the high-resolution simulation and the smoothing-spline function was employed for this purpose. Figure 7-18 shows the comparison between the smoothed and original saturation profile after 4 hours of injection.

To verify the the averaged-and-smoothed saturation profile of the high-resolution simulation with the semi-analytical approach, the two profiles were plotted and shown in Figure 7-19. It indicates that the prediction underestimated the saturation behind the finger and overestimated the saturation within the fingered region. However, there is an excellent match in the value of the real velocity of the front (6.5cm/hr) between the prediction and the simulation. This shows that the method can be used to verify breakthrough time even in extreme cases where the variation of composition within the fingered region is not linear.

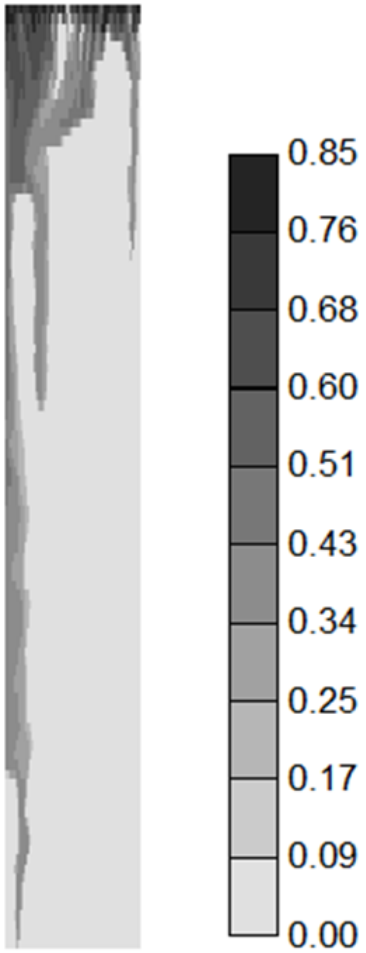

Figure 7-16: Gas saturation profile along the core after 4hrs injection from (80x100) model simulation of experiment 4.

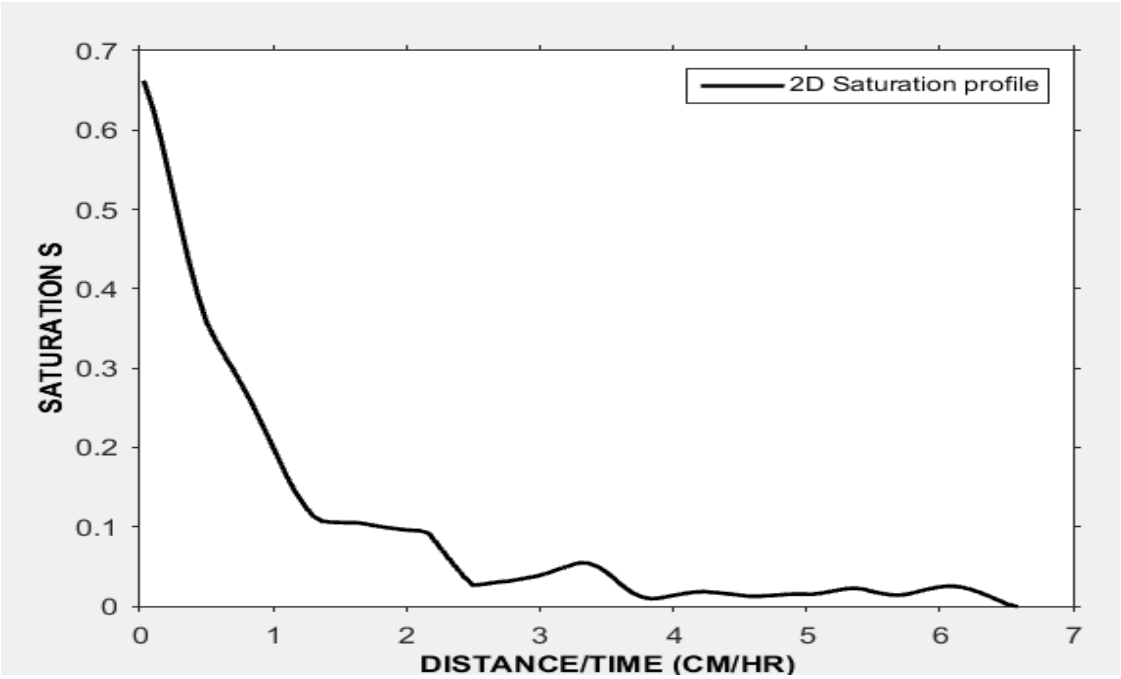

Figure 7-17: Averaged gas saturation profile after 4hrs injection plotted against the gas velocity.

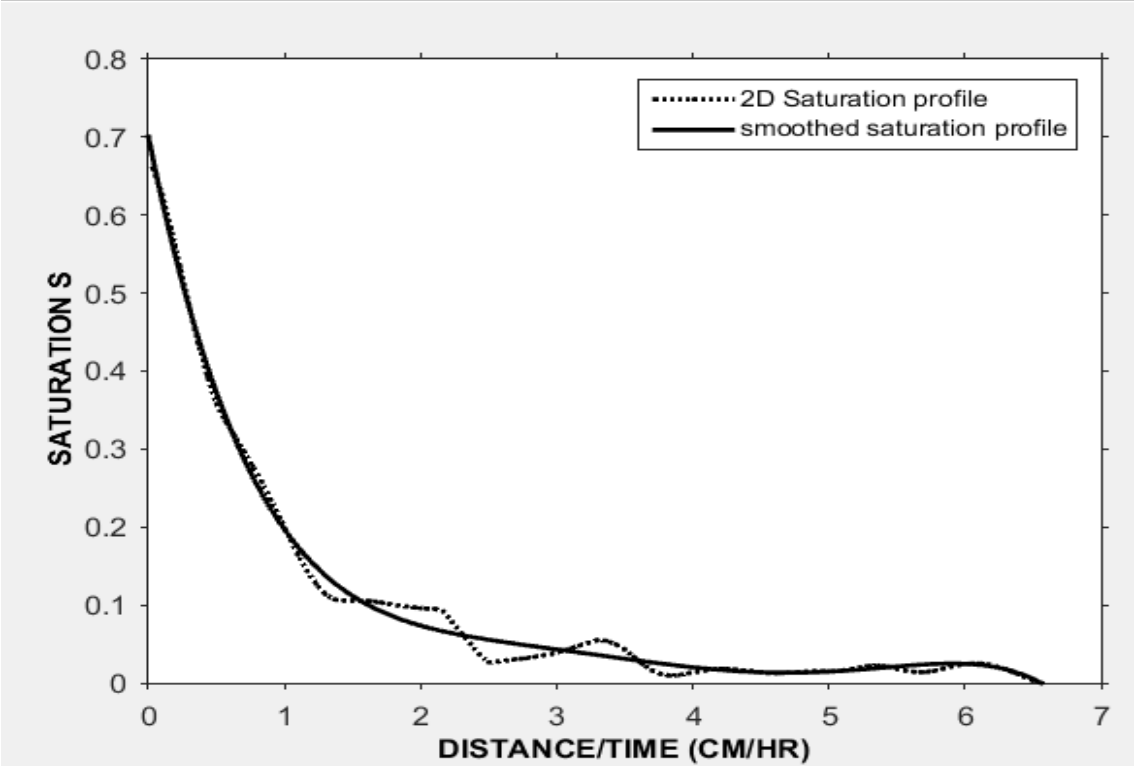

Figure 7-18: Comparison between the smoothed and the original gas saturation profile obtained from the high-resolution model.

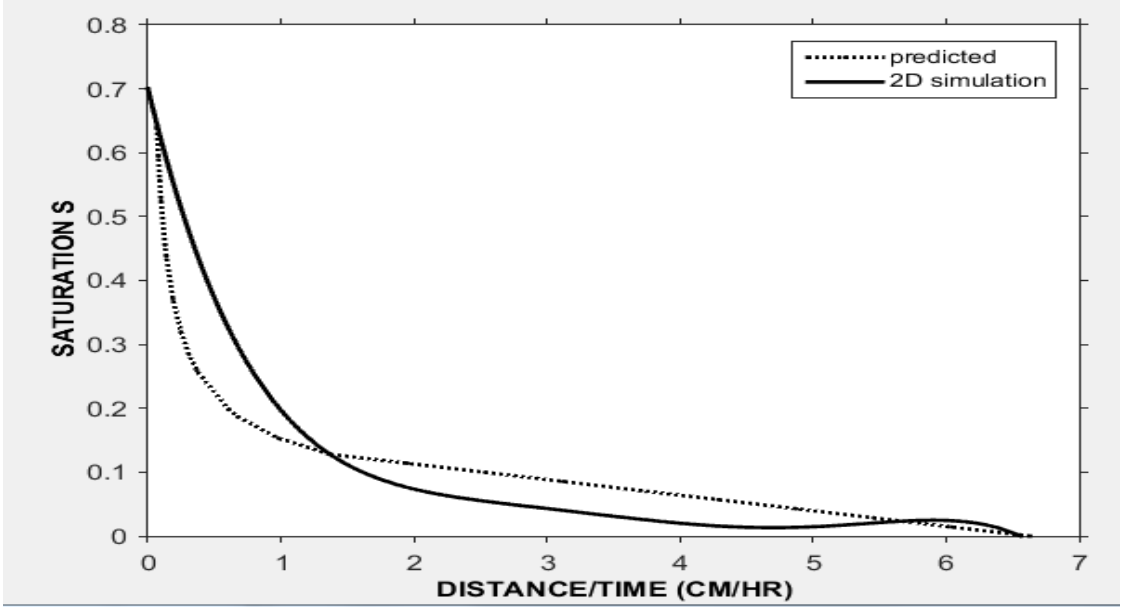

Figure 7-19: Comparison between predicted saturation profile and the averaged (smoothed) saturation profile obtained from high-resolution simulation.

7.7 CONCLUSION

The main objective of this chapter was to develop a simple theoretical tool for predicting viscous fingering in displacements with instability and to semi-analytically verify the

estimated relative permeability curves. The following conclusions were drawn from the studies.

The theory of viscous fingering in compositional displacement, which was developed based on material balance and Koval's empirical equation for light and conventional oils has been extended to predict the saturation (composition) in heavy oil displacement by immiscible gas. The theory is also based on the assumption of linear variation of composition within the fingered region and has shown that it can reasonably predict the saturation profile within the fingered region in an unstable displacement for horizontal displacement.

The saturation profile of a CO_2 injection into horizontal core saturated with heavy oil was predicted using the relative permeability curves estimated from previous history matching studies. The saturation profile reasonably agrees with the average saturation profile obtained from the high-resolution simulation of a similar experiment. This indicates the capability of the proposed semi-analytical method to predict viscous fingering in such displacements. For the second case where CO_2 was injected from the top into a vertical core saturated with heavy oil, the theory could not satisfactorily predict the saturation profile. This could mainly be due to the gravitational effect that has not been factored into the equation.

CHAPTER 8

COARSE-SCALE APPROACH TO ESTIMATION OF TWO-PHASE RELATIVE PERMEABILITY FROM UNSTABLE DISPLACEMENT BY HISTORY MATCHING

8.1 INTRODUCTION

In modelling of subsurface flow such as in a reservoir, the accuracy of the model largely depends on the availability and the quality of the reservoir description. The sophistication of current characterization techniques has made it possible to obtain a large amount of detailed and more reliable information that can be used to sufficiently model the reservoir. These include detailed information obtainable from core analysis, good logs and seismic interpretations as well as dynamic production data that can be obtained from core experiments, field appraisal as well as early and later production periods. It is important to systematically integrate all these various sources of information to reduce the uncertainty and increase the reliability of the model.

However, the full detailing may lead to a model with hundreds of millions of grid-cells that would be near impossible, at this fine-scale, to perform a direct reservoir simulation studies, even with the current modern computing capabilities. The major difficulty of the direct solution here would be the scale of the computation, as a fine-scale model would require a tremendous amount of computer memory and CPU time, which can easily exceed the limit of today's computing capabilities. For these reasons, therefore, upscaling methods such as scalable mathematical formulations and other techniques have been developed to deal with large problems in a robust and efficient manner (Dogru et al., 2002, Al-Shaalan et al., 2003, Cao et al., 2009, Zhou and Tchelepi, 2012).

The use of the upscaling method allows for the application of a relatively coarse model to perform the simulation of a complex flow and transport computations with accuracy similar to that of a high-resolution model. In multiscale approach, an attempt is made to resolve fine-scale information without the direct solution of the global fine-scale problem. Hou and Wu (1997) have used a Multiscale Finite Element Method (MsFEM) to compute for the flow of compositional fluid in porous media by capturing the fine-scale information through the construction of special basis. However, this approach is not mass conservative. Therefore, the need to develop methods that also conserve mass led Jenny et al. (2006) to propose a Multiscale Finite Volume method (MsFVM). Therefore, the need to develop methods that also conserve mass led Jenny et al, (2006) to propose a Multiscale Finite Volume method (MsFVM).

Here, a compositional displacement in which unstable flow regimes and mass transport occur as a result of the injection of a soluble gas such as, CO_2, into heavy oil was considered. The injection leads to the dissolution of the gas in the oil thereby significantly reducing the oil viscosity and relatively increasing its density (Paracello et al., 2012). In addition, the large viscosity difference between the gas and heavy (viscous) oil would lead to an unfavourable mobility ratio resulting in a severe instability in the displacement. This is a well-researched phenomenon that is known as viscous fingering (Cuthiel et al., 2006). The large density difference between the gas and the oil would lead to gravity segregation, aggravating the instability in the displacement process (Nasrabadi et al., 2009). To effectively model this displacement, which would take into account the detail of the complex compositional interaction and the instability, a high-resolution model is necessary. Christie (1989) has previously used a high resolution (130x130) two-dimensional (2D) finite-difference grid model to simulate unstable miscible displacement. His method of triggering the fingers was by introducing a small permeability variation using a small variance in a stochastically distributed permeability field. However, the approach using the fine-scale model is time and resource demanding, making such approach near impossible for running multiple realisations or scenarios that are typical of a reservoir simulation studies.

Specifically, in this work, the aim was to develop an efficient method for the estimation of gas/oil relative permeability from displacement in which instability and compositional effects existed. The objective is to use a set of coarse models (as opposed to the high-resolution model) in a history-matching procedure in order to estimate relative

permeability with accuracy similar to that obtained using high-resolution model. The desired goal is to reduce the overall simulation time and resources that are required for the estimation of relative permeability from unstable displacement.

8.2 BACKGROUND THEORY

Generally, relative permeability curves are obtained through laboratory coreflood displacement experiment where dynamic production data such as cumulative oil, water and gas production, the differential pressure across the core and the saturation profile during the displacement are measured and evaluated. There are two main ways of conducting the coreflood experiment; the steady state, and the unsteady state method (2.3). In the unsteady displacement method, the measured production data can be analysed explicitly using an analytical technique such as the one developed by JBN(Johnson et al., 1959). These are designed, based on the one-dimensional Buckley-Leverett fractional flow concept, where the front, or the interface between the injected fluid and the resident fluid, is assumed to be piston-like and with constant saturation. However, moving from laboratory scale to a larger reservoir or a field scale, the displacement may be highly unstable. The instability can be due to viscous fingering resulting from adverse mobility ratio or gravity tonguing as a result of gravity difference. In these cases, the fronts cannot be assumed to be piston-like, and the one-dimensional simplification described by the Buckley-Leverett theory, which forms the basis of the JBN method, does not hold. These larger scales are, therefore, generally represented with a three-dimensional model which can adequately account for the instability. As described in (chapter 5) using relative permeability obtained from one-dimensional displacement to simulate displacement that is prone to instability may be highly erroneous. This chapter has also described in detail how to use a high-resolution 2D model to estimate relative permeability for use in displacement with instability.

8.2.1 Conventional History Matching and Parameter Estimation

Fluid flow in porous media can be affected by many factors; these include physical parameters such as oil viscosity or inferred parameters such as relative permeability. Even though they are known to influence the flow significantly, they are often difficult to be determined through available measurement techniques. However, these are still needed to be accounted for in order to model a reservoir or to simulate fluid flow for the purpose of reservoir performance and prediction. These unknown parameters are

therefore estimated to achieve the aim. If the parameters are estimated with reasonable accuracy, the predicted results would be accepted with more confidence. Many techniques such as those by Lu and Horne (2000) which is based on wavelet analysis and Yan (2002) that is based on correlating available data from different sources to establish a relationship that can be used to estimate the unknown parameter have been proposed. These techniques, however, often result in inaccurate estimates when numerical forecasts are compared with history data (O'sullivan, 2004). An inverse process where production data measured from displacement experiments with core or field operations at a set time interval, termed 'history-data' is matched with simulated data through updating parameter value is known as history-matching. In this process, the parameter values are verified or updated by measuring the misfit between the history data and simulated data. The limited history data available are compared with the simulated data and if there exist an error above the set tolerance, a parameter in the simulation model is adjusted and new simulation data generated; the process is repeated until the tolerance between the history data, and simulated data is reached (O'sullivan, 2004). History matching is often the preferred technique when a parameter needs to be estimated.

8.2.2 Optimisation Algorithm and Misfit in History-Matching

The implicit estimation of relative permeability by history matching is a non-linear inverse and ill-conditioned problem (O'sullivan, 2004). Some modern non-linear optimisation techniques for solving this type of problem include the Ensemble Kalman Filter (EnKF) optimizer (Li et al., 2009) and the Designed Exploration and Controlled Evolution (DECE) optimizer (Yang et al., 2009). The DECE is a proprietary optimisation technique developed by Computer modelling group (CMG) and is an integral part of their CMOST optimisation software. It uses an iterative optimisation process that first applies a designed exploration stage to search space in a designed random manner such that maximum information about the solution space can be obtained; this is followed by a controlled evolution stage, which performs statistical analysis of the simulation result obtained in the previous stage.

The misfit function which measures the deviation of the simulation from the experimental value can range in form from a simple least square model (LSM) to more advanced Plus Mean Error (PEM) and the Full Error Model (FEM). The LSM (equation 54) is defined as the sum of the squares of the difference between the observed and simulated data and

has only one parameter for measuring the degree of the variance, the standard variance, σ^2. It also assumes that the error is normally distributed, which implies that the data points are randomly distributed or independent of each other. In a situation where the error is also correlated with time, a single parameter of measuring variance is not sufficient and as such the least square method would not hold.

$$M = \sum_{i=1}^{n} \frac{(o_i - s_i)^2}{2\sigma^2} \quad 54$$

Where *o* is the observed data and *s* is the simulated data.

The Least Square Misfit (LSM) model can be modified to include the mean error, $\bar{e}$, into the summation term. This would reduce the bias effect of the LSM model and improve the accuracy of the error model by shifting the likelihood into a region of the parameter space and is termed as the Plus Mean Error (PME) given by equation (55).

$$M = \sum_{i=1}^{n} \frac{(o_i - s_i - \bar{e})^2}{2\sigma^2} \quad 55$$

The third type of misfit, which is more advanced, is the Full Error Model (FEM) given equation (56). It includes both the mean error, $\bar{e}$, and full inverse covariance, C^{-1}, which help in accurately representing the variance in the parameter estimation. Quite noteworthy, establishing the full error model is a rigorous process because calculating the true mean error and the covariance matrix is time consuming and may not be feasible for fine grid simulation (O'sullivan, 2004).

$$M = \frac{1}{2}(o - s - \bar{e})^T C^{-1}(o - s - \bar{e}) \quad 56$$

Figure 8-1 shows a typical history matching algorithm for the estimation of relative permeability using a simple misfit. The automatic estimation process starts with an initial guess of the kr function parameter values, and the coreflood is simulated using the computed relative permeability curves, the results of the simulation such as fluid production and saturation profile are compared with the actual experimental data to determine the misfit. If this value is less than a set tolerance, the relative permeability curves computed are accepted as the representative curves for the displacement.

However, if the misfit is somewhat greater than the tolerance and optimisation procedure is used to choose another set of the relative permeability function parameter values. The new set of parameter values are now used to recalculate a new relative permeability curve, and the whole process is repeated until a relative permeability curve with misfit value less than the tolerance is achieved.

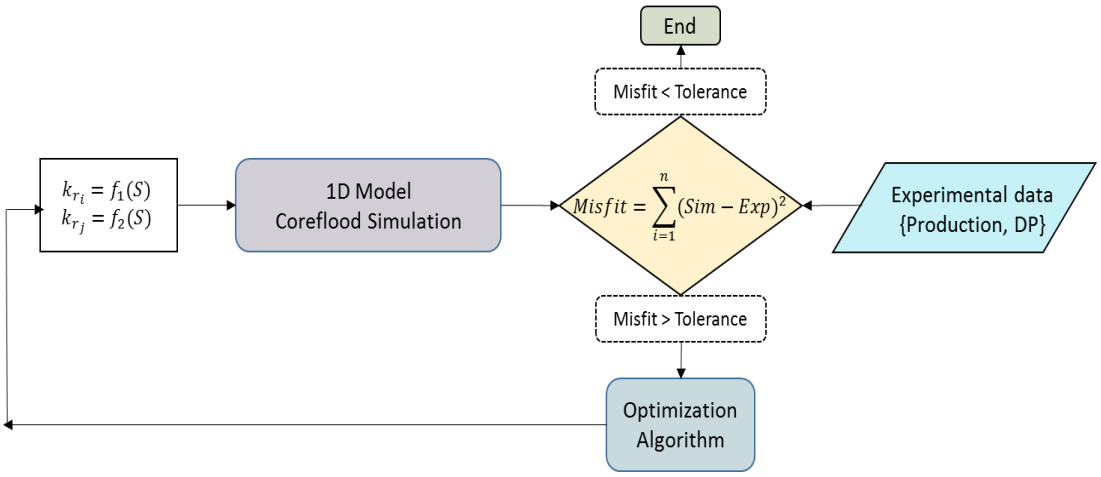

Figure 8-1: Conventional history-matching procedure for estimation of relative permeability

8.3 METHODOLOGY

As stated earlier, using a high-resolution model during the history-matching process would be enormously time-consuming. It is also worthy to note that relative permeability for an unstable system is highly dependent upon grid size. Therefore, a set of relative permeability curves estimated using a coarse grid model cannot be used directly in a high-resolution model as that may lead to huge error. In this research, a set of relatively coarse-grid models of the same experiment, which are relatively faster to simulate were generated, the relative permeability for each of the models were estimated by history matching and the estimated curves were then used to compute the relative permeability for a high-resolution model of the same experiment. This approach has two potential advantages; firstly, the total time it takes to simulate the set of coarse grid models would be less than the time it takes to simulate a single high-resolution model; secondly, the lower memory and computational requirement for simulating the coarse models would hitherto enable less powerful computers to be used for the estimation of relative permeability for high-resolution simulation.

The proposed multiscale approach for the estimation of the relative permeability is described below:

1. Generate a set of 2D coarse grid models by sequentially refining the grid size until a reasonably refined grid model is achieved. It is important here to ensure symmetry in the sequence as this would be easier to a relationship in the relative permeability parameter values that would be estimated later. It can be for example an arithmetic or geometric sequence (for example the x-axis of the models can be 10, 20, 30 grid cells).

2. The relative permeability curves for each of the 2D coarse-grid models are estimated by history matching procedure using a suitable relative permeability function. In this case, the more versatile three-parameter function proposed by Lomeland (2005) is employed. It is chosen because of its versatility in honouring the S-behaviour that is typical of gas relative permeability curves. The misfit is calculated using the Plus Mean Error (PME) because using a least square model would result in a significant bias in the result (O'sullivan, 2004).

3. For each of the parameters (in this case L, E and T), the values of the parameters for each of the coarse grid models obtained during the history matching in step 2 above are plotted against the grid size. The curve for each of the parameters can then be extrapolated to determine the relative permeability at the required fine grid size.

4. The extrapolated parameter values obtained from the plots can then be used to simulate the high-resolution model.

8.4 RESULTS

To demonstrate the methodology, two physical experiments were considered based on the similarity between them. Both were heavy oil displacement by CO_2 in a horizontal core. However, they differ in their degree of mass transfer, fluid viscosity ratio and hence displacement instability. This allows for the observation of any change in the flow functions resulting from the mass transfer effect. Table 8-1 recaps the test conditions and fluids used in the selected coreflood experiments. The details of the experimental procedure can be found in Chapter 2.

1) Experiment-1: CO_2 injection into a horizontal core saturated with dead crude oil (Crude-J).
2) Experiment-3: CO2 injection into a horizontal core saturated with live crude oil (Crude J saturated with methane).

Table 8-1 Description of the coreflood experiment selected for this simulation study

Exp. No.	Description	Fluids	Core Orientation	Test Conditions
1	Secondary CO_2 injection into Dead Crude-J	Injection fluid: CO_2 Resident oil: dead Crude-J Resident brine: 20000 ppm	Horizontal	T=28°C, P=1500 psig
3	Secondary CO_2 injection into Live Crude-J	Injection fluid: CO_2 Resident oil: dead Crude-J saturated with methane Resident brine: 20000 ppm	Horizontal	T=28°C, P=1500 psig

8.4.1 Experiment-1: CO_2 injection into a horizontal core saturated with dead crude J

In this experiment, CO2 was injected into a horizontally oriented core saturated with dead Crude-J, as described in previous chapters. Viscosities of the displacing (CO_2) and displaced (crude oil) fluids were 0.077cp and 617cp, respectively, which made the displacement prone to viscous fingering. The CO_2 was soluble in the heavy oil which led to reduction in its viscosity from the original 617cP to 15cp when it was fully saturated in the oil (Emadi et al., 2013). On the other hand, compared to the resident crude oil, the injection fluid has lower density resulting in gravitational segregation. (Fayers and Newley, 1988). These phenomena cannot be modelled in conventional one-dimensional simulation as stated in the previous section since it does not take into account component and phase dispersion, as well as fingering and overrides, which require another dimension to be considered.

Consequently, using a 2D model for the displacement, the grid sensitivity studies carried out on the core model in chapter 3 has shown that the model is most sensitive on the direction perpendicular to flow or across the core diameter. The optimum grid size for the displacement was also found to be 100x80. Based on this grid size, the set of 100x10,

100x20, 100x30 and 100x40 coarse grid models were chosen. Note that only the z-axis was varied because it is the axis that is more sensitive to instability.

Table 8-2 shows the L E and T parameter values obtained from history matching of the experiment using the four grid models. Figure 8-2 shows the match of the cumulative oil recovered for the different models. Good matches were obtained for all the models, but the matching improved when the grid size was increased from 10 to 20. Similarly, Figure 8-3 shows the result of the history matching of the pressure across the core during the injection for the four different models. Good matches were also obtained especially after breakthrough, particularly for models with grid size above 20. The mismatch at the beginning of the injection, as stated earlier, can likely be attributed to the simulator's assumption of instantaneous thermodynamic equilibrium and hence not capable of taking into account the in-situ dynamic viscosity variation that takes place with mass transfer. Likewise, Figure 8-4 shows the result of the history matching of the cumulative gas produced for the different models, it can be observed that the matching improved with increase in grid size as expected. However, knowing that there is huge uncertainty associated with the gas measurement, a lower weighting was assigned for the cumulative gas recovered in the calculation of misfit during the history matching process. Moreover, for the four different core models labelled from A to D, the values of the misfits obtained using Plus Mean Error (PME) for all the core models were less than 2%.

Table 8-2: Relative permeability function (L.E.T) parameter values obtained at the end of the history-matching procedure for the four coarse core models

Parameter	**A(100X10)**	**B(100X20)**	**C(100X30)**	**D(100X40)**
L_o	6.67	7.6	6.652	5.705
E_o	3.888	3	3.127	3.253
T_o	1.04	1.49	1.34	1.185
L_g	1.165	2.68	2.419	2.157
E_g	1.845	1.245	1.125	0.99
T_g	1.57	1.725	3.432	5.15
Misfit (Error) %	1.41	1.21	1.01	2.03

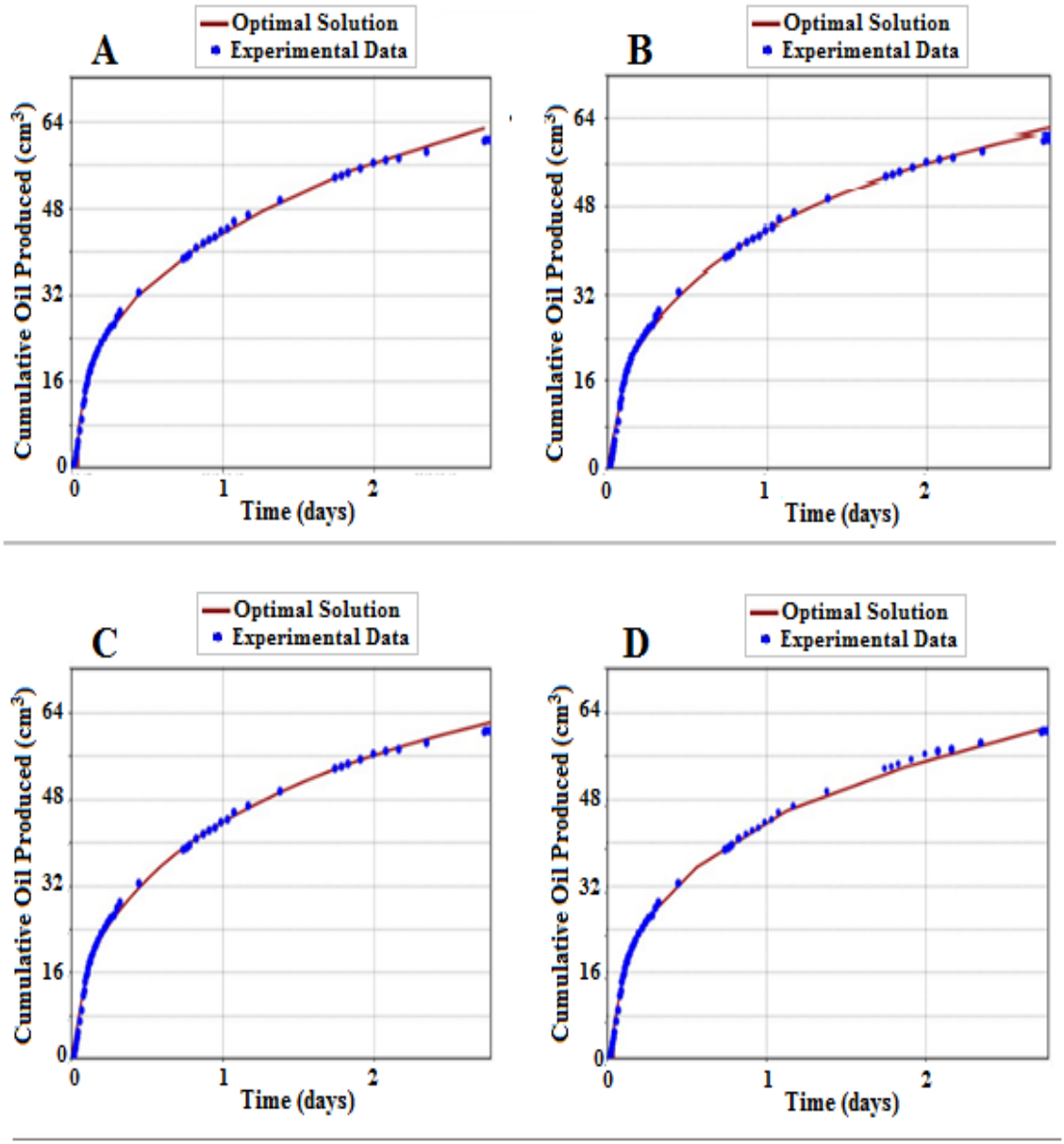

Figure 8-2: Shows the result of cumulative oil recovered from the history matching (solid red line) in comparison with the experimental data (blue dots) for four coarse models. A: 100x10; B:100x20; C:100x30; D: 100x40

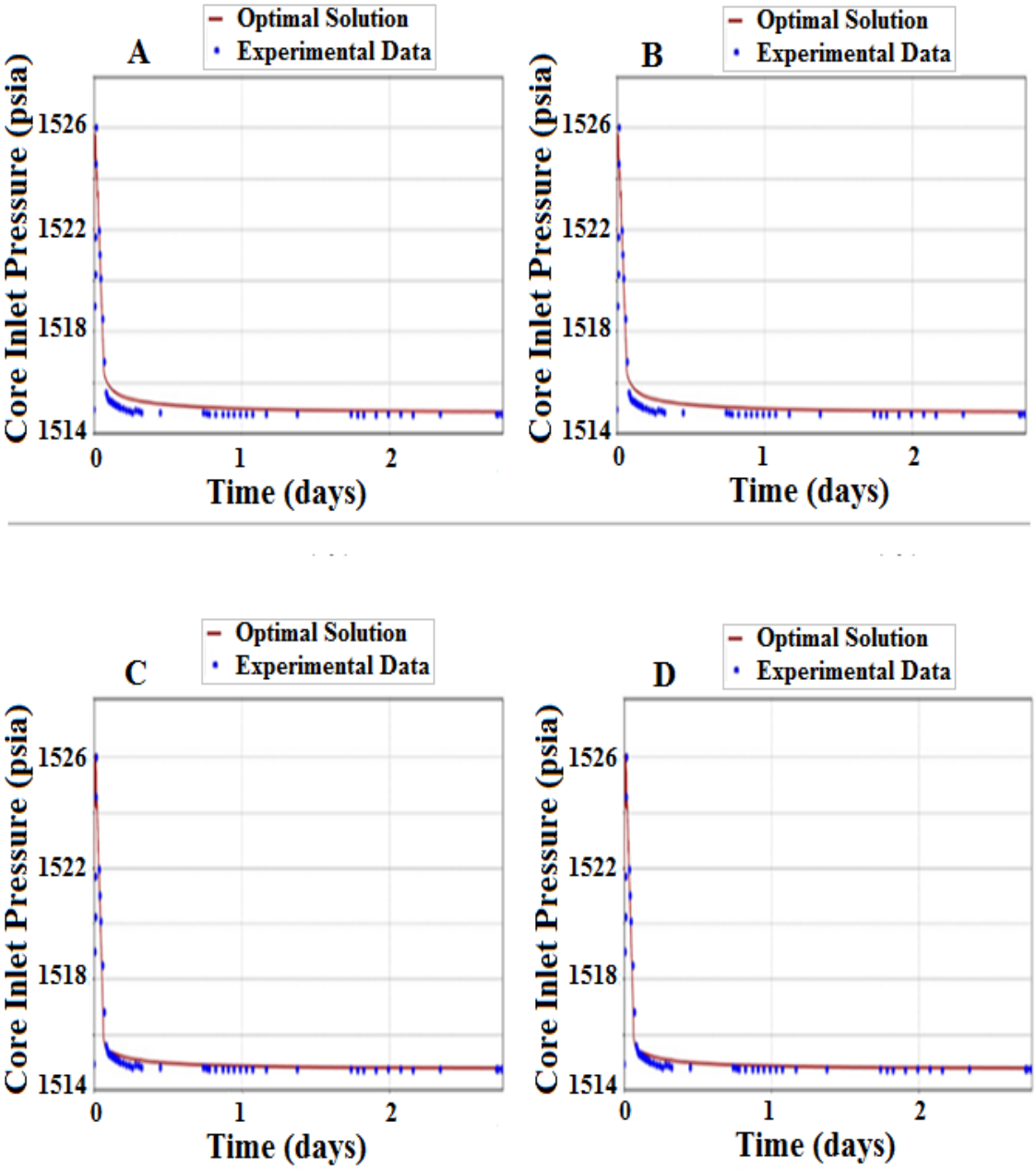

Figure 8-3: Shows the result of the pressure across the core from the history matching (solid red line) in comparison with the experimental data (blue dots) for four coarse models. A: 100x10; B:100x20; C:100x30; D:100x40.

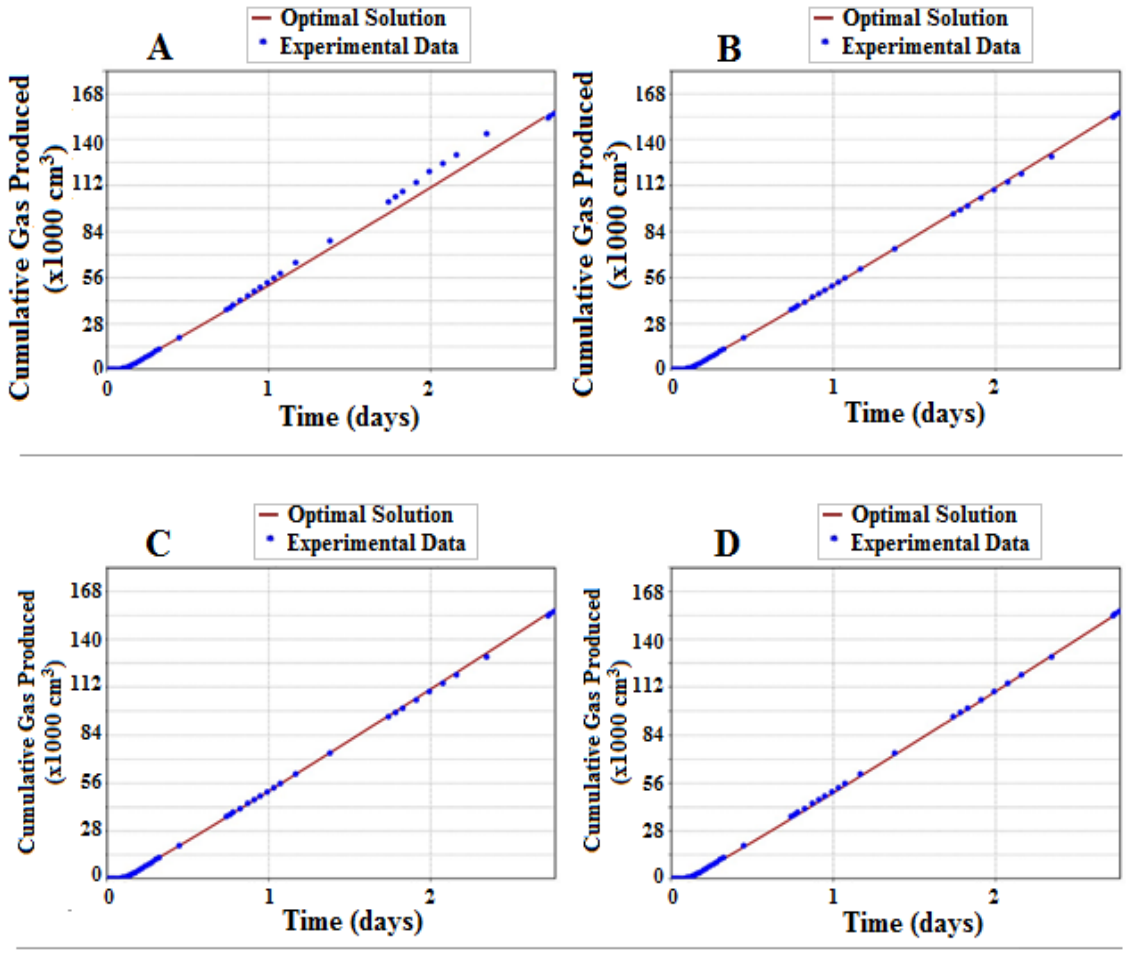

Figure 8-4: Shows the result of the cumulative gas produced from the history matching (solid red line) in comparison with the experimental data (blue dots) for four coarse models. A: 100x10; B:100x20; C:100x30; D: 100x40

Figure 8-5 shows the gas saturation after 0.1 pore volume of injection for the four different models. It indicated the occurrence of gas override at the top of the core for all the models. As the grid size increased, the finger became sharper as expected. Accordingly, Figure 8-6 shows the gas saturation at the end of the injection period, again, all the models showed similar sweeping behaviour with a swept area at the top of the core and a bypassed region at the bottom the core. The recovery mechanism that led to this sweeping behaviour has been described in section (4.3). Similarly, this also shows that all the models have same 'residual oil saturation' since by definition it is the residual immobile oil at the end of the injection and does not indicate the distribution of the saturation in the porous media. Therefore, even though the saturation distribution within the swept area are different for all the models, they have the same residual oil saturation value because it is the sum of the residual oil, trapped in pores in the swept area, and the

bypassed oil. Hence, residual oil saturation for unstable displacement has a different meaning from that of stable displacement and does not indicate the amount of capillary trapped oil.

$$Residual\ Oil\ Sat_{(unstable\ displacement)} = trapped\ Oil + Bypassed\ Oil \qquad 57$$

Figure 8-7 shows the gas/oil relative permeability obtained from the history matching for the four different models, demonstrating a clear symmetry in the shape of the relative permeability curves as it moved from A(100x10) to D (100x40). The oil relative permeability (kr_o) shifted to the right as it moved from A to D while the gas relative permeability (kr_g) shifted up as it moved from A to D and this shows that relationship existed between the grid size and the shape of the relative permeability.

Figure 8-5: Shows the saturation gas profile after 0.1 pore volume injection for the four different core models.

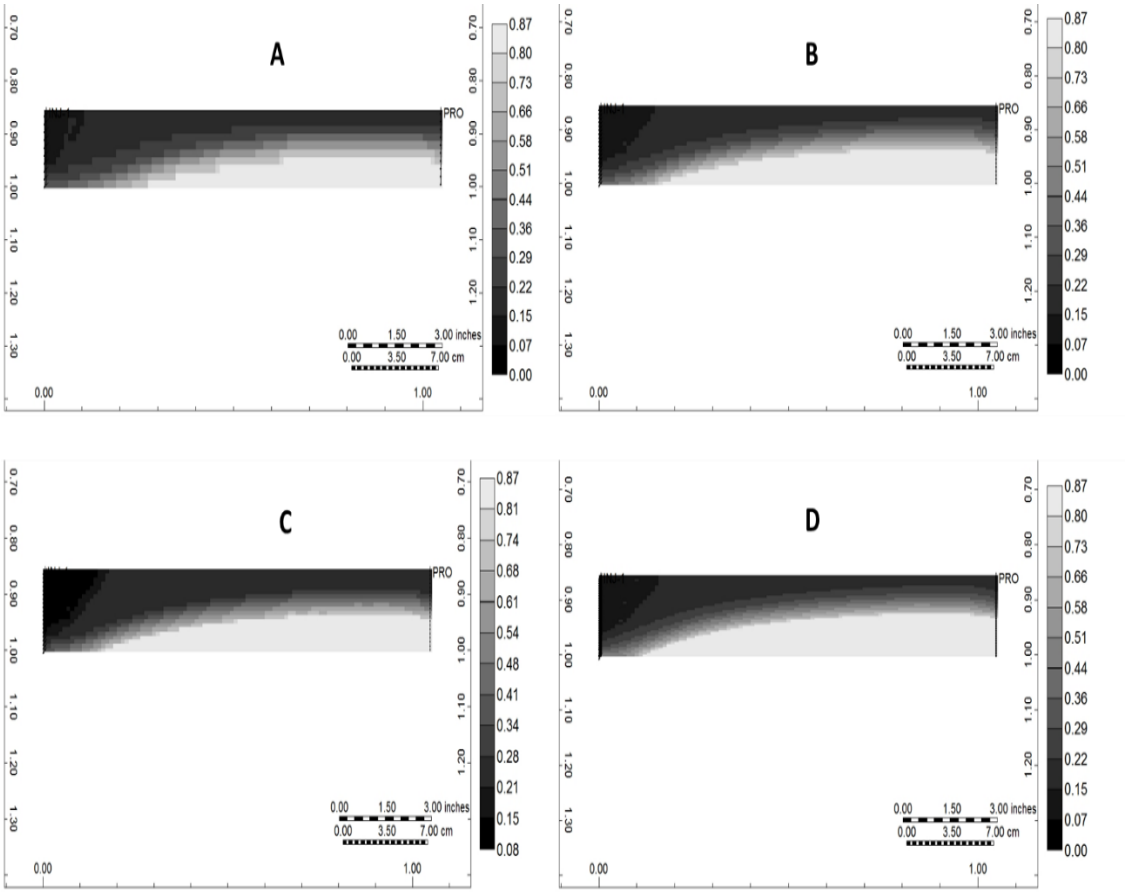

Figure 8-6: Shows the result of the saturation profile at the end of the injection period for the four history matched core models. A: 100x10; B:100x20; C:100x30; D:100x40.

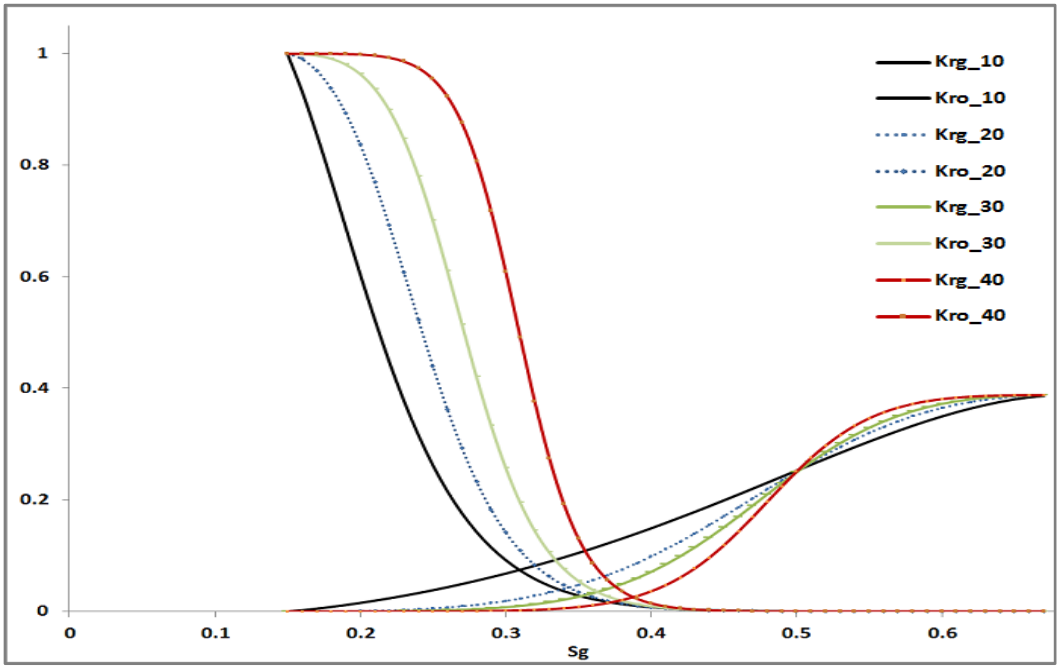

Figure 8-7: Shows the plot of the history matched gas-oil relative permeability curves as a function of gas saturation for the four core models.

To obtain the relationship between the shape of the relative permeability curve and the grid size, the parameter values (Table 8-2) were plotted against the grid size as seen in Figure 8-8. It shows that from model with grid size 20 (on the z-axis) to 40, there was a linear relationship between the parameter values. The relationship, however, did not start with the coarsest grid model (100x10) and therefore indicates that there is a minimum threshold of grid size required to establish the linear relationship. Therefore, by extrapolating this relationship, the relative permeability of the fine grid, high-resolution model (100x80) can be estimated. Figure 8-8 shows the extrapolated parameter values for the fine grid model plotted against the grid size while Figure 8-9 shows the relative permeability obtained using the extrapolated values. Figure 8-10 shows a comparison of the result of the simulation of cumulative oil recovered using the computed relative permeability curves against the experimental data. A good match was obtained between the simulation and the experiment. Similarly, Figure 8-11 shows the differential pressure across the core obtained from the simulation. The match for the DP, similar to that in the direct history matching of the high-resolution model, was not perfect for the period before breakthrough, however, it is acceptable for such a complex system.

To evaluate the efficiency of the multiscale approach with regards to reduction in time, the total time it took to simulate the set of coarse models was compared to that for the high-resolution model. Figure 8-12 shows that the multiscale approach has a huge benefit in runtime as it only required about one-fifth of the time needed to simulate the high-resolution model. Likewise, in terms of memory, Figure 8-13 shows that the virtual memory size requirement of the coarse models is only about half of that required for running the high-resolution model. Also, Figure 8-14 shows that the total number of Newton's iteration required by the solver to simulate the set of coarse models was less than half the amount required to simulate the single high-resolution model.

Conclusively, this example shows that the multiscale approach has a huge benefit in terms of simulation time and can also help in reducing the memory requirement for history matching process, which involves running a large number of simulations.

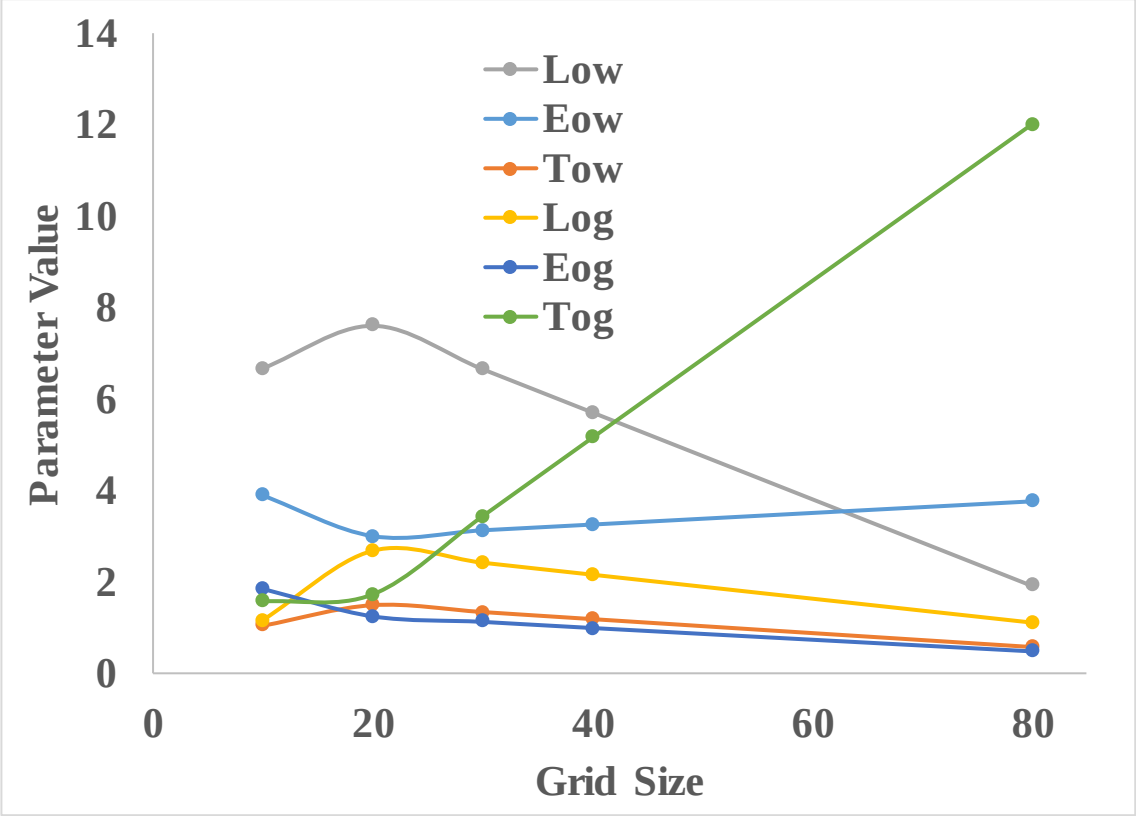

Figure 8-8: Plot of relative permeability function parameter (L.E.T) values against grid size showing the extrapolated values for grid size (100x80).

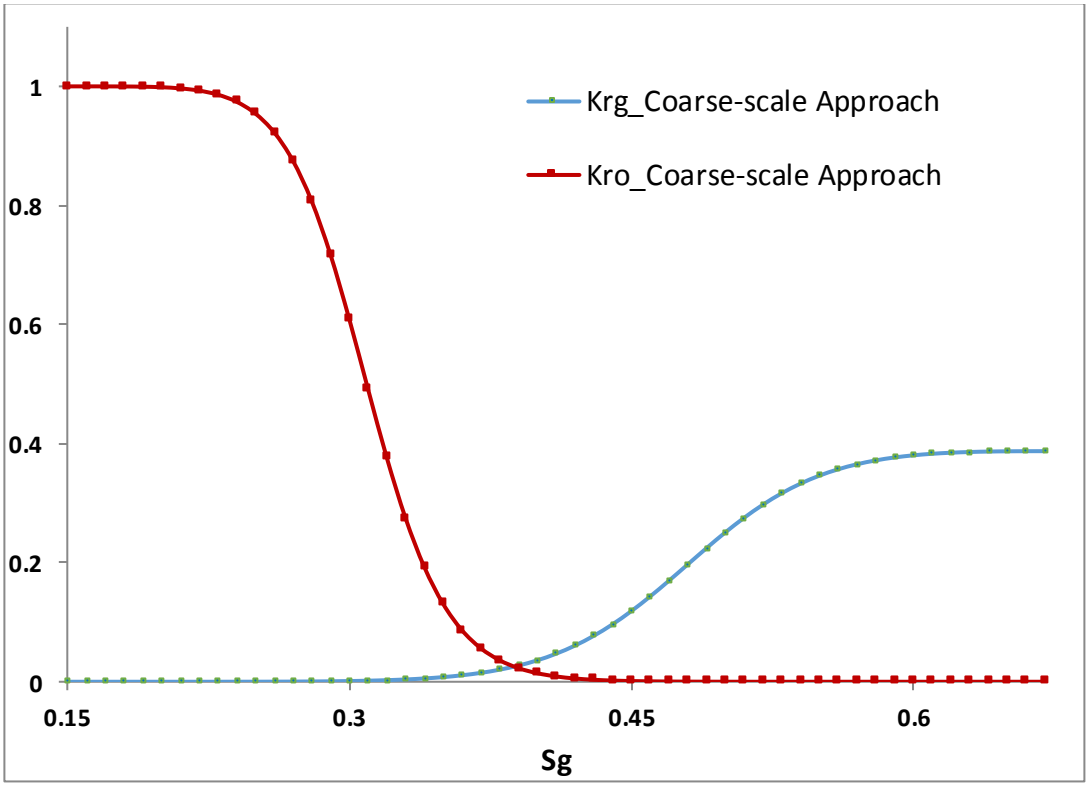

Figure 8-9: Predicted relative permeability of the high-resolution model (100x80) obtained using the coarse-scale approach

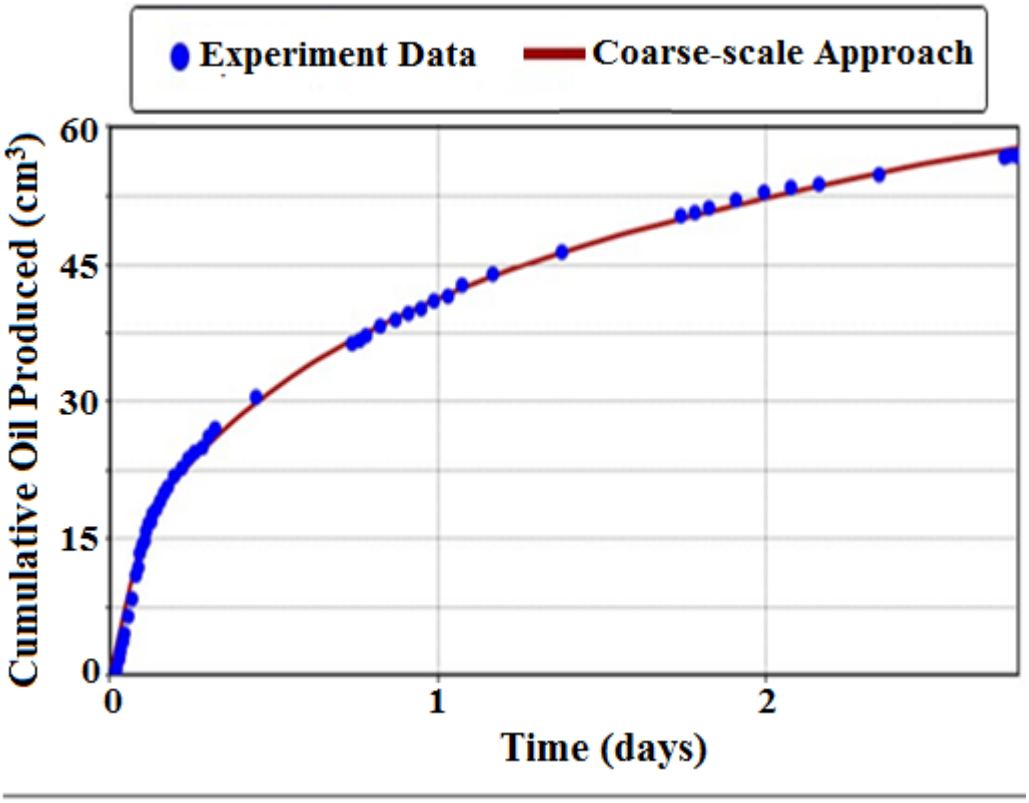

Figure 8-10: Shows the cumulative Oil recovered obtained from the simulation of the high-resolution model (100x80) using relative permeability obtained from the coarse-scale approach.

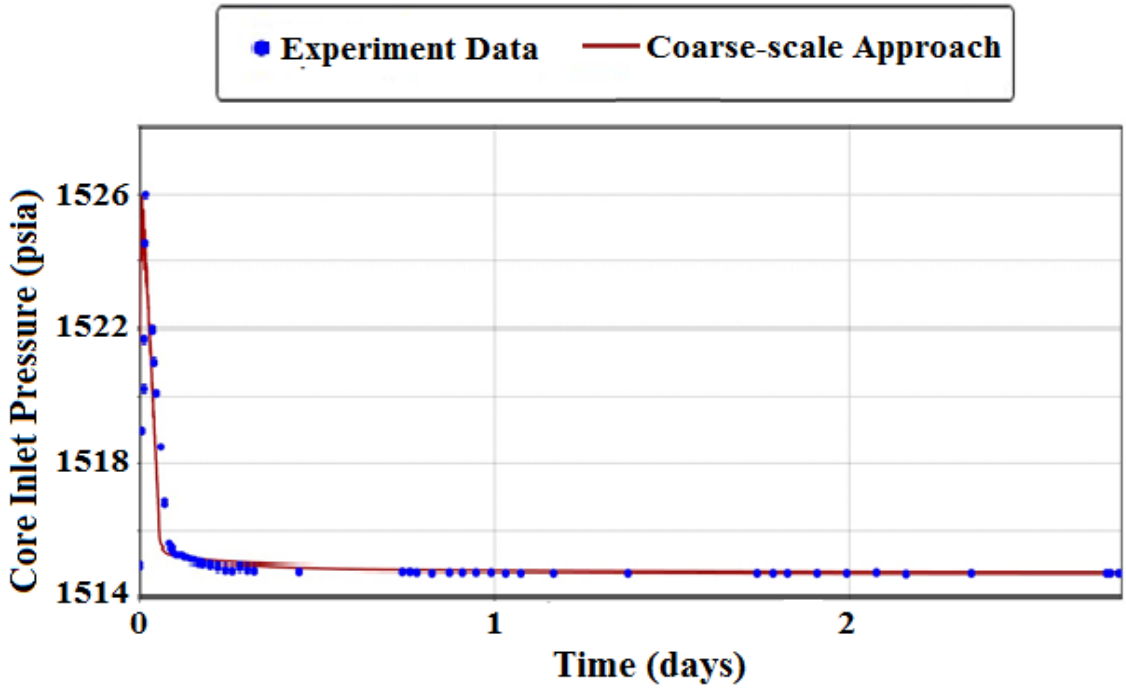

Figure 8-11: Shows the differential pressure across the core obtained from the simulation of the high-resolution model (100x80) using relative permeability obtained from the coarse-scale approach.

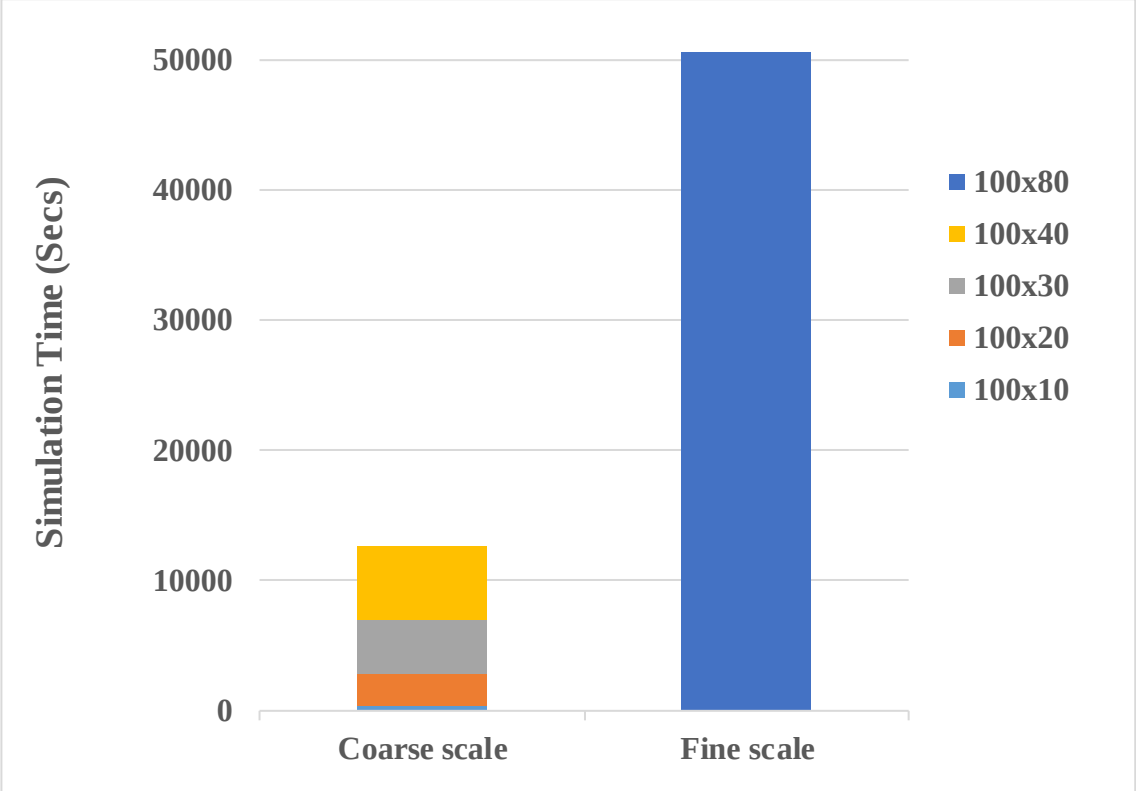

Figure 8-12: A chart of the simulation time for the coarse models compared with that of the fine scale, high-resolution model (100x80).

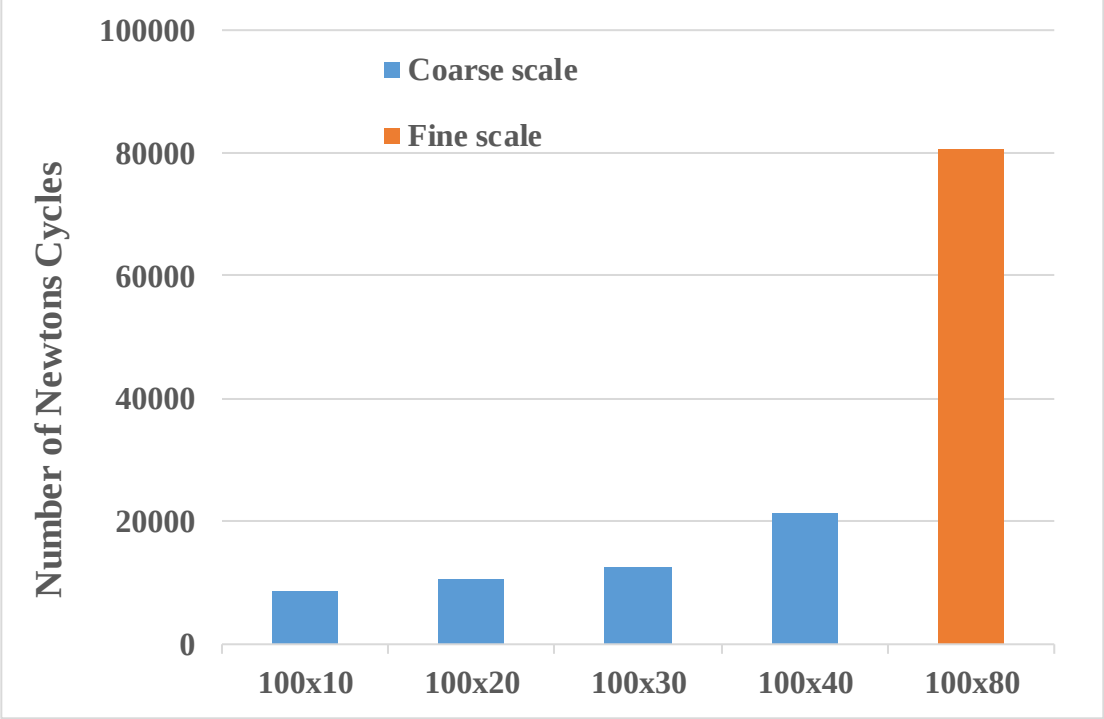

Figure 8-13: Comparison of the virtual memory Size usage (MB) required for the simulation of the fine scale and the coarse scale models.

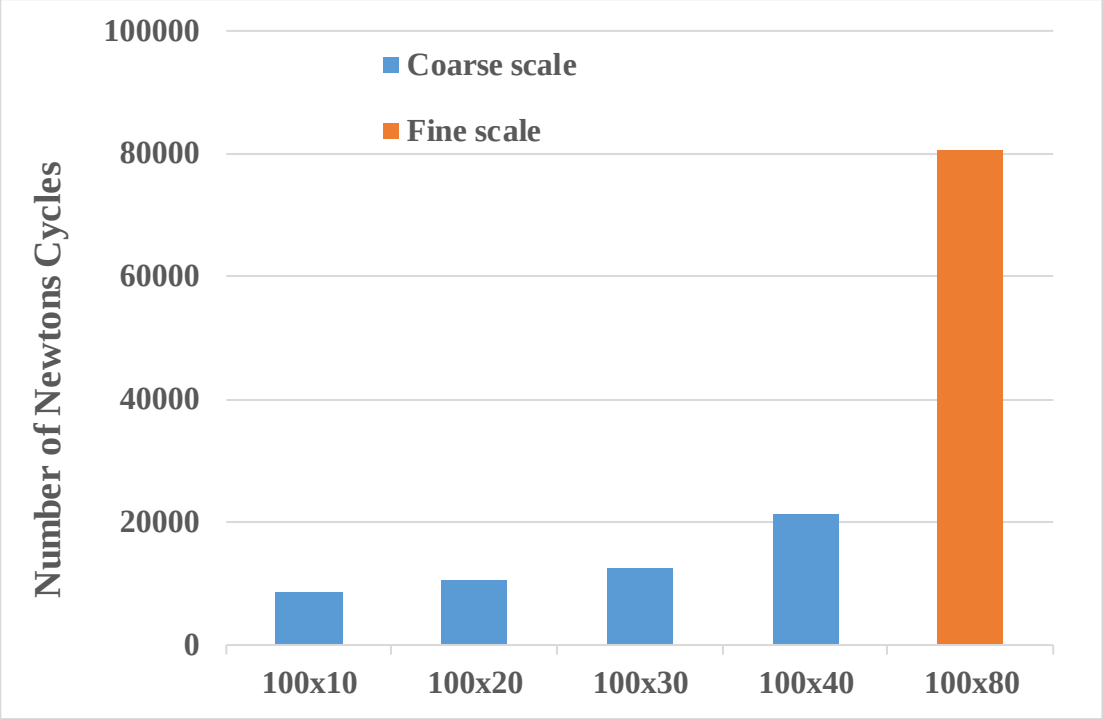

Figure 8-14: Comparison of the number of Newton's iterations completed during the simulation of the fine scale and coarse models.

8.4.2 Experiment-3: CO_2 injection into a horizontal core saturated with live crude J

In this experiment, CO_2 was injected into live crude J (crude J saturated with methane) in a horizontal core. The experimental conditions are similar to that in example one, but the live oil had an estimated viscosity of about 100cp, much lower than that of the dead oil (617cp). The experiment and the simulation results (section 6.7) have shown that the hydrocarbon solution gas (dissolved methane) has reduced the amount of the CO_2 that can otherwise be dissolved in the oil. The CO_2, having a higher potential, had to displace the methane from the oil into the gas phase before it can dissolve in the oil. Hence, the displacement benefits less from the viscosity reduction potential of the CO_2 as indicated by its lower recovery compared to the dead oil displacement. It also indicated an early breakthrough due to the lower viscosity of the CO_2-methane mixture in the bulk gas phase (Figure 6.24).

Previously, in Section 6.7 the detail of the simulation and the estimation of the relative permeability by history matching using the single, fine grid, high-resolution model approach has been described. The same relative permeability was estimated using the multiscale approach. A set of three coarse grid models were used which are 100x20, 100x30 and 100x40 in order to estimate the relative permeability of the high-resolution

model. Figure 8-15 shows the result of the history matching of the cumulative oil recovered for the three different coarse grid models indicating good matches for all the models.

Table 8-3 shows the result of the relative permeability function (L.E.T) parameter values for the models, which were obtained from the history matching, while Figure 8-16 shows the estimated gas/oil relative permeability curves of the coarse models, also obtained from the history matching. It clearly shows a trend in the shape of the relative permeability curves, similar to that achieved in the previous example. To estimate the relative permeability of the high-resolution model (100x80), therefore, the parameter values of the coarse grid models were plotted and extrapolated to determine the parameter values for the high-resolution model. Figure 8-17 shows the plot of the relative permeability function parameter values obtained from the history matching for the coarse grid models. Linear relationship existed for all the parameters which were extrapolated to estimate the values for the high-resolution model. Table 8-3 also shows the estimated parameter value for the high-resolution model while Figure 8-18 shows the estimated gas/oil relative permeability curves.

To verify the estimated relative permeability curves obtained from the multiscale approach, the high-resolution model of the experiment (100x80) was simulated using the estimated relative permeability. Figure 8-19 shows the result of the simulation of the cumulative oil recovered in comparison with the experiment. A good match similar to that obtained by the direct history matching of the high-resolution model was achieved. Similarly, Figure 8-20 and Figure 8-21 show the match of the pressure at the inlet of the core and the cumulative gas produced. This indicates that the estimated relative permeability curves using the multiscale approach were appropriate for the high-resolution model. Additionally, Figure 8-22 shows a chart of the total simulation runtime requirement for the multiscale coarse grid models and the time needed to run the single high-resolution model. It indicates that only about one-third of the time needed for the simulation of the high-resolution model was required to run the models in the multiscale approach, a huge benefit in terms of simulation time. In a similar vein, Figure 8-23 shows the average memory requirement for each of the models while Figure 8-24 indicates the average number of Newton's iterations needed during the simulation of each model. Bearing in mind the highly computational nature of history matching optimisation

process, the lower memory size and computations required in the multiscale approach using coarse models means that a less powerful computer can be used to estimate relative permeability curves for an unstable displacement with accuracy similar to that obtained using a single high-resolution model approach.

Table 8-3: Relative Permeability function (L.E.T) parameter values obtained from the history matching of the coarse grid models. The values for the high-resolution model (100x80) were extrapolated from the values of the coarse grid models.

Parameter	Model(100x20)	Model(100x30)	Model(100x40)	Model(100x80)
Lo	1.2	1.2933	1.3867	1.76
Eo	1.5	1.4896	1.4792	1.4375
To	1.5	1.6950	1.8708	2.6125
Lg	2.68	3.1000	3.4533	5
Eg	1.245	1.2697	1.2943	1.392975
Tg	1.725	1.7235	1.7200	1.716
Error Misfit%	1.23	2.17	1.79	2.3

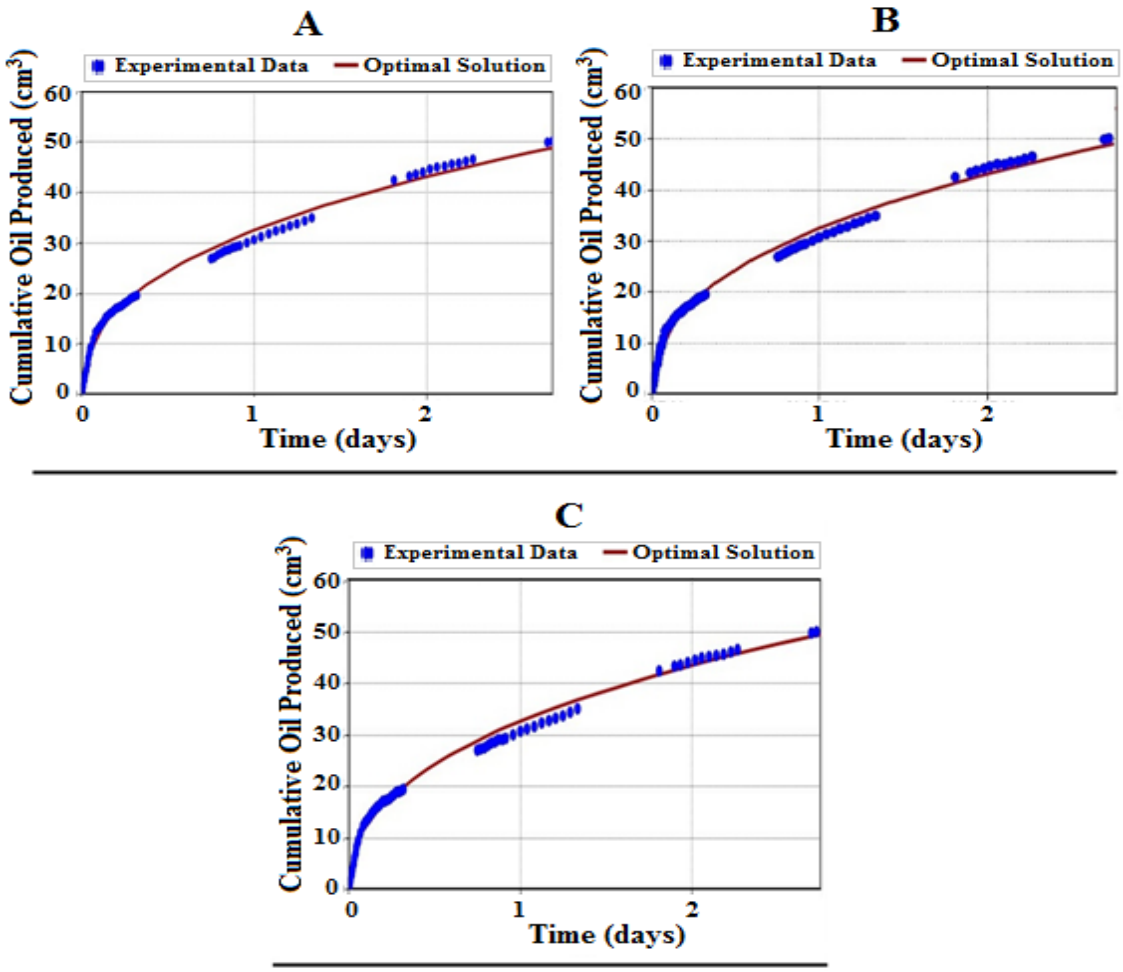

Figure 8-15: Shows the result of simulation of cumulative oil recovered obtained from the history matching of Experiment-3 in comparison with the experimental data for three coarse models. A: 100x20; B:100x30; C:100x40.

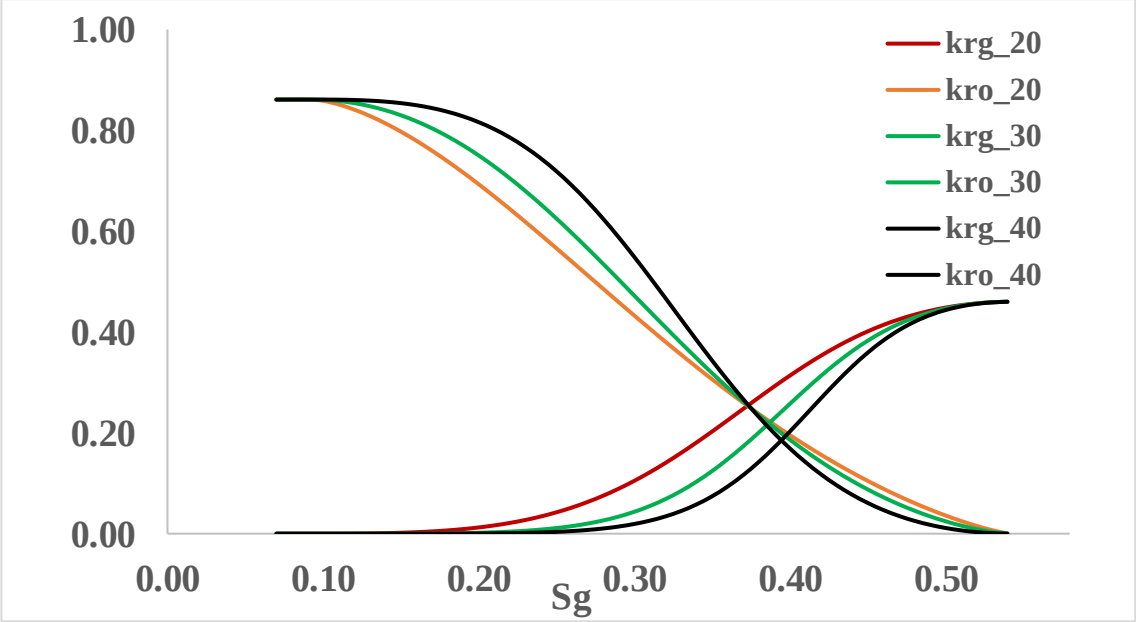

Figure 8-16: Shows the gas/oil relative permeability curves for the three coarse grid models obtained from the history matching process.

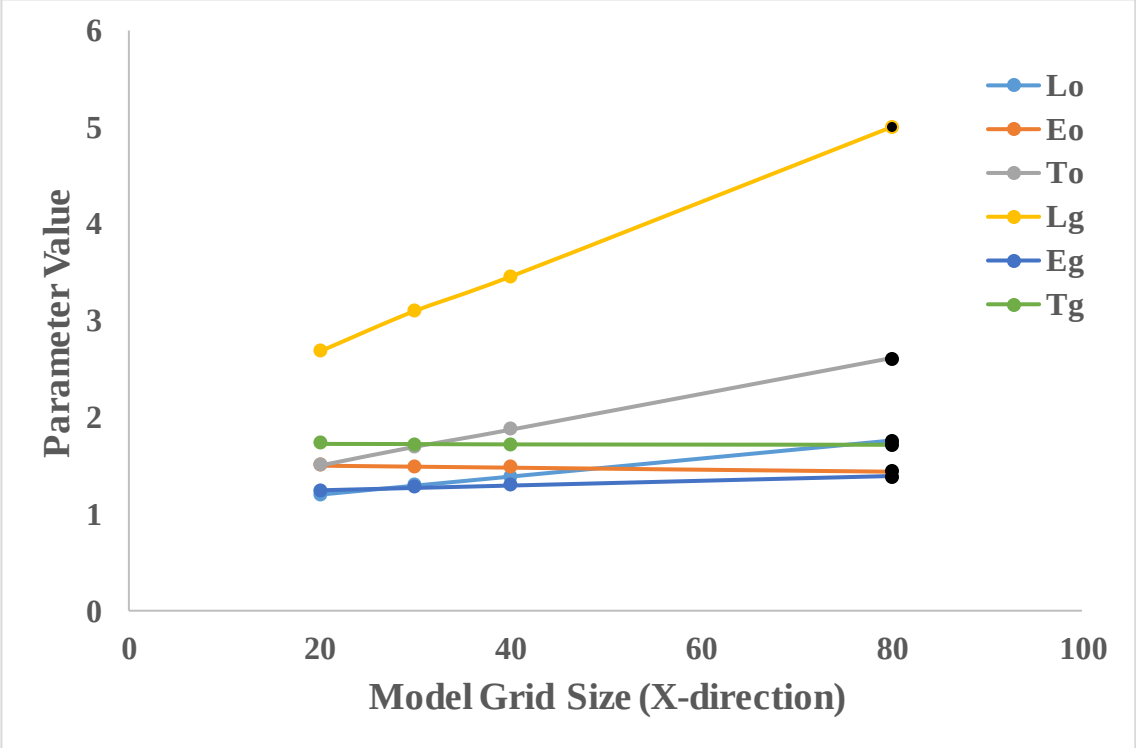

Figure 8-17: Plot of the relative permeability function parameter values obtained from the history-matching of the coarse grid models of Experiment-3 (CO_2 injection into live oil) and the extrapolated values for the high-resolution models (black dots).

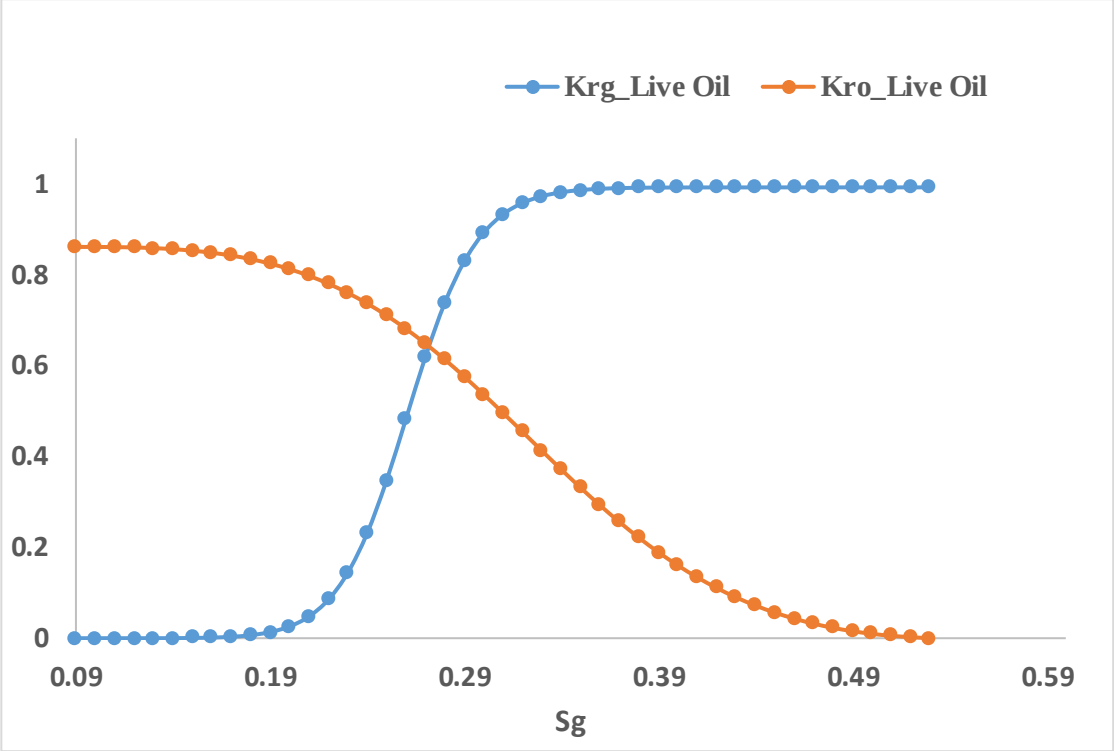

Figure 8-18: Predicted relative permeability curves for Experiment-3 (CO_2 injection into live oil) obtained using the coarse-scale approach.

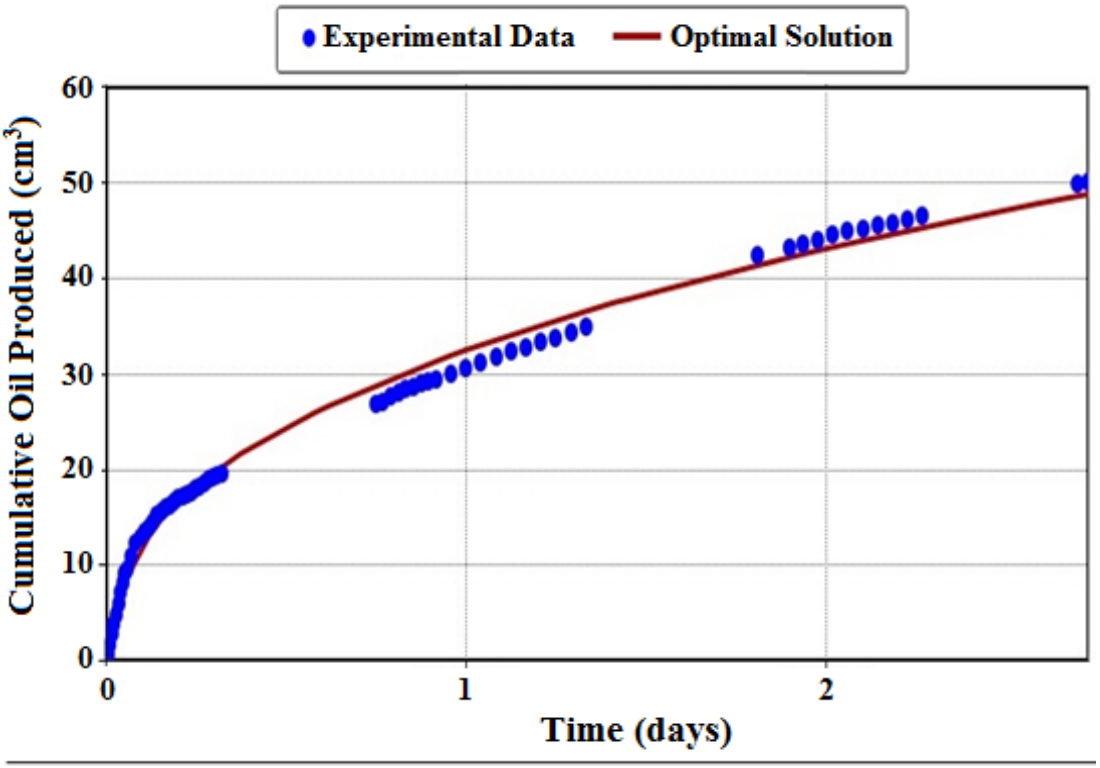

Figure 8-19: A match of the cumulative oil recovered obtained from the simulation of experiment-3 using a high-resolution model (100x80) and a relative permeability obtained from the multiscale approach.

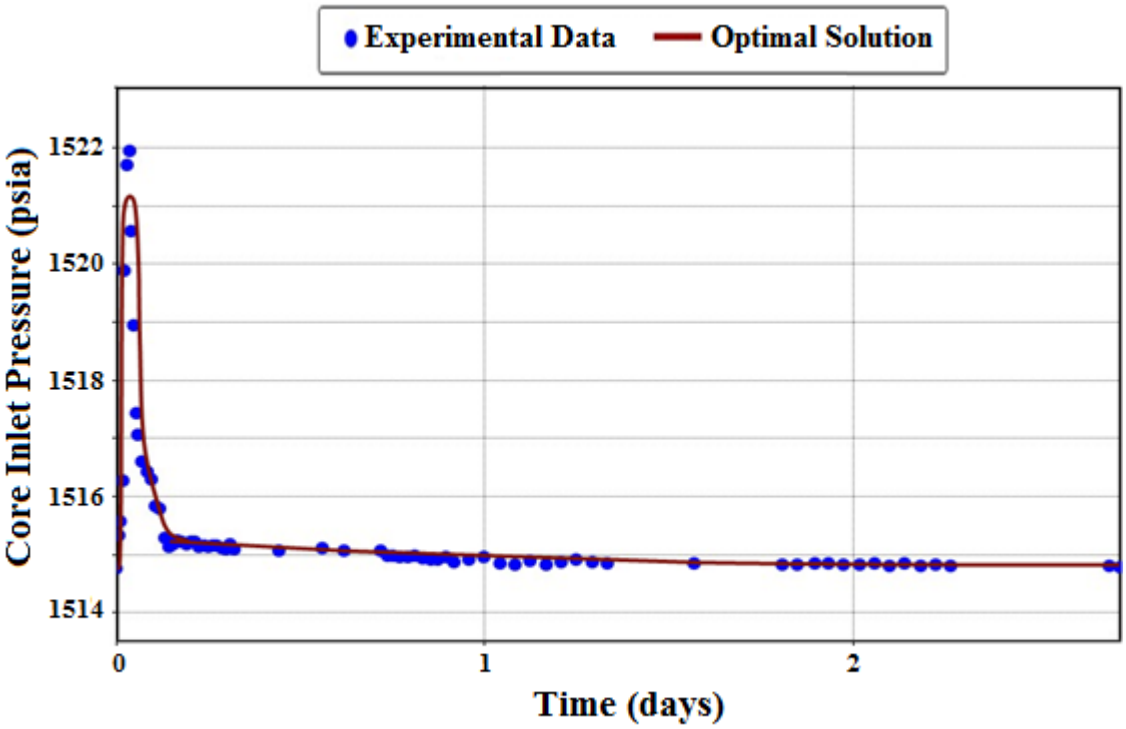

Figure 8-20: A match of the pressure at the inlet of the core obtained from the simulation of experiment-3 using a high-resolution model (100x80) and a relative permeability obtained from the multiscale approach.

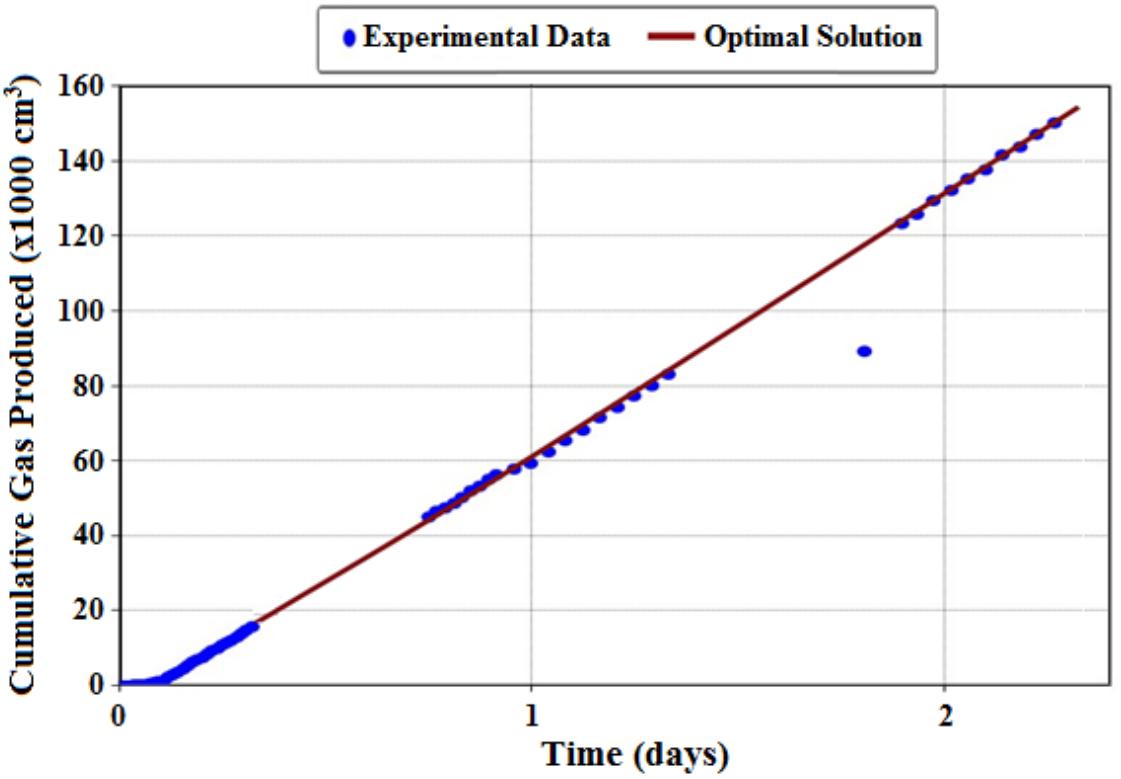

Figure 8-21: A match of the cumulative gas produced obtained from the simulation of experiment-3 using a high-resolution model (100x80) and a relative permeability obtained from the multiscale approach.

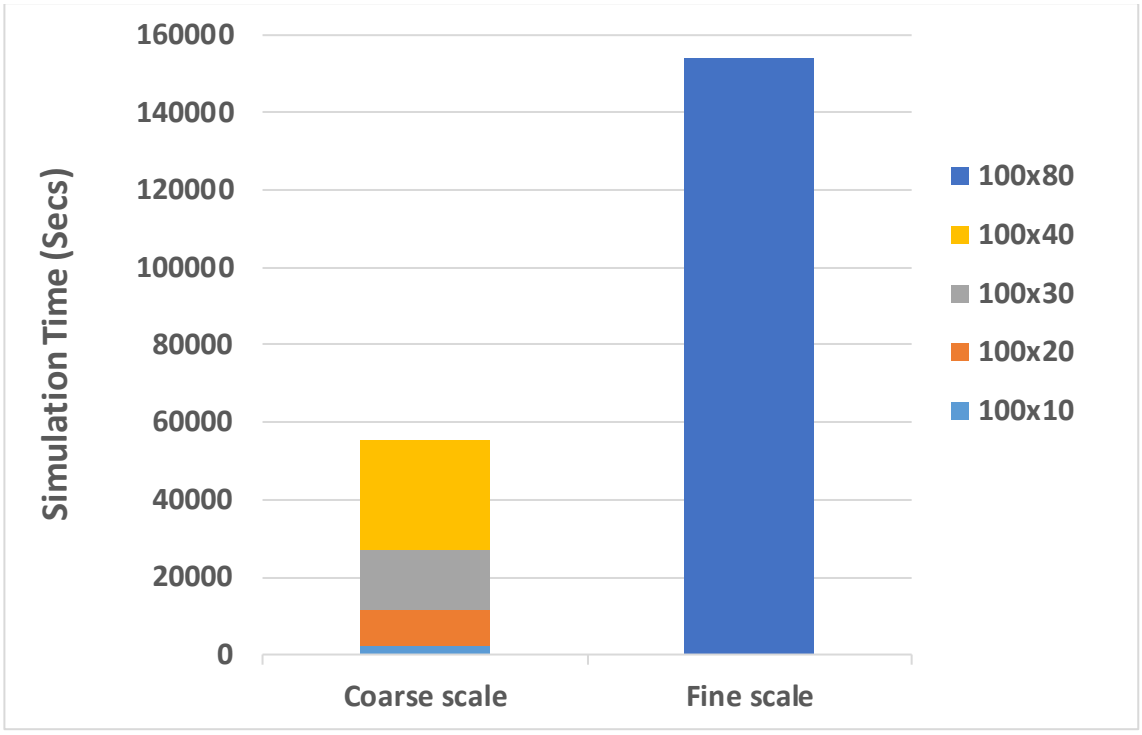

Figure 8-22: A chart of the simulation time for the coarse models compared with that of the fine scale, high-resolution model (100x80).

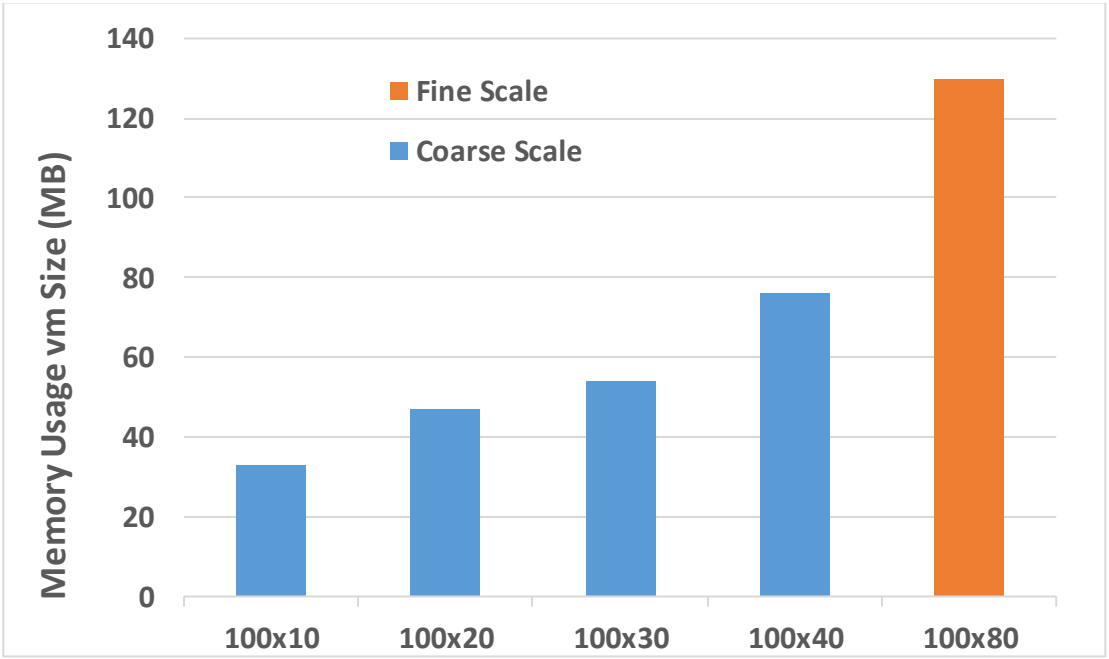

Figure 8-23: Comparison of the virtual memory Size usage (MB) required for the simulation of the coarse scale and the high-resolution models.

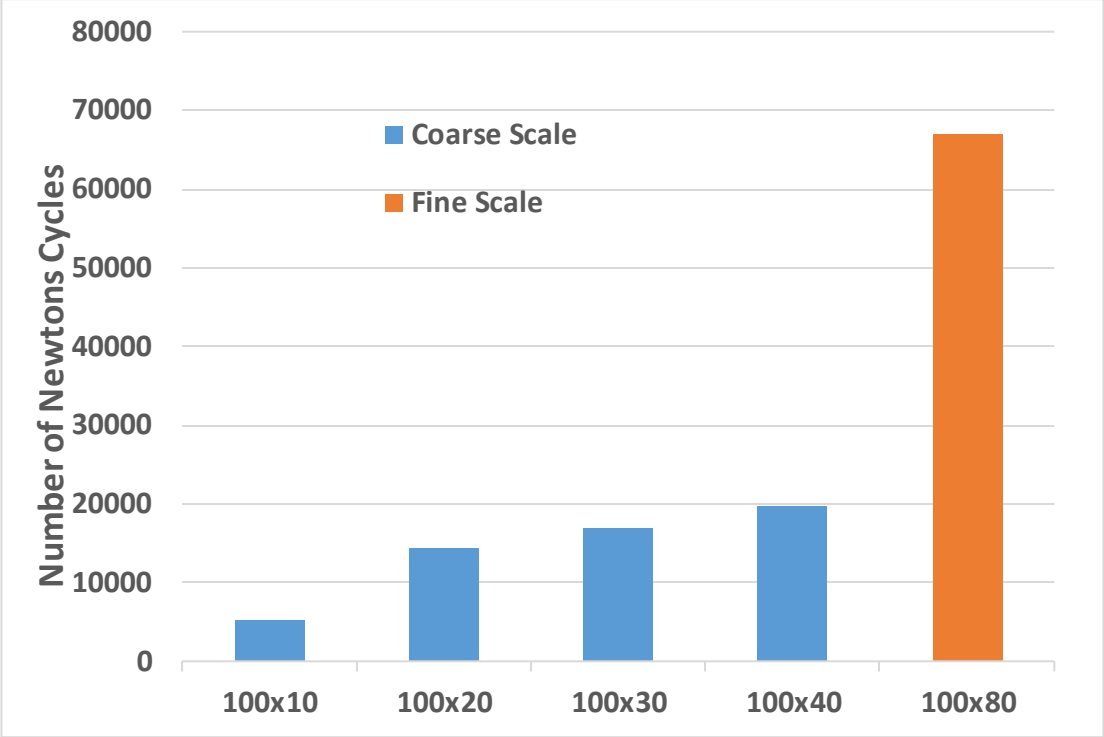

Figure 8-24: Comparison of the average Number of Newton's iterations needed for the simulation of the coarse and the high-resolution models.

8.5 CONCLUSION

Relative permeability is an important flow function that is essential in the simulation of multiphase flow, however, difficulty in measurement, artefact and cumbersome analysis of result makes the determination of this important parameter using experimental technique untenable or quite often unreliable. History matching of experimental data, an inverse technique which has gained wider acceptance due to advances in processing and memory capacity of computers is often utilised to estimate this important flow function. The limits of these hitherto powerful computers can, however, be tested when the displacement is highly unstable and especially when the fluid is compositional, as this would require a high-resolution multi-dimensional model (2D or 3D) to simulate the displacement. As simulation time is proportional to the number of grids in the models and the number of equations to be solved, it is clear that a computer's capacity can easily be exhausted in such a scenario. In this chapter, gas/oil relative permeability was estimated from an unstable compositional displacement using a multiscale approach involving the history matching of a set of coarse models to determine relative permeability for use in a high-resolution model of a similar experiment. The following conclusions were drawn from the approach.

1. It shows that a relationship can exist between relative permeability function parameter values for a set of coarse models which can be extended to estimate the parameter values for a high-resolution model.

2. The relative permeability estimated from an unstable displacement using the multiscale approach, was appropriate for use in the simulation of a high-resolution model, as it was able to match the experimental production data correctly.

3. The total time required for the simulation of the multiscale coarse models was only about one-third the time needed to simulate the single high-resolution model for the examples considered, a huge benefit in terms of simulation time.

4. The memory requirement of the multiscale coarse models for the experiments considered was only about a half required for the simulation of the high-resolution model. Therefore, the lower memory size and computations required in the multiscale approach using coarse models means that a less powerful computer can be used to estimate the relative permeability curves for unstable displacements with accuracy similar to that obtained using a high-resolution model approach.

CHAPTER 9

CONCLUSION AND RECOMMENDATION

Two-phase and three-phase flow occur during many important processes in oil reservoirs, these include waterflooding, solvent and gas injection as well as the combination of different injection fluids and strategies. The concept of relative permeability is generally accepted and used to describe the fractional flow of a particular phase during a multiphase flow in porous media. Several direct and indirect standard methods are being used to estimate this parameter for input into reservoir simulators. However, in displacement with instability, such as viscous or gravity fingering, the main assumption behind these methods, which is that the flow is stable and the front is a Buckley-Leverett type shock front, is violated. Therefore, conventional methods of estimation of relative permeability cannot be applied. In this study, the methodologies used for characterization of relative permeability in relation to heavy oil displacement by waterflooding or immiscible gas injections in which viscous and gravity instabilities occur were reviewed and a new methodology for its estimation was proposed. The methodology was verified using a semi-analytical approach and a procedure for reducing the time required for the estimation was proposed. The main conclusions drawn from this work followed by some recommendation for future studies are presented in the following sections

9.1 CONCLUSION

A summary of the work and the main findings derived from each chapter are as follows:

Chapter 2: Background Material and Underpinning Data

The chapter mainly reviewed the concept of relative permeability and explained the experimental and analytical approaches for the estimation of this important flow function. The procedure for estimation of relative permeability by history matching was discussed

and the inadequacy of the conventional method of history matching using one-dimensional model was highlighted. Numerical dispersion error resulting from the choice of grid size and other sources were then discussed. The injection strategy, the fluid types and the displacement mechanisms of the experiments considered in this work were then presented and finally the core modelling approach was discussed and the optimum grid size of the 2D model of the most unstable displacement experiment was then determined for use in all subsequent simulations.

Chapter 3: Simulation Model

This chapter forms the core framework of the studies by providing an in-depth background of the modelling approach and presented some of the main components of the studies. Hence, the following conclusions were drawn:

1. Compositional displacement processes involving CO_2 and other gases were first reviewed, and the use of the equation of state (EOS) in the characterization of heavy oil for simulation of compositional displacement was highlighted. The stages involved in the tuning of EOS to match experimental data and relevant correlations used in conventional oil PVT modelling were discussed to show they can be misleading when used for matching heavy oil experiments.

2. In the procedure for tuning the EOS, a new methodology for lumping the heavy oil components into pseud-components was proposed. The method was based on the behaviour of the produced fluids components rather than the arbitrary scheme of lumping of components in conventional methods. The new procedure showed a better matching of the fluid properties and its behaviour during simulation.

3. One-dimensional core model simulation of CO_2 injection into a horizontal saturated with a dead heavy oil (Experiment-1) was carried out and was shown to be incapable of simulating compositional displacement where there is instability at the front due to viscous fingering or gravity drainage.

4. Grid sensitivity study was therefore carried out on a two-dimensional model of the core to determine the optimum size that would sufficiently resolve the finger in such displacements. The sensitivity study was based on the variation in the cumulative oil recovered and the differential pressure across the core. It was

observed that the gridding was more sensitive in the direction perpendicular to the flow. The optimum model for the horizontal core was found to be 100 grids in the horizontal direction and 80 grids in the vertical direction. The core was assumed to be homogenous in porosity while the permeability field was stochastically populated using a normal distribution with small variability to trigger the finger during displacement. The modelling approach was able to capture the finger and its behaviour.

Chapter 4: Estimation of Two-Phase Flow Functions from Unsteady State Heavy Oil Coreflood Experiments with Instability

This chapter discussed a methodology for estimation of two-phase relative permeability from unstable heavy oil displacement experiments. The following conclusions were derived from the work.

1. Experimental and analytical methods for estimation of two-phase relative permeability in conventional oil displacement processes were reviewed, and the incapability of these methods to handle displacements in which instability and mass transfer take place, such as CO_2 injection into heavy oil were highlighted.

2. To estimate relative permeability in such displacements, an implicit history-matching approach where a high-resolution 2D model of the core was used in the history matching of the unsteady-state coreflood data was considered. The unknown flow function in the history matching process was represented by a versatile L.E.T type parametric equation. The procedure using 2D model and a versatile function to represent the relative permeability curve was able to estimate this important flow function sufficiently.

3. Some parameters, which could control the shape of the curves, were investigated. The key conclusion on this sensitivity is that the estimated relative permeability curves were solely controlled by the type of instability

and viscosity ratio; the transition zone where the exchange of mass takes places does not have a significant effect on the shape of the curves.

4. The two-phase, gas/oil relative permeability curves estimated from secondary CO_2 injection into heavy oil (Experiment-1) was basically similar to that estimated from N_2 injection (Experiment-2), an indication that the shape of the curves does not depend on the gas type but rather on the viscosity ratio and the extent of the instability.

5. A one-dimensional model simulation and analysis of the two displacements (Experiment-1 and Experiment-2) showed that there was competition between gravitational and viscous forces in dictating the stability of the displacement. Moreover, the analysis which did not take into account the effect of capillary pressure showed that the N_2 injection into the vertical core was dominated by viscous fingering while gravitational force dominated the CO2 injection into the horizontal core, with a prominent gravitational override feature.

6. The history matching of a secondary waterflood for the displacement of heavy oil (Experiment-4), where data for drainage capillary pressure curve was included in the simulation model, showed that the displacement was stable with a sharp, Buckley-Leverett type front. It, therefore, highlights the importance of capillary pressure in stabilising the fronts of these type of displacements.

Chapter 5: Estimation of Three-Phase Relative Permeability from Unsteady-state Heavy Oil Coreflood Experiments with Instability

This chapter examined the mechanism of tertiary waterflood injection. Tertiary relative permeability was estimated by history matching an experiment in which water was used to chase a CO_2 flood (Experiment-1). The result of the simulation demonstrated a different three-phase CO_2/oil/water flow mechanism. The estimated tertiary oil/water relative permeability had different critical values and endpoints compared to that obtained from secondary waterflood. The following conclusions were derived from the chapter:

1. The simulation results obtained from the history-matched model of the tertiary water injection showed that water preferred to follow the path already opened up by the previously injected CO_2. This displacement mechanism was different from conventional Water Alternating Gas Injection (WAG) where water, because of its higher density than both gas and oil would open up a new path different from that of the gas. In here, the water preferred to follow the path of the CO_2, because its dissolution in the oil had significantly reduced the viscosity of the trapped oil along its path. Hence, the lower resistance in the CO_2 path compared to that in the bypassed oil makes it more preferable for the tertiary water to follow.

2. An attempt was made to simulate a Simultaneous Water and Gas (SWAG) injection experiment (Experiment-5) in which CO_2 and brine were simultaneously injected. Two approaches were followed; In one, a secondary gas-oil and secondary water-oil relative permeability curves that have been estimated previously were combined using Stone's (ii) model as the three-phase relative permeability model in order to simulate the experiment. In the second, a secondary gas/oil and a tertiary oil/water relative permeability curves were combined in the Stone's model (ii) for the three-phase relative permeability.

3. The results of the simulation of the SWAG experiment showed a better match with the experimental production data for the second case, where tertiary water-oil relative permeability was employed in the three-phase Stone's (ii) model. This is because CO_2 has significantly higher mobility compared to water and hence moved ahead of the water.

4. In these simulations, a notable discrepancy, in differential pressure across the core, between the simulation and the experimental results was observed. This could mainly be attributed to the diffusive flow of CO_2, which was not neglected in the simulation due to substantially higher computation cost. As a recommendation, it would be worthwhile to include the diffusive flow of CO_2 into the simulations to sensitise its impact.

In the displacement of heavy oil by water, gas or solvent, several processes are dynamically changing, making the modelling of such displacement difficult to achieve. These include the mass transfer between phases, which can lead to a continuous change in phase properties and capillary pressure changes due to the change in interfacial tension. In addition, there is also the issue of viscous fingering resulting from the large mobility ratio. These are complex processes that require a tremendous amount of experimental and theoretical information to adequately model and simulate. It is for these reasons that the model is gauged against the effect of some of these complex processes. The following conclusions were drawn from the work in this chapter:

1. The two-phase gas/oil relative permeability obtained from the history matching of secondary CO_2 injection in a horizontal orientation (Experiment-1) was used to simulate similar experiment that was conducted in a vertical orientation (Experiment-5). The results of the simulation showed a perfect match with the experimental data for the vertical injection experiment, indicating that the method used for the estimation of relative permeability from the unstable displacement was not influenced by gravity or orientation.

2. The results of the simulation also showed that gravity drainage mechanism similar to that in vapour extraction (VAPEX) processes occurred in the vertical injection, indicating the ability of CO_2 to extract component under the influence of gravity through density-driven current.

3. The shape of the relative permeability estimated by history matching when capillary pressure curve was included was different from that estimated when the capillary pressure was not included. They showed significantly different critical saturation values and residual oil saturation, even though the core was homogenous with relatively high permeability. This understates the importance of capillary pressure when estimating relative permeability in heavy oil displacement.

4. The simulation of secondary waterflood in which experimental drainage capillary pressure curve was included showed a stable, Buckley-type of front

while the simulation of the same experiment, where capillary pressure curve was not included showed an unstable front with multiple viscous fingers. This highlights the importance of capillary pressure in the stability of fronts in the simulation of heavy oil displacement processes.

5. Effect of Fickian (molecular) diffusion on the residual oil and the recovery was investigated. The analysis showed that only about 10% of the bypassed oil could be affected by static diffusion. However, this could be significantly higher when dynamic diffusion which includes convective currents and dispersion effects is considered.

6. The viscosity of injected gas phase in heavy oil displacement can dynamically change as it gradually extracts lighter components from the oil. This would have a significant effect on the amount of trapped oil in the pores and hence, the recovery. Since most simulators assume instantaneous equilibrium as the injected gas comes in contact with the oil, it is important to determine the effect of the change on recovery. This was achieved by varying the viscosity of the contacted gas in the simulation of a gas injection into heavy oil. An increase of about 10% in the contacted viscosity led to about 5% increase incremental ultimate oil recovery, a significant improvement that was partly due to extracted lighter components that were produced in the gas phase.

7. A peculiar property of CO_2 is its ability to increase oil density in solution. This phenomenon could lead to density current which can significantly affect recovery. The result of simulation of a CO_2 injection into heavy oil showed that dynamic change in density resulted in density-driven current and eddies which improved recovery from the bypassed oil region.

8. Hydrocarbon solution gas in heavy oil can limit the amount of CO_2 that can dissolve in the oil thereby hampering its beneficial viscosity reduction effect. The comparison of the simulation result for dead oil (Experiment-1) and live oil (Experiment-3) showed that the recovery of the latter was lower due to the competition between the two solvents (methane and CO_2).

9. The relative permeability curves of live oil are markedly different from that of the dead oil due to change in fluid viscosity and possibly as a result of changes in rock properties such as wettability and contact angle, which need to be verified through physical experiment.

Chapter 7: Theoretical predictive model for Viscous Fingering in Heavy Oil Compositional Displacement

The main purpose of this chapter was to develop a simple theoretical tool for predicting viscous fingering in displacements with instability and to analytically verify estimated relative permeability curves. The following conclusions were drawn from the studies.

The theory of viscous fingering in compositional displacement, which was developed, based on material balance and Koval's empirical equation for light and conventional oils was extended to predict composition in heavy oil displacement by immiscible gas.

1. The theory, which is based on the assumption of linear variation of composition within a fingered region, has shown the potential to predict saturation profile within a fingered region in an unstable displacement, such as heavy oil displacement processes.

2. The saturation profile of CO_2 injection into horizontal core (Experiment-1) and vertical core (Experiment-4), saturated with heavy oil, were predicted using the relative permeability curves estimated from previous history matching studies. The saturation profiles reasonably agreed with the average saturation profile obtained from high-resolution simulation of the similar experiment. In particular, the breakthrough time was accurately predicted in both cases while the saturation and width of the fingered region in the horizontal case was also accurately predicted. For the vertical case, the theory could not satisfactorily predict the saturation and the width of the fingered region due to the gravitational effect that was factored into the equation. However, it has shown the capability of the proposed semi-analytical method to predict viscous fingering in such displacements.

3. Therefore, this method can be used to verify the relative permeability obtained from history matching of unstable displacement processes.

Chapter 8: Multiscale Approach to Estimation of Two-Phase Relative Permeability from Unstable Displacements Using History Matching

The difficulty in measurement, artefact and cumbersome analysis of result has made the determination of relative permeability using experimental technique untenable or quite often unreliable. History matching is often resorted to in order to estimate this important flow function. However, history matching is time and resource consuming, and even more so when confronted with an unstable displacement that requires a high-resolution fine grid model. The limits of hitherto powerful computers can easily be tested in such scenarios, and it is, therefore, expedient to develop a methodology that would reduce the computational time and resource requirement of the history matching process. For this objective, a novel multiscale approach that uses a set of coarse grid model in the history matching process instead of a single high-resolution fine grid model was proposed. The following conclusions were drawn from the approach.

1. It shows that a relationship can exist between relative permeability function parameter values for a set of coarse models which can be extended to estimate the parameter values for a high-resolution model.

2. The relative permeability estimated from an unstable displacement using the multiscale approach, was appropriate for use in the simulation of a high-resolution model, as it was able to match the experimental production data correctly.

3. The total time required for the simulation of the multiscale coarse models was only about one-third the time needed to simulate the single high-resolution model for the examples considered, a huge benefit in terms of simulation time.

4. The memory requirement of the multiscale coarse models for the experiments considered was only about a half required for the simulation of the high-resolution model. Therefore, the lower memory size and computations required in the multiscale approach using coarse models means that a less powerful computer can be used to estimate the relative permeability curves for unstable displacements with accuracy similar to that obtained using a high-resolution model approach.

9.2 RECOMMENDATION

The work to advance the numerical simulation of unstable displacements exacerbated by mass transfer is far from complete, and there are huge areas for improvements. Based on the work presented in this thesis, the following recommendations can be proposed for future works.

1. Although the approach to PVT modelling was able to capture the overall behaviour of the fluid components in the experiment, however, it was insufficient in matching quantitatively, the composition of the produced fluid from the experiment. This understates the importance of sufficient experimental data and therefore more PVT experiments would be required to effectively model the phase behaviour of the components in order to achieve a better match.

2. In the CO_2 injection experiment, there was a gradual dissolution of the gas into oil, however, the commercial simulator used (CMG-GEM) is based on an equation of state that assumes instantaneous equilibrium. This can be inaccurate and may lead to an erroneous result. A higher order numerical simulator capable of handling this compositional effect should be used to understand fully how the exchange of components affect recovery.

3. Capillary pressure is one of the prevailing parameters affecting fluid distribution and recovery in oil reservoirs and is routinely measured in the oil industry using displacement test methods such as centrifuging for two-phase flow. However, reliable measurements are difficult to obtain for heavy oil systems due to the nature of the fluid. Sensitivity study had shown the stabilising effect of capillary pressure on displacement. This shows that capillary pressure can affect significantly influence the stability of fronts in such displacements and extensive experimental and theoretical work should be conducted to gain a better understanding of capillary pressure.

4. The multiscale approach for the estimation of relative permeability of an unstable displacement by history matching has shown a promising result when applied at core scale and its applicability at a larger scale should be investigated.

REFERENCES

AGARWAL, R. K., LI, Y. K., NGHIEM, L. X. & COOMBE, D. A. 1991. Multiphase Multicomponent Isenthalpic Flash Calculations. *Journal of Canadian Petroleum Technology,* 30**,** 69-75.

AKHLAGINIA, M., TORABI, F. & CHAN, C. W. 2013. Estimation of Three-Phase Relative Permeability Isoperms in HeavyOil/Water/Carbon Dioxide and Heavy Oil/Water/Methane Systems. *SPE Heavy Oil Conference Canada*. Calgary, Alberta, Canada.

AL-SHAALAN, T. M., FUNG, L. S. K. & DOGRU, A. H. 2003. A Scalable Massively Parallel Dual-Porosity Dual-Permeability Simulator for Fractured Reservoirs with Super-K Permeability. *SPE Annual Technical Conference and Exhibition*. Denver, Colorado, USA: Society of Petroleum Engineers.

ALKINDI, A., AL-WAHAIBI, Y. & MUGGERIDGE, A. H. 2011. Experimental and numerical investigations into oil-drainage rates during vapor extraction of heavy oils. *SPE Journal,* 16**,** 343-357.

ALKINDI, A., MUGGERIDGE, A. H. & AL-WAHAIBI, Y. 2008. The Influence of Dispersion and Diffusion on Heavy Oil Recovery by VAPEX. *SPE International Thermal Operations and Heavy Oil Symposium*. Calgary, Alberta, Canada.

AMBROSE, D. & TSONOPOULOS, C. 1995. Vapor-Liquid Critical Properties of Elements and Compounds. 2. Normal Alkanes. *Journal of Chemical & Engineering Data,* 40**,** 531-546.

ARAKTINGI, U. G. & ORR JR, F. M. 1993. Viscous Fingering in Heterogeneous Porous Media. *spe Advance Technology Series,* 1**,** 71-80.

BACHU, S. & BENNION, B. 2008. Effects of in-situ conditions on relative permeability characteristics of CO2-brine systems. *Environmental Geology,* 54**,** 1707-1722.

BAKER, L. E. 1988. Three-Phase Relative Permeability Correlations. *SPE/DOE Enhanced Oil Recovery Symposium*. Tulsa, Oklahoma, USA: Society of Petroleum Engineers.

BARKER, J. W. & EVANS, S. C. 1995. Predictive Model for Viscous Fingering in compositional wag. *SPE Reservoir Engineering,* 10**,** 116-121.

BENHAM, A. L. & OLSON, R. W. 1963. A Model Study of Viscous Fingering. *Society of petroleum engineers journal***,** 138-144.

BLACKWELL, R. J., RAYNE, J. R. & TERRY, W. M. 1959. Factors Influencing the Efficiency of Miscible Displacement. *Petroleum Transactions,* 217**,** 1-8.

BLUNT, M. J. 2000. An Empirical Model for Three-Phase Relative Permeability. *SPE Journal,* 5**,** 435-445.

BLUNT, M. J., BARKER, W. J., RUBIN, B., MANSFIELD, M., CULVERWELL, I. D. & CHRISTIE, M. A. 1994. Predictive Theory for Viscous Fingering in Compositional Displacement. *SPE Reservoir Engineering***,** 73-80.

BLUNT, M. J. & CHRISTIE, M. A. 1994. Theory of Viscous Fingering in Two Phase, Three Component Flow. *Spe Advance Technology Series,* 2**,** 52-60.

BOUKADI, F. H., BEMANI, A. S. & BABADAGLI, T. 2005. Investigating Uncertainties in Relative Permeability Measurements. *Energy Sources,* 27**,** 719-728.

BOUSTANI, A. & MAINI, B. B. 2001. The Role of Diffusion and Convective Dispersion in Vapour Extraction Process. *Journal of Canadian Petroleum Technology,* 40**,** 68-77.

BRAUN, E. M. & HOLLAND, R. F. 1995. Relative permeability hysteresis: Laboratory measurements and a conceptual model. *SPE Reservoir Engineering,* 10**,** 222-228.

BUCKLEY, S. E. & LEVERETT, M. 1942. Mechanism of fluid displacement in sands. *Transactions of the AIME,* 146**,** 107-116.

BUTLER, R. M. 1991. *Thermal recovery of oil and bitumen,* Old Tappan, NJ, USA, Prentice Hall Inc.

CAMY, J. P. & EMANUEL, A. S. 1977. Effect of Grid size in the Compositional Simulation of CO2 Injection. *52nd Full Annual Technical Conference and Exhibition of the Society of Petroleum Engineers of AIME*. Denver, Colorado, USA.

CAO, H., CRUMPTON, P. I. & SCHRADER, M. L. 2009. Efficient General Formulation Approach For Modeling Complex Physics. *2009 Reservoir Simulation Symposium*. Woodlands7, Texas, USA: Society of Petroleum Engineers.

CARLSON, F. M. Simulation of relative permeability hysteresis to the nonwetting phase. 56th Annual Fall Technical Conference and Exhibition of the SPE of AIME, 5-7, October 1981 San Antonio, texas, USA. Society of Petroleum Engineers.

CASTILLO, A. F., R., P. E., ROJAS, J. A. & ZAPATA, J. F. 2009. Numerical and Experimental Modelling of Relative Permeability in Heavy Oil Reservoir. *SPE Latin American and Caribbean Petroleum Engineering Conference*. Cartagena, Colombia.

CHARDAIRE-RIVIERE, C., CHAVENT, G., JAFFRE, J. & JUN, L. 1990. Multiscale Representation for Simultaneous Estimation of Relative Permeabilities and Capillary Pressure. *65th Annual Technical Conference and Exhibition of the Society of Petroleum Engineers*. New Orleans, LA, USA: Society of Petroleum Engineers.

CHARDAIRE-RIVIERE, C., CHAVENT, G., JAFFRE, J., LIU, J. & BOURBIAUX, B. J. 1992. Simultaneous Estimation of Relative Permeabilities and Capillary Pressure. *SPE Formation Evaluation,* 7.

CHIERICI, G. L. 1984. Novel Relations for Drainage and Imbibition Relative Permeabilities. *society of petroleum engineers journal,* 24**,** 275-276.

CHRISTIANSEN, R. L., KALBUS, J. S. & HOWARTH, S. M. 1997. Evaluation of Methods for Measuring Relative Permeabillity of Anhydrite from the Salado Formation: Sensitivity Analysis and Data Reduction. New Mexico, USA: Sandia National Laboratories.

CHRISTIE, M. A. 1989. High.Resolution Simulation of Unstable Flows in Porous Media. *SPE Reservoir Engineering,* 4**,** 297-203.

CHRISTIE, M. A. & BOND, D. J. 1987. Detailed Simulation of Unstable Processes in Miscible Flooding. *SPE Reservoir Engineering,* 2**,** 514-522.

CHRISTIE, M. A., JONES, A. D. W. & MUGGERIDGE, A. H. 1990. Comparison between Laboratory Experiments and Detailed Simulations of Unstable Miscible Displacement Influenced by Gravity. *In:* BULLER, A. T., BERG, E., HJELMELAND, O., KLEPPE, J., TORSÆTER, O. & AASEN, J. O. (eds.) *North Sea Oil and Gas Reservoirs—II: Proceedings of the 2nd North Sea Oil and Gas Reservoirs Conference organized and hosted by the Norwegian Institute of Technology (NTH), Trondheim, Norway, May 8–11, 1989*. Dordrecht: Springer Netherlands.

CHRISTIE, M. A., MUGGERIDGE, A. H. & BARLEY, J. J. 1993. 3D Simulation of Viscous Fingering and WAG Schemes. *SPE Reservoir Engineering***,** 19-26.

CHUNG, F. T. H., JONES, R. A. & NGUYEN, H. T. 1998. Measurements and Correlations of the Physical Properties of CO2-Heavy Crude Oil Mixtures. *SPE Reservoir Eng.,* 3**,** 822-828.

CIVAN, F. & DONALDSON, E. C. 1989. Relative Permeability From Unsteady-State Displacements With Capillary Pressure Included. *SPE Formation Evaluation,* 4**,** 189-193.

COATS, K. H. 1980. An Equation of State Compositional Model. *SPE Journal,* 20**,** 363-376.

COREY, A. T. 1954. The Interrelation Between Gas and Oil Relative Permeabilities. *Producers Monthly,* 19**,** 38-41.

CUTHIEL, D., KISSEL, G., JACKSON, C., FRAUENFELD, T., FISHER, D. & RISPLER, K. 2006. Viscous Fingering Effects in Solvent Displacement of Heavy Oil. *Journal of Canadian Petroleum Technology,* 45**,** 29-39.

DAUBA, C., QUETTIER, L., CHRISTENSEN, J., LE GOFF, C. & CORDELIER, P. An integrated experimental and numerical approach to assess the performance of solvent injection into heavy oil. SPE Annual Technical Conference and Exhibition, 29 September - 2 October 2002 San Antonio, Texas, USA. Society of Petroleum Engineers.

DESCH, J. B., LARSEN, W. K., LINDSAY, R. F. & NETTLE, R. L. 1984. Enhanced Oil Recovery by CO2 Miscible Displacement in the Little Knife Field, Billings County, North Dakota. *Journal of Petroleum Technology,* 36**,** 1592-16-2.

DÍAZ, O. C., MODARESGHAZANI, J., SATYRO, M. A. & YARRANTON, H. W. 2011. Modelling the Phase Behavior of Heavy Oil and Solvent Mixtures. *Fluid Phase Equilibria,* 304**,** 74-85.

DOGRU, A. H., SUNAIDI, H. A., FUNG, L. S., HABIBALLAH, W. A., AL-ZAMEL, N. & LI, K. G. 2002. A Parallel Reservoir Simulator for Large-Scale Reservoir Simulation. *SPE Reservoir evaluation and Engineering,* 5**,** 11-23.

DOWNIE, J. & CRANE, F. E. 1961. Effect of Viscosity on Relative Permeability. *SPE Journal,* 1**,** 59-60.

DUMORE, J. M. 1964. Stability Considerations in Downward Miscible Displacements. *SPE Journal,* 4**,** 356-362.

ELSHARKAWY, A. M. 2001. Characterization of the Plus Fraction and Prediction of the Dewpoint Pressure for Gas Condensate Reservoirs. *SPE Western Regional Meeting*. Bakersfield: Society of Petroleum Engineers.

EMADI, A. 2011. Mechanistic Study of Improved Heavy Oil Recovery by CO2-Foam Injection. *SPE Enhanced Oil Recovery Conference*. Kuala Lumpur, Malaysia.

EMADI, A. 2012. *Enhanced heavy oil recovery by water and carbon dioxide flood.* PhD, Heriot-Watt University.

EMADI, A., SOHRABI, M., FARZANEH, S. & IRELAND, S. 2013. Experimental Investigation of Liquid-CO2 and CO2-Emulsion Application for Enhanced Heavy Oil Recovery. *EAGE Annual Conference & Exhibition incorporating SPE Europec*. London, UK: Society of Petroleum Engineers.

EMADI, A., SOHRABI, M., JAMIOLAHMADY, M., IRELAND, S. & ROBERTSON, G. 2011a. Reducing heavy oil carbon footprint and enhancing production through CO2 injection. *Chemical Engineering Research and Design,* 89**,** 1783-1793.

EMADI, A., SOHRABI, M., JAMIOLAHMADY, M., IRLAND, S. & ROBERTSON, G. 2011b. Mechanistic Study of Improved Heavy Oil Recovery by CO2-Foam Injection. *SPE Enhanced Oil Recovery Conference*. Kuala Lumpur, Malaysia: Society of Petroleum Engineers.

FAROUQ ALI, S. M. 1974. Heavy Oil Recovery - Principles, Practicality, Potential, and Problems. Society of Petroleum Engineers.

FAROUQ ALI, S. M. 1976. Non Thermal heavy Oil Recovery Methods. *Rocky Mountian Regional Meeting of the Society of Petroleum engineers AIME* Wyoming, USA.

FARZANEH, S. A. 2014. *Non-thermal EOR from Heavy Oils.* PhD, Heriot-Watt University.

FARZANEH, S. A., SEYYEDSAR, S. M. & SOHRABI, M. 2016. Enhanced Heavy Oil Recovery by Liquid CO2 Injection under Different Injection Strategies. *SPE Annual Technical Conference and Exhibition*. Dubai, UAE: Society of Petroleum Engineers.

FAYERS, F. J. & NEWLEY, T. M. J. 1988. Detailed Validation of an Empirical Model for Viscous Fingering With Gravity Effects. *SPE Reservoir Engineering*, 542-550.

FAYERS, F. J. & SHELDON, J. W. 1959. The effect of capillary pressure and gravity on two-phase fluid flow in a porous medium. *Petrol. Trans. AIME,* 216, 147.

FOROOZESH, J. & MOGHADDAM, R. N. 2015. The Convective-Diffusive Mechanism in CO2 Sequestration in Saline Aquifers: Experimental and Numerical Simulation Study. *EUROPEC 2015*. Madrid, Spain: Society of Petroleum Engineers.

GARCIA, F. M. 1983. A Successful Gas-Injection Project in a Heavy Oil Reservoir. *58th Annual Technical Conference and Exhibition*. San Francisco, CA, USA: Society of Petroleum Engineers.

GERRITSEN, M. G. & DURLOFSKY, L. J. 2005. Modeling fluid flow in oil reservoirs. *Annu. Rev. Fluid Mech.,* 37, 211-238.

GHOODJANI, E. & BOLOURI, S. H. 2011. Experimental Study and Calculation of CO2-Oil Relative Permeability`. *Petrolum and Coal,* 53, 123-131.

GLASS, R. J., PARLANGE, J. Y. & STEENHUIS, T. S. 1991. Immiscible displacements in porous media: Stability analysis of three-dimensional, axisymmetric disturbances with application to gravity-driven wetting front instability. *Water Resour. Res.,* 27, 1947.

GOOSSENS, A. G. 1996. Prediction of Molecular Weight of Petroleum Fractions. *Industrial & Engineering Chemistry Research,* 35, 985-988.

GROGAN, A. T., PINCZEWSKI, V. W., RUSKAUFF, G. R. & ORR JR, F. M. 1988. Diffusion of CO2 at Reservoir conditions: Models and Measurements. *SPE Reservoir Engineering,* 39, 591-602.

HOLM, L. W. 1982. CO2 Flooding: Its Time Has Come. *Society of petroleum engineers journal,* 32, 2,739 - 2,745.

HOLM, L. W. 1986. Miscibility and Miscible Displacement. *Journal Of Petroleum Technology,* 38, 817-818.

HONARPOUR, M. M., KOEDERITZ, F. & HERBERT, A. 1986. *Relative permeability of petroleum reservoirs,* CRC Press Inc,Boca Raton, FL; None.

HONG, K. C. 1982. Lumped-Component Characterization of Crude Oils for Compositional Simulation. *SPE Enhanced Oil Recovery Symposium*. Tulsa, Oklahoma, USA: Society of Petroleum Engineers.

HOU, T. Y. & WU, X.-H. 1997. A Multiscale Finite Element Method for Elliptic Problems in Composite Materials and Porous Media. *Journal of Computational Physics,* 134, 169-189.

JAHANBAKHSH, A. & SOHRABI, M. 2015. A New Approach for Simultaneous Estimation of Relative Permeability and Capillary Pressure from Coreflood Experiments. *SPE Annual Technical Conference and Exhibition*. Houston, Texas, USA: Society of Petroleum Engineers.

JAMES, L. A., REZAEI, N. & CHATZIS, I. 2008. VAPEX, Warm VAPEX and Hybrid VAPEX – The State of Enhanced Oil Recovery for In-Situ Heavy Oils in Canada. *Journal of Canadian Petroleum Technology,* 47, 1-7.

JENNINGS , H. Y. & HABRA, L. 1966. Waterflood Behavior of High Viscosity Crudes in Preserved Soft and Unconsolidated Cores. *Journal Of Petroleum Technology*, 116-120.

JENNINGS, J. W., JR., MCGREGOR, D. S. & MORSE, R. A. 1988. Simultaneous Determination of Capillary Pressure and Relative Permeability by Automatic History Matching. *SPE Formation Evaluation,* 3**,** 322-328.

JENNY, P., LEE, S. H. & TCHELEPI, H. A. 2006. Adaptive fully implicit multi-scale finite-volume method for multi-phase flow and transport in heterogeneous porous media. *Journal of Computational Physics,* 217**,** 627-641.

JERAULD, G. R. 1997. General three-phase relative permeability model for Prudhoe Bay. *SPE reservoir Engineering,* 12**,** 255-263.

JERAULD, G. R., NITSCHE, L. C., TELETZKE, G. F., DAVIS, H. T. & SCRIVEN, L. E. 1984. Frontal Structure and Stability in Immiscible Displacement. *SPE Enhanced Oil Recovery Symposium*. Tulsa, Oklahoma, USA: Society of Petroleum Engineers.

JERAULD, G. R. & SALTER, S. J. 1990. The effect of pore-structure on hysteresis in relative permeability and capillary pressure: pore-level modeling. *Transport in porous media,* 5**,** 103-151.

JESSEN, K., STENBY, E. H. & ORR, F. M. 2004. Interplay of Phase Behavior and Numerical Dispersion in Finite-Difference Compositional Simulation. *Society of petroleum engineers journal,* 9**,** 193-201.

JHA, K. N. 1986. A Laboratory Study of Heavy Oil Recovery with Carbon Dioxide. *Journal of Canadian Petroleum Technology*, 54-63.

JOHNSON, E. F., BOSSLER, D. P. & NAUMANN, V. O. 1959. Calculation of Relative Permeability from Displacement Experiments. *Petroleum Transactions of AIME,* 216**,** 370-372.

JONES, S. C. & ROSZELLE, W. O. 1978. Graphical Techniques for Determining Relative Permeability From Displacement Experiments. *Journal Of Petroleum Technology,* 30**,** 807-817.

JOSSI, J. A., STIEL, L. I. & THODOS, G. 1962. The viscosity of pure substances in the dense gaseous and liquid phases. *AIChE Journal,* 8**,** 59-63.

KANTAR, K., KARAOGUZ, D., ISSEVER, K. & VARANA, L. 1985. Design Concepts of a Heavy-Oil Recovery Process by an Immiscible CO2 Application. *Journal of Petroleum Technology,* 37**,** 275-283.

KAVOUSI, A., TORABI, F. & CHAN, C. 2013. Experimental Measurement of CO2 Solubility in Heavy Oil and Its Diffusion Coefficient calculation at Both Static and Dynamic Conditions. *SPE Heavy Oil Conference Canada*. Calgary, Alberta, Canada.

KECHUT, N. I., JAMIOLAHMADY, M. & SOHRABI, M. 2011. Numerical simulation of experimental carbonated water injection (CWI) for improved oil recovery and CO2 storage. *Journal of Petroleum Science and Engineering,* 77**,** 111-120.

KING, M. J. 1987. Viscous Fingering Utilizing Probabilistic Simulation. *62nd Annual Coneference and Exhibition of the Society of Petroleum Engineers.* Dallas, Texas, USA.

KOKAL, S. & MAINI, B. B. 1990. An Improved Model For Estimating Three-Phase Oil-Water-Gas Relative Permeabilities From Two-Phase Oil-Water And Oil-Gas Data. *Journal of Canadian Petroleum Technology,* 29**,** 105-113.

KOVAL, E. J. 1963. A Method for Predicting the Performance of Unstable Miscible Displacement in Heterogeneous Media. *Society of petroleum engineers journal*, 145-154.

KUEPER, B. H. & FRIND, E. O. 1988. An overview of immiscible fingering in porous media. *Journal of Contaminant Hydrology,* 2**,** 95-110.

KULKARNI, K. N. & DATTA-GUPTA, A. 2000. Estimating Relative Permeability From Production Data: A Streamline Approach. *Society of petroleum engineers journal,* 5**,** 402-411.

KUMAR, A. & OKUNO, R. 2012a. Critical parameters optimized for accurate phase behavior modeling for heavy n-alkanes up to C100 using the Peng–Robinson equation of state. *Fluid Phase Equilibria,* 335**,** 46-59.

KUMAR, A. & OKUNO, R. 2012b. Fluid Characterization Using an EOS for Compositional Simulation of Enhanced Heavy-Oil Recovery. *SPE annual Technical Conference and Exhibition*. San Antonio, Texas, USA: Society of Petroleum Engineers.

LAKE, L. W. 1989. *Enhanced oil recovery,* Englewood Cliffs, New Jersey, USA, Prentice Hall.

LAND, C. S. 1968. Calculation of Imbibition Relative Permeability for Two- and Three-Phase Flow From Rock Properties. *SPE Journal,* 8**,** 149-156.

LANSANGAN, R. M. & SMITH, J. L. 1993. Viscosity, Density, and Composition Measurements of CO2/West Texas Oil Systems. *SPE Reservoir Engineering,* 8**,** 175-182.

LEE, A. L. & EAKIN, B. E. 1964. Gas-Phase Viscosity of Hydrocarbon Mixtures. *Society of petroleum engineers journal,* 4**,** 247-249.

LEE, B. I. & KESLER, M. G. 1975. A generalized thermodynamic correlation based on three-parameter corresponding states. *AIChE Journal,* 21**,** 510-527.

LI, H., CHEN, S., YANG, D. & TONTIWACHWUTHIKUL, P. 2009. Estimation of Relative Permeability by Assisted History Matching Using the Ensemble Kalman Filter Method. *Canadian International Petroleum Conference*. Calgary, Alberta, Canada: Petroleum Society of Canada.

LI, K., SHEN, P. & QING, T. 1994. A New Method for Calculating Oil-Water Relative Permeabilities with

Consideration of Capillary Pressure. *Mechanics and Practice,* 16**,** 46-52.

LI, Y. K. & NGHIEM, L. X. 1982. The Development of a General Phase Envelope Construction Algorithm for Reservoir Fluid Studies. *SPE Annual Technical Conference and Exhibition*. New Orleans, Louisiana, USA: Society of Petroleum Engineers.

LIM, G. B., KRY, P. R., LEBEL, J. P. & KWAN, M. Y. 2004. Cyclic solvent process for in-situ bitumen and heavy oil production. Google Patents.

LINDELOFF, N., PEDERSEN, K. S., RONNINGSEN, H. P. & MILTER, J. 2004. The Corresponding States Viscosity Model Applied to Heavy Oil Systems. *Journal of Canadian Petroleum Technology,* 43**,** 47-53.

LOHRENZ, J., BRAY, B. G. & CLARK, C. R. 1964. Calculating Viscosities of Reservoir Fluids From Their Compositions. *Journal Of Petroleum Technology,* 16**,** 1171-1176.

LOLLEY, C. S. & RICHARDSON, W. C. 1997. Compositional Input for Thermal Simulation of Heavy Oils With Application to the San Ardo Field. *International Thermal Operations and Heavy Oil Symposium*. Bakersfield, California, USA: Society of Petroleum Engineers.

LOMELAND, F., EBELTOFT, E. & THOMAS, W. K. 2005. A NEW VERSATILE RELATIVE PERMEABILITY CORRELATION. *International Symposium of the Society of Core Analysts*. Toronto, Canada: Society of Core Analyst.

LU, P. & HORNE, R. N. 2000. A Multiresolution Approach to Reservoir Parameter Estimation Using Wavelet Analysis. *SPE Annual Technical Conference and Exhibition*. Dallas, Texas, USA: Society of Petroleum Engineers.

M., H. G. 1987. Viscous fingering in porous media. *Annu. Rev. Fluid Mech.,* 19**,** 1.

MA, T. D., RUGEN, J. A., STOISITS, R. F. & VOUNGREN, G. K. 1995. Simultaneous Water and Gas Injection Pilot at the Kuparuk River Field, Reservoir Impact. *SPE Annual Technical Conference and Exhibition*. Dallas, Texas, USA: Society of Petroleum Engineers.

MAI, A., BRYAN, J., GOODARZI, N. & KANTZAS, A. 2009. Insights Into Non-Thermal Recovery of Heavy Oil. 48**,** 27-35.

MAI, A. & KANTZAS, A. 2009. Heavy Oil Waterflooding: Effects of Flow Rate and Oil Viscosity. *Journal of Canadian Petroleum Technology,* 48.

MAINI, B. 1998. Is it Futile to measure Relative Permeability for Heavy Oil Reservoir. *Journal of Canadian Petroleum Technology,* 37**,** 56-62.

MARTIN, F. D. & TABER, J. J. 1992. Carbon Dioxide Flooding. *Journal Of Petroleum Technology***,** 398-400.

MAYER, E. H., EARLOUGHER, R. C., SPIVAK, A. & COSTA, A. 1988. Analysis of Heavy-Oil Immiscible CO2 Tertiary Coreflood Data. *SPE Reservoir Engineering,* 3**,** 69-75.

MEANEY, K. & PATERSON, L. 1996. Relative Permeability in Coal. *SPE Asia Pacific Oil and Gas Conference*. Adelaide, Australia: Society of Petroleum Engineers.

MILLER, K. A. 1994. Heavy Oil and Bitumen Not Glamorous, but Often Profitable.

MITRA, P. P., SEN, P. N. & SCHWARTZ, L. M. 1993. Short-time behavior of the diffusion coefficient as a geometrical probe of porous media. *Physical Review B,* 47**,** 8565-8574.

MODARESGHAZANI, J., MOORE, R. G., MEHTA, S. A. & FRAASSEN, K. C. V. 2015. Determination of Two-Phase and Three-Phase Relative Permeabilities in Heavy Oil/Water/Gas Systems. *SPE Canada Heavy Oil Conference*. Calgary, Alberta, Canada: Society of Petroleum Engineers.

MOHANTY, K. K., MASINO, W. H., JR., MA, T. D. & NASH, L. J. 1995. Role of Three-Hydrocarbon-Phase Flow in a Gas Displacement Process. *SPE Reservoir Engineering,* 10**,** 214-221.

MOORTGAT, J., FIROOZABADI, A., LI, Z. & ESPO´SITO, R. 2013. CO2 Injection in Vertical and Horizontal Cores: Measurements and Numerical Simulation. *SPE Journal***,** 1-14.

MUQEEM, M. A., BENTSEN, R. G. & MAINI, B. B. 1993. An Improved Steady-State Technique For Three-Phase Relative Permeability Measurements. *Annual Technical Meeting*. Calgary, Alberta: Petroleum Society of Canada.

MUTORU, J. W., LEAHY-DIOS, A. & FIROOZABADI, A. 2011. Modeling infinite dilution and Fickian diffusion coefficients of carbon dioxide in water. *AIChE Journal,* 57**,** 1617-1627.

NASEHI, M. & ASGHARI, K. 2010. Use of CO2 in Heavy Oil Waterflooding. *SPE International Conference on CO2-Capture, Storage and Utilization*. New Orleans, Louisiana.

NASRABADI, H., FIROOZABADI, A. & AHMED, T. K. 2009. Complex Flow and Composition Path in CO2 Injection Schemes from Density Effects in 2 and 3D. *2009 SPE Annual Technical Conference and Exhibition*. New Orleans, Louisiana, USA: Society of Petroleum Engineers.

NEHRING, R., HESS, N., AND KAMIONSKI, M. 1983. The Heavy Oil Resources of the United States. *In:* ENERGY, U. S. D. O. (ed.).

NGHIEM, L. X. & SAMMON, P. H. 1997. A Non-Equilibrium Equation-of-State Compositional Simulator. *1997 SPE 7Reservoir Simulation Symposium*. Dallas, Texas, USA: Society of Petroleum Engineers.

NORDTVEDT, J. E., MEJIA, G., YANG, P.-H. & WATSON, A. T. 1993. Estimation of Capillary Pressure and Relative Permeability Functions From Centrifuge Experiments. *SPE Reservoir Eng.,* 8**,** 292-298.

O'SULLIVAN, A. E. 2004. *MODELLING SIMULATION ERROR FOR IMPROVED RESERVOIR PREDICTION*. Doctor of Philosophy, Heriot-Watt University.

ODEH, A. S. 1959. Effect of viscosity ratio on relative permeability. *Petroleum Transactions of AIME,* 216**,** 346-353.

ODEH, A. S. & DOTSON, B. J. 1985. A Method for Reducing the Rate Effect on Oil and Water Relative Permeabilities Calculated From Dynamic Displacement Data. *Journal Of Petroleum Technology,* 37**,** 2051-2058.

OECD/IEA 2013. Resources to Reservoirs 2013. *Oil, Gas and Coal Technologies for the Energy Markets of the Future*. France: International Energy Agency.

OLIVER, D. S., REYNOLDS, A. C. & LIU, N. 2008. *Inverse Theory for Petroleum Reservoir Characterization and History Matching,* Cambridge, Cambridge University Press.

ORTIZ-ARANGO, J. D. & KANTZAS, A. 2011. Pore-Level Investigation of Oil-Mobility Enhancement In Heavy Oil Reservoirs *Journal of Canadian Petroleum Technology***,** 59-74.

OUTMANS, H. D. 1962. Nonlinear theory for frontal stability and viscous fingering in porous media. *Society of Petroleum Engineers Journal,* 2**,** 165-176.

PAPATZACOS, P. & SKJÆVELAND, S. M. 2002. Relative Permeability From Capillary Pressure. *SPE Annual Technical Conference and Exhibition*. San Antonio, Texas, USA: Society of Petroleum Engineers.

PARACELLO, V. P., BARTOSEK, M., DE SIMONI, M. & MALLARDO, C. 2012. Experimental Evaluation of CO2 Injection in a Heavy Oil Reservoir. *International Petroleum Technology Conference*. Bangkok, Thailand.

PATHAK, V., BABADAGLI, T. & EDMUNDS, N. 2012. Mechanics of heavy-oil and bitumen recovery by hot solvent injection. *SPE Reservoir Evaluation & Engineering,* 15**,** 182-194.

PEDERSEN, K. S. & CHRISTENSEN, P. L. 2007. *Phase Behaviour of Petroleum Reservoir Fluids,* Boca Raton, Florida, USA, CRC Press, Taylor and Francis Group.

PEDERSEN, K. S. & FREDENSLUND, A. 1987. An improved corresponding states model for the prediction of oil and gas viscosities and thermal conductivities. *Chemical Engineering Science,* 42**,** 182-186.

PEDERSEN, K. S., FREDENSLUND, A., CHRISTENSEN, P. L. & THOMASSEN, P. 1984a. Viscosity of crude oils. *Chemical Engineering Science,* 39**,** 1011-1016.

PEDERSEN, K. S., THOMASSEN, P. & FREDENSLUND, A. 1983. SRK-EOS calculation for crude oils. *Fluid Phase Equilibria,* 14**,** 209-218.

PEDERSEN, K. S., THOMASSEN, P. & FREDENSLUND, A. 1984b. Thermodynamics of petroleum mixtures containing heavy hydrocarbons. 1. Phase envelope calculations by use of the Soave-Redlich-Kwong equation of state. *Industrial & Engineering Chemistry Process Design and Development,* 23**,** 163-170.

PEI, H., ZHANG, G., GE, J., JIN, L. & LIU, X. 2011. Analysis of microscopic displacement mechanisms of alkaline flooding for enhanced heavy-oil recovery. *Energy & Fuels,* 25**,** 4423-4429.

PENG, D. Y. & ROBINSON, D. B. 1976. A New Two-Constant Equation of State. *Industrial & Engineering Chemistry Fundamentals,* 15**,** 59-64.

PENG, D. Y. & ROBINSON, D. B. 1978. *The characterization of the heptanes and heavier fractions for the GPA Peng-Robinson programs,* Tulsa, Okla., Gas Processors Association.

PERKINS, T. & JOHNSTON, O. 1963. A review of diffusion and dispersion in porous media. *Society of Petroleum Engineers Journal,* 3**,** 70-84.

PETERS, E. J. & FLOCK, D. L. 1981. The Onset of Instability During Two-Phase Immiscible Displacement in Porous Media. *SPE Journal,* 21**,** 249-258.

PETERS, E. J. & KHATANIAR, S. 1987. The Effect of Instability on Relative Permeability Curves Obtained by the Dynamic-Displacement Method. *SPE Formation Evaluation***,** 6.

PIRI, M. & BLUNT, M. J. 2005. Three-Dimensional Mixed-wet Random Pore-scale Network odeling of Two and Three-Phase Flow in Porous Media. II. Results. *Physical Review E,* 71**,** 026302.

POOLADI-DARVISH, M. & FIROOZABADI, A. 1999. Solution-gas drive in heavy oil reservoirs. *Journal of Canadian Petroleum Technology,* 38.

QUIÑONES-CISNEROS, S. E., ZÉBERG-MIKKELSEN, C. K. & STENBY, E. H. 2003. Friction theory prediction of crude oil viscosity at reservoir conditions based on dead oil properties. *Fluid Phase Equilibria,* 212**,** 233-243.

RAHNEMA, H., KHARRAT, R. & ROSTAMI, B. Experimental and numerical study of vapor extraction process (VAPEX) in heavy oil fractured reservoir. Canadian International Petroleum Conference, 1777-19, June 2008 Calgary, Alberta, Canada. Petroleum Society of Canada.

RIAZ, A. & TCHELEPI, H. A. 2006. Influence of Relative Permeability on the Stability Characteristics of Immiscible Flow in Porous Media. *Transport in Porous Media,* 64**,** 315-338.

RIAZ, A., TCHELEPI, H. A. & B., H. 2004. Linear stability analysis of immiscible two-phase flow in porous media with capillary dispersion and density variation. *Physics of Fluids,* 16**,** 4727-4737.

RIAZI, M. R. & AL-SAHHAF, T. A. 1996. Physical properties of heavy petroleum fractions and crude oils. *Fluid Phase Equilibria,* 117**,** 217-224.

RODRIGUEZ, I. & HAMOUDA, A. A. 2008. An Approach for Characterization and Lumping of Plus Fractions of Heavy Oil. *International Thermal operations and Heavy Oil Symposium*. Calgary, Alberta, Canada: Society of Petroleum Engineers.

ROJAS, G. A., ZAO, T., DYER, S. B., THOMAS, S. & FAROUQ ALI, S. M. 1991. Scaled Model Studies of CO2 Floods. *SPE Reservoir Engineering*.

RONGY, L., HAUGEN, K. B. & FIROOZABADI, A. 2012. Mixing from Fickian diffusion and natural convection in binary non-equilibrium fluid phases. *AIChE Journal,* 58**,** 1336-1345.

SAHNI, A., BURGER, J. & BLUNT, M. J. 1998. Measurement of Three-Phase Relative Permeability during Gravity Drainage using CT. *SPE/DOE Improved Oil Recovery Symposium*. Tulsa, Oklahoma, USA: Society of Petroleum Engineers.

SALEHI, A., VOSKOV, D. V. & TCHELEPI, H. A. 2013. Thermodynamically Consistent Transport Coefficients for Upscaling of Compositional Processes. *SPE Reservoir Simulation Symposium*. The Woodlands, Texas, USA: Society of Petroleum Engineers.

SANCET, G. F. 2007. Heavy Fraction C7+ Characterization for PR-EOS. *SPE annual Technical Conference and Exhibition*. Anaheim, California, USA: Society of Petroleum Engineers.

SANDBERG, C. R., GOURNAY, L. S. & SIPPEL, R. F. 1958. The Effect of Fluid-Flow Rate and Viscosity on Laboratory Determinations of Oil-Water Relative Permeabilities. *Petroleum Transactions of AIME,* 21**,** 36-43.

SANER, W. B. & PATTON, J. T. 1986. CO2 Recovery of Heavy Oil: Wilmington Field Test. *Journal Of Petroleum Technology*.

SANKUR, V. & EMMANUEL, A. S. 1983. A Laboratory Study of Heavy Oil Recovery With C02 Injection. *1983 California Regional Meeting*. Ventura, California, USA.

SEYYEDSAR, S. M., FARZANEH, S. A. & SOHRABI, M. 2015. Enhanced Heavy Oil Recovery by Intermittent CO2 Injection. *SPE annual Technical Conference and Exhibition*. Houston, Texas, USA: Society of Petroleum Engineers.

SHAHVERDI, H. & SOHRABI, M. 2011. Relative Permeability Characterization for Water-Alternating-Gas Injection in Oil Reservoirs. *Journal of Petroleum Science and Engineering,* 21**,** 799-808.

SHAHVERDI, H. & SOHRABI, M. 2013. An Improved Three-Phase Relative Permeability and Hysteresis Model for the Simulation of a Water-Alternating-Gas Injection. *SPE Journal,* 18**,** 841-850.

SHARMA, J., INWOOD, S. B. & KOVSCEK, A. 2012. Experiments and Analysis of Multiscale Viscous Fingering During Forced Imbibition. *SPE Journal,* 17**,** 1142-1159.

SHERWOOD, J. D. 1987. Unstable fronts in a porous medium. *Journal of Computational Physics,* 68**,** 485-500.

SHOKRI, A. R. & BABADAGLI, T. 2012. An Approach to Model CHOPS and Post-CHOPS Application. *SPE Annual Technical Conference and exhibition*. San Antonio, Texas, USA.

SHU, W. R. & HARTMAN, K. J. 1986. Thermal recovery method for viscous oil. Google Patents.

SIGMUND, P. M. 1976. Prediction of Molecular Diffusion At Reservoir Conditions. Part 1- Measurement And Prediction of Binary Dense Gas Diffusion Coefficients. *Journal of Canadian Petroleum Technology***,** 48-57.

SIGMUND, P. M. & MCCAFFERY, F. G. 1979. An Improved Unsteady-State Procedure for Determining the Relative-Permeability Characteristics of Heterogeneous Porous Media (includes associated papers 8028 and 8777). *Society of petroleum engineers journal,* 19**,** 15-28.

SIMON, R., ROSMAN, A. & ZANA, E. 1978. Phase-Behavior Properties of CO2 - Reservoir Oil Systems. *Society of petroleum engineers journal,* 18**,** 20-26.

SKAUGE, A. & POULSEN, S. 2000. Rate Effects on Centrifuge Drainage Relative Permeability. *SPE Annual Technical Conference and Exhibition*. Dallas, Texas, USA: Society of Petroleum Engineers.

SMITH, G. E. 1992. Waterflooding Heavy Oils. *SPE Rocky Mountain Regional Meeting*. Casper, Wyoming: SPE.

SOAVE, G. 1972. Equilibrium constants from a modified Redlich-Kwong equation of state. *Chemical Engineering Science,* 27**,** 1197-1203.

SOHRABI, M. & EMADI, A. 2012. Novel Insights into the Pore-Scale Mechanisms of Enhanced Oil Recovery by CO2 Injection. *EAGE Annual Conference and Exhibition Incorporating SPE Europec*. Copenhagen, Denmark.

SOHRABI, M. & FATEMI, S. M. 2013. Experimental and Numerical Investigation of the Impact of Design Parameters on the Performance of WAG and SWAG Injection in Water-Wet and Mixed-Wet Systems. *SPE Enhanced Oil Recovery Conference*. Kuala Lumpur, Malaysia: Society of Petroleum Engineers.

SPITERI, E. J. & JUANES, R. 2006. Impact of relative permeability hysteresis on the numerical simulation of WAG injection. *Journal of Petroleum Science and Engineering,* 50**,** 115-139.

SPITERI, E. J., JUANES, R., BLUNT, M. J. & ORR, F. M. 2008. A new model of trapping and relative permeability hysteresis for all wettability characteristics. *Spe Journal,* 13**,** 277-288.

SPIVAK, A. 1984. Mechanisms of Immiscible CO2 Injection in Heavy Oil

Reservoirs, Wilmington Field, CA. *California regional meeting*. Long beach, California, USA.

STALKUP, F. I., LO, L. L. & DEAN, R. H. 1990. Sensitivity to Gridding of Miscible Flood Predictions Made With Upstream Differenced Simulators. *SPE/DOE Seventh Symposium on Enhanced Oil Recovery*. Tulsa, Oklahoma, USA: Society of Petroleum Engineers.

STERN, D. 1991. Mechanisms of Miscible Oil Recovery: Effects of Pore-Level Fluid Distribution. *SPE Annual Technical Conference and Exhibition*. Dallas, Texas, USA: Society of Petroleum Engineers.

STONE, H. L. 1970. Probability Model for Estimating Three-Phase Relative Permeability. *Journal Of Petroleum Technology,* 22**,** 214-218.

STONE, H. L. 1973. Estimation of Three-Phase Relative Permeability And Residual Oil Data. *Journal of Canadian Petroleum Technology,* 12**,** 54-61.

SUN, S. & FIROOZABADI, A. 2009. Compositional Modeling in Three-Phase Flow for CO2 and other Fluid Injections using Higher-Order Finite Element Methods. *SPE Annual Technical Conference and exhibition*. New Orleans, Louisiana.

TAURA, U., MAHZARI, P., SOHRABI, M. & FARZANEH, S. A. 2016. A New Methodology for Improved Estimation of Two-Phase Relative Permeability Functions for Heavy Oil Displacement Involving Compositional Effects and Instability. *SPE International Heavy Oil Conference and Exhibition*. Mangaf, Kuwait: Society of Petroleum Engineers.

TERWILLIGER, P. L., WILSEY, L. E., HALL, N. H., BRIDGES, P. M. & MORSE, R. A. 1951. An experimental and theoretical investigation of gravity drainage performance. *Petrol. Trans. AIME,* 192**,** 285.

THEODOROPOULOU, M. A., SYGOUNI, V., KAROUTSOS, V. & TSAKIROGLOU, C. D. 2005. Relative permeability and capillary pressure functions of porous media as related to the displacement growth pattern. *International Journal of Multiphase Flow,* 31**,** 1155-1180.

THOMAS, S., SCOULAR, J. R., VERKOCZY, B. & FAROUQ ALI, S. M. 1999. CHEMICAL METHODS FOR HEAVY OIL RECOVERY. *THE EIGHTH PETROLEUM CONFERENCE OF THE SOUTH SASKATCHEWAN SECTION, THE PETROLEUM SOCIETY OF CIM*. Regina, Canada.

TODD, M. R. & LONGSTAFF, W. J. 1972. The Development, Testing, and Application Of a Numerical Simulator for Predicting Miscible Flood Performance. *Journal Of Petroleum Technology,* 253**,** 874-882.

TORABI, F., JAMALOEI, B. Y., ZARIVNYY, O., PAQUIN, B. A. & RUMPEL, N. J. 2012a. The Evaluation of Variable-Injection Rate Waterflooding, Immiscible CO2Flooding, and Water-alternating-CO2Injection for Heavy Oil Recovery. *Petroleum Science and Technology,* 30**,** 1656-1669.

TORABI, F., YADALI JAMALOEI, B., STENGLER, B. M. & JACKSON, D. E. 2012b. The evaluation of CO2-based vapour extraction (VAPEX) process for heavy-oil recovery. *Journal of Petroleum Exploration and Production Technology,* 2**,** 93-105.

TRAN, T. D., NEOGI, P. & BAI, B. 2017. Stability of CO2 Displacement of an Immiscible Heavy Oil in a Reservoir. *SPE Journal,* 22**,** 539-547.

TRIPATHI, I. & MOHANTY, K. K. 2008. Instability due to wettability alteration in displacements through porous media. *Chemical Engineering Science,* 63**,** 5366-5374.

TWU, C. H. 1985. Internally consistent correlation for predicting liquid viscosities of petroleum fractions. *Industrial & Engineering Chemistry Process Design and Development,* 24**,** 1287-1293.

VAN DIJKE, M. I. J., MCDOUGALL, S. R. & SORBIE, K. S. 2001a. Three-Phase Capillary Pressure and Relative Permeability Relationships in Mixed-Wet Systems. *Transport in Porous Media,* 44**,** 1-32.

VAN DIJKE, M. I. J., SORBIE, K. S. & MCDOUGALL, S. R. 2001b. Saturation-dependencies of three-phase relative permeabilities in mixed-wet and fractionally wet systems. *Advances in Water Resources,* 24**,** 365-384.

VOSKOV, D. V. & TCHELEPI, H. A. 2012. Comparison of nonlinear formulations for two-phase multi-component EoS based simulation. *Journal of Petroleum Science and Engineering,* 82–83**,** 101-111.

WAKEHAM, W. A., CHOLAKOV, G. S. & STATEVA, R. P. 2002. Liquid Density and Critical Properties of Hydrocarbons Estimated from Molecular Structure. *Journal of Chemical & Engineering Data,* 47**,** 559-570.

WAN, T., MENG, X., SHENG, J. J. & WATSON, M. Compositional modeling of EOR process in stimulated shale oil reservoirs by cyclic gas injection. SPE Improved Oil Recovery Symposium, 2014. Society of Petroleum Engineers.

WANG, J., DONG, M. & ASGHARI, K. 2006a. Effect of Oil Viscosity on Heavy Oil/Water Relative Permeability Curves. *Symposium on Improved Oil Recovery*. Tulsa, Oklahoma, USA.

WANG, J., WALTERS, D. A., SETTARI, A. & WAN, R. G. 2006b. Simulation of cold heavy oil production using an integrated modular approach with emphasis on foamy oil flow and sand production effects. *1st Heavy Oil Conference*. Calgary, Alberta, Canada.

WEISSBERG, H. L. 1963. Effective diffusion coefficient in porous media. *Journal of Applied Physics,* 34**,** 2636-2639.

WELGE, H. J. 1949. Displacement of Oil from Porous Media by Water or Gas. *Transactions of the AIME,* 179**,** 133-145.

WHITSON, C. H. 1983. Characterizing Hydrocarbon Plus Fractions. *society of petroleum engineers of AIME*.

WHITSON, C. H. 1984. Critical Properties Estimation From an Equation of State. *SPE Enhanced Oil Recovery Symposium*. Society of Petroleum Engineers.

WHITSON, C. H. & BRULÉ, M. R. 2000. *Phase behavior,* Richardson, Texas, USA, Henry L. Doherty Memorial Fund of AIME, Society of Petroleum Engineers Richardson, TX.

WILKE, C. R. & CHANG, P. 1955. Correlation of diffusion coefficients in dilute solutions. *AIChE Journal,* 1**,** 264-270.

WINPROP, C. 2015. WINPROP USER GUIDE Phase-Behaviour & Fluid Property Program. 2015 ed. Calgary, Alberta, Canada: Computer Modelling Group.

YAN, J. 2002. Reservoir parameters estimation from well log and core data: a case study from the North Sea. *Petroleum Geoscience,* 8**,** 63-69.

YANG, C., CARD, C. & NGHIEM, L. 2009. Economic Optimization and Uncertainty Assessment of Commercial SAGD Operations. *Journal of Canadian Petroleum Technology,* 48**,** 33-40.

YANG, P. H. & WATSON, A. T. 1991. A Bayesian Methodology for Estimating Relative Permeability Curves. *SPE Reservoir Engineering*, 259-265.

YAZDANI, A. & MAINI, B. B. 2008. Modeling of the VAPEX Process in a Very Large Physical Model. *Energy & Fuels*, 22, 535-544.

ZHANG, Y., SONG, C., ZHENG, S. & YANG, D. 2012. Simultaneous Estimation of Relative Permeability and Capillary Pressure for Tight Formations from Displacement Experiments. *SPE Canadian Unconventional Resources Conference*. Calgary, Alberta, Canada: Society of Petroleum Engineers.

ZHOU, H. & TCHELEPI, H. A. 2012. Two-Stage Algebraic Multiscale Linear Solver for Highly Heterogeneous Reservoir Models. *SPE Journal*, 17, 523-539.

ZUBOV, V. R., INDRUPSKIY, I. M. & BOGACHEV, K. Y. Compositional Simulator with Non-equilibrium Phase Transitions. *SPE Russian Petroleum Technology Conference and Exhibition*. Moscow, Russia: Society of Petroleum Engineers.